

Under the Influence of Light

New Chromatographic
Tools for Elucidating
Photodegradation
Mechanisms

Mimi den Uijl

Under the Influence of Light

New Chromatographic Tools for Elucidating
Photodegradation Mechanisms

Mimi den Uijl

2022

Under the Influence of Light

New Chromatographic Tools for Elucidating
Photodegradation Mechanisms

ISBN: 978-94-6458-538-4

Provided by thesis specialist Ridderprint, ridderprint.nl

Printing: Ridderprint

Layout & Design: Jules Verkade, persoonlijkproefschrift.nl

For additional information: <https://linktr.ee/mimidenuyl>

Copyright © 2022 by Mimi J. den Uijl, Amsterdam

Under the Influence of Light
-
New Chromatographic Tools for Elucidating
Photodegradation Mechanisms

ACADEMISCH PROEFSCHRIFT

ter verkrijging van de graad van doctor
aan de Universiteit van Amsterdam
op gezag van de Rector Magnificus
prof. dr. ir. P.P.C.C. Verbeek
ten overstaan van een door het College voor Promoties ingestelde commissie,
in het openbaar te verdedigen in de Aula der Universiteit
op vrijdag 7 oktober 2022, te 14:00 uur

Door
Mimi Josefien den Uijl
Geboren te Amsterdam

ACADEMISCH PROEFSCHRIFT

Promotores: Prof. dr. ing. M.R. van Bommel
Universiteit van Amsterdam

Prof. dr. ir. P.J. Schoenmakers
Universiteit van Amsterdam

Copromotores: Dr. B.W.J. Pirok
Universiteit van Amsterdam

Overige leden: Prof. dr. D. Cabooter
KU Leuven

Prof. dr. ir. J.G.M. Janssen
Wageningen University & Research

Dr. I. Degano
University of Pisa

Prof. dr. K. Keune
Universiteit van Amsterdam

Prof. dr. ing. T. Noël
Universiteit van Amsterdam

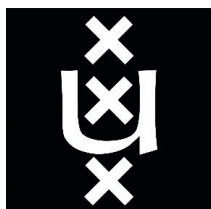
Prof. dr. S. Woutersen
Universiteit van Amsterdam

Dr. A. Gargano
Universiteit van Amsterdam

The work in this thesis was financially supported by the TooCOLD project, which is funded by the TTW Open Technology Programme, which is (partly) financed by the Netherlands Organisation for Scientific Research (NWO). Project number 15506.



Academic partners:



Industrial partners:



Table of contents

Part I: Introduction

Chapter 0	Prologue	11
Chapter 1	Introduction	15
	<i>Scope of the thesis</i>	27

Part II: Retention modelling

Chapter 2	Recent applications of retention modelling in liquid chromatography	37
Chapter 3	Measuring and using scanning-gradient data for use in method optimization for liquid chromatography	85
Chapter 4	Assessing the Feasibility of Stationary-Phase-Assisted Modulation for Two-Dimensional Liquid-Chromatography Separations	113

Part III: Photodegradation research

Chapter 5	Comparing different light-degradation approaches for the degradation of Crystal Violet and Eosin Y	141
Chapter 6	Combining photodegradation in a liquid-core-waveguide cell with multiple-heart-cut two-dimensional liquid chromatography	163
Chapter 7	Incorporating a liquid-core-waveguide cell in recycling liquid chromatography for detailed studies of photodegradation reactions	183

Part IV: Evaluation

Chapter 8	Conclusions and Future Perspectives	201
Chapter 9	Epilogue	231

Part V: Summary

Chapter 10	Summary	239
-------------------	---------	------------

Part VI: Supporting Information

Chapter 11	Sundries	249
	<i>List of publications</i>	250
	<i>Overview of co-authors' contribution</i>	252
	<i>List of abbreviations</i>	255
	<i>List of symbols</i>	257
Chapter 12	Appendices	261
	<i>Appendix A (related to Chapter 3)</i>	262
	<i>Appendix B (related to Chapter 4)</i>	274
	<i>Appendix C (related to Chapter 5)</i>	280
	<i>Appendix D (related to Chapters 6 & 7)</i>	285
	<i>Appendix E (related to Chapter 7)</i>	291
Chapter 13	Acknowledgements	297

PART I

Introduction

CHAPTER 0

Prologue

'To develop a complete mind: Study the science of art; Study the art of science. Learn how to see. Realize that everything connects to everything else.' (Leonardo da Vinci)

Throughout history, chemistry and art always went hand in hand. As a painter, one was limited by the resources available. Organic dyes, *i.e.* dyes with structures consisting mainly of carbon and other light elements, used to dye textiles were extracted from natural resources, such as plants (*e.g.* roots, leaves, wood) or animals (insects, mollusks), and inorganic pigments, such as earth pigments and minerals, were available to prepare paint. Pigments were also discovered in a more accidental way. For example when paint maker Diesbach made a red lake pigment of cochineal, a scale insect used for the dye carmine, he accidentally discovered Prussian blue while using a sample of potassium contaminated with iron.

As a painter before the 1820s, you had several choices for pigments ranging in quality and price. While some pigments were derived from rare materials and were very expensive, other ones were cheaper, because of their high abundance. In those days the colorants used were never mass produced. They were created in workshops, studios, and small laboratories. This all changed during the first industrial revolution (mid-18th century to mid-19th century). In this period, the iron-production process grew enormously after charcoal was replaced by cokes. The latter material was also used to fuel stoves and forges. Cokes is made in the coking process, in which coal is heated in the absence of oxygen. This process resulted in three main products, *i.e.* coke, coal tar, and coal gas. The latter was used to heat the furnace, but the coal tar was an unused waste product. Scientists currently know that coal tar, which has a high concentration of polycyclic aromatic hydrocarbons (PAHs), constitutes a great health risk. Although a feared substance in current society, scientists in the 19th century were trying to make something out of this waste.

August Wilhelm von Hoffman was one of these scientists. He discovered a way to convert benzene and xylene obtained from coal tar to their nitro and amine derivatives. The resulting product, aniline, was already known to man, but it was only prepared from the dye indigotin, which was retrieved from different types of indigo plants. Because aniline was known to be one of the building blocks of indigotin, it was then used as a starting material to produce more-useful products.

One of Von Hoffmans students, William Henry Perkin, was trying to synthesize quinine, which was used as a medicine to treat malaria. While these attempts failed, Perkin discovered a purple colorant, later identified as the first synthetic (*i.e.* man-made) organic dye. Although Perkin at 18-years old may have been just in the right place at the right time, he made

history with one of the great examples of serendipity in science by showing persistence after obtaining the disappointing result. He later perfected the synthesis route of mauveine to obtain a patent in 1856. He then decided to market his discovery, offering a cheaper and better alternative to the purple dyes extracted from natural sources, which were less bright than mauveine.

Within 5 years, 'mauve' was a fashion trend, both in France and in England, especially after its display at the 1862 International Exhibition. Perkin eventually made a fortune with its production and started the 'race on dyes'. Scientists tried to make other colorants from aniline, creating a new class of aniline-dyes, of which we can still see the influence in companies such as BASF (Badische Aniline- & Soda Fabrik) and Bayer. Some of the colorants discussed in this thesis, such as crystal violet and fuchsin, were synthesized shortly after the discovery of mauveine and are still used today in many fields.

Perkin's invention started a revolution in organic chemistry and started a whole new industry that produced a rainbow of colours, but also fertilizers, explosives, and plastics, and so on. Eventually, the lightfastness and the production-yield of mauveine were lower than that of newly produced colorants. As a result, the production of mauveine could not keep up with the demand. Later, it was also found to be carcinogenic, which makes another science-history story.

What I love about this story is that we, as chemists, often do not realize how variable our field is. Only in the 19th century, scientists started to mass produce chemicals and to slowly understand molecular structures. Many of the compounds we study contain more information than only their molecular structure or lightfastness. An example may be how these components were used and how they were synthesized. I believe it is important to know the history of our chemical world to put our research in a broader perspective. After all, without Perkin (and his supervisor!), mauveine would have been just a (group of) undiscovered molecules that faded when exposed to light.

CHAPTER 1

Introduction

1.1. Light and molecules

The world around us consists of atoms and molecules and our world is illuminated by the sun. Everything we see, we owe to light reflecting from objects. Light has a dual character, it can be treated as both wave and particle, *i.e.* photons (Greek: **φωτός**, photos = light), which interact with the atoms and molecules around us. Without these interactions the world as we know it would not exist.

The properties of light depend greatly on the energy of the photons, which corresponds to a specific wavelength. The sun, for example, emits a very broad spectrum of light, including ultraviolet light (UV, 100 to 400 nm), visible light (vis, 400 to 750 nm), and infrared light (IR, 750 nm to 1 mm) [1,2]. Shorter wavelengths include X-rays and gamma rays, while longer wavelengths include microwaves and radio waves. Shorter wavelengths correspond to higher-energy photons, which are more harmful to life on earth [3].

When photons collide with molecules reactions can take place, depending on the molecular structure and the energy of the photon. The surroundings of the molecule, called the matrix, may also play a role [4]. When a photon is absorbed by a molecule, indicated with the purple arrow in Fig. 1.1, the molecule enters a higher energy state, for example with excited electrons (indicated by *a*) [5,6]. A number of excited states exist, indicated by the dark blue lines in Fig. 1.1. Singlet or triplet states (S and T) can be distinguished. Each electronic state consists of a group of vibrational or rotational states, indicated by the light-blue lines. From an excited state, many processes can happen, such as internal conversion (*c*), vibrational relaxation (*R*), intersystem crossing (*d*), fluorescence (*b*), phosphorescence (*e*), or energy transfer to a different molecule. These processes were described by Jablonksi and Kasha and are depicted in Fig. 1.1 [6–8].

Some of these processes can lead to photochemical reactions. The absorbed energy can be used for reactions within the molecule, such as isomerization or disintegration, or for intermolecular reactions. For a photon to induce a chemical reaction, its energy must be sufficient to *i)* be absorbed and *ii)* be high enough to break chemical bonds. Breaking a bond formed by two electrons may result in the formation of reactive radicals [9]. Photochemical reactions can be divided into two types, *i.e.* direct or photosensitized reactions [7]. The former includes reactions such as ionization, isomerization, aggregation, radical dissociation, and degradation. Which of these reactions occur depends on the energy of the photon and the structure of the molecule. Photosensitized oxidation reactions need an auxiliary compound, a so-called photosensitizer, to absorb the light and to deliver the energy needed for the

reaction [10]. Without the photosensitizer the reaction would not occur. Photosensitized reactions include photolytic auto-oxidation and photo-isomerization. The most-common reaction around us is photo-oxidation. In this process a sensitizer absorbs the light and enters a triplet state through inter-system crossing. In this active state it can then either react with a substrate molecule in a radical reaction, followed by a reaction between the substrate and triplet oxygen (type I), or the sensitizer can react directly to oxygen, leading to a reaction between singlet oxygen and the substrate (type II), shown in Fig. 1.2. Both reactions result in an oxidized substrate. The type-I reaction rate depends on the type and concentrations of sensitizers and substrates, while the rate of the type-II reaction is dependent on the concentration of oxygen [7,10].

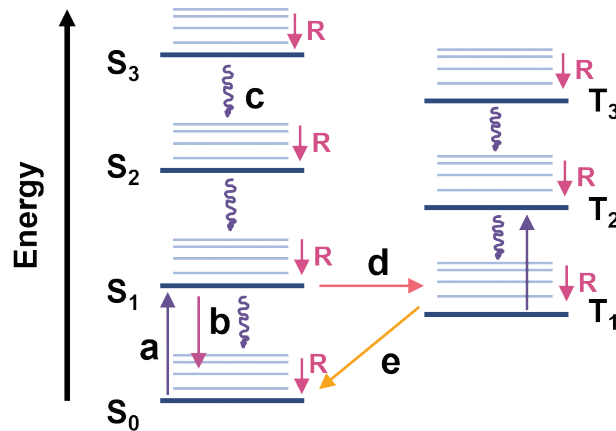


Figure 1.1. Jablonski Diagram. In the figure, the singlet states (left, S₀, S₁, S₂, S₃) and triplet states (right, T₁, T₂, T₃) are shown. Six processes are illustrated, viz. a) absorption, b) fluorescence, c) internal conversion, d) intersystem crossing, e) phosphorescence, and R) relaxation. This figure was reproduced from [6,8].

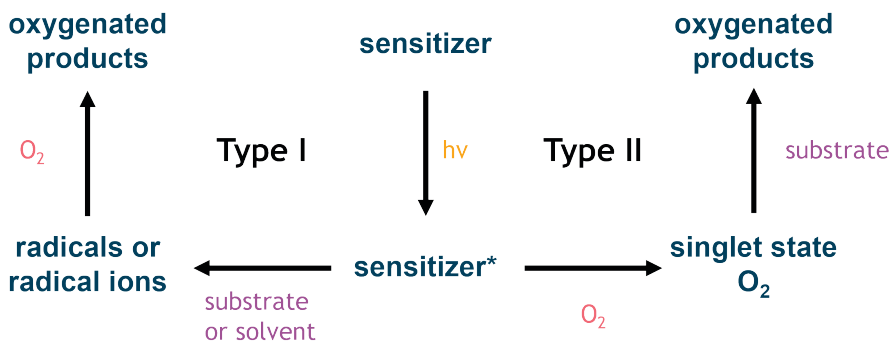


Figure 1.2. Schematic overview of type-I and type-II reaction mechanisms. This figure was reproduced from [11].

1.2. Photodegradation in our daily life

While the above reactions seem rather abstract, they occur in the world around us. This gives rise to challenges, such as those encountered in the cultural-heritage field. The rich history of the world can be retold to future generations together, alongside many objects, such as paintings, tapestries, furniture, or drawings depicting scenes or referring to cultural events. However, because colorants fade through photodegradation, these objects slowly lose their esthetical value which affects how we interpret these. One example to demonstrate photodegradation in cultural heritage is the *Bedroom* of Van Gogh. Three replicates exist of this painting, which have been stored under different conditions over time. Currently, the colours of these three paintings no longer look similar. Since Van Gogh wrote about his bedroom in many letters, we know that the colours he observed differ from the current colours [12,13]. Because of the different preservation and conservation histories of these three paintings they are currently all very different. Understanding photodegradation can result in a better understanding of how to conserve paintings, by altering windows, lamps, or illumination times to preserve them for future generations. In addition, the original appearance of faded artwork will be better known, which is of relevance for art historians, and, on several occasions, has led to digital reconstructions [14,15] or retouching with coloured light to disseminate this knowledge to the museum public [16].

Another field where the prevention of photodegradation can have a major impact is the food industry. Some products are highly susceptible to light and must be carefully packaged and stored. However, products that should be stored for long times, *i.e.* products with long shelf-lives, may receive a much higher dose of light when using transparent packaging [17,18]. In either case this can lead to loss of nutritional value by degradation of healthy food components (*e.g.* vitamins), to the loss of colour, or even to the formation of unwanted by-products [19–21]. Food samples are usually based on natural products and are highly complex. Many components, such as carotenoids or flavanols, are added because of both their antioxidative and colorant properties. When such compounds are present in foodstuff contained in transparent packaging, they absorb the radiation of light, causing them to degrade and to lose their nutritional value [22]. Ideal product packaging should be transparent to appeal to the consumer, have a low oxygen-transfer rate and a low moisture-vapor-transfer rate, and needs to be puncture resistant and freezer safe. For a material to fulfil (many of) these requirements, the food industry resorted to multi-layered plastics, which cannot be recycled. Since recycling or, preferably, circular processes are increasingly becoming the norm, new, better, and monolayered materials should be developed. Understanding photodegradation can lead to a major shift in the food industry towards recyclable packaging

materials, the light-blocking ability of which will need to be evaluated [1,23]. Improved knowledge will lead to better storage possibilities, increased shelf life, and healthier products.

One field where irradiation with UV light is advantageous is that of water purification. When water is disposed through the sewage system, it is processed in a waste-water treatment plant, before it enters the environment. Production of drinking water requires a purification plant, where the water is filtered and treated in several steps. One of these steps may be an advanced oxidation process (AOP). AOPs are a group of processes that use a combination of UV light and either ozone or hydrogen peroxide to lower the levels of possibly harmful substances in drinking water [24]. In such a process, radicals will be formed that react with the contaminants in the water. Alternatively, organic matter may undergo direct photolysis. AOPs, however, yield many different degradation products, producing complex mixtures, at very low concentrations [25,26]. Understanding AOPs better will contribute to the design of optimized facilities.

1.3. Photodegradation research

To conduct photodegradation research, dissolution and illumination of the compound of interest is often performed [27]. Since water research concerns samples in solution, much of these photodegradation studies are performed in such a fashion. The sample is often illuminated from the top with a collimated-beam setup [26,28]. Such a setup, however, has some problems, *viz.* *i)* manual sample handling is required for these experiments, leading to a high chance of errors, *ii)* the solvent can evaporate, leading to concentration differences in time series, *iii)* the sample is illuminated inefficiently, *iv)* large sample volumes are needed, and *v)* degradation experiments can be very lengthy [29,30].

However, sample degradation can be different when analytes are present in pure form or on a substrate. Because many samples in food science and all samples in cultural-heritage research are solid, degradation research performed in solution may not be representative. To circumvent this, the compounds can be degraded directly on their substrate, but this complicates the sample handling procedure due to the extraction step needed for analysis. Extraction is not only time consuming, it also carries risks of altering the components of interest or of selectively extracting certain compounds. In other words, not all degradation products are extracted to an equal extent and without modification. After the degradation and eventual extraction, samples may, for example, be analysed with liquid chromatography (LC) coupled to a diode-array detector (DAD) or a mass spectrometer (MS). Within cultural-heritage research photodegradation techniques are used, such as the Xenotest (XT) and the

Microfading Tester (MFT), that illuminate substrates, such as textile or a painting, directly. These techniques are mainly used to determine the light fastness of materials, and not aimed at elucidating the chemical processes of photodegradation [31–33]. In food science, so called light rooms are employed to accelerate studies into the shelf life of products [34,35] although not focussed on understanding the chemical degradation reactions.

The three types of samples described above, *i.e.* art, food, and water, all contain very diverse sets of different molecules, making them very complex. Studying photodegradation in such samples is nearly impossible with the techniques described above, because all compounds present in the sample will degrade simultaneously. One compound may degrade into several products, which can already be a challenge to investigate on its own [27]. Also, degradation products tend to be structurally similar to the main product. When studying a mixture it will be nearly impossible to determine which degradation products derive from which parent molecule, making it impossible to understand the photodegradation pathways. While some of these problems can be circumvented by performing photodegradation research on single compounds and analysing these samples with chromatography and spectroscopy, some problems still persist.

1.4. Toolbox for studying the Chemistry of Light-Induced Degradation

A novel methodology to conduct photodegradation research is needed that can apply both spectroscopy and chromatography for efficient characterisation of degradation products which can be used to understand degradation mechanisms. To investigate and develop these methods, the TooCOLD project was conceived (Toolbox for studying the Chemistry Of Light-induced Degradation). The TooCOLD project aimed at developing a light cell that can be implemented in a multi-dimensional-liquid-chromatography (mDLC) setup to study single compounds from complex samples. The goals were to speed up photodegradation research by more efficient illumination, to eliminate manual sample-handling and extraction procedures, and to make the light-exposure cell, now referred to as light cell, adjustable for specific applications. Within the TooCOLD project Groeneveld *et al.* developed a light cell based on a liquid-core-waveguide (LCW) principle [36]. This LCW cell comprises of an amorphous-Teflon (AF2400) tubing, which has a lower refractive index ($RI = 1.29$) than typical solvents [37]. When the LCW cell is filled, the light, focussed in the axial direction, is guided through the cell by total internal reflection, irradiating the sample inside. Because this cell is designed for liquid samples, it can directly be coupled to the exit (effluent) or entrance (injection) of an LC column.

1.5. Liquid chromatography

Because of its separation power, liquid chromatography (LC) will be an important technique to be implemented in the photodegradation setup [27,38,39]. In LC an analyte is distributed between a non-moving stationary phase and a moving mobile phase. How the analyte distributes itself between these two phases determines how long it will take to move through the column (t_R) and this is reflected in the retention factor (k). These two parameters are connected through the following formula

$$t_R = t_0(1 + k) \quad (1.1)$$

where t_0 is the column dead time. The retention factor is related to the distribution coefficient (K) through

$$k = \frac{q_s}{q_m} = \frac{c_s}{c_m} \frac{V_s}{V_m} = K \frac{V_s}{V_m} \quad (1.2)$$

In this formula q_m and q_s are the total mass of analyte in the mobile and the stationary phase, respectively, c_m and c_s are the analyte concentrations in the two phases and V_m and V_s are the total volumes of each phase in the column. K is the distribution coefficient in terms of concentrations. The retention factor is analyte specific and dependent on different factors, such as temperature, pH, and mobile phase composition (volume fraction of strong solvent, φ). In Eq. 1.1 these factors are supposed to be constant during the LC run (*i.e.* isocratic elution), but more often the organic-modifier concentration (φ) is increased over time (gradient elution). In isocratic mode, the longer is the retention time, the broader become the peaks. This implies that late-eluting compounds will be highly diluted and harder to detect. Moreover, the time required to elute all components from the column can be very long, especially if the polarities of the compounds in the mixture cover a broad range. Therefore, countless applications of LC use gradient elution. When φ is increased over time, k values are gradually reduced, leading to sharp peaks at the time of elution for all components in the mixture, even though these are very different. Gradient elution will be described in more detail elsewhere in this thesis.

There are various modes of LC that are employed, of which reversed-phase LC (RPLC) is the most popular technique. In RPLC the stationary phase is hydrophobic (low polarity) and the mobile phase is hydrophilic (high polarity) [40]. Over the course of the run, the mobile-phase polarity is decreased, by replacing the aqueous solution by solvents such as methanol (MeOH), acetonitrile (ACN), or tetrahydrofuran (THF). Varying stationary phases are available, such as silicas modified with long carbon chains (C8, C18), phenyl rings (phenyl, diphenyl), or cyano groups (CN), to achieve the best separation for a specific sample.

1.6. Multidimensional liquid chromatography

For complex samples, however, gradient elution is often not sufficient to achieve complete separation. A single dimension of LC can only separate a limited number of components which are represented as peaks in the chromatogram. This so-called peak capacity may amount to hundreds of peaks in theory, but is much lower in practice due to randomly distributed retention times of unrelated analytes [41,42]. A powerful solution for complex mixtures is provided by two-dimensional LC (2DLC) [43]. In 2DLC, fractions of the effluent of a first-dimension (1D) separation are collected in loops installed on a 10-port or 8-port valve. After the modulation time (t_{mod}), the valve is switched and the contents of the loop are injected onto the second-dimension (2D) separation. There are several ways to perform 2DLC, depending on the number of cuts taken from the 1D separation. When one or several cuts are transferred, (multiple) heart-cut two-dimensional LC (mHC-2DLC) is employed. In this method, the 2D separation time is not linked to the modulation time. If the entire effluent of the 1D separation is transferred to the 2D , we speak of comprehensive 2DLC (LC \times LC). In this situation, the 2D separation must be performed within the modulation time. We speak of selective LC \times LC (sLC \times LC) when the same terms apply, but only one or more series of fractions from the 1D separation are transferred to the 2D separation. A schematic overview of the different 2DLC modes is given in Fig. 1.3.

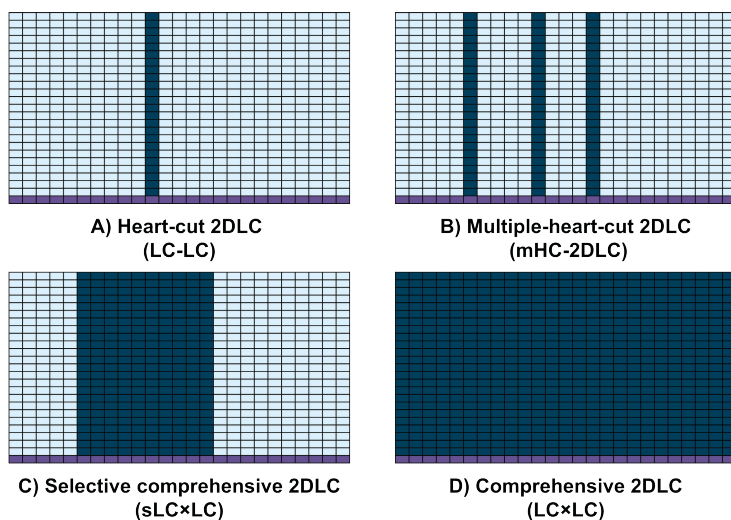


Figure 1.3. Different modes of 2DLC. A) heart-cut 2DLC (LC-LC), B) multiple-heart-cut 2DLC (mHC-2DLC), C) Selective comprehensive 2DLC, D) Comprehensive 2DLC (LC \times LC). The 1D separation is shown in purple, while the 2D separations are shown in dark blue. Absent modulations are shown in light blue, present in A-C. Figure adopted from [44][45].

The peak capacity in LC×LC is at least an order of magnitude higher than that of 1DLC and the times required for high-resolution separations are much shorter, but this increase in separation power can only be coined if the two separations are as different as possible. If the retention time in the second dimension (2t_R) is completely independent of that in the first dimension (1t_R) we speak of orthogonal separations and the entire separation space can be used [46,47]. The 1D and 2D separation modes can be chosen to match the dimensions of the sample, *i.e.* the ways in which sample components differ [48,49]. For example, in the case of a mixture of *n*-alkanes, the only dimension of the sample is the length of the alkane chain and the sample dimensionality is one. Such a sample would not be separated any better if it would be analysed with two-dimensional chromatography. However, if the sample were to also contain alcohols its dimensionality would be increased, which would make it amenable with a two-dimensional separation. If the two separation systems would be similar, *i.e.* not completely orthogonal, for example in the combination of RPLC with C18 and phenyl, it would lead to elution along the diagonal of the separation space [47,50]. If a sample is altered between its dimensions, for example when it undergoes a reaction or if it is dissolved in a different solvent changing its secondary structure, the concept of orthogonality suddenly changes. In this case, identical separation systems could be used to obtain information about the two states, making the method fully orthogonal.

With the increasing number of dimensions, method optimization becomes dramatically more complex. One way to make this process less time-consuming – and potentially automatic – is to use retention modelling, for example with semi-empirical retention models [51]. This thesis contains three chapters (Chapter 2-4) in which this type of retention modelling and the gradient-scanning methods that provide the required data are discussed in detail.

As described before, 2DLC can be performed by using loops. This is called passive modulation and it is the most-applied method to collect and transfer fractions, shown in Fig. 1.4A [45]. There are some disadvantages, however, associated with this straightforward approach. The volume in the loop becomes the injection volume for the 2D separation, potentially leading to band broadening and reduced sensitivity [45,52]. Also, passive modulation can lead to distorted peaks, peak splitting, or breakthrough phenomena when two separation modes are incompatible, for example hydrophilic interaction liquid chromatography (HILIC, requiring a high concentration of organic modifier) and RPLC (requiring significant concentrations of water to ensure retention of analytes at the start of the gradient).

Active modulation (AM) can help circumvent these problems [53–55]. In AM, the analytes in the effluent of the 1D column are concentrated prior to or during injection on the 2D column.

There are several types of AM techniques, which have been mainly developed in the last decade. The two most-used techniques are active-solvent modulation (ASM, Fig. 1.5) [53,56] and stationary-phase-assisted modulation (SPAM, Fig. 1.4B) [57–60], but there are some relatively new techniques as well, such as thermal modulation and cold trapping [61–67], evaporative membrane modulation [68], and vacuum evaporation [69,70].

In ASM, the sample is focused at the top of the ²D column after dilution of the loop volume, most conveniently by using a specially designed 10-port valve [53]. This process is displayed in Fig. 1.5. This valve allows the introduction of the (starting) ²D mobile phase at both the entrance and the exit of the loop, thereby allowing dilution of the sample solvent with a weak ²D eluent. The ratio between the two flows can be adjusted. In ASM, between 50% and 80% of the loop volume is the maximum volume of ¹D effluent per modulation, to ensure that all will be injected into the ²D separation [71,72]. This percentage depends on the analyte and the filling conditions used, which affect the Poiseuille-flow profile of the analyte band. Some efforts have been made to increase the maximum filling percentage by avoiding the Poiseuille-flow profile.

If separation modes and detectors are incompatible, for example, the salts used in ion-exchange chromatography (IEX) that cannot be introduced in the mass spectrometer, there is no possibility to eliminate the ¹D solvent [42,73,74]. Other methods exist to dilute the collected fraction before it enters the ²D column, such as at-column dilution (ACD), which are based on a similar principle [55]. In SPAM, the loops are replaced by short guard columns to trap the sample from the ¹D effluent onto a stationary phase. To ensure trapping of the analytes, the ¹D effluent is actively diluted with an isocratic pump before entering the trap column. From the trap column it is then quickly desorbed before injection onto the ²D column. In this method, the total injection volume entering the ²D column can be greatly reduced, although dilution may again be required if the desorption solvent is too strong a ²D eluent. Most importantly, SPAM allows for the ¹D effluent to be replaced by another solvent, which can be very beneficial in case of compatibility issues. There is a chance, however, that sample will be lost when analytes have insufficient retention on the trap columns. This issue will be addressed in detail in Chapter 4 of this thesis. Both these AM techniques have been increasingly applied in 2DLC in recent years [45].

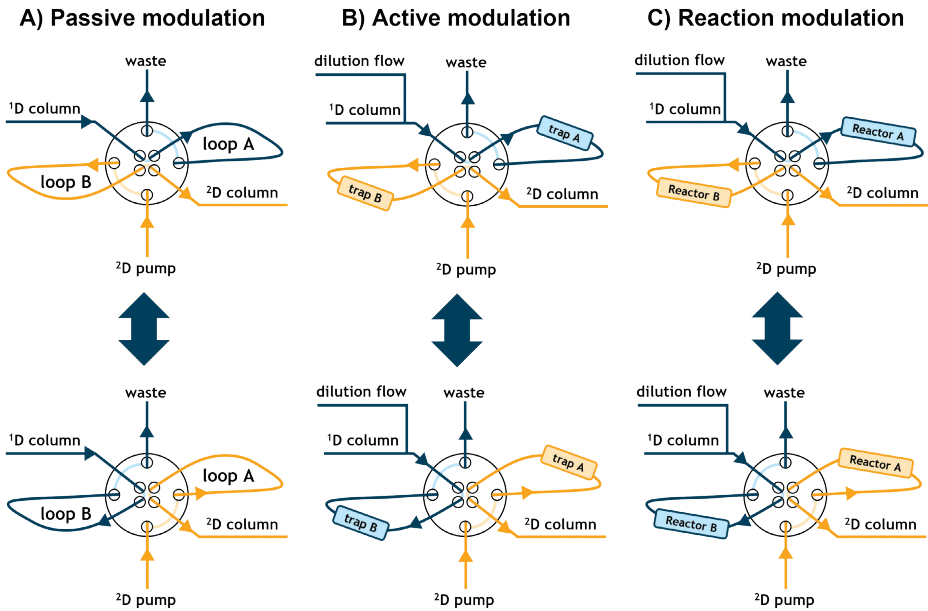


Figure 1.4. Schematic overview of A) passive modulation, B) stationary-phase-assisted modulation, a form of active modulation, and C) reaction modulation. The ^1D and ^2D flow path are indicated by blue and yellow, respectively. The dilution flow in both B and C is not essential for the technique. Figure adopted and extended from [45].

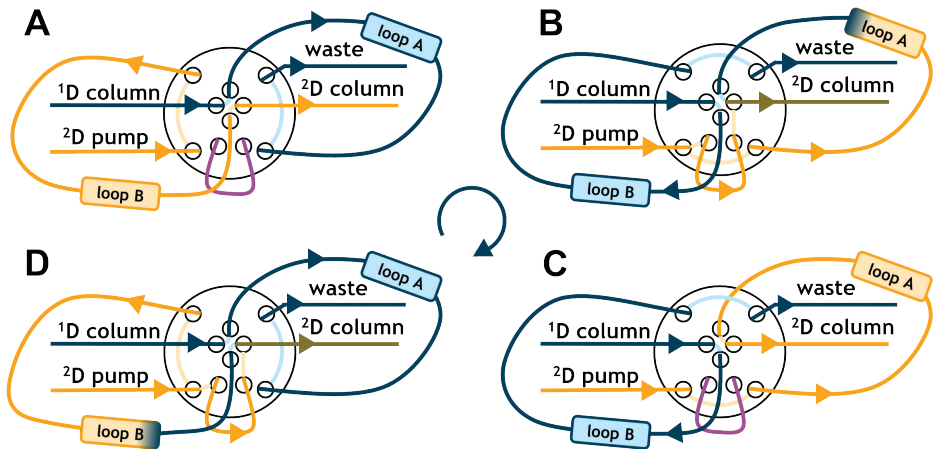


Figure 1.5. Schematic overview of an active-solvent modulation valve for coupling two separations in 2DLC. The ^1D and ^2D flow paths are depicted in blue and yellow, respectively. The non-active bypass is indicated in purple. In A and C, the setup is identical to the passive-modulation setup from Fig. 1.4. In B and D, the ^2D flow is split to elute the fraction from the loop and simultaneously dilute the fraction at the exiting flow from the loop through the bypass capillary.

A different family of analytical methods has emerged that is based on 2DLC instrumentation, but uses reaction modulation, shown in Fig. 1.4C. In this case, the fraction collected from the ^1D separation is actively transformed before entering a ^2D separation. Because the sample changes, there is no need for orthogonal separation in ^1D and ^2D systems. The orthogonality is no longer in the retention mechanisms, but in the sample. Our group has been trying to employ various forms of reaction modulation, for example with immobilized-enzyme reactors, protein digestion, or by breaking up nanoparticles [60,75–78]. Reaction modulation on a specific part of the separation by means of a mHC-2DLC setup can be seen as a form of online sample treatment. As described before, the performance parameters of 2DLC, such as total peak capacity and orthogonality, lose their meaning when reaction modulation is performed. The ^2D separation is not added to obtain more separation power or to add additional selectivity. Instead, it is used to separate a (completely) new sample. This means that even a ^2D separation that is identical to the ^1D separation suddenly becomes meaningful in 2DLC with reaction modulation. Using different separation mechanisms before and after the reaction may actually complicate the data analysis, as described in Chapter 6 of this thesis.

Reaction modulation may alleviate the previously described problems encountered in photodegradation research [43,74,75,77]. If a light cell were to be developed that could be implemented in a 2DLC system, the ^1D separation could function to separate the compound of interest from other sample components, after which the degradation could take place. The ^2D separation would then separate the compound of interest from its degradation products. It will then be easy to connect degradation products with parent compounds and this may lead to efficient photodegradation research.

1.7. Method optimization and retention modelling

To achieve the best possible separation in 1DLC various parameters need to be optimized, such as flow rate, gradient program, total analysis time, and modifier composition. Because these parameters can be interdependent and because peak cross-overs may lead to many local optima, it can be quite hard to find the optimal conditions using trial-and-error experiments. The available computer power has increased dramatically during the last 40 years, and this has led to the development of computerized method-optimization programs that rely on retention modelling [51,79,80]. In general, a retention model is a function that relates retention to analyte and system parameters. The complexity of an LC method increases enormously when extra dimensions are added, since not only another separation needs to be optimized. Additional factors need to be considered, such as the modulation time. The so-called sampling rate or number of “cuts” per peak is determined by the ^1D

separation and the modulation time. The latter parameter is usually identical to the ²D cycle time (time needed for analysis and reconditioning). The loop volume is usually fixed, with few options available, and impractical to change. It also cannot be optimized without considering the parameters of the ¹D separation and the modulation time.

When AM techniques are employed, this complexity is amplified further. Retention modelling is almost indispensable for method optimization in 2DLC, as is evident from the number of computerized methods published [45,58,80–84]. Because of the great number of parameters to optimize in 2DLC, the technique is mostly used in academia and hardly – if at all – applied in routine methods in industry. Retention modelling may accelerate the proliferation of 2DLC and associated modulation strategies.

Retention modelling and 2DLC can strengthen the entire field of chromatography to achieve better separations and yield more information on complex samples, but the question is how these techniques can also support photodegradation research.

First, liquid chromatography is an indispensable technique to separate photodegradation products from their parent compound or to isolate compounds from a mixture to study its photodegradation. 2DLC can yield more information by combining two different separation mechanisms [58] or by implementing photodegradation at the modulation stage, as a form of reaction modulation. Active-modulation strategies may be used to reduce dilution of the sample, either in a conventional 2DLC setup or after reaction modulation. These combinations of techniques, however, make the optimization even more challenging.

1.8. Scope of this thesis

Developments in online photodegradation in two-dimensional liquid chromatography (2DLC) are impractical if developments in method optimization of multi-dimensional liquid chromatography lag behind. For that reason, two research lines are described in this thesis. The first one consists of improvements made in retention modelling, research with a broad impact in 2DLC applications. The second part concerns the implementation of our new light cell in (multidimensional) liquid chromatography and its comparison to other techniques for photodegradation research.

Retention modelling

In Chapter 2 state-of-the-art methods for retention modelling with semi-empirical retention models are described and discussed. Recent improvements from the period 2015-2020 are

summarized and categorized based on the goal of the publication. Five distinct retention-modelling goals were identified.

Chapter 3 focusses on the experiments needed to perform retention modelling. These so-called scanning-gradient experiments had up to that point been applied in a rather random fashion, which was further investigated. The aims of this chapter were to present a clear protocol to arrive at the optimal set of scanning-gradient experiments and to find the best retention model based on two different experimental data sets.

While Chapter 3 focusses solely on one-dimensional liquid chromatography (1DLC) methods, Chapter 4 focusses on the application of stationary-phase assisted modulation (SPAM). In this chapter, a tool is presented to facilitate method optimization of SPAM in 2DLC. To support this tool, system parameters, method parameters and analyte parameters were examined to optimize retention prediction on SPAM columns.

Photodegradation research

The liquid-core-waveguide (LCW) cell was developed within the TooCOLD (Toolbox for studying the Chemistry Of Light-induced Degradation) project as a tool to study photodegradation. Chapter 5 focusses on the difference and similarities between photodegradation in this cell and other, more established photodegradation techniques within cultural-heritage research. Degradations were performed both in solution and on textile.

Chapter 6 describes the research performed implementing the photoreactor in multidimensional liquid chromatography. In this work, the light cell was installed within a multiple-heart-cut 2DLC method. This facilitated the degradation of single compounds from a mixture and the subsequent analysis of the degradation products.

Since the work described in Chapter 6 concerned a rather complex setup with some limitations, Chapter 7 encompasses the work performed to reduce this complexity and resolve those limitations. By reducing the number of modules in the 2DLC setup, we aim to achieve more information about degradation pathways.

Chapter 8 consists of the work to develop another light cell, which can be implemented in comprehensive 2DLC (LC×LC). Next to that it includes some future perspectives about the world of reaction-modulation 2DLC, retention modelling and 2DLC, and the future of photodegradation. It will create the link between the first and the second part of the thesis.

References

- [1] Krehula LK, Papić A, Krehula S, Gilja V, Foglar L, Hrnjak-Murgić Z. Properties of UV protective films of poly(vinyl-chloride)/TiO₂ nanocomposites for food packaging. *Polym Bull* 2017;74:1387–404. <https://doi.org/10.1007/S00289-016-1782-4/FIGURES/11>.
- [2] Duncan SE, Chang HH. Implications of Light Energy on Food Quality and Packaging Selection. *Adv. Food Nutr. Res.*, vol. 67, Academic Press Inc.; 2012, p. 25–73. <https://doi.org/10.1016/B978-0-12-394598-3.00002-2>.
- [3] Butcher G. *Tour of the Electromagnetic Spectrum*. 3rd ed. National Aeronautics and Space Administration.; 2016.
- [4] Murov SL, Carmichael I, Hug GL. *Handbook of Photochemistry*, Second Edition. 1993.
- [5] Kang D, Zhu S, Liu D, Cao S, Sun M. One- and Two-Photon Absorption: Physical Principle and Applications. *Chem Rec* 2020;20:894–911. <https://doi.org/10.1002/TCR.202000038>.
- [6] Jabłoński A. Efficiency of Anti-Stokes Fluorescence in Dyes. *Nat* 1933 1313319 1933;131:839–40. <https://doi.org/10.1038/131839b0>.
- [7] Min DB, Boff JM. Chemistry and Reaction of Singlet Oxygen in Foods. *Compr Rev Food Sci Food Saf* 2002;1:58–72. <https://doi.org/10.1111/J.1541-4337.2002.TB00007.X>.
- [8] Lewis GN, Kasha Vol M, Gilbert Lewis BN, Kasha M. Phosphorescence and the Triplet State 1938;71:191.
- [9] Koutchma T, Orłowska M, Zhu Y. Fruits and Fruit Products Treated by UV Light. *Food Eng Ser* 2018:457–504. https://doi.org/10.1007/978-1-4939-3311-2_17.
- [10] Baptista MS, Cadet J, Di Mascio P, Ghogare AA, Greer A, Hamblin MR, et al. Type I and Type II Photosensitized Oxidation Reactions: Guidelines and Mechanistic Pathways. *Photochem Photobiol* 2017;93:912–9. <https://doi.org/10.1111/PHP.12716>.
- [11] Sharman WM, Allen CM, Van Lier JE. [35] Role of activated oxygen species in photodynamic therapy. *Methods Enzymol* 2000;319:376–400. [https://doi.org/10.1016/S0076-6879\(00\)19037-8](https://doi.org/10.1016/S0076-6879(00)19037-8).
- [12] Hendriks E, Leo Jansen, Johanna Salvant, Élisabeth Ravaud, Myriam Eveno, Michel Menu, et al. A comparative study of Vincent van Gogh's Bedroom Series. *Stud Old Master Paint Technol Pract Natl Gall Tech Bull 30th Anniv Conf Post Prints, Archetype* 2011:237–43.
- [13] Vincent van Gogh: The Paintings (Vincent's Bedroom in Arles) n.d. http://www.vggallery.com/painting/p_0482.htm (accessed June 16, 2022).
- [14] Menu M, Salvant J, Ravaud EH, Hendriks E, Jansen L, Ravaud É, et al. A comparative study of Vincent van Gogh's Bedroom series A comparative study of Vincent van Gogh's Bedroom series n.d.
- [15] Original colours of Van Gogh's paintings Research project REVIGO n.d.
- [16] Van Bommel MR, Van Adrichem FB, Boonstra JJ. *Bringing Back Color: Retouching Faded Furniture With Colored Light*. AIC Wooden Artifacts Gr Postprints, Houston, Texas, 2018 2018.
- [17] Bosset JO, Gallmann PU, Sieber R. Influence of light transmittance of packaging materials on the shelf-life of milk and dairy products — a review. *Food Packag Preserv* 1994:222–68. https://doi.org/10.1007/978-1-4615-2173-0_13.
- [18] Manzocco L, Kravina G, Calligaris S, Nicoli MC. Shelf Life Modeling of Photosensitive Food: The Case of Colored Beverages. *J Agric Food Chem* 2008;56:5158–64. <https://doi.org/10.1021/JF800072U>.
- [19] Patras A, Julakanti S, Yannam S, Bansode RR, Burns M, Vergne MJ. Effect of UV irradiation on aflatoxin reduction: a cytotoxicity evaluation study using human hepatoma cell line. *Mycotoxin Res* 2017;33:343–50. <https://doi.org/10.1007/S12550-017-0291-0/FIGURES/6>.
- [20] Mao J, He B, Zhang L, Li P, Zhang Q, Ding X, et al. A Structure Identification and Toxicity Assessment of the Degradation Products of Aflatoxin B1 in Peanut Oil under UV Irradiation. *Toxins* 2016, Vol 8, Page 332 2016;8:332. <https://doi.org/10.3390/TOXINS8110332>.

- [21] Chandra S, Patras A, Pokharel B, Bansode RR, Begum A, Sasges M. Patulin degradation and cytotoxicity evaluation of UV irradiated apple juice using human peripheral blood mononuclear cells. *J Food Process Eng* 2017;40:e12586. <https://doi.org/10.1111/JFPE.12586>.
- [22] Verduin J, Den Uijl MJ, Peters RJ, Van Bommel MR. Photodegradation Products and their Analysis in Food. *J Food Sci Nutr* 2020;6. <https://doi.org/10.24966/FSN-1076/100067>.
- [23] Han JH. New technologies in food packaging: Overview. *Innov Food Packag* 2005;3–11. <https://doi.org/10.1016/B978-012311632-1/50033-4>.
- [24] Oturan MA, Aaron J-J, Oturan MA, Aaron J-J. Advanced Oxidation Processes in Water/Wastewater Treatment: Principles and Applications. A Review. <https://doi.org/10.1080/106433892013829765>. <https://doi.org/10.1080/10643389.2013.829765>.
- [25] Brunner AM, Bertelkamp C, Dingemans MML, Kolkman A, Wols B, Harmsen D, et al. Integration of target analyses, non-target screening and effect-based monitoring to assess OMP related water quality changes in drinking water treatment. *Sci Total Environ* 2020;705:135779. <https://doi.org/10.1016/J.SCITOTENV.2019.135779>.
- [26] Kolkman A, Martijn BJ, Vughs D, Baken KA, van Wezel AP. Tracing Nitrogenous Disinfection Byproducts after Medium Pressure UV Water Treatment by Stable Isotope Labeling and High Resolution Mass Spectrometry. *Environ Sci Technol* 2015;49:4458–65. <https://doi.org/10.1021/es506063h>.
- [27] Confortin D, Neevel H, Brustolon M, Franco L, Kettelarij AJ, Williams RM, et al. Crystal violet: Study of the photo-fading of an early synthetic dye in aqueous solution and on paper with HPLC-PDA, LC-MS and FORS. *J. Phys. Conf. Ser.*, vol. 231, Institute of Physics Publishing; 2010, p. 012011. <https://doi.org/10.1088/1742-6596/231/1/012011>.
- [28] Kuo J, Chen C, Nellor M. Standardized Collimated Beam Testing Protocol for Water/Wastewater Ultraviolet Disinfection. *J Environ Eng* 2003;129:774–9. [https://doi.org/10.1061/\(ASCE\)0733-9372\(2003\)129:8\(774\)](https://doi.org/10.1061/(ASCE)0733-9372(2003)129:8(774)).
- [29] den Uijl MJ, Lokker A, van Dooren B, Schoenmakers PJ, Pirok BWJ, van Bommel MR. Comparing different light-degradation approaches for the degradation of crystal violet and eosin Y. *Dye Pigment* 2022;197:109882. <https://doi.org/10.1016/J.DYEPIG.2021.109882>.
- [30] Confortin D, Neevel H, van Bommel MR, Reissland B. Study of the degradation of an early synthetic dye (crystal violet) on cotton linters, lignin and printing paper by the action of UV-Vis and Vis light and evaluation of the effect of gum arabic on degradation products and on colour change. *Creat 2010 Conf Proc - 'Colour Coded'* 2010;81–5.
- [31] Friele LFC. A Comparative Study of Natural and Xenotest Exposure Condition: for Measuring Fading and Degradation. *J Soc Dye Colour* 2008;79:623–31. <https://doi.org/10.1111/j.1478-4408.1963.tb02522.x>.
- [32] Whitmore PM, Bailie C, Connors SA. Micro-fading tests to predict the result of exhibition: progress and prospects. *Stud Conserv* 2000;45:200–5. <https://doi.org/10.1179/sic.2000.45.supplement-1.200>.
- [33] Whitmore PM, Pan X, Bailie C. Predicting the fading of objects: Identification of fugitive colorants through direct nondestructive lightfastness measurements. *J Am Inst Conserv* 1999;38:395–409. <https://doi.org/10.1179/019713699806113420>.
- [34] Martínez ML, Penci MC, Ixtaina V, Ribotta PD, Maestri D. Effect of natural and synthetic antioxidants on the oxidative stability of walnut oil under different storage conditions. *LWT - Food Sci Technol* 2013;51:44–50. <https://doi.org/10.1016/J.LWT.2012.10.021>.
- [35] Verardo V, Ferioli F, Riciputi Y, Iafelice G, Marconi E, Caboni MF. Evaluation of lipid oxidation in spaghetti pasta enriched with long chain n-3 polyunsaturated fatty acids under different storage conditions. *Food Chem* 2009;114:472–7. <https://doi.org/10.1016/J.FOODCHEM.2008.09.074>.
- [36] Groeneveld I, Schoemaker SE, Somsen GW, Ariese F, van Bommel MR. Characterization of a liquid-core waveguide cell for studying the chemistry of light-induced degradation. *Analyst* 2021. <https://doi.org/10.1039/D1AN00272D>.

- [37] Dijkstra RJ, Bader AN, Hoornweg GP, Brinkman UAT, Gooijer C. On-line coupling of column liquid chromatography and Raman spectroscopy using a liquid core waveguide. *Anal Chem* 1999;71:4575–9. <https://doi.org/10.1021/ac9902648>.
- [38] Andrisano V, Gotti R, Leoni A, Cavrini V. Photodegradation studies on Atenolol by liquid chromatography. *J Pharm Biomed Anal* 1999;21:851–7. [https://doi.org/10.1016/S0731-7085\(99\)00223-X](https://doi.org/10.1016/S0731-7085(99)00223-X).
- [39] Detomaso A, Mascolo G, Lopez A. Characterization of carbofuran photodegradation by-products by liquid chromatography/hybrid quadrupole time-of-flight mass spectrometry. *Rapid Commun Mass Spectrom* 2005;19:2193–202. <https://doi.org/10.1002/RCM.2036>.
- [40] Snyder LR, Dolan JW, Gant JR. Gradient elution in high-performance liquid chromatography. I. Theoretical basis for reversed-phase systems. *J Chromatogr A* 1979;165:3–30. [https://doi.org/10.1016/S0021-9673\(00\)85726-X](https://doi.org/10.1016/S0021-9673(00)85726-X).
- [41] Davis JM, Stoll DR. Likelihood of total resolution in liquid chromatography: Evaluation of one-dimensional, comprehensive two-dimensional, and selective comprehensive two-dimensional liquid chromatography. *J Chromatogr A* 2014;1360:128–42. <https://doi.org/10.1016/J.CHROMA.2014.07.066>.
- [42] Pirok BWJ, Gargano AFG, Schoenmakers PJ. Optimizing separations in online comprehensive two-dimensional liquid chromatography. *J Sep Sci* 2018;41:68–98. <https://doi.org/10.1002/jssc.201700863>.
- [43] Pirok BWJ, Stoll DR, Schoenmakers PJ. Recent Developments in Two-Dimensional Liquid Chromatography: Fundamental Improvements for Practical Applications. *Anal Chem* 2018;91:240–63. <https://doi.org/10.1021/ACS.ANALCHEM.8B04841>.
- [44] Stoll DR, Carr PW. Two-Dimensional Liquid Chromatography: A State of the Art Tutorial. *Anal Chem* 2016;89:519–31. <https://doi.org/10.1021/ACS.ANALCHEM.6B03506>.
- [45] Pirok BWJ, Stoll DR, Schoenmakers PJ. Recent Developments in Two-Dimensional Liquid Chromatography: Fundamental Improvements for Practical Applications. *Anal Chem* 2019;91:240–63. <https://doi.org/10.1021/acs.analchem.8b04841>.
- [46] Gilar M, Olivova P, Daly AE, Gebler JC. Orthogonality of Separation in Two-Dimensional Liquid Chromatography. *Anal Chem* 2005;77:6426–34. <https://doi.org/10.1021/AC0509231>.
- [47] Schure MR, Davis JM. Orthogonal separations: Comparison of orthogonality metrics by statistical analysis. *J Chromatogr A* 2015;1414:60–76. <https://doi.org/10.1016/J.CHROMA.2015.08.029>.
- [48] Giddings JC. Sample dimensionality: A predictor of order-disorder in component peak distribution in multidimensional separation. *J Chromatogr A* 1995;703:3–15. [https://doi.org/10.1016/0021-9673\(95\)00249-M](https://doi.org/10.1016/0021-9673(95)00249-M).
- [49] Schure MR. The dimensionality of chromatographic separations. *J Chromatogr A* 2011;1218:293–302. <https://doi.org/10.1016/J.CHROMA.2010.11.016>.
- [50] Camenzuli M, Schoenmakers PJ. A new measure of orthogonality for multi-dimensional chromatography. *Anal Chim Acta* 2014;838:93–101. <https://doi.org/10.1016/J.ACA.2014.05.048>.
- [51] Pirok BWJ, Pous-Torres S, Ortiz-Bolsico C, Vivó-Truyols G, Schoenmakers PJ. Program for the interpretive optimization of two-dimensional resolution. *J Chromatogr A* 2016;1450:29–37. <https://doi.org/10.1016/j.chroma.2016.04.061>.
- [52] Chapel S, Rouvière F, Peppermans V, Desmet G, Heinisch S. A comprehensive study on the phenomenon of total breakthrough in liquid chromatography. *J Chromatogr A* 2021;1653:462399. <https://doi.org/10.1016/J.CHROMA.2021.462399>.
- [53] Stoll DR, Shoykhet K, Petersson P, Buckenmaier S. Active Solvent Modulation: A Valve-Based Approach To Improve Separation Compatibility in Two-Dimensional Liquid Chromatography. *Anal Chem* 2017;89:9260–7. <https://doi.org/10.1021/ACS.ANALCHEM.7B02046>.
- [54] Gargano AFG, Duffin M, Navarro P, Schoenmakers PJ. Reducing Dilution and Analysis Time in Online Comprehensive Two-Dimensional Liquid Chromatography by Active Modulation. *Anal Chem* 2016;88:1785–93. https://doi.org/10.1021/ACS.ANALCHEM.5B04051/SUPPL_FILE/AC5B04051_SI_001.PDF.

- [55] Chen Y, Li J, Schmitz OJ. Development of an At-Column Dilution Modulator for Flexible and Precise Control of Dilution Factors to Overcome Mobile Phase Incompatibility in Comprehensive Two-Dimensional Liquid Chromatography. *Anal Chem* 2019;91:10251–7. https://doi.org/10.1021/ACS.ANALCHEM.9B02391/SUPPL_FILE/AC9B02391_SI_001.PDF.
- [56] Stoll DR, Lhotka HR, Harmes DC, Madigan B, Hsiao JJ, Staples GO. High resolution two-dimensional liquid chromatography coupled with mass spectrometry for robust and sensitive characterization of therapeutic antibodies at the peptide level. *J Chromatogr B Anal Technol Biomed Life Sci* 2019;1134–1135. <https://doi.org/10.1016/j.jchromb.2019.121832>.
- [57] Sun M, Sandahl M, Turner C. Comprehensive on-line two-dimensional liquid chromatography × supercritical fluid chromatography with trapping column-assisted modulation for depolymerised lignin analysis. *J Chromatogr A* 2018;1541:21–30. <https://doi.org/10.1016/J.CHROMA.2018.02.008>.
- [58] Pirok BWJ, Den Uijl MJ, Moro G, Berbers SVJ, Croes CJM, Van Bommel MR, et al. Characterization of Dye Extracts from Historical Cultural-Heritage Objects Using State-of-the-Art Comprehensive Two-Dimensional Liquid Chromatography and Mass Spectrometry with Active Modulation and Optimized Shifting Gradients. *Anal Chem* 2019. <https://doi.org/10.1021/acs.analchem.8b05469>.
- [59] Vonk RJ, Gargano AFG, Davydova E, Dekker HL, Eeltink S, Koning LJ de, et al. Comprehensive Two-Dimensional Liquid Chromatography with Stationary-Phase-Assisted Modulation Coupled to High-Resolution Mass Spectrometry Applied to Proteome Analysis of *Saccharomyces cerevisiae*. *Anal Chem* 2015;87:5387–94. <https://doi.org/10.1021/ACS.ANALCHEM.5B00708>.
- [60] Pirok BWJ, Abdulhussain N, Brooijmans T, Nabuurs T, de Bont J, Schellekens MAJ, et al. Analysis of charged acrylic particles by on-line comprehensive two-dimensional liquid chromatography and automated data-processing. *Anal Chim Acta* 2019;1054:184–92. <https://doi.org/10.1016/J.ACA.2018.12.059>.
- [61] Groskreutz SR, Weber SG. Temperature-assisted solute focusing with sequential trap/release zones in isocratic and gradient capillary liquid chromatography: Simulation and experiment. *J Chromatogr A* 2016;1474:95–108. <https://doi.org/10.1016/j.chroma.2016.10.062>.
- [62] Creese ME, Creese MJ, Foley JP, Cortes HJ, Hilder EF, Shellie RA, et al. Longitudinal On-Column Thermal Modulation for Comprehensive Two-Dimensional Liquid Chromatography. *Anal Chem* 2016;89:1123–30. <https://doi.org/10.1021/ACS.ANALCHEM.6B03279>.
- [63] Groskreutz SR, Horner AR, Weber SG. Temperature-based on-column solute focusing in capillary liquid chromatography reduces peak broadening from pre-column dispersion and volume overload when used alone or with solvent-based focusing. *J Chromatogr A* 2015;1405:133–9. <https://doi.org/10.1016/J.CHROMA.2015.05.071>.
- [64] Van de Ven HC, Gargano AFG, Van der Wal SJ, Schoenmakers PJ. Switching solvent and enhancing analyte concentrations in small effluent fractions using in-column focusing. *J Chromatogr A* 2016;1427:90–5. <https://doi.org/10.1016/J.CHROMA.2015.11.082>.
- [65] Niezen LE, Staal BBP, Lang C, Pirok BWJ, Schoenmakers PJ. Thermal Modulation To Enhance Two-Dimensional Liquid Chromatography Separations of Polymers. *J Chromatogr A* 2021;1653:462429. <https://doi.org/10.1016/J.CHROMA.2021.462429>.
- [66] Verstraeten M, Pursch M, Eckerle P, Luong J, Desmet G. Thermal modulation for multidimensional liquid chromatography separations using low-thermal-mass liquid chromatography (LC). *Anal Chem* 2011;83:7053–60. https://doi.org/10.1021/AC201207T/ASSET/IMAGES/LARGE/AC-2011-01207T_0005.JPG.
- [67] Verstraeten M, Pursch M, Eckerle P, Luong J, Desmet G. Modelling the thermal behaviour of the Low-Thermal Mass Liquid Chromatography system. *J Chromatogr A* 2011;1218:2252–63. <https://doi.org/10.1016/J.CHROMA.2011.02.023>.
- [68] Fornells E, Barnett B, Bailey M, Hilder EF, Shellie RA, Breadmore MC. Evaporative membrane modulation for comprehensive two-dimensional liquid chromatography. *Anal Chim Acta* 2018;1000:303–9. <https://doi.org/10.1016/J.ACA.2017.11.053>.
- [69] Tian H, Xu J, Guan Y. Comprehensive two-dimensional liquid chromatography (NPLC×RPLC) with vacuum-evaporation interface. *J Sep Sci* 2008;31:1677–85. <https://doi.org/10.1002/JSSC.200700559>.

- [70] Tian H, Xu J, Xu Y, Guan Y. Multidimensional liquid chromatography system with an innovative solvent evaporation interface. *J Chromatogr A* 2006;1137:42–8. <https://doi.org/10.1016/J.CHROMA.2006.10.005>.
- [71] Moussa A, Lauer T, Stoll D, Desmet G, Broeckhoven K. Numerical and experimental investigation of analyte breakthrough from sampling loops used for multi-dimensional liquid chromatography. *J Chromatogr A* 2020;1626:461283. <https://doi.org/10.1016/j.chroma.2020.461283>.
- [72] Moussa A, Lauer T, Stoll D, Desmet G, Broeckhoven K. Modelling of analyte profiles and band broadening generated by interface loops used in multi-dimensional liquid chromatography. *J Chromatogr A* 2021;1659:462578. <https://doi.org/10.1016/J.CHROMA.2021.462578>.
- [73] Luo H, Zhong W, Yang J, Zhuang P, Meng F, Caldwell J, et al. 2D-LC as an on-line desalting tool allowing peptide identification directly from MS unfriendly HPLC methods. *J Pharm Biomed Anal* 2017;137:139–45. <https://doi.org/10.1016/J.JPBA.2016.11.012>.
- [74] Groeneveld G, Pirok BWJ, Schoenmakers PJ. Perspectives on the future of multi-dimensional platforms. *Faraday Discuss* 2019;218:72–100. <https://doi.org/10.1039/C8FD00233A>.
- [75] Wouters B, Pirok BWJ, Soulis D, Garmendia Perticarini RC, Fokker S, van den Hurk RS, et al. On-line microfluidic immobilized-enzyme reactors: A new tool for characterizing synthetic polymers. *Anal Chim Acta* 2019;1053:62–9. <https://doi.org/10.1016/J.ACA.2018.12.002>.
- [76] Wouters B, Currivan SA, Abdulhussain N, Hankemeier T, Schoenmakers PJ. Immobilized-enzyme reactors integrated into analytical platforms: Recent advances and challenges. *TrAC Trends Anal Chem* 2021;144:116419. <https://doi.org/10.1016/J.TRAC.2021.116419>.
- [77] Pirok BWJ, Abdulhussain N, Aalbers T, Wouters B, Peters RAH, Schoenmakers PJ. Nanoparticle Analysis by Online Comprehensive Two-Dimensional Liquid Chromatography combining Hydrodynamic Chromatography and Size-Exclusion Chromatography with Intermediate Sample Transformation. *Anal Chem* 2017;89:9167–74. <https://doi.org/10.1021/ACS.ANALCHEM.7B01906>.
- [78] Camperi J, Goyon A, Guillaume D, Zhang K, Stella C. Multi-dimensional LC-MS: the next generation characterization of antibody-based therapeutics by unified online bottom-up, middle-up and intact approaches. *Analyst* 2021;146:747–69. <https://doi.org/10.1039/D0AN01963A>.
- [79] Molnar I. Computerized design of separation strategies by reversed-phase liquid chromatography: Development of DryLab software. *J Chromatogr A* 2002;965:175–94. [https://doi.org/10.1016/S0021-9673\(02\)00731-8](https://doi.org/10.1016/S0021-9673(02)00731-8).
- [80] Sarrut M, D'Attoma A, Heinisch S. Optimization of conditions in on-line comprehensive two-dimensional reversed phase liquid chromatography: Experimental comparison with one-dimensional reversed phase liquid chromatography for the separation of peptides. *J Chromatogr A* 2015;1421:48–59. <https://doi.org/10.1016/j.chroma.2015.08.052>.
- [81] van Schaick G, Pirok BWJ, Haselberg R, Somsen GW, Gargano AFG. Computer-aided gradient optimization of hydrophilic interaction liquid chromatographic separations of intact proteins and protein glycoforms. *J Chromatogr A* 2019;1598:67–76. <https://doi.org/10.1016/j.chroma.2019.03.038>.
- [82] Bernardin M, Masle A Le, Bessueille-Barbier F, Lienemann CP, Heinisch S. Comprehensive two-dimensional liquid chromatography with inductively coupled plasma mass spectrometry detection for the characterization of sulfur, vanadium and nickel compounds in petroleum products. *J Chromatogr A* 2020;1611. <https://doi.org/10.1016/j.chroma.2019.460605>.
- [83] Iguiniz M, Heinisch S. Two-dimensional liquid chromatography in pharmaceutical analysis. Instrumental aspects, trends and applications. *J Pharm Biomed Anal* 2017;145:482–503. <https://doi.org/10.1016/J.JPBA.2017.07.009>.
- [84] Muller M, Tredoux AGJ, de Villiers A. Predictive kinetic optimisation of hydrophilic interaction chromatography × reversed phase liquid chromatography separations: Experimental verification and application to phenolic analysis. *J Chromatogr A* 2018;1571:107–20. <https://doi.org/10.1016/j.chroma.2018.08.004>.

PART II

Retention modelling

CHAPTER 2

Applications of Retention Modelling

2. Recent applications of retention modelling in liquid chromatography

Abstract

Recent applications of retention modelling in liquid chromatography (2015-2020) are comprehensively reviewed. The fundamentals of the field, which date back much longer, are summarized. Retention modelling is used in retention-mechanism studies, for determining physical parameters, such as lipophilicity, and for various more-practical purposes, including method development and optimization, method transfer, and stationary-phase characterization and comparison. The review focusses on the effects of mobile-phase composition on retention, but other variables and novel models to describe their effects are also considered. The five most-common models are addressed in detail, *i.e.* the log-linear (linear-solvent-strength) model, the quadratic model, the log-log (adsorption) model, the mixed-mode model and the Neue-Kuss model. Isocratic and gradient-elution methods are considered for determining model parameters and the evaluation and validation of fitted models is discussed. Strategies in which retention models are applied for developing and optimizing one- and two-dimensional liquid chromatographic separations are discussed. The review culminates in some overall conclusions and several concrete recommendations.

Publication

Recent applications of retention modelling in liquid chromatography

Mimi J. den Uijl, Peter J. Schoenmakers, Bob W.J. Pirok, and Maarten R. van Bommel

J. Sep. Sci., **2021**, *44*, 88–114, DOI: 10.1002/jssc.202000905

2.1. Introduction

Liquid chromatography (LC) is one of the most essential and pervasive techniques in the toolbox of analytical chemists. Retention modelling serves as a useful technique available for analytical chemists to rapidly develop methods. In LC, an analyte is distributed between a non-moving stationary phase and a moving mobile phase. The time it takes for the analyte to migrate through the column is referred to as the retention time, t_R , which can be expressed as

$$t_R = t_0(1 + k) \quad (2.1)$$

where t_0 is the dead time or hold-up time of the column and k is the analyte retention factor, which is related to the distribution coefficient (K) through

$$k = \frac{q_s}{q_m} = \frac{c_s}{c_m} \frac{V_s}{V_m} = K \frac{V_s}{V_m} \quad (2.2)$$

where q_m and q_s are the total mass of analyte in the mobile and the stationary phase, respectively, c_m and c_s are the analyte concentrations in the two phases and V_m and V_s are the total volumes of each phase in the column. The retention factor is dependent on many different parameters, such as pH, temperature, and mobile-phase composition (volume fractions of strong solvent, φ). Many equations have been described to relate k to one or more of these parameters and are typically referred to as retention models. Retention modelling is the process of fitting such a model to the experimental data.

LC can be performed in isocratic or gradient mode. In isocratic mode, the mobile-phase composition is not changed over the course of the run, which means that the total mass of analyte in both phases does not change, with the result of a constant retention factor. This is not the case in gradient mode, where the mobile-phase strength is increased over the run. This increases the total mass of analyte in the mobile phase and thus decreases the retention factor. To relate k to the solvent strength in gradient elution, the gradient equation has to be used. When a compound elutes before the start of the gradient, the retention time can be calculated through Eq. 2.1, in which the k is the retention factor at the initial organic-modifier concentration. If a compound elutes during the gradient, the retention time can be calculated with the general equation of linear gradients [1].

$$\frac{1}{B} \int_{\varphi_{init}}^{\varphi_{init} + B(t_R - \tau)} \frac{d\varphi}{k(\varphi)} = t_0 - \frac{t_{init} + t_D}{k_{init}} \quad (2.3)$$

In this equation $k(\varphi)$ is the retention model (see Section 2.2.1), describing the relationship between the retention (k) and the organic modifier concentration (φ). The change in φ as a function of time (*i.e.* the slope of the gradient) is shown with B ($\varphi = \varphi_{\text{init}} + Bt$) and τ is the sum of the dwell time (t_D), the time before the start of the gradient (t_{init}) and the dead time (t_0). In the case that the analyte elutes after the gradient, the retention time can be calculated by

$$\frac{1}{B} \int_{\varphi_{\text{init}}}^{\varphi_{\text{final}}} \frac{d\varphi}{k(\varphi)} + \frac{t_R - \tau - t_G}{k_{\text{final}}} = t_0 - \frac{t_{\text{init}} + t_D}{k_{\text{init}}} \quad (2.4)$$

in which t_G represents the gradient time.

Retention modelling is mostly used to facilitate rapid and efficient method development in many modes of liquid chromatography (LC) and supercritical-fluid chromatography (SFC). The applications of retention modelling in method development can be divided in several areas. Retention models can be used to characterize newly developed stationary phases and to establish the underlying retention mechanism. In method optimization retention modelling is used to achieve better separations. In method transfer, methods developed or implemented on different systems are harmonized with the aid of retention models. Retention models are used to better understand and more-accurately describe retention. Additionally, retention modelling is applied outside the field of chromatography, for example in pharmaceutical and environmental science, to determine the octanol-water partition coefficient ($\log k_{ow}$) of a newly synthesized product or to determine the persistence of a pollutant in the ecosystem [2,3]. There are different strategies to perform retention modelling, depending on the aim of the study. The general form of a retention model can be described as a relation between a retention parameter and a function combining system and analyte parameters.

In a specific set of models, called linear-free-energy relationships (LFER), the function consists of the sum of a small number (typically five) of product terms, each consisting of a system parameter (s_i) and an analyte parameter (a_i).

$$\log k_{i,s} = \sum_{i=1}^n a_i s_i \quad (2.5)$$

Each term is loosely connected with a specific type of interaction between analyte and the stationary phase. Examples are the (hydrophobic-subtraction) model of Snyder (HSM) [4,5] and the model of Abraham [6,7]. Snyder defined the stationary-phase parameters in his model as hydrophobicity, steric hindrance, hydrogen-bond acidity and basicity, and cation-exchange activity [4,5]. Abraham identified contributions of molar refraction, solute polarizability, effective hydrogen-bond acidity and basicity, and the McGowan

characteristic volume [6,7]. In either case, the values of the system parameters depend on the values assigned to a set of reference analytes. The goal of these models is not to predict retention, but to characterize and classify stationary phases. The model does not describe the effect of the mobile-phase composition. Characterizing analytes is laborious (requiring measurements on different columns), but characterizing systems is easy. Despite the influence of the mobile phase, system parameters are usually interpreted as column or stationary-phase parameters and values for many stationary phases have been tabulated [8,9].

A different angle to retention modelling is the use of quantitative structure-retention relationships (QSRR) which are statistically derived relationships between a number of structural descriptors of an analyte and its retention [10]. Such models, based on large sets of structural parameters and retention data of many compounds, can be used to predict retention of new compounds if their structural parameters can be computed. Similar approaches have been applied to evaluate the pharmacological activity and physicochemical parameters of compounds (quantitative structure-activity relationships, QSAR, and quantitative structure-property relationships, QSPR, respectively). The most-important structural descriptors are identified in the process [11].

A third approach utilizes artificial neural networks (ANNs) to describe retention for (very large) input data sets. An ANN is a computational modelling tool that is inspired by the architecture of the human brain. It consists of an input and an output layer, with one or more hidden layers in between [12], and ANN models are known to require a vast data set-[13].

The final approach to retention modelling is based on (semi-) empirical models that contain abstract parameters to describe retention. Different models have been developed for and applied to many specific modes of LC. Few input data are needed to describe retention and to predict new data through inter- or extrapolation. This renders the class of (semi-) empirical models eminently useful to assist in LC method development [14–17] and the remainder of this review will focus solely on such models.

Empirical retention models typically feature several parameters that are abstract (*i.e.* not linked to a specific interaction/mechanism in chromatography), yet which relate analyte- and measurement parameters (e.g. volume fraction of organic modifier, salt concentration, pH, *etc.*) to k . Often the common logarithm or the natural logarithm of the retention factor, *i.e.* $\log_{10} k$ or $\ln k$ is used. Other variables that are not represented by the model (e.g. the stationary phase, temperature) must be kept constant at specified values for the model to remain valid. The model is typically fitted through all data points available.

With increasing computer resources, *in-silico* techniques become much-more attractive than exhaustive trial-and-error experiments for LC method development. In this review, recent developments in and applications of retention modelling will be discussed, with focus on method optimization, method transfer, stationary-phase characterization, understanding and describing retention, and lipophilicity determination.

2.2. (Background) Theory

Several models have been developed and applied for retention modelling. In most cases, the volume fraction of modifier (φ) is the most-important variable. Only a handful of two- or three-parameter models have been used extensively, *viz.* the linear-solvent-strength model (LSS), the quadratic model (Q), the adsorption model (ADS), the mixed-mode model (MM) and the Neue-Kuss model (NK). Optimization programs, such as Drylab [18], PEWS² [19], and MOREPEAKS [20], rely on one or more of these retention models, which are all based on the volume fraction of the modifier (φ) and are two- or three-parameter models. In the following section, the models and their applications will be briefly discussed. The requirements for input data will also be discussed, such as the elution mode and the number of datapoints.

2.2.1. Models

2.2.1.1. Linear solvent strength model

The log-linear model for reversed-phase liquid chromatography (RPLC) was introduced by Snyder *et al.* to describe retention as a function of mobile-phase composition (φ) [21]. It is often referred to as the LSS model (occasionally it is also referred to as the partitioning model). The common form of the model is

$$\ln k = \ln k_0 - S_{LSS}\varphi \quad (2.6)$$

where $\ln k$ is the natural logarithm of the retention factor at a specific modifier concentration, $\ln k_0$, often also denoted $\ln k_w$, refers to the isocratic retention factor of a solute in pure water, φ refers to the volume fraction of the (organic) modifier in the mobile phase, and the slope S_{LSS} is related to the interaction of the solute and the (organic) modifier. The LSS model parameters can be calculated from the retention of an analyte in two isocratic runs with different φ . Of the 90 references found for the LSS model in the last six years (2015-2020), 55% concern one-dimensional RPLC, leaving the rest for other applications such as two-dimensional LC (2DLC), hydrophilic interaction chromatography (HILIC) and supercritical-fluid chromatography (SFC), shown in Fig. 2.1A.

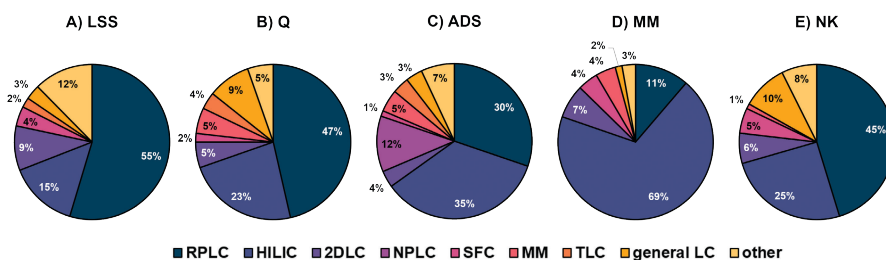


Figure 2.1. Application to different modes of chromatography for all five models. The data is based on the total number of references published from 2015 to 2020.

2.2.1.2. Quadratic model

Schoenmakers *et al.* introduced the quadratic model (Q), which can be seen as an extension of the log-linear model with another parameter. This renders the relation between the $\ln k$ and φ convex rather than linear [22].

$$\ln k = \ln k_0 + S_{1,Q}\varphi + S_{2,Q}\varphi^2 \quad (2.7)$$

In this and subsequent retention-model equations, $S_{1,Q}$ and $S_{2,Q}$ are empirical coefficients used to describe the influence of the organic modifier on the retention of the analyte. The other parameters in the Q model are identical to those of the LSS model. Of the 45 works reported in literature that use the Q model in the last six years (2015-2020), summarized in Fig. 2.1B, the main application is RPLC (47%). The Q model has also been investigated for describing HILIC retention (23%).

2.2.1.3. Adsorption model

The adsorption model (ADS) was introduced by multiple researchers during the nineteen sixties and seventies. Soczewinski *et al.* [23], Jandera *et al.* [24], and Snyder *et al.* [25] all presented the model in their work on normal-phase liquid chromatography (NPLC), and thin layer chromatography (TLC). The model, which was designed to account for adsorption, has also been described as the log-log model or the Snyder-Soczewinski model [23–26].

$$\ln k = \ln k_0 - n_{\text{ADS}} \ln \varphi \quad (2.8)$$

In this model, the n_{ADS} parameter is the so-called solvation number, which represents the ratio of surface areas occupied by adsorbed molecules of the strong eluent component and the analyte. In contrast to the log-linear LSS model, here $\ln k$ is linearly correlated with $\ln \varphi$ (log-log model). While the model was initially intended for NPLC (12%), it is now mainly used for retention modelling in HILIC (35%) and RPLC (30%) (Fig. 2.1C).

2.2.1.4. Mixed-mode model

The mixed-mode model (MM) was developed by Jin *et al.* to describe retention in HILIC. The idea is that it can account for both retention modes of HILIC and RPLC. The model is a combination of the LSS and ADS models [27].

$$\ln k = \ln k_0 + S_{1,M}\varphi + S_{2,M} \ln \varphi \quad (2.9)$$

Jin *et al.* related $S_{1,M}$ to the solute's interaction with the solvents and $S_{2,M}$ to the solute's interaction with the stationary phase [27]. The model will be discussed more extensively in Section 2.3.3.2. The main application of the MM model is for HILIC (69%), as shown in Fig. 2.1D.

2.2.1.5. Neue-Kuss model

The most-recent of the five main models is the three-parameter Neue-Kuss (NK) model which was based on another model described by Nikitas *et al.* [28,29].

$$\ln k = \ln k_0 - \ln(1 + S_{1,NK}\varphi) - \frac{\varphi S_{2,NK}}{1 + S_{1,NK}\varphi} \quad (2.10)$$

Where the $S_{1,NK}$ -parameter represents the slope and the $S_{2,NK}$ -parameter represents the curvature of the $\ln k$ vs. φ plot. When integrating this equation to obtain gradient-elution retention times an exact solution can be found. Neue [30] suggested that this model could describe the curvature observed in $\ln k$ vs. φ relationships. Later, Neue and Kuss published the following version of the model in 2010 [31].

$$\ln k = \ln k_0 + 2 \ln(1 + S_{1,NK}\varphi) - \frac{\varphi S_{2,NK}}{1 + S_{1,NK}\varphi} \quad (2.11)$$

Note that the only differences between Eq. 2.10 and Eq. 2.11 are the sign before and the factor 2 in the second term. In Eq. 2.11, the $S_{1,NK}$ -parameter represents the slope and the $S_{2,NK}$ -parameter represents the curvature of the $\ln k$ vs. φ plot. The NK model was developed for gradient RPLC, which is clear from the number of applications (45%). However, it is also often applied to HILIC (25%), as shown in Fig. 2.1E.

2.2.2. Measurement and use of data

The way in which these empirical models can be used depends on the number and type (isocratic or gradient) of data points that are used to fit the model.

2.2.2.1. Isocratic or gradient data

All the empirical models covered in this review have been used for optimizing both isocratic and linear-gradient separations. Isocratic data points would need to be collected at different organic-modifier concentrations. This can be a tedious task, since not all compounds elute at a reasonable time for every value of φ . Many organic-modifier concentrations are often required to calculate the model parameters for every compound in a mixture. One way to get around this problem is to use gradient elution. This allows all analytes to be eluted within one run in a reasonable time. To compute the gradient-elution retention time or the organic-modifier concentration at the time of elution during or after the gradient, the retention model used must be numerically integrated in the gradient equation (Eq. 2.3 and 2.4) [20]. Here $k(\varphi)$ in Eq. 2.3 and Eq. 2.4 refers to one of the above retention models. To use gradient-elution experiments (known as scanning gradients) to establish model parameters, this process must be followed in opposite order. It is necessary to vary the effective steepness of the gradient between experiments. The effective steepness (b) is the product of the slope of the $\ln k$ vs. φ curve (e.g. S_{LSS}), the slope of the gradient ($B = \Delta\varphi / \Delta\tau$) and the hold-up time of the column (t_0)

$$b_{LSS} = S_{LSS} B t_0 = \frac{S_{LSS} B V_0}{F} \quad (2.12)$$

where V_0 is the hold-up volume and F is the flow rate. The effective slope can be varied by changing one of three parameters (i) the slope of the gradient (B), (ii) the column volume, or (iii) the flow rate.

The accuracy of prediction is influenced by the selected elution mode. An error-analysis approach was described by Vivó-Truyols *et al.* for translating gradient data to isocratic elution or *vice versa* [32]. The authors concluded that input data obtained using isocratic experiments yielded the most accurate predictions [32]. Isocratic elution could also be predicted using models constructed based on gradient experiments, but such models were only found accurate across limited ranges of solvent composition [32–35]. Gradient retention data can be predicted from gradient-scanning experiments [36–39], but little research has been performed on the requirements for the experimental data. In a recent paper it was shown that the prediction accuracy of the model depended on many factors, including the proximity of the slope of the predicted gradient to that of the scanning gradients, whether interpolation or extrapolation is applied, and the experimental precision [40].

2.2.2.2. Number of input datapoints & model evaluation

When calculating the parameters of the empirical models of Section 2.2.1, referred to as retention parameters, there is a limitation as to the minimal number of input datapoints. Generally, the number of parameters determines the number of necessary input runs. Two-parameter models, such as ADS and LSS, need at least two datapoints for each component, while three-parameter models, such as MM, NK and Q, require at least three. Some of these models, for example NK, have mostly been used with larger numbers of data [31].

Adding more parameters to a model increases the risk that the model will overfit the data. When multiple models are tested on a dataset, the number of parameters may betray the actual quality of the model. To correct for this bias, the Akaike Information Criterion (AIC) can be used, which contains a penalty when more parameters are added [41].

$$AIC = 2p + n \left[\ln \left(\frac{2\pi \cdot SSE}{n} \right) + 1 \right] \quad (2.13)$$

The AIC value is calculated upon fitting the data to the model. The sum-of-squares error (SSE) is corrected by the number of parameters (p) and the number of observations (n). A lower (more negative) value represents a better fit, thus aiding in the selection of a correct model [37,42–46]

Another way of choosing between two- or three-parameter models is to perform an F-test of regression to examine whether adding a third term is significant. This test does not evaluate the goodness-of-fit, but only the difference between a three-parameter model and its reduced form. From the five empirical models, the F-test of regression can be performed on (i) the Q and the LSS models, (ii) the MM and the LSS model, and (iii) the MM and the ADS model. These three combinations have been examined by Roca *et al.* for modelling the retention of peptides in HILIC [38]. Baczek *et al.* performed an F-test on the LSS and Q models in RPLC [47].

2.3. Methods

Upon reviewing the literature, we have identified five main domains where retention modelling is applied, and these will be discussed. These five domains and their workflows are summarized in Fig. 2.2. For reference, the lower section of the figure contains a reference to the corresponding paragraphs in the text.

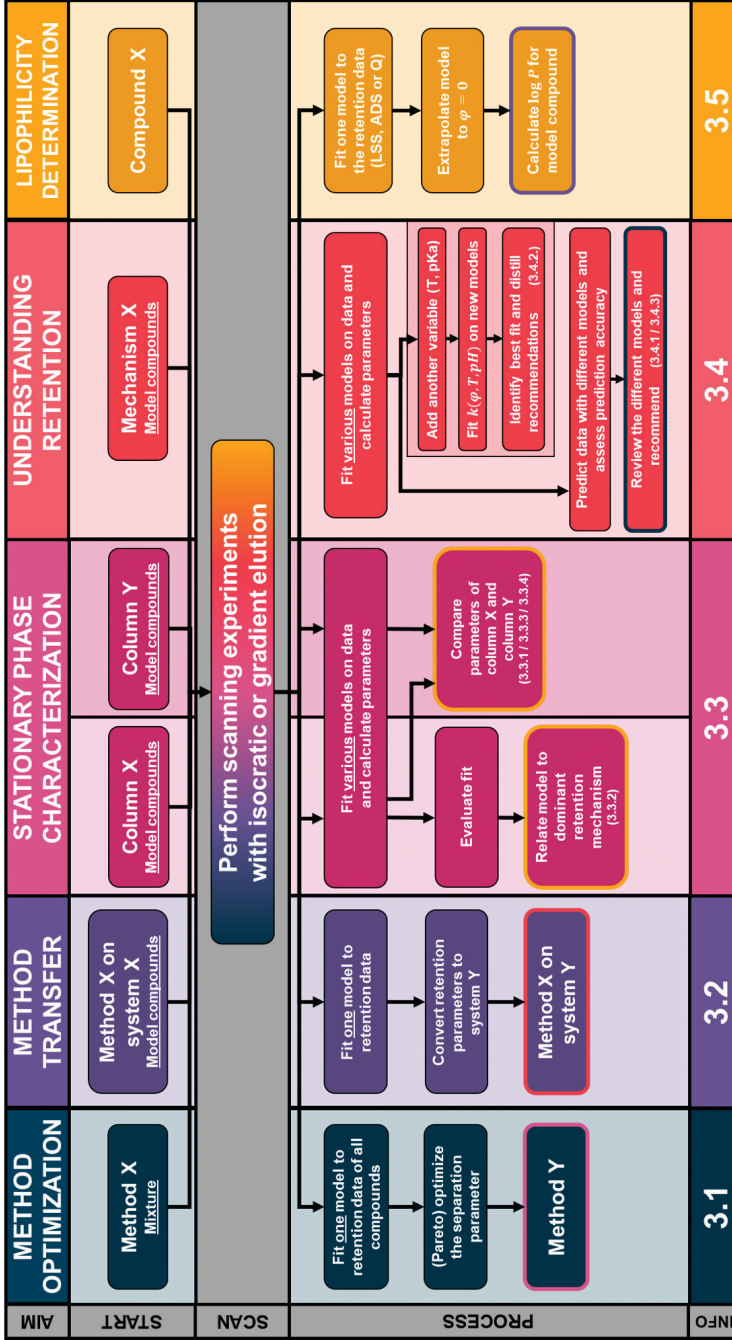


Figure 2.2. Overview of workflows of the main application domains of retention modelling in recent literature. At the top of the figure, the different aims are shown with the starting point indicated directly below. All domains will require input data which is obtained in the scan step. Next, the different processes are shown in their matching colour underneath. The number of models used is indicated in the box and the final goal, whether it is a method, a number or a degree of similarity, is indicated with the coloured line around the box. Beneath the workflows, the section number of the corresponding paragraph can be found. The workflows indicated in the figure are generalized and individual works may deviate from it.

2.3.1. Method optimization

In the development and optimization of an LC method, retention modelling can be an important tool. In this section we review recent literature on method optimization with the aid of retention modelling. The next two sections focus on one- and two-dimensional methods, whereas a final section addresses elaborate strategies and optimization packages.

2.3.1.1. Optimization of one-dimensional separations

After the mobile-phase components and the stationary phase have been selected, retention modelling can be used to optimize separations. For example, for a separation of a vegetable oil employing a porous-graphitic-carbon column, Zhang *et al.* used the LSS model to optimize the separation with an isopropanol-toluene gradient [48]. The authors tested the effect of the toluene fraction (φ_{tol}) on the retention through the S_{LSS} -parameter, which was found to be similar for all triacylglycerols, resulting in the same selectivity at all toluene concentrations. Conversely, differences between S_{LSS} -parameters can indicate to what extent the modifier concentration can be used to optimize selectivity. Fekete *et al.* reported very large S_{LSS} values for proteins (calculated from two scanning gradients) and a 10-fold decrease in retention when the organic-modifier concentration was increased by 0.8% [49]. Such high S_{LSS} values are one of the reasons why gradient elution is indispensable in RPLC of proteins. Selectivity could be improved by serially coupling columns with increasing retentive capacity and applying multi-step gradients [50,51].

Apart from the mobile-phase composition, the sample solvent should be considered. A large difference in elution strength between the eluent and the sample solvent may lead to incidents such as breakthrough or peak deformation [52,53]. Jeong *et al.* simulated separations to study the effect of an injection with a high-elution-strength solvent into a weaker eluent [52]. The LSS and NK models were used for calculating local retention factors. The peak widths were predicted by considering the retention of the analyte in the injection solvent and the in mobile phase. The simulated chromatograms (red) were confirmed with experimental data (black), which is indicated in Fig. 2.3.

Boateng *et al.* [54] improved a separation of three regioisomers of methoxyphenidine by optimizing the temperature, pH, and organic-modifier concentration. Retention data were fitted using an ADS model to describe the effects of pH, the LSS or Q model for mobile-phase composition (φ) or the Van 't Hoff equation for temperature (T). By varying the three parameters at three different levels, producing a 3×3 input data set, an optimized separation was developed with prediction errors lower than 5%. Vaňková *et al.* investigated the effect of gradient steepness on peak compression using LSS retention models. They determined the

mobile-phase composition at time of elution (φ_e) and the corresponding retention factor (k_e) [55]. k_e was then related to the peak width. Using this information, the peak compression by the gradient was calculated. A ratio of gradient time to column dead time of 12 was found to give the best kinetic performance for small molecules. Gritti [56] discussed peak compression more extensively and derived a new expression based on the NK model, predicting peak broadening for complex gradient programs. When the peak compression predicted by linear and non-linear models was compared, no significant difference was observed.

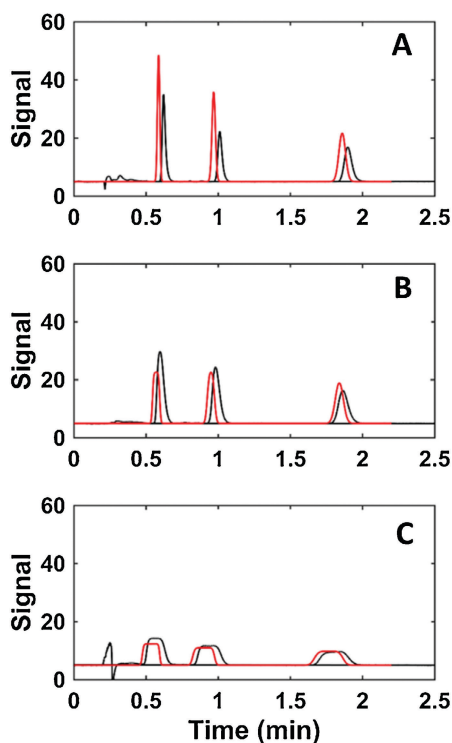


Figure 2.3. Comparison of the experimental (black) and simulated (red) chromatograms for isocratic separations of alkylbenzenes. Mobile-phase composition was 30% water and 70% ACN. The injection volume was 100 μL of (A) 50%, (B) 70%, and (C) 90% ACN in water. Reproduced from [52] with permission.

Another objective of method optimization may be to maximize the sensitivity. One way to achieve this is by on-column focusing, retaining all analytes at the column inlet by decreasing the solvent strength or by changing the temperature [57,58]. Rerick *et al.* [58] used an extended form of the NK model that included the effects of temperature. The model was extrapolated to predict retention in case cooling was employed. This model will be further discussed in Section 2.3.4.2. Chang *et al.* used the retention parameters of the LSS and ADS model for their peak-picking algorithm [59]. Clustering based on similarity of retention

behaviour and isotope ratios was performed. Using this strategy, the authors could rapidly identify 206 precursor ions in a complicated natural extract.

2.3.1.2. Optimization of two-dimensional separations

Two-dimensional liquid chromatography (2DLC) is increasingly applied [60]. Its success can be ascribed to the combination of two different separation mechanisms (*i.e.* targeting different sample dimensions) and the concurrent increase in peak capacity. However, the combination of two dimensions renders method optimization a more complicated endeavour [61]. When retention modelling is applied in the development of two-dimensional separations, the LSS model is often used to optimize the individual (gradient) dimensions [62–65]. The S_{LSS} parameter has also been used as a measure for orthogonality (*i.e.* the degree to which the two dimensions have different selectivities) [66,67]. S_{LSS} is expected to be similar for compounds of similar molecular weight, but for a given sample it may vary. For that reason, it was decided to use the average S_{LSS} -parameter of all compounds in the sample of the two separations to calculate the degree of orthogonality (O_d).

$$O_d = \gamma \cdot S_{LSS,1} \cdot S_{LSS,2} \cdot \Delta\varphi_{e,1} \cdot \Delta\varphi_{e,2} \quad (2.14)$$

It is calculated by multiplying the average S_{LSS} for both dimensions and the organic modifier concentration difference of the gradient of both dimensions ($\Delta\varphi_{e,1}$ and $\Delta\varphi_{e,2}$) with the correction factor with respect to the theoretical retention area (γ). This approach was developed by D'Attoma *et al.* [67] and applied to a RPLC×RPLC separation for peptides of Iguiniz *et al.* [66], which was able to separate more compounds than the prior 1DLC method. The use of LSS parameters for the degree of orthogonality is novel, although more studies are required to validate the approach.

One of the challenges in coupling two dimensions in 2DLC is the possibility of solvent mismatches, *i.e.* a weak solvent in one mechanism can be a strong solvent in the other. This has already been discussed to a certain extent in Section 2.3.1.1. Stoll *et al.* modelled ²D separations with gradient conditions, specifically a solvent mismatch between the injection solvent (*i.e.* the ¹D eluent) and the ²D mobile phase [68]. The loop volumes were varied (*i.e.* larger loops) and different loop fillings were employed. To make these simulations, the retention behaviour was assumed to be non-linear following the NK model. Muller *et al.* tried to model the effect of the dilution factor, which is often applied to reduce the solvent strength of the ¹D effluent, when coupling HILIC to RPLC [69]. The NK and the LSS model were used to calculate the retention factor at the time of elution (k_e) and the retention factor in the sample solvent (k_{ss}). The effect of several chromatographic parameters of these two

retention factors is modelled to find the optimal setup for HILIC×RPLC. It was found that the predictions of k_{SS} and k_e made with LSS and NK are similar.

2.3.1.3. Optimization programs and strategies

Many tools and software packages have been developed for liquid chromatography optimization because of growing computing power. These strategies have been developed over the years with increasing knowledge of the parameters influencing retention. An example of this is the development of the Drylab, ChromSword and PEWS² method development software [18,19,43,70–72]. Many of these papers are limited to RPLC, but there are three software packages that can be used for liquid chromatography in general.

Fasoula *et al.* developed a package of Excel VBA macros for modelling gradient retention data obtained in multilinear gradients [73]. The procedure consists of three steps: first the initial gradient retention data of each compound is fitted to a model and the parameters of that model are calculated. The model is then tested for accurate prediction of different gradients. Lastly, the optimized gradient method is determined. The package comprises ten retention models, of which the two-parameter models, especially the ADS model, describe simulated and experimental data very well. It was found that implementing more parameters, such as the Q model, increases the accuracy of the prediction, but also consumed more computational resources. The same group published a recent paper on a more elaborate program developed in R [74]. Next to an optimized gradient separation, the software aids in other aspects of the optimization such as peak shapes and base-line correction, and it is applied to ionized solutes too. The program contains the same 10 retention models as the Excel package of Fasoula *et al.* to optimize isocratic, gradient and multigradient separations [73,74].

Pirok *et al.* developed an optimization program (PIOTR) for 2DLC separations in Matlab [20]. With this program both a strong ion-exchange separation (IEX) and an ion-pair reversed-phase separation were optimized. The LSS model was used for optimization in RPLC and the ADS model for optimization in IEX, replacing φ by the salt concentration $[c]$. The input data for the program is the retention data of two comprehensive liquid chromatography (LC×LC) runs, of which the gradient slopes in both dimensions differ by a factor three. The workflow of the program is shown in Fig. 2.4.

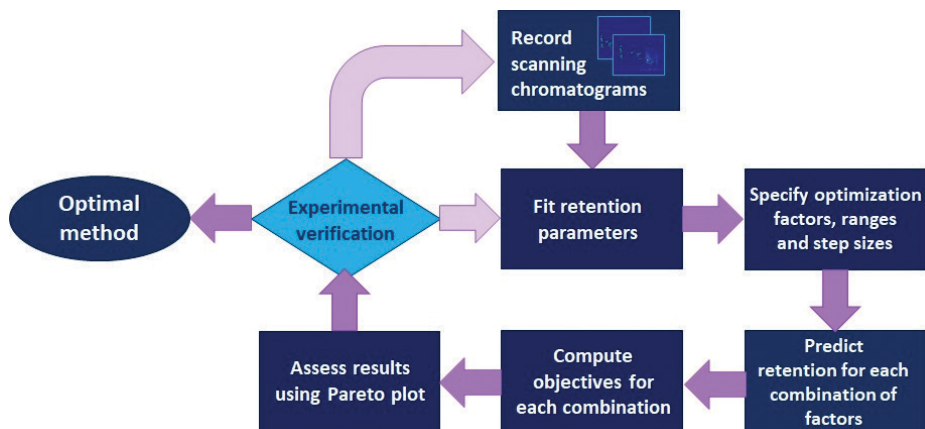


Figure 2.4. Pareto optimization strategy discussed by Pirok *et al.* Recorded scanning gradients are used to calculate the retention parameters by fitting the model. By specifying the ranges and step sizes in which the method can be optimized, the program predicts the retention for each component in each combination. The results are assessed in the Pareto plot and the best separation combination is verified through experimental verification. Depending on the verification, more scanning gradients are performed, or the optimal method is chosen. Adapted from [20] with permission.

The model gave an accurate description of the retention time but could not account for the band broadening. The program also served as a good tool for peptide separation in HILIC, when the NK, the MM and the Q model were added to the software [15,38,75]. Muller *et al.* reported on a predictive kinetic optimization tool for online HILIC×RPLC which allowed all chromatographic parameters to be optimized simultaneously within experimental restrictions [69]. The method was applied to a phenolic separation, in which the retention was modelled. Another approach was developed by Khalaf *et al.* for the development of RPLC separations for peptides [76]. The LSS model, the Van 't Hoff equation and an analytical solution for the mass balance on the column were combined, which was successfully applied to the separation of 5 different peptide mixtures. It is good to note that optimization approaches can also be conducted differently. For example, for RPLC specifically, multiple optimization algorithms have been proposed. Zhang *et al.* developed a new algorithm to simulate and optimize RPLC data with the aid of genetic algorithms (GA), in which the computation mimics the genetic mechanisms in all live form to adapt to the environment, and multi-layer perceptron artificial neural networks (MLP-ANNs) [77]. Alvarez-Segura *et al.* compared the use of GAs to that of multi-scale optimization (MSO), in which the level of detail in the solution is increased along the search by using subdivision schemes, for the optimization of multi-linear gradients, simulated by the NK model [78]. The reason for this is that GAs have a hard time fine-tuning the method. It was found that both methods yielded similar results.

2.3.2. Method-transfer

Retention modelling can also be used to speed up the transfer of methods to different hardware. When gradient methods are transferred, analysts often run into the problem of different dwell volumes and gradient profiles, caused by different mixers, pumps and tubing. Bos *et al.* developed a response-function-based algorithm to determine analyte parameters with a geometry-induced deformation correction [79]. The LSS parameters for a small set of compounds were determined on different systems with and without a correction of gradient shape, only considering the dwell time. This yielded a decrease of the inter-system retention prediction error from 9.8% to 2.1% between the first and the second system and 12.2% to 6.5% between the first and the third system. While the study was limited to geometry-induced deformation, the authors noted that other effects such as those induced by solvent properties, as well as solvatochromic effects still required further study.

Jandera *et al.* applied four different retention models on the prediction of the retention of a series of standard analytes in short monolithic columns with fast gradients [80]. A prediction error between 0.7% and 1.5% was found for 1 min gradients starting at 100% water for all 4 models, indicating the validity of the retention models to predict retention in short columns. Next to that, the ADS model provided the most accurate prediction in the fast gradients. The predicted retention of the models is compared to the experimental data in Fig. 2.5.

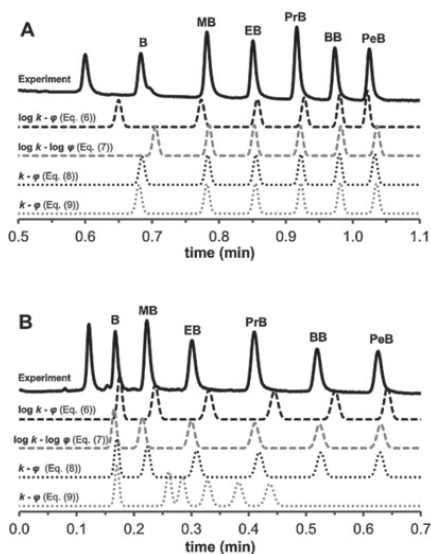


Figure 2.5. Comparison of experimental and predicted chromatogram of one-minute gradients from (A) 0-100% ACN and (B) 50-100% ACN. The four models used are (i) LSS model, (ii) ADS model, (iii) model developed by Jandera *et al.*, and (iv) the NK model. Reproduced from [80] with permission.

Gritti studied the transfer of a gradient method between two columns with similar particles but different average pore diameter [81]. He proposed three different gradient transfer methods to maintain the selectivity, based on either the LSS or the NK model. The first method is the “vertical” transfer, in which it was assumed that the LSS model applies for both models and that there is no change in the S_{LSS} -parameter when changing columns. The retention factor on the two columns would then only vary with the change in column phase ratio ($\ln \frac{\phi_1}{\phi_2}$). The second method was referred to as the “horizontal” transfer and assumed that the new retention factor was equal to the old retention factor after shifting the eluent composition from φ to $\varphi + \Delta\varphi_{1 \rightarrow 2}$ and that the shift in eluent composition ($\Delta\varphi_{1 \rightarrow 2}$) was unique for each compound. These directions refer to the shift in the $\ln k$ vs. φ plots. The third method is the *in-silico* approach, in which the best optimal method is found by changing the gradient steepness and the starting concentration of modifier.

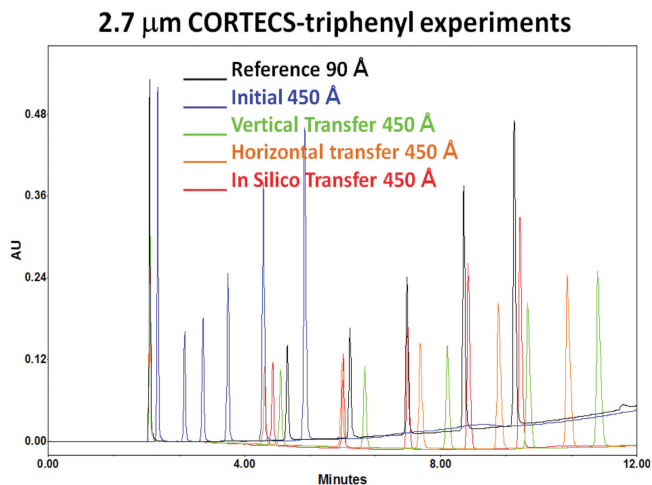


Figure 2.6. Gradient method transfer between two columns (2.7 μm CORTECS-triphenyl) with different pore size (90 Å – 450 Å). In the figure, the reference gradient chromatogram is shown in black. The direct transfer to a column with a larger pore size is shown in blue. The three different transfer methods are indicated with green (vertical transfer), brown (horizontal transfer) and red (in silico transfer). It is visible that the black line is most similar to the red line, revealing the best gradient method transfer. Reproduced from [81] with permission.

In Fig. 2.6, the reference chromatogram of the column with a pore diameter of 90 Å is shown with the initial chromatogram in a 450 Å pore diameter column, and the three different transfer methods. The vertical transfer was found to perform worst, while the *in-silico* approach performed best. The reason for this was that the linearity of the LSS model is only an approximation.

2.3.3. Stationary phase characterization and comparison

Retention modelling is frequently used in the development and characterization of columns and stationary phases. The main part of retention modelling in column characterization is performed with models such as LFER and HSM, leading all the way to enormous column databases [82]. In these methods, the extent of different interactions occurring in a separation and the effect of these interaction on the total retention process are established [7,83]. The models have been more extensively described in the introduction, but will not further be discussed in this review. Two other approaches to compare columns are classification of stationary phases by performing chromatographic tests or statistical tests and predicting retention behaviour with mathematical models, requiring large amounts of data [84,85]. Since statistical tests yield more than only retention model descriptors [86] and mathematical models often provide information on mechanical and physicochemical properties, which is often not based on any chromatographic retention data [84,87], these two goals will not be discussed further. The fourth approach for column characterization is the application of semi-empirical models. In this method, the fit to a model indicates which of the retention mechanisms is dominant, such as mixed-mode [88], reversed phase [89–91], normal phase [92], but mostly HILIC [93]. In the last years, HILIC has gained popularity, leading to a better understanding of the mechanism and the influence of several parameters (see Section 2.3.4.), which led to the development of many additional HILIC stationary phases. Stationary phases that can be used in the RPLC and the HILIC mode, depending on the level of organic modifier, have also gained in popularity.

2.3.3.1. Column Comparison

New columns or stationary phase materials are often compared to existing methods by, for example, analysing the differences in the retention of probe compounds. A C30 bonded silica stationary phase was characterized by Vyňuchalová *et al.* [94,95]. The column was compared to other RPLC columns, such as C4, C8 and C18 columns, concerning the retention of homologous non-polar alkylbenzenes with an extended LSS model. This model included parameters for the methylene group selectivity (α) and the contribution of the end group in the series (β). In Eq. 2.15, the constants a and m increase with the number of repeats (n).

$$\log k = \log \beta + n \log \alpha = \alpha_0 + \alpha_1 n - (m_0 + m_1 n) \varphi \quad (2.15)$$

The retention parameters a_0 , a_1 , m_0 , m_1 were compared between columns, and it was found that the C30 column yielded lower parameters than the standard RPLC columns, indicating lower contributions of methylene groups and end groups and weaker effects of the organic solvent on the decrease of methylene selectivity. Similar stationary phases can be used for

different purposes, for example when performing flash purification chromatography. Some manufacturers are producing flash purification stationary phases identical to the analytical stationary phase, only adapting the geometry of the column. Héron *et al.* compared these with a model based on the LSS model [96], where the change in S is described with the $\ln k_w$.

$$S = p + q \ln k_w \quad (2.16)$$

$$q = \frac{\Delta \ln \alpha_{CH_2}}{\ln \alpha_{CH_2-H_2O}} \quad (2.17)$$

Where p and q are constant for a binary solvent system. The q -parameter can then be correlated to the methylene selectivity measured in pure water ($\ln \alpha_{CH_2-H_2O}$) and the decrease in selectivity due to an increase of the organic modifier concentration ($\Delta \ln \alpha_{CH_2}$). As an alternative to C18 bonded phases, graphitic carbon can separate both polar and non-polar analytes. Lunn *et al.* [97] compared this phase to other regular RPLC stationary phases regarding its pre-concentration capability at the top of the column. The retention parameters were calculated by the NK model from isocratic retention data of small molecules on the different columns. The $\ln k_0$ parameter was used as a marker for its focusing ability, since the extrapolated values predict retention in 100% water

2.3.3.2. Classification of new fabricated stationary phases

With the increasing popularity of HILIC and mixed-mode separations over the last years, there has been a rise in the number of stationary phases developed for these two separation modes. Most of the developments in RPLC, the workhorse of LC, are either developments of the geometrical shape of the column, such as pillar-array separations or channel shape [90,98] (discussed in Section 2.3.3.4.), or the addition of other separating mechanisms like ion-exchange, creating a mixed-mode separation [89] (discussed in this section). Few new stationary phases for NPLC have been introduced. In 2015, Peristyy *et al.* investigated the retention behaviour of some small molecules on synthetic polycrystalline diamond and fitted the data on the ADS model [92]. Examining the parameters calculated by the model, a higher n -value (Eq. 2.8), the parameter that indicates the slope of the $\ln k$ vs. $\ln \varphi$ plot, is found for the more polar compounds than for the polycyclic aromatic hydrocarbons (PAHs). This indicates hydrogen bonding on the surface of the diamond and weak dispersive forces between the PAH molecules and the flat stationary phase.

In the last years, many different stationary phases have been developed for HILIC. To confirm the HILIC retention mechanism, the retention of some probe compounds is often measured at different levels of φ and fitted to the MM model. High regression coefficients indicate

a good fit and thus confirm the HILIC mechanism, which is often indicated by a U-profile retention (*i.e.* high retention at φ levels close to 0 and 1, but lower retention in between). This retention plot is shown in Fig. 2.7.

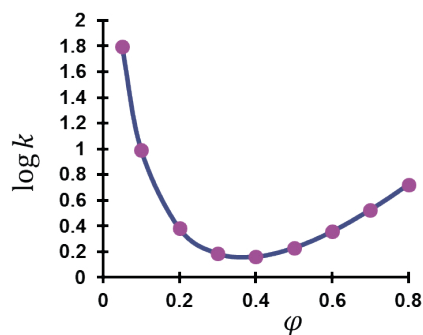


Figure 2.7. Retention behaviour of gallic acid showing higher $\log k$ values at the extreme φ values. Note that φ in this figure concerns the amount of water in the mobile phase, since this is the strong solvent in HILIC. On the right side, gallic acid demonstrates HILIC behaviour and on the right side it exhibits RP behaviour. The model is shown in Eq. 2.18 and the φ_{min} is given by Eq. 2.19. Plot based on the data in ref [99].

Since the MM model is built by combining both the LSS and the ADS model, the retention data may also be fitted to these two models separately to find the dominant retention mechanism [44,100–102]. Many of the developed stationary phases for HILIC are based on a polymeric structure, such as a hyperbranched polyethylenimine stationary phase [103] and a poly(vinyl alcohol)-cationic cellulose copolymer [104]. Other used polymer functionalized silica stationary phases for HILIC separations are based on polyglycerol [105,106], polyacrylamide [107], poly(vinyl alcohol) [108], and poly(glycidyl methacrylate-divinylbenzene) [101].

With the synthesis of new stationary phases, the retention mechanism is often not limited to one specific selectivity, sometimes leading to a mixed-mode mechanism [88]. For example, this can be based on RPLC with ion repulsion [89,109], using the LSS model to describe the relation between retention and organic modifier. Another mixed-mode selectivity was prepared by polymerizing a mixture of glycidyl methacrylate and 2-dimethylaminoethylmethacrylate, yielding a dual retention mechanism of HILIC and IEX chromatography [110]. The mixed-mode behaviour was confirmed by fitting the retention data to the LSS, ADS and MM model. It was found that acidic and neutral compounds behaved purely on an adsorption mechanism, while the basic compounds fitted best with the MM model. A perhaps more relevant and contemporary combination of selectivities is the HILIC mechanism with a RP mechanism, dependent on the level of organic modifier in the mobile phase. High levels of organic modifier induce HILIC behaviour, whereas high levels of water

induce RP behaviour, leading to higher retention in both ends of the φ -scale [91,111]. The dual retention behaviour can be described by the mixed-mode model of Jin.

$$\log k = a + m_{\text{RP}} \cdot \varphi_{\text{H}_2\text{O}} - m_{\text{HILIC}} \cdot \log \varphi_{\text{H}_2\text{O}} \quad (2.18)$$

Here, a is related to the size of the molecule and to the interaction between analyte and stationary and mobile phase, m_{RP} relates to the interaction between the solutes and the solvents and m_{HILIC} refers to the direct analyte-stationary phase interaction [112,113]. The minimum of the $\log k$ vs. $\varphi_{\text{H}_2\text{O}}$ plots (φ_{min}), which is shown in Fig. 2.7, can be calculated by the following equation and corresponds to the transition between RPLC and HILIC behaviour of analytes. It depends on both the polarity of the sample and the stationary phase [113,114].

$$\varphi_{\text{min}} = \frac{0.434 \cdot m_{\text{HILIC}}}{m_{\text{RP}}} \quad (2.19)$$

2.3.3.3. Column comparison between SFC and LC

SFC is experiencing a renaissance in the last years and it was recently compared to LC [84]. Vera *et al.* published two papers in 2015 on the difference in selectivity of linear polynuclear aromatic hydrocarbons in SFC and LC [115,116]. In the first paper the retention of the hydrocarbons was modelled with the LSS model [115]. The effect of the organic modifier on the S -parameter was determined on two different stationary phases. It was found that in SFC using a similar percentage of acetonitrile reduced the retention time by half compared to the use of methanol. This led to the conclusion that retention optimization in SFC is very different from that in HPLC. In the second paper, the same selectivity's in HPLC and SFC were compared and it was concluded that PAHs yield different retention between RPLC and RPSFC on the same columns [116].

2.3.3.4. Comparing different column geometries

Besides optimizing the bonded stationary phase, there also have been improvements in the geometrical fabrication of existing stationary phases. These developments ranged from macrolevel to microlevel, which will be discussed in this order. In 2018, Gilar *et al.* tested the chromatographic performance of straight and serpentine microfluidic channels [98]. The LSS model was applied for the intrinsic gradient steepness ($b = S_{\text{LSS}} \cdot \Delta\varphi \cdot \frac{t_0}{t_g}$) to model the difference in gradient elution. A negative effect of turns on the efficiency was found, but this was reduced when gradient mode was employed. Gritti *et al.* evaluated the performance of conically shaped columns to standard cylindrical columns, where the LSS model was used for the retention in gradient elution [117]. The research indicated that, when in gradient mode, a conically shaped column could be advantageous to cylindrical columns, since it reduced

peak tailing. Several scientists have devoted their attention to (the simulation of) stationary phase gradients [52,68,118,119]. In one example, the isocratic retention data on the gradient stationary-phase-gradient columns was fitted to the NK model, which was then used to predict retention in gradient elution mode [118]. It was stated that the simulated retention fitted very well with the experimental data. This model was then applied to other stationary-phase gradient geometries and no large differences between using a uniform mixed-mode or a gradient column were found, but differences were found in the retention depending on the orientation of the stationary-phase gradient (*i.e.* the solute retention factor either increases or decreases in the direction of the flowrate) [119].

2.3.4. Understanding, describing, and predicting retention

One of the objectives of retention modelling is to obtain a better understanding of retention mechanisms. Especially in HILIC, retention modelling can improve the understanding of the mechanism and at the same time reduce the time needed for method optimization. Models that only consider the organic-modifier concentration, however, cannot describe the retention behaviour completely. Other parameters such as buffer concentration, pH and temperature influence the separation efficiency. This section will be subdivided in three parts. The first part will consider the use of the models in Section 2.2.1 to gain a better understanding of retention interactions. The second part focuses on new proposed models to describe more parameters in the separation besides the modifier. The third and final part will cover approaches to perform retention modelling.

2.3.4.1. Using existing models for understanding retention

2.3.4.1.1. Reversed-phase liquid chromatography

In many cases of retention modelling applied to RP separations the LSS model is applied. While higher-order models often yield a better description of the data, such as the Q and the NK model, such models also require more input data and risk overfitting the data. Gilar *et al.* [17] investigated this problem and compared retention prediction by NK and the LSS model. The LSS parameters were calculated in three different ways: looking at the full experimental range, only on experimental data of $\ln k > 0$ and a k range from 1 to 30, leading to significantly different parameters. The authors concluded that non-linear models describe the data best. The authors also recommended that if an LSS model is used it is better to omit data for $\ln k < 0$. Tyteca *et al.* [120] found a similar deviation from the LSS model for small molecules and peptides and found a better fit for the Q and the NK model. Next to smaller molecules, the retention data of proteins was also investigated, which led to the conclusion that, because of the very steep $\ln k$ vs. φ curves, non-linear retention behaviour in proteins could not be proven. A recent study on the use of scanning gradients for RPLC optimization

found that when a limited number of input experiments was desirable, good fits could be found for the two-parameter models (LSS and ADS) [40]. However, with increasing number of sampled measurements the fit was best for the ADS model. Next to that, the research showed that the gradient-slope factor, *i.e.* the ratio between slopes of the fastest and the slowest scanning gradients, which is often assumed to be at least three, is less important than the proximity of the slope of the predicted gradient to that of the scanning gradients.

For the determination of retention parameters towards the extreme values of φ , Jandera *et al.* [121] developed a three-parameter model (ABM model) to allow estimation of retention in pure strong and pure weak solvent ($\varphi = 0$ and $\varphi = 1$).

$$k = (a + b\varphi)^{-m} \quad (2.20)$$

Where a , b and m are experimental constants depending on the solute, the stationary phase and the mobile phase [121,122]. The authors state that in high organic-modifier concentration, the a -parameter could be neglected. This model allowed better prediction than the LSS or the ADS model and could also be used for HILIC. One of the drawbacks of the LSS model is that it cannot account for the non-linearity, making it only applicable to the narrow linear range. Baeza-Baeza *et al.* [123] extended the LSS model to include the elution strength changes with the elution degree, g . This parameter was assumed equal to 1 when the solvent strength followed the LSS model. It is larger than 1 when the elution strength decreased along with the organic-modifier concentration and, reversely, smaller than 1 when it increased with the organic-modifier concentration. In this way, it affected the linearity of the LSS model. The model could also be applied to other modes of LC.

When performing scanning experiments, it can be advantageous to reduce the time needed for the runs. Baeza-Baeza *et al.* combined the accuracy of isocratic data with the speed of gradient experiments by adding solvent concentration pulses in the isocratic runs [124]. The predicted parameters were found to agree with those obtained from isocratic experiments. Gradients have also been investigated in this context, with reports focussing on the fundamental equation of gradient elution [125], non-linear gradients [126] and pre-elution of solute in the initial mobile phase [127].

2.3.4.1.2. Normal-phase liquid chromatography

Because of decreased popularity, there has been little development in the field of normal-phase liquid chromatography (NPLC) with respect to retention modelling. One study compared the slight difference in the ADS model as seen by Snyder and by Soczewinski

[128]. There exist some different perspectives about the n -term in the ADS model, where Soczewinski wrote that polar solutes and the polar solvent absorb 1:1 with the absorption sites in the silica [23], whereas Snyder defined n to be the ratio of molecular area of the solute required when adsorbed on the stationary phase versus the molecular area of the strong solvent [25]. Wu *et al.* applied these models to classic NPLC bonded phases with literature data and to the charge transfer 2,4-dinitroanilinopropyl (DNAP) column [128]. While the Snyder model predicted better on the classed NPLC phases, the Soczewinski model predicted the charge transfer phase better.

2.3.4.1.3. Hydrophilic interaction liquid chromatography

With the potential of HILIC for the separations of highly polar and ionic compounds, the number of applications of HILIC has recently grown [129,130]. Since the actual retention mechanism of HILIC is not yet completely understood, there have been many published reviews in recent years that attempt to describe the interactions occurring in the column [114,131–133].

Recently, papers have focused on the optimization of a complete method, looking at different parameters such as buffers, salts, their concentrations, pH, the organic-modifier content, temperature and stationary phase. When optimizing the modifier content, a number of studies used the LSS model [134–138], the ADS model [102,134–139], the Q model [102,139] and the MM model [134,136]. Often, more than one model is used to distinguish for example between the partitioning mechanism and the adsorption mechanism [113,114]. The effect of pH was only found to significantly influence the retention in bare silica columns, since it has a major effect on the charge of the column [102,137]. There are several other papers that focus on the retention modelling itself. Euerby *et al.* [14] applied seven existing models to describe the retention as a function of the organic-modifier concentration and three models to predict the effect of temperature. These models were added to the developed retention-modelling program, in which the prediction accuracy could be assessed. The importance of the method parameters was ranked for retention and selectivity with statistical approaches and it was found that for retention the observed order of importance was organic-modifier content>stationary phase>temperature \approx pH \approx buffer concentration and for selectivity it was stationary phase>pH>buffer concentration>temperature>organic-modifier content. It was concluded that with gradient results, isocratic experiments could not be predicted. Cesla *et al.* [140] applied five existing models to the retention of oligosaccharides on different columns for which the magnitude of several mechanisms occurring in the different columns was determined. All five models fitted the retention data to a similar extent. In different studies, the LSS, ADS, Q, MM, and NK model were used by Rácz *et al.* [141] in Drylab and

by Roca *et al.* [38] in MOREPEAKS. The former study concerned method development for a hallucinogenic mushroom extract on the organic modifier, the pH and the temperature for different columns. The predicted chromatograms by the Q model deviated more from the experimental results than those of the LSS model [141]. In the work of Roca *et al.* a tryptic digest of bovine-serum-albumin was analysed and retention modelling was used to determine the best combination of column, organic modifier concentration and additive. To confirm the selection of the model, the F-test of regression was applied [38]. This retention modelling program was applied by Pirok *et al.* to separate metabolites with HILIC [15]. The ADS model was found to perform best, only requiring two scanning gradients and yielded acceptable accuracy and linearity. Next to that different stationary-phase materials were analysed, where the prediction accuracy in diol columns was found to be better than amide columns.

One aspect which renders the use of gradient data for the retention modelling challenging is the distortion of the gradient shape by the solvent-delivery system [79]. Therefore, when such data is used to calculate the retention model parameters, such small errors can yield wrong φ values and thus complicate the retention prediction. Wang *et al.* [142] used a back-calculation methodology for gradient imperfections and compared their HILIC results to those of RPLC. The authors concluded that column distortion plays a much more important role in HILIC retention projection compared to RPLC.

2.3.4.1.4. Mixed-mode chromatography

When optimizing mixed-mode separations, scientists often discuss the dual retention mechanism of RPLC and HILIC, depending on the level of organic modifier. This behaviour can be described by the U-profile retention plots, shown in Fig. 2.7, where the minimum describes the φ where the main retention mechanism switches from HILIC to reversed phase (See Eq. 2.19) [132,143]. Obradovic *et al.* investigated the retention of imidazoline and serotonin receptor ligands on a mixed-mode column and were able to fit the retention data at different mobile phase concentrations to a MM model, thereby confirming the retention mechanism [144]. Balkatzopoulou *et al.* applied retention modelling to a mixed-mode reversed-phase and weak anion-exchange column. It was found that the retention behaviour could be described by a U-profile plot, *i.e.* MM model, confirming the RPLC and HILIC behaviour of the compounds in lower and higher organic modifier concentration respectively [145].

2.3.4.1.5. Other chromatographic modes

Retention modelling has also been applied to more uncommon forms of LC, such as micellar LC (MLC), critical chromatography (LCCC) and chiral chromatography. Since other

mechanisms play a role in these types of chromatography, it is obvious that the standard retention models are not applicable to these methods. Navarro-Huerta *et al.* optimized MLC by isocratic or gradient elution and applied a wide range of models, some of which are developed for RPLC or specifically for MLC [146]. The most accurate predictions were found from the following model with fixed surfactant concentration:

$$\frac{1}{k} = c_0 + c_1\varphi + c_2\varphi^2 + c_3\varphi^3 + c_4\sqrt{\varphi} \quad (2.21)$$

Where c_0 , c_1 , c_2 , c_3 , and c_4 are the adjustable fit coefficients of the model. Hegade *et al.* applied the concept of stationary-phase optimized selectivity (SOSLC), in which the Q model was applied to the chiral separation of enantiomers [147]. The prediction error of the retention of enantiomers on polysaccharide stationary phases was found to be within 2% and 7% for isocratic and 0% and 12% for gradient elution.

Supercritical-fluid chromatography (SFC) often follows similar retention mechanisms as LC [84]. Vera *et al.* published two papers on the study of retention of polynuclear aromatic hydrocarbons on phenyl-type stationary phases [115,116]. These papers are discussed in Section 2.3.3.3. Tyteca *et al.* modelled SFC retention data and applied that in computer assisted method optimization [148]. The MM model, the Q model and the NK model were applied on isocratic and gradient data. The NK and MM model yielded the best retention-prediction accuracy. The conversion of isocratic to gradient data and vice versa resulted in more difficulties due to pressure differences. De Pauw *et al.* [149] investigated this pressure-related problem. Pressure and temperature definition of parameters such as fluidic CO_2 volumes, volumetric flow rates and mobile phase fractions, may differ between systems. The authors found that the retention in SFC could best be described through the mass fraction instead of volume fraction of the organic modifier.

2.3.4.2. Developing new models for understanding retention

2.3.4.2.1. Reversed-phase liquid chromatography

In many retention models, the elution mode for which the input data is measured should be the same as the preferred elution mode for prediction. For example, when recording isocratic data, the output is more reliable in isocratic mode. The same goes for gradient elution, which has even more restrictions, since the input gradient slopes should be like those predicted [40]. There have been developments to convert such data by defining the retention of analytes in gradient and isocratic elution and transferring this information to the data. This approach is referred to as the *iso-to-grad* approach [32]. Stankov *et al.* tried to apply this approach to dual-species eluent (*i.e.* a combination of two organic modifiers,

such as methanol and acetonitrile), and developed and tested four isocratic models with 3, 4, 5, and 8 parameters based on the Q model and the LSS model [150]. The authors deemed their prediction better than those of other models, referring to an average root-mean square error/minute of 0.743 for the compounds measured in gradient elution. Claiming a better prediction with increasing number of parameters, the authors stated that the models did not overfit the retention data. The best model was as follows:

$$\begin{aligned} \log k = a_0 + a_1 \cdot \varphi(\text{MeOH}) + a_2 \cdot \varphi(\text{ACN}) + a_3 \cdot \varphi^2(\text{MeOH}) + a_4 \cdot \varphi^2(\text{ACN}) + a_5 \\ \cdot \varphi(\text{MeOH}) \cdot \varphi(\text{ACN}) + a_6 \cdot \varphi^2(\text{MeOH}) \cdot \varphi(\text{ACN}) + a_7 \cdot \varphi(\text{MeOH}) \\ \cdot \varphi^7(\text{ACN}) + a_8 \cdot \varphi^2(\text{MeOH}) \cdot \varphi^2(\text{ACN}) \end{aligned} \quad (2.22)$$

Where $a_0, a_1, a_2, a_3, a_4, a_5, a_6, a_7$ and a_8 are regression coefficients for each analyte, solvent and column system. This model requires (at least) 9 data points. Tsui *et al.* [151] developed a three-parameter-equilibrium constant stoichiometric displacement retention model for RPLC, which considers the interaction between solute-sorbent, solute-ACN (ACN being the mobile phase), and ACN-sorbent, leading to the following model:

$$\ln k = -\ln(1 + K_{\text{SL-ACN}} C_{\text{ACN}}^y) - x \ln(1 + K_{\text{ACN}} C_{\text{ACN}}) + \ln k_0 \quad (2.23)$$

Where $K_{\text{SL-ACN}}$ and K_{ACN} are the equilibrium constants of solute-ACN and ACN-sorbent, respectively, C_{ACN} is the free ACN concentration and x, y and k_0 are the adjustable parameters. The authors plotted both $\ln k$ vs. C_{ACN} and $\ln k$ vs $\ln C_{\text{ACN}}$, in which concave upward and concave downward curves were found, respectively. The developed model was able to account for the non-linearity in the full ACN range. Unfortunately, the work was not compared to conventional retention models, and as such its performance is difficult to assess.

Gritti developed a solvent-retention model for the description of retention in combined solvent- and temperature gradient liquid chromatography (CST-GLC) by combining the LSS model with the Van 't Hoff relationship [152]. In this equation, the retention as a factor of the organic modifier concentration and the temperature is written as:

$$k'(\varphi, T) = k'(0) e^{-S_{\text{LSS}}(\varphi - \varphi_0)} e^{\frac{Q_{\text{st}}}{RT_0^2}(T - T_0)} \quad (2.24)$$

where $k'(0)$ is the retention factor at the initial φ and temperature, S_{LSS} is the S -parameter from the LSS model, Q_{st} is the isosteric heat of adsorption specific for the analyte, T is the temperature, and R is the ideal gas constant. The author stated that the model described the

retention of smaller compounds well over a modified range of temperature from ambient to 90°C. In the work of Wilson *et al.* temperature-assisted on-column solute focusing (TASF) was performed [57]. To model the effect of temperature on the retention, three different models were employed. Two models could be used for a fixed temperature (*i.e.* one-dimensional model dependent on φ), one based on the LSS model (Eq. 2.25) and one on the NK model (Eq. 2.26), and a third model based on the NK model (Eq. 2.27) included a temperature dependence (*i.e.* two-dimensional model dependent on φ and T).

$$\ln k = \ln k_0(T) - S(T)\varphi \quad (2.25)$$

$$\ln k = \ln k_0(T) + 2 \ln(1 + a(T)\varphi) - \frac{S(T)\varphi}{1 + a(T)\varphi} \quad (2.26)$$

$$\ln k = \ln k_0 + \frac{D}{T} + 2 \ln(1 + a\varphi) - \left(a + \frac{D}{T}\right) \frac{S\varphi}{1 + a\varphi} \quad (2.27)$$

In these equations, k_0 and $k_0(T)$ is the retention in pure water, S and $S(T)$ describe the solvent strength, a and $a(T)$ account for the curvature in the relationship between $\ln k$ and φ , and D indicates the effect of temperature. It was found that from the three descriptions of retention, the second equation yielded the most accurate predictions, which was calculated by measuring the retention at an organic modifier fraction of 0.05 at different temperatures. The last model (Eq. 2.27), which was first published by Neue and Kuss, was also used for the modelling of retention in TASF by Groskreutz *et al.* [31,153]. Retention data of parabens and hydroxyphenones was fitted to the model from 12 different solvent compositions and 6 column temperatures, yielding an R^2 -value of 0.9996. It was claimed that the model could predict retention and shape of the peak under both isocratic and gradient elution conditions. Horner *et al.* evaluated three temperature- and mobile-phase-dependent retention models, of which one was Eq. 2.27. The other two models were based on the Pappa-Louisi partition (Eq. 2.28) and Pappa-Louisi adsorption (Eq. 2.29) equations.

$$\ln k = \frac{1}{T} (A\varphi^2 + B\varphi + C) + D\varphi^2 + E\varphi + F \quad (2.28)$$

$$\ln k = A + \frac{B}{T} - \frac{\varphi \left(C + \frac{D}{T} \right) e^{\frac{E+F}{T}}}{1 + \varphi \left(e^{\frac{E+F}{T}} - 1 \right)} \quad (2.29)$$

Where both equations have 6 variable parameters A , B , C , D , E , and F . The model with the best fit, calculated with the AIC value (Section 2.2.2.2), was Eq. 2.29. It was followed by Eq. 2.28 and the worst fit was found with Eq. 2.27. The authors found that Eq. 2.27 (NK), with the lowest number of parameters, still yielded a decent estimate of the retention.

When the retention of analytes with acid-base properties is modelled, the retention not only depends on the organic-modifier concentration, but also on the dissociation constant (K). Andrés *et al.* developed a simplified model, based on a polarity-parameter model [154]. This two-parameter model, which is a simplified form of the LFER by Abraham, was originally developed for neutral compounds in RPLC [155].

$$\log k = q + pP_m^N \quad (2.30)$$

In this model, P_m^N describes the polarity of the mobile phase (related to the volume fraction and the different organic modifiers) and p and q are the fitting parameters. This model was extended to model retention of acid-base compounds for separations with acetonitrile and validated for separations with methanol [154,156]:

$$\log k = q + pP_m^N + \log[1 - D(1 - f)] \quad (2.31)$$

where P_m^N , p and q are similar to Eq. 2.30, D describes the ionization degree of the analytes related to the pK_a , and f is the ratio between the retention factors of the pure ionized and the pure neutral compound. The model was tested with different types of gradients with methanol (linear, convex, concave and combinations of those) and at three pH values. In Fig. 2.8 on the left, the predicted retention times for a wide range of acid-base compounds are plotted against the experimental retention times for the three pH values. On the right, the residuals are shown. From this figure, it can be seen that a higher pH lowers the prediction error [156].

The authors claimed that the model was not size dependent, since it performed as good for small as for complex molecules [156]. Sasaki *et al.* found that the model of Andrés *et al.* gave good accuracy, but it could not model compounds that presented multiple-curved retention behaviour, *i.e.* molecules with multiple pK_a values, when changing the pH [157]. In their work, pH-modifier models were combined in an optimization program to predict the optimal separation in pH and organic modifier, based on the data of 33 runs. While the model of Andrés *et al.* needed information *a priori* such as the pK_a , the software package of Sasaki *et al.* could predict retention from the retention input data alone and needed no physiological or chemical information of the target analyte.

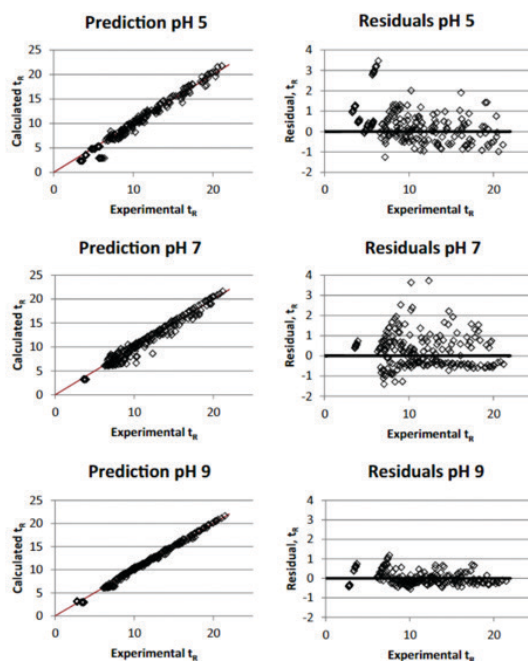


Figure 2.8. Prediction retention times, calculated with the model in Eq. 2.31, compared to experimental retention times for pH = 5, pH = 7, and pH = 9. On the left the two retention times are plotted for each compound and on the right the residuals of the left plot are shown. Retention time is in minutes. Reproduced from [156] with permission.

2.3.4.2.2. Hydrophilic interaction and mixed-mode chromatography

As could be seen in Section 2.3.4.1.3, HILIC is often described by the MM model. Wang *et al.* [158] studied the multiple interactions in HILIC further, and described the interactions between the solute, the solvent and the stationary phase into a stoichiometric displacement model for retention (SDM-R), which is defined as follows:

$$\log k = \log I - Z \log[W] \quad (2.32)$$

where $\log I$, which represents the affinity of 1 mol amount of solute to stationary phase, and Z are both constant, and $\log[W]$ is the logarithm of the concentration of water in the mobile phase. The model was compared to the LSS and ADS model, and outperformed both models on the retention prediction of proteins in HILIC.

Obradovic *et al.* developed a novel computational approach to identify the optimal fitting models for dual retention behaviour of HILIC and RPLC, typically described with a U-profile [159]. The considered models were analysed on their predictive ability of retention and on the accuracy of the turning point (φ_{\min}). The research yielded multiple models that outperformed the

standard Q and MM model, which were correlated to other parameters that are influencing the separation. These parameters were based on the average retention in HILIC mode, the average retention in RPLC mode and the average retention in the whole range of organic modifier.

2.3.4.3. Approaches to perform retention modelling

The exact method of conducting retention modelling is not always clear. Tyteca *et al.* investigated fitting problems encountered when modelling retention [160]. The LSS, ADS, NK, MM, and an extended four-parameter Neue model, as well as combinations thereof were tested on HILIC and SFC retention data. It was found that adding more scanning experiments and switching to higher-order models could improve the fitting and modelling of the data. For highly retained compounds, the authors recommended to use very slow gradients (high $\frac{t_G}{t_0}$) or to start at a higher organic-modifier concentration. Next to that, modelling retention of less retained compounds benefits from faster gradients. Another problem encountered when fitting HILIC retention data to retention models is that the retention in HILIC changes as a result of small changes in the mobile phase concentration. For that reason, Tumpa *et al.* divided the experimental space into different segments with an interpolated polynomial for each part, which is known as spline interpolation [161]. The MM, Q, ADS and LSS model were tested in this study. The spline interpolation technique was cross validated with the standard retention modelling approach, yielding the new technique with the best values. The prediction error of the retention parameters was below 10% for all compounds.

2.3.5. Lipophilicity determination

Lipophilicity is an important parameter to describe physicochemical properties and is often used in quantitative structure-activity relationships (QSARs) for several classes of compounds, such as environmental pollutants, pharmaceuticals, and bioactive compounds. It is generally described as the logarithm of the n-octanol/water coefficient: $\log P$. Lipophilicity is a critical parameter in drug discovery, since it plays a crucial role in determining the ADMET (adsorption, distribution, metabolism, excretion, and toxicity) of the potential candidate [162]. For successful drug discovery, drugs are assessed on their pharmacokinetic properties, such as biological half-life and extent of protein binding, but next to that they are assessed on the delivery to these target sites. After uptake, the drugs must cross several membranes, either passively or actively. These are generally more hydrophobic and thus prefer compounds with higher lipophilicity. In recent years, the average lipophilicity value of potential drugs has increased, exposing its value and influence on the drug industry [162]. Moreover, lipophilicity plays an important role in environmental chemistry, where it is used in the estimation of bioaccumulation in plants and animals, the prediction of adsorption of pollutants in soil and sediments and the assessment of health risks of emerging contaminants [163].

There are various methods, computational and experimental, which can be divided into direct and indirect methods, to calculate lipophilicity, but there are limitations to the direct experimental methods as these (i) cost time, (ii) are labour intensive, (iii) require a lot of sample, and (iv) are often limited by the dynamic range of the detector [164]. For that reason, many indirect methods have been introduced based on separations, of which the most common approach is based on RPLC. When using RPLC as a tool, the descriptor of lipophilicity is the logarithm of the retention parameter ($\log k$), which can be calculated from the retention time and the dead time (Eq. 2.1) [2]. At first, isocratic retention factors at specific organic modifier levels were used to correlate the $\log P$ to the $\log k$, but later the authors opted that the retention factor in 100% water was more demonstrative [165]. This led to the Collander Equation, which is a linear dependence between $\log P$ and $\log k$ [166,167]:

$$\log P = a \log k_w + b \quad (2.33)$$

where a and b are parameters that are characteristic for the non-polar solvent used in the chromatographic separation. Performing analyses at 100% water, which is thought to lead to major retention loss and to be catastrophic for the column life time [168], leads to large retention times of hydrophobic compounds and to very broad peaks, is omitted. For that reason, often the $\log k_w$ is estimated from the Snyder-Soczewinski Equation (Eq. 2.8). When calculating retention factors from 4 isocratic runs at different organic modifier levels, the $\log k_w$ can be extrapolated [164]. Liang *et al.* [169] revised the methodology of lipophilicity determination and argued to use gradients instead of isocratic runs to save time. If gradient runs are performed instead of isocratic runs, the $\log k_w$ found with three gradient runs agreed better with the $\log k_w$ determined with isocratic runs than if two gradient runs were used. Next to RPLC, Sobánska argues that TLC can serve as an alternative for lipophilicity determination, since it is inexpensive, fast, and readily available [170].

The extent to which a drug can penetrate biological membranes, such as the blood-brain barrier, cell membranes, and skin, depends heavily on the $\log P$. A number of groups publish the lipophilicity parameters of many newly synthesized drug candidates [171–184]. In drug-discovery research the LSS model is often used to obtain the $\log P$, but Hawrył *et al.* acknowledge the concave structure of the retention plots [177]. For this reason, the Q model was used next to the LSS model to determine the intercept. The Q model gave more accurate results when acetonitrile was used as organic modifier, whereas retention data in methanol fitted better with the LSS model [1,177]. The same quadratic relation was found by Klose *et al.* for wide φ ranges [173]. However, other authors found a linear relationship when using acetonitrile [182]. Sztanke *et al.* [171] compared modifier systems with methanol, acetonitrile and dioxane and found that

methanol systems yield the best experimental lipophilicity indices. However, the research stresses the differences and thus the complexity when performing these scanning gradients.

2.4. Discussion

In retrospect, the application of retention modelling by means of (semi-) empirical models has led to a better understanding of general HPLC, specifically RPLC and HILIC. It can be stated that it plays a key-role in the different fields of application. In the published work on retention modelling, however, a clear distinction between the workflows of the different applications becomes evident, which can be seen in Figs. 2.2 and 2.9. For method optimization and lipophilicity determination retention modelling is often approached as a black box. Often only one model is applied which is chosen by convention, although there seems to be enough evidence that these models have their inaccuracies. For example, with lipophilicity determination, the $\ln k_w$ is mostly determined by extrapolating the LSS model, while it has often been shown that there is a clear deviation from linearity, especially in the lower φ range [123]. For this reason, lipophilicity determination is ranked with the lowest complexity of the retention modelling, followed by the method optimization (Fig. 2.9). In stationary-phase characterization, often more models are investigated. Any good performance of a specific model is sometimes used as supporting evidence to conclude that a certain retention mechanism mainly determines the selectivity. In contrast, most work in the domain of method transfer and understanding retention use retention modelling to a much-sophisticated extent. Researchers also appear to implement increasingly more parameters to conduct retention modelling in these latter domains, attempting to describe each contributing effect.

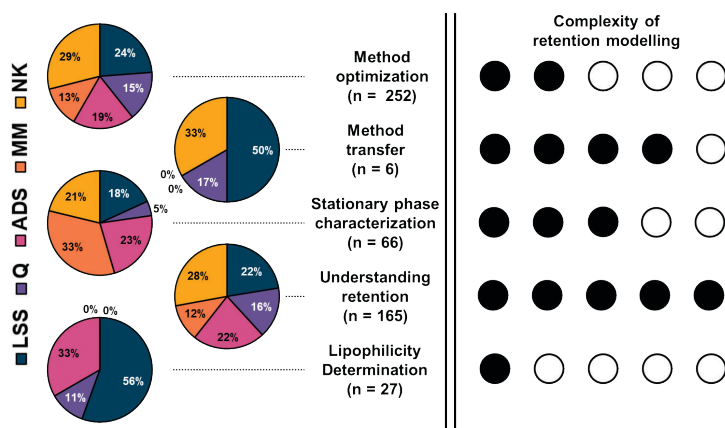


Figure 2.9. Overview of the different models applied per application. The total number of research papers is found under the title of the application. On the right the degree of complexity is given for the five different application fields.

2.5. Concluding remarks

The aim of this review was to provide a comprehensive overview of strategies for and applications of retention modelling. After reviewing the recent literature, we can also make a number of recommendations.

- > Studies on retention modelling are typically limited to specific purposes, such as method optimization or method transfer. However, from a mathematical point of view, retention modelling is ultimately an exercise in regression statistics and insights obtained in one study should – in principle – be applicable for all purposes.
- > To our surprise, numerical information on the outcome of retention modelling (e.g. residuals) are rarely reported. Also, in retention-modelling studies the experimental (raw) input data and relevant conditions, such as the column dead volume and the dwell volume, are often not reported. It is repeatedly unclear how specific regression results or model parameters were obtained. Unfortunately, all these factors affect the accuracy and precision of the reported retention model parameters [32,33,40]. Therefore, it is often not possible to reproduce or critically evaluate published work.
- > The main application of retention modelling lies in the understanding, description and prediction of retention. There is currently no consensus on the quality of retention models, which frustrates the comparison and evaluation of models. Reported prediction errors range from 0.1% to 10%, but almost all authors speak of “accurate” or “good” models. Some uniformity is badly needed. Given the high efficiency of LC separations, small variations in retention times may result in large variations in resolution. Therefore, retention models for application in method development and optimization require predictions (well) within 1%.
- > A potentially important application of retention modelling is method transfer. Given the enormous diversity in columns and the continuous innovation in instrumentation, method transfer is increasingly needed. Retention (model) parameters may facilitate a successful transfer of existing methods without a need for renewed method optimization.
- > If better care is taken of the quality of measurements and reporting, model parameters may eventually be used as system-independent retention data, which is an attractive proposition.

References

- [1] Schoenmakers, P. J., Billiet, H. A. H., Tussen, R., De Galan, L., Gradient selection in reversed-phase liquid chromatography. *J. Chromatogr. A* 1978, 149, 519–537.
- [2] Martel, S., Gillerat, F., Carosati, E., Maiarelli, D., Tetko, I. V., Mannhold, R., Carrupt, P. A., Large, chemically diverse dataset of log P measurements for benchmarking studies. *Eur. J. Pharm. Sci.* 2013, 48, 21–29.
- [3] Xiang, Q., Shan, G., Wu, W., Jin, H., Zhu, L., Measuring log Kow coefficients of neutral species of perfluoroalkyl carboxylic acids using reversed-phase high-performance liquid chromatography. *Environ. Pollut.* 2018, 242, 1283–1290.
- [4] Marchand, D. H., Snyder, L. R., Dolan, J. W., Characterization and applications of reversed-phase column selectivity based on the hydrophobic-subtraction model. *J. Chromatogr. A* 2008, 1191, 2–20.
- [5] Snyder, L. R., Dolan, J. W., Carr, P. W., The hydrophobic-subtraction model of reversed-phase column selectivity. *J. Chromatogr. A* 2004, 1060, 77–116.
- [6] Abraham, M. H., Scales of solute hydrogen-bonding: Their construction and application to physicochemical and biochemical processes. *Chem. Soc. Rev.* 1993, 22, 73–83.
- [7] Abraham, M. H., Rosés, M., Poole, C. F., Poole, S. K., Hydrogen bonding. 42. Characterization of reversed-phase high-performance liquid chromatographic C18 stationary phases. *J. Phys. Org. Chem.* 1997, 10, 358–368.
- [8] Snyder, L. R., Dolan, J. W., Marchand, D. H., Carr, P. W., The hydrophobic-Subtraction model of reversed-phase column selectivity. *Adv. Chromatogr.* 2015, 50, 297–376.
- [9] Græsbøll, R., Nielsen, N. J., Christensen, J. H., Using the hydrophobic subtraction model to choose orthogonal columns for online comprehensive two-dimensional liquid chromatography. *J. Chromatogr. A* 2014, 1326, 39–46.
- [10] Kaliszán, R., QSRR: Quantitative structure-(chromatographic) retention relationships. *Chem. Rev.* 2007, 107, 3212–3246.
- [11] Kaliszán, R., Baczek, T., Buciński, A., Buszewski, B., Sztupecka, M., Prediction of gradient retention from the linear solvent strength (LSS) model, quantitative structure-retention relationships (QSRR), and artificial neural networks (ANN). *J. Sep. Sci.* 2003, 26, 271–282.
- [12] Novotná, K., Havlíš, J., Havel, J., Optimisation of high performance liquid chromatography separation of neuroprotective peptides: Fractional experimental designs combined with artificial neural networks. *J. Chromatogr. A* 2005, 1096, 50–57.
- [13] Barron, L. P., McEneff, G. L., Gradient liquid chromatographic retention time prediction for suspect screening applications: A critical assessment of a generalised artificial neural network-based approach across 10 multi-residue reversed-phase analytical methods. *Talanta* 2016, 147, 261–270.
- [14] Euerby, M. R., Hulse, J., Petersson, P., Vazhentsev, A., Kassam, K., Retention modelling in hydrophilic interaction chromatography. *Anal. Bioanal. Chem.* 2015, 407, 9135–9152.
- [15] Pirok, B. W. J., Molenaar, S. R. A., van Outersterp, R. E., Schoenmakers, P. J., Applicability of retention modelling in hydrophilic-interaction liquid chromatography for algorithmic optimization programs with gradient-scanning techniques. *J. Chromatogr. A* 2017, 1530, 104–111.
- [16] Tyteca, E., Périat, A., Rudaz, S., Desmet, G., Guillaume, D., Retention modeling and method development in hydrophilic interaction chromatography. *J. Chromatogr. A* 2014, 1337, 116–127.
- [17] Gilar, M., Hill, J., McDonald, T. S., Gritti, F., Utility of linear and nonlinear models for retention prediction in liquid chromatography. *J. Chromatogr. A* 2020, 1613, 460690.
- [18] Molnar, I., Computerized design of separation strategies by reversed-phase liquid chromatography: Development of DryLab software. *J. Chromatogr. A* 2002, 965, 175–194.

- [19] Tyteca, E., Liekens, A., Clicq, D., Fanigliulo, A., Debrus, B., Rudaz, S., Guillaume, D., Desmet, G., Predictive elution window stretching and shifting as a generic search strategy for automated method development for liquid chromatography. *Anal. Chem.* 2012, 84, 7823–7830.
- [20] Pirok, B. W. J., Pous-Torres, S., Ortiz-Bolsico, C., Vivó-Truyols, G., Schoenmakers, P. J., Program for the interpretive optimization of two-dimensional resolution. *J. Chromatogr. A* 2016, 1450, 29–37.
- [21] Snyder, L. R., Dolan, J. W., Gant, J. R., Gradient elution in high-performance liquid chromatography. I. Theoretical basis for reversed-phase systems. *J. Chromatogr. A* 1979, 165, 3–30.
- [22] Schoenmakers, P. J., Billiet, H. A. H., Tijssen, R., De Galan, L., Gradient selection in reversed-phase liquid chromatography. *J. Chromatogr. A* 1978, 149, 519–537.
- [23] Soczewinski, E., Solvent Composition Effects in Thin-Layer Chromatography Systems of the Type Silica Gel-Electron Donor Solvent. *Anal. Chem.* 1969, 41, 179–182.
- [24] Jandera, P., Churáček, J., Gradient elution in liquid chromatography. I. The influence of the composition of the mobile phase on the capacity ratio (retention volume, band width, and resolution) in isocratic elution - theoretical considerations. *J. Chromatogr. A* 1974, 91, 207–221.
- [25] Snyder, L. R., Poppe, H., Mechanism of solute retention in liquid—solid chromatography and the role of the mobile phase in affecting separation. *J. Chromatogr. A* 1980, 184, 363–413.
- [26] Soczewiński, E., Mechanistic molecular model of liquid-solid chromatography: Retention-eluent composition relationships. *J. Chromatogr. A* 2002, 965, 109–116.
- [27] Jin, G., Guo, Z., Zhang, F., Xue, X., Jin, Y., Liang, X., Study on the retention equation in hydrophilic interaction liquid chromatography. *Talanta* 2008, 76, 522–527.
- [28] Nikitas, P., Pappa-Louisi, A., Agrafiotou, P., Effect of the organic modifier concentration on the retention in reversed-phase liquid chromatography: II. Tests using various simplified models. *J. Chromatogr. A* 2002, 946, 33–45.
- [29] Nikitas, P., Pappa-Louisi, A., Agrafiotou, P., Effect of the organic modifier concentration on the retention in reversed-phase liquid chromatography: I. General semi-thermodynamic treatment for adsorption and partition mechanisms. *J. Chromatogr. A* 2002, 946, 9–32.
- [30] Neue, U. D., *Chromatographia*. Springer 2006, pp. S45–S53.
- [31] Neue, U. D., Kuss, H. J., Improved reversed-phase gradient retention modeling. *J. Chromatogr. A* 2010, 1217, 3794–3803.
- [32] Vivó-Truyols, G., Torres-Lapasió, J. R., García-Alvarez-Coque, M. C., Error analysis and performance of different retention models in the transference of data from/to isocratic/gradient elution. *J. Chromatogr. A* 2003, 1018, 169–181.
- [33] Vivó-Truyols, G., Torres-Lapasió, J. R., García-Alvarez-Coque, M. C., *Journal of Chromatography A*. Elsevier 2004, pp. 31–39.
- [34] Tyteca, E., Guillaume, D., Desmet, G., Use of individual retention modeling for gradient optimization in hydrophilic interaction chromatography: Separation of nucleobases and nucleosides. *J. Chromatogr. A* 2014, 1368, 125–131.
- [35] Jandera, P., Hájek, T., Vyňuchalová, K., Retention and bandwidths prediction in fast gradient liquid chromatography. Part 2-Core-shell columns. *J. Chromatogr. A* 2014, 1337, 57–66.
- [36] Schellinger, A. P., Carr, P. W., A practical approach to transferring linear gradient elution methods. *J. Chromatogr. A* 2005, 1077, 110–119.
- [37] Pirok, B. W. J., Molenaar, S. R. A., van Outersterp, R. E., Schoenmakers, P. J., Applicability of retention modelling in hydrophilic-interaction liquid chromatography for algorithmic optimization programs with gradient-scanning techniques. *J. Chromatogr. A* 2017, 1530, 104–111.

- [38] Roca, L. S., Schoemaker, S. E., Pirok, B. W. J., Gargano, A. F. G., Schoenmakers, P. J., Accurate modelling of the retention behaviour of peptides in gradient-elution hydrophilic interaction liquid chromatography. *J. Chromatogr. A* 2019, DOI: 10.1016/j.chroma.2019.460650.
- [39] Nikitas, P., Pappa-Louisi, A., Papageorgiou, A., Simple algorithms for fitting and optimisation for multilinear gradient elution in reversed-phase liquid chromatography. *J. Chromatogr. A* 2007, 1157, 178–186.
- [40] den Uijl, M. J., Schoenmakers, P. J., Schulte, G. K., Stoll, D. R., van Bommel, M. R., Pirok, B. W. J., Measuring and using scanning-gradient data for use in method optimization for liquid chromatography. *J. Chromatogr. A* 2021, 1636, 461780.
- [41] Akaike, H., A New Look at the Statistical Model Identification. *IEEE Trans. Automat. Contr.* 1974, 19, 716–723.
- [42] Horner, A. R., Wilson, R. E., Groskreutz, S. R., Murray, B. E., Weber, S. G., Evaluation of three temperature- and mobile phase-dependent retention models for reversed-phase liquid chromatographic retention and apparent retention enthalpy. *J. Chromatogr. A* 2019, 1589, 73–82.
- [43] Bos, T. S., Knol, W. C., Molenaar, S. R. A., Niezen, L. E., Schoenmakers, P. J., Somsen, G. W., Pirok, B. W. J., Recent applications of chemometrics in one- and two-dimensional chromatography. *J. Sep. Sci.* 2020, DOI: 10.1002/jssc.202000011.
- [44] Li, R., Sun, W., Xiao, X., Chen, B., Wei, Y., Retention of stevioside polar compounds on a sulfonic acid-functionalized stationary phase. *J. Chromatogr. A* 2020, DOI: 10.1016/j.chroma.2020.460978.
- [45] Komendová, M., Urban, J., Dual-retention mechanism of dopamine-related compounds on monolithic stationary phase with zwitterion functionality. *J. Chromatogr. A* 2020, 1618, DOI: 10.1016/j.chroma.2020.460893.
- [46] Česla, P., Vaňková, N., Křenková, J., Fischer, J., Comparison of isocratic retention models for hydrophilic interaction liquid chromatographic separation of native and fluorescently labeled oligosaccharides. *J. Chromatogr. A* 2016, 1438, 179–188.
- [47] Baczek, T., Markuszewski, M., Kaliszan, R., Straten, M. A. van, Claessens, H. A., Linear and Quadratic Relationships between Retention and Organic Modifier Content in Eluent in Reversed Phase High-Performance Liquid Chromatography: A Systematic Comparative Statistical Study. *J. High Resolut. Chromatogr.* 2000, 23, 667–676.
- [48] Zhang, S.-D., Gong, C., Lu, Y., Xu, X., Separation of Triacylglycerols from Edible Oil Using a Liquid Chromatography-Mass Spectrometry System with a Porous Graphitic Carbon Column and a Toluene-Isopropanol Gradient Mobile Phase. *J. Am. Oil Chem. Soc.* 2018, 95, 1253–1266.
- [49] Fekete, S., Beck, A., Veuthey, J. L., Guillaume, D., Proof of Concept to Achieve Infinite Selectivity for the Chromatographic Separation of Therapeutic Proteins. *Anal. Chem.* 2019, 91, 12954–12961.
- [50] Fekete, S., Ritchie, H., Lawhorn, J., Veuthey, J. L., Guillaume, D., Improving selectivity and performing online on-column fractioning in liquid chromatography for the separation of therapeutic biopharmaceutical products. *J. Chromatogr. A* 2020, DOI: 10.1016/j.chroma.2020.460901.
- [51] Alvarez-Segura, T., Camacho-Molinero, C., Torres-Lapasíó, J. R., García-Alvarez-Coque, M. C., Analysis of amino acids using serially coupled columns. *J. Sep. Sci.* 2017, 40, 2741–2751.
- [52] Jeong, L. N., Sajulga, R., Forte, S. G., Stoll, D. R., Rutan, S. C., Simulation of elution profiles in liquid chromatography—I: Gradient elution conditions, and with mismatched injection and mobile phase solvents. *J. Chromatogr. A* 2016, 1457, 41–49.
- [53] Gritti, F., Gilar, M., Hill, J., Mismatch between sample diluent and eluent: Maintaining integrity of gradient peaks using in silico approaches. *J. Chromatogr. A* 2019, 1608, DOI: 10.1016/j.chroma.2019.460414.
- [54] Boateng, B. O., Fever, M., Edwards, D., Petersson, P., Euerby, M. R., Sutcliffe, O. B., Chromatographic retention behaviour, modelling and optimization of a UHPLC-UV separation of the regioisomers of the Novel Psychoactive Substance (NPS) methoxphenidine (MXP). *J. Pharm. Biomed. Anal.* 2018, 153, 238–247.

- [55] Vaňková, N., De Vos, J., Tyteca, E., Desmet, G., Edge, T., Česlová, L., Česla, P., Eeltink, S., Effect of gradient steepness on the kinetic performance limits and peak compression for reversed-phase gradient separations of small molecules. *J. Chromatogr. A* 2015, 1409, 152–158.
- [56] Gritti, F., General theory of peak compression in liquid chromatography. *J. Chromatogr. A* 2016, 1433, 114–122.
- [57] Wilson, R. E., Groskreutz, S. R., Weber, S. G., Improving the Sensitivity, Resolution, and Peak Capacity of Gradient Elution in Capillary Liquid Chromatography with Large-Volume Injections by Using Temperature-Assisted On-Column Solute Focusing. *Anal. Chem.* 2016, 88, 5112–5121.
- [58] Rerick, M. T., Groskreutz, S. R., Weber, S. G., Multiplicative On-Column Solute Focusing Using Spatially Dependent Temperature Programming for Capillary HPLC. *Anal. Chem.* 2019, 91, 2854–2860.
- [59] Chang, Q., Shao, Y., Yang, Y., Yu, H., Wang, R., Chromatographic retention assisted deconvolution of liquid chromatography-mass spectrometry chromatogram of natural products. *Anal. Sci.* 2019, 35, 201–206.
- [60] Pirok, B. W. J., Stoll, D. R., Schoenmakers, P. J., Recent Developments in Two-Dimensional Liquid Chromatography: Fundamental Improvements for Practical Applications. *Anal. Chem.* 2019, 91, 240–263.
- [61] Pirok, B. W. J., Gargano, A. F. G., Schoenmakers, P. J., Optimizing separations in online comprehensive two-dimensional liquid chromatography. *J. Sep. Sci.* 2018, 41, 68–98.
- [62] Sarrut, M., D'Attoma, A., Heinisch, S., Optimization of conditions in on-line comprehensive two-dimensional reversed phase liquid chromatography: Experimental comparison with one-dimensional reversed phase liquid chromatography for the separation of peptides. *J. Chromatogr. A* 2015, 1421, 48–59.
- [63] Sarrut, M., Rouvière, F., Heinisch, S., Theoretical and experimental comparison of one dimensional versus on-line comprehensive two dimensional liquid chromatography for optimized sub-hour separations of complex peptide samples. *J. Chromatogr. A* 2017, 1498, 183–195.
- [64] Bernardin, M., Masle, A. Le, Bessueille-Barbier, F., Lienemann, C. P., Heinisch, S., Comprehensive two-dimensional liquid chromatography with inductively coupled plasma mass spectrometry detection for the characterization of sulfur, vanadium and nickel compounds in petroleum products. *J. Chromatogr. A* 2020, 1611, DOI: 10.1016/j.chroma.2019.460605.
- [65] Sarrut, M., Corgier, A., Fekete, S., Guillarme, D., Lascoux, D., Janin-Bussat, M. C., Beck, A., Heinisch, S., Analysis of antibody-drug conjugates by comprehensive on-line two-dimensional hydrophobic interaction chromatography x reversed phase liquid chromatography hyphenated to high resolution mass spectrometry. I – Optimization of separation conditions. *J. Chromatogr. B Anal. Technol. Biomed. Life Sci.* 2016, 1032, 103–111.
- [66] Iguiniz, M., Rouvière, F., Corbel, E., Roques, N., Heinisch, S., Comprehensive two dimensional liquid chromatography as analytical strategy for pharmaceutical analysis. *J. Chromatogr. A* 2018, 1536, 195–204.
- [67] D'Attoma, A., Grivel, C., Heinisch, S., On-line comprehensive two-dimensional separations of charged compounds using reversed-phase high performance liquid chromatography and hydrophilic interaction chromatography. Part I: Orthogonality and practical peak capacity considerations. *J. Chromatogr. A* 2012, 1262, 148–159.
- [68] Stoll, D. R., Sajulga, R. W., Voigt, B. N., Larson, E. J., Jeong, L. N., Rutan, S. C., Simulation of elution profiles in liquid chromatography – II: Investigation of injection volume overload under gradient elution conditions applied to second dimension separations in two-dimensional liquid chromatography. *J. Chromatogr. A* 2017, 1523, 162–172.
- [69] Muller, M., Tredoux, A. G. J., de Villiers, A., Predictive kinetic optimisation of hydrophilic interaction chromatography x reversed phase liquid chromatography separations: Experimental verification and application to phenolic analysis. *J. Chromatogr. A* 2018, 1571, 107–120.

- [70] Hewitt, E. F., Lukulay, P., Galushko, S., Implementation of a rapid and automated high performance liquid chromatography method development strategy for pharmaceutical drug candidates. *J. Chromatogr. A* 2006, 1107, 79–87.
- [71] Taheri, M., Moazeni-Pourasil, R. S., Sheikh-Olia-Lavasani, M., Karami, A., Ghassempour, A., Central composite design with the help of multivariate curve resolution in loadability optimization of RP-HPLC to scale-up a binary mixture. *J. Sep. Sci.* 2016, 39, 1031–1040.
- [72] Tyteca, E., Bieber, S., Letzel, T., Desmet, G., Possibilities and Limitations of Computer-Assisted Method Development in HILIC: A Case Study. *Chromatographia* 2017, 80, 771–781.
- [73] Fasoula, S., Zisi, C., Gika, H., Pappa-Louisi, A., Nikitas, P., Retention prediction and separation optimization under multilinear gradient elution in liquid chromatography with Microsoft Excel macros. *J. Chromatogr. A* 2015, 1395, 109–115.
- [74] Zisi, C., Pappa-Louisi, A., Nikitas, P., Separation optimization in HPLC analysis implemented in R programming language. *J. Chromatogr. A* 2020, 1617, DOI: 10.1016/j.chroma.2019.460823.
- [75] van Schaick, G., Pirok, B. W. J., Haselberg, R., Somsen, G. W., Gargano, A. F. G., Computer-aided gradient optimization of hydrophilic interaction liquid chromatographic separations of intact proteins and protein glycoforms. *J. Chromatogr. A* 2019, 1598, 67–76.
- [76] Khalaf, R., Baur, D., Pfister, D., Optimization of reversed-phase chromatography methods for peptide analytics. *J. Chromatogr. A* 2015, 1425, 198–203.
- [77] Zhang, Y., Computer simulation and optimization for reversed-phase HPLC separation: A novel algorithm simulating and optimizing the non-linear and non-ideal separation process in analytical chromatography. *Chemom. Intell. Lab. Syst.* 2015, 149, 73–80.
- [78] Alvarez-Segura, T., López-Ureña, S., Torres-Lapasió, J. R., García-Alvarez-Coque, M. C., Multi-scale optimisation vs. genetic algorithms in the gradient separation of diuretics by reversed-phase liquid chromatography. *J. Chromatogr. A* 2020, 1609, DOI: 10.1016/j.chroma.2019.460427.
- [79] Bos, T. S., Niezen, L. E., den Uijl, M. J., Molenaar, S. R. A., Lege, S., Schoenmakers, P. J., Somsen, G. W., Pirok, B. W. J., Reducing the influence of geometry-induced gradient deformation in liquid chromatographic retention modelling. *J. Chromatogr. A* 2021, 1635, 461714.
- [80] Jandera, P., Hájek, T., Possibilities of retention prediction in fast gradient liquid chromatography. Part 3: Short silica monolithic columns. *J. Chromatogr. A* 2015, 1410, 76–89.
- [81] Gritti, F., Gradient method transfer after changing the average pore diameter of the chromatographic stationary phase I – One-dimensional sample mixture. *J. Chromatogr. A* 2019, 1597, 119–131.
- [82] Stoll, D., Boswell, P., Caldow, S., HPLC Columns - HPLC column selectivity measurements of more than 600 reversed phase columns from over 30 manufacturers, <http://hplccolumns.org/about/index.php> (last time accessed: August 19, 2020).
- [83] Abraham, M. H., Chadha, H. S., Leo, A. J., Hydrogen bonding. XXXV. Relationship between high-performance liquid chromatography capacity factors and water-octanol partition coefficients. *J. Chromatogr. A* 1994, 685, 203–211.
- [84] Sykora, D., Vozka, J., Tesarova, E., Chromatographic methods enabling the characterization of stationary phases and retention prediction in high-performance liquid chromatography and supercritical fluid chromatography. *J. Sep. Sci.* 2016, 39, 115–131.
- [85] Žuvela, P., Skoczylas, M., Jay Liu, J., Baczek, T., Kaliszan, R., Wong, M. W., Buszewski, B., Bączek, T., Kaliszan, R., Wong, M. W., Buszewski, B., Baczek, T., Kaliszan, R., Wong, M. W., Buszewski, B., Bączek, T., Kaliszan, R., Wong, M. W., Buszewski, B., Baczek, T., Kaliszan, R., Wong, M. W., Buszewski, B., Bączek, T., Kaliszan, R., Wong, M. W., Buszewski, B., Column Characterization and Selection Systems in Reversed-Phase High-Performance Liquid Chromatography. *Chem. Rev.* 2019, 119, 3674–3729.

- [86] Visky, D., Vander Heyden, Y., Iványi, T., Baten, P., De Beer, J., Kovács, Z., Noszál, B., Roets, E., Massart, D. L., Hoogmartens, J., Characterisation of reversed-phase liquid chromatographic columns by chromatographic tests. Evaluation of 36 test parameters: Repeatability, reproducibility and correlation. *J. Chromatogr. A* 2002, 977, 39–58.
- [87] Galea, C., Mangelings, D., Vander Heyden, Y., Characterization and classification of stationary phases in HPLC and SFC - a review. *Anal. Chim. Acta* 2015, 886, 1–15.
- [88] Wang, L., Wei, W., Xia, Z., Jie, X., Xia, Z. Z., Recent advances in materials for stationary phases of mixed-mode high-performance liquid chromatography. *TrAC - Trends Anal. Chem.* 2016, 80, 495–506.
- [89] Khalaf, R., Forrer, N., Buffolino, G., Butté, A., Morbidelli, M., Model-based description of peptide retention on doped reversed-phase media. *J. Chromatogr. A* 2015, 1407, 169–175.
- [90] Lincoln, D. R., Lavrik, N. V., Kravchenko, I. I., Sepaniak, M. J., Retention in Porous Layer Pillar Array Planar Separation Platforms. *Anal. Chem.* 2016, 88, 8741–8748.
- [91] Li, Y., Zhu, N., Chen, T., Wei, M., Ma, Y., Stationary Phase Based on β -Cyclodextrin and Poly(N-isopropylacrylamide) for HILIC and RPLC. *Chromatographia* 2016, 79, 29–36.
- [92] Peristyy, A., Paull, B., Nesterenko, P. N., Chromatographic performance of synthetic polycrystalline diamond as a stationary phase in normal phase high performance liquid chromatography. *J. Chromatogr. A* 2015, 1391, 49–59.
- [93] Qiao, L., Shi, X., Xu, G., Recent advances in development and characterization of stationary phases for hydrophilic interaction chromatography. *TrAC - Trends Anal. Chem.* 2016, 81, 23–33.
- [94] Vyňuchalová, K., Jandera, P., Comparison of a C30 bonded silica column and columns with shorter bonded ligands in reversed-phase LC. *Chromatographia* 2015, 78, 861–871.
- [95] Jandera, P., Reversed-phase liquid chromatography of homologous series. A general method for prediction of retention. *J. Chromatogr. A* 1984, 314, 13–36.
- [96] Héron, S., Charbonneau, D., Albisson, P., Estievenart, G., Groni, S., Tchaplá, A., A new methodology to determine the isoelutropic conditions on ultra-performance flash purification stationary phases from analytical reversed liquid chromatography stationary phase. *J. Chromatogr. A* 2015, 1397, 59–72.
- [97] Lunn, D. B., Yun, Y. J., Jorgenson, J. W., Retention and effective diffusion of model metabolites on porous graphitic carbon. *J. Chromatogr. A* 2017, 1530, 112–119.
- [98] Gilar, M., McDonald, T. S., Gritti, F., Roman, G. T., Johnson, J. S., Bunner, B., Michienzi, J. D., Collamati, R. A., Murphy, J. P., Satpute, D. D., Bannon, M. P., DellaRovere, D., Jencks, R. A., Dourdeville, T. A., Fadgen, K. E., Gerhardt, G. C., Chromatographic performance of microfluidic liquid chromatography devices: Experimental evaluation of straight versus serpentine packed channels. *J. Chromatogr. A* 2018, 1533, 127–135.
- [99] Jandera, P., Staňková, M., Hájek, T., New zwitterionic polymethacrylate monolithic columns for one- and two-dimensional microliquid chromatography. *J. Sep. Sci.* 2013, 36, 2430–2440.
- [100] Douša, M., 1H-Tetrazole-5-amine Immobilized on Substituted Polymer Gel/Silica as a New Stationary Phase for Hydrophilic Interaction Chromatography. *Chromatographia* 2018, 81, 349–357.
- [101] Li, S., Li, Z., Zhang, F., Geng, H., Yang, B., A polymer-based zwitterionic stationary phase for hydrophilic interaction chromatography. *Talanta* 2020, 216, DOI: 10.1016/j.talanta.2020.120927.
- [102] Kalíková, K., Voborná, M., Tesařová, E., Chromatographic behavior of new deazapurine ribonucleosides in hydrophilic interaction liquid chromatography. *Electrophoresis* 2018, 39, 2144–2151.
- [103] Peng, Y., Hou, Y., Zhang, F., Shen, G., Yang, B., A hyperbranched polyethylenimine functionalized stationary phase for hydrophilic interaction liquid chromatography. *Anal. Bioanal. Chem.* 2016, 408, 3633–3638.
- [104] Peng, Y., Zhang, F., Pan, X., Hou, Y., Yang, B., Poly(vinyl alcohol)-cationic cellulose copolymer encapsulated SiO₂ stationary phase for hydrophilic interaction liquid chromatography. *RSC Adv.* 2017, 7, 21336–21341.

- [105] Li, H., Zhang, X., Zhang, L., Cang, H., Kong, F., Fan, D., Wang, W., Hyperbranched polyglycerol functionalized silica stationary phase for hydrophilic interaction liquid chromatography. *Anal. Sci.* 2018, 34, 433–438.
- [106] Geng, H., Jing, J., Zhang, F., Zhang, F., Yang, B., A polar stationary phase obtained by surface-initiated polymerization of hyperbranched polyglycerol onto silica. *Talanta* 2020, 209, DOI: 10.1016/j.talanta.2019.120525.
- [107] Wang, Y., Bu, H., Wang, L., Wang, L., Guo, Y., Liang, X., Wang, S., High efficiency and simple preparation of polyacrylamide coated silica stationary phase for hydrophilic interaction liquid chromatography. *J. Chromatogr. A* 2019, 1605, DOI: 10.1016/j.chroma.2019.07.011.
- [108] Hou, Y., Zhang, F., Liang, X., Yang, B., Liu, X., Dasgupta, P. K., Poly(vinyl alcohol) Modified Porous Graphitic Carbon Stationary Phase for Hydrophilic Interaction Liquid Chromatography. *Anal. Chem.* 2016, 88, 4676–4681.
- [109] Ding, L., Guo, Z., Hu, Z., Liang, X., Mixed-mode reversed phase/positively charged repulsion chromatography for intact protein separation. *J. Pharm. Biomed. Anal.* 2017, 138, 63–69.
- [110] Wang, X., Bo, C., Wang, C., Wei, Y., Controllable preparation of a hydrophilic/ion-exchange mixed-mode stationary phase by surface-initiated atom transfer radical polymerization using a mixture of two functional monomers. *J. Sep. Sci.* 2017, 40, 1861–1868.
- [111] Staňková, M., Jandera, P., Dual Retention Mechanism in Two-Dimensional LC Separations of Barbiturates, Sulfonamides, Nucleic Bases and Nucleosides on Polymethacrylate Zwitterionic Monolithic Micro-Columns. *Chromatographia* 2016, 79, 657–666.
- [112] Jin, G., Guo, Z., Zhang, F., Xue, X., Jin, Y., Liang, X., Study on the retention equation in hydrophilic interaction liquid chromatography. *Talanta* 2008, 76, 522–527.
- [113] Komendová, M., Ribeiro, L. F., Urban, J., Controlling selectivity of polymer-based monolithic stationary phases. *J. Sep. Sci.* 2019, 42, 952–961.
- [114] Jandera, P., Janás, P., Recent advances in stationary phases and understanding of retention in hydrophilic interaction chromatography. A review. *Anal. Chim. Acta* 2017, 967, 12–32.
- [115] Vera, C. M., Shock, D., Dennis, G. R., Samuelsson, J., Enmark, M., Fornstedt, T., Shalliker, R. A., A preliminary study on the selectivity of linear polynuclear aromatic hydrocarbons in SFC using phenyl-type stationary phases. *Microchem. J.* 2015, 121, 136–140.
- [116] Vera, C. M., Shock, D., Dennis, G. R., Samuelsson, J., Enmark, M., Fornstedt, T., Shalliker, R. A., Contrasting selectivity between HPLC and SFC using phenyl-type stationary phases: A study on linear polynuclear aromatic hydrocarbons. *Microchem. J.* 2015, 119, 40–43.
- [117] Gritti, F., Belanger, J., Izzo, G., Leveille, W., On the performance of conically shaped columns: Theory and practice. *J. Chromatogr. A* 2019, 1593, 34–46.
- [118] Jeong, L. N., Rutan, S. C., Simulation of elution profiles in liquid chromatography – III. Stationary phase gradients. *J. Chromatogr. A* 2018, 1564, 128–136.
- [119] Cain, C. N., Forzano, A. V., Rutan, S. C., Collinson, M. M., Experimental- and simulation-based investigations of coupling a mobile phase gradient with a continuous stationary phase gradient. *J. Chromatogr. A* 2019, 1602, 237–245.
- [120] Tyteca, E., De Vos, J., Vankova, N., Cesla, P., Desmet, G., Eeltink, S., Applicability of linear and nonlinear retention-time models for reversed-phase liquid chromatography separations of small molecules, peptides, and intact proteins. *J. Sep. Sci.* 2016, 39, 1249–1257.
- [121] Jandera, P., Hájek, T., Šromová, Z., Mobile phase effects in reversed-phase and hydrophilic interaction liquid chromatography revisited. *J. Chromatogr. A* 2018, 1543, 48–57.
- [122] Jandera, P., Kučerová, M., Prediction of retention in gradient-elution normal-phase high performance liquid chromatography with binary solvent gradients. *J. Chromatogr. A* 1997, 759, 13–25.

- [123] Baeza-Baeza, J. J., García-Alvarez-Coque, M. C., Extension of the linear solvent strength retention model including a parameter that describes the elution strength changes in liquid chromatography. *J. Chromatogr. A* 2020, 1615, DOI: 10.1016/j.chroma.2019.460757.
- [124] Navarro-Huerta, J. A., Gisbert-Alonso, A., Torres-Lapasió, J. R., García-Alvarez-Coque, M. C., Benefits of solvent concentration pulses in retention time modelling of liquid chromatography. *J. Chromatogr. A* 2019, 1597, 76–88.
- [125] Blumberg, L. M., Migration and elution equations in gradient liquid chromatography. *J. Chromatogr. A* 2019, 1599, 35–45.
- [126] De Luca, C., Felletti, S., Macis, M., Cabri, W., Lievore, G., Chenet, T., Pasti, L., Morbidelli, M., Cavazzini, A., Catani, M., Ricci, A., Modeling the nonlinear behavior of a bioactive peptide in reversed-phase gradient elution chromatography. *J. Chromatogr. A* 2020, 1616, DOI: 10.1016/j.chroma.2019.460789.
- [127] Hao, W., Wang, K., Yue, B., Chen, Q., Huang, Y., Yu, J., Li, D., Influence of the pre-elution of solute in initial mobile phase on retention time and peak compression under linear gradient elution. *J. Chromatogr. A* 2020, 1618, DOI: 10.1016/j.chroma.2020.460858.
- [128] Wu, D., Lucy, C. A., Study of the slope of the linear relationship between retention and mobile phase composition (Snyder-Soczewiński model) in normal phase liquid chromatography with bonded and charge-transfer phases. *J. Chromatogr. A* 2016, 1475, 31–40.
- [129] Kartsova, L. A., Bessonova, E. A., Somova, V. D., Hydrophilic Interaction Chromatography. *J. Anal. Chem.* 2019, 74, 415–424.
- [130] Guo, Y., Recent progress in the fundamental understanding of hydrophilic interaction chromatography (HILIC). *Analyst* 2015, 140, 6452–6466.
- [131] McCalley, D. V., Understanding and manipulating the separation in hydrophilic interaction liquid chromatography. *J. Chromatogr. A* 2017, 1523, 49–71.
- [132] Jandera, P., Hájek, T., Mobile phase effects on the retention on polar columns with special attention to the dual hydrophilic interaction–reversed-phase liquid chromatography mechanism, a review. *J. Sep. Sci.* 2018, 41, 145–162.
- [133] Taraji, M., Haddad, P. R., Amos, R. I. J., Talebi, M., Szucs, R., Dolan, J. W., Pohl, C. A., Chemometric-assisted method development in hydrophilic interaction liquid chromatography: A review. *Anal. Chim. Acta* 2018, 1000, 20–40.
- [134] Maksić, J., Tumpa, A., Stajić, A., Jovanović, M., Rakić, T., Jancic-Stojanovic, B., Hydrophilic interaction liquid chromatography in analysis of granisetron HCl and its related substances. Retention mechanisms and method development. *J. Pharm. Biomed. Anal.* 2016, 123, 93–103.
- [135] Douša, M., Doubský, J., Separation of structurally related primary aliphatic amines using hydrophilic interaction chromatography with fluorescence detection after postcolumn derivatization with o-phthaldialdehyde/mercaptoethanol. *J. Sep. Sci.* 2017, 40, 4689–4699.
- [136] Xu, X., Gevaert, B., Bracke, N., Yao, H., Wynendaele, E., De Spiegeleer, B., Hydrophilic interaction liquid chromatography method development and validation for the assay of HEPES zwitterionic buffer. *J. Pharm. Biomed. Anal.* 2017, 135, 227–233.
- [137] Kokotou, M. G., Thomaidis, N. S., Characterization of the retention of artificial sweeteners by hydrophilic interaction liquid chromatography. *Anal. Lett.* 2018, 51, 49–72.
- [138] Kasagić-Vujanović, I., Jančić-Stojanović, B., Ivanović, D., Investigation of the retention mechanisms of amlodipine besylate, bisoprolol fumarate, and their impurities on three different HILIC columns. *J. Liq. Chromatogr. Relat. Technol.* 2018, 41, 523–531.
- [139] Tircova, B., Kozlik, P., HILIC-MS/MS Method for Analysis of Ephedrine in Internet-available Drugs. *Chromatographia* 2017, 80, 523–528.

- [140] Česla, P., Vaňková, N., Křenková, J., Fischer, J., Comparison of isocratic retention models for hydrophilic interaction liquid chromatographic separation of native and fluorescently labeled oligosaccharides. *J. Chromatogr. A* 2016, 1438, 179–188.
- [141] Rácz, N., Nagy, J., Jiang, W., Veress, T., Modeling Retention Behavior on Analysis of Hallucinogenic Mushrooms Using Hydrophilic Interaction Liquid Chromatography. *J. Chromatogr. Sci.* 2019, 57, 230–237.
- [142] Wang, N., Boswell, P. G., Accurate prediction of retention in hydrophilic interaction chromatography by back calculation of high pressure liquid chromatography gradient profiles. *J. Chromatogr. A* 2017, 1520, 75–82.
- [143] Jandera, P., Hájek, T., Utilization of dual retention mechanism on columns with bonded PEG and diol stationary phases for adjusting the separation selectivity of phenolic and flavone natural antioxidants. *J. Sep. Sci.* 2009, 32, 3603–3619.
- [144] Obradović, D., Oljačić, S., Nikolić, K., Agbaba, D., Investigation and prediction of retention characteristics of imidazoline and serotonin receptor ligands and their related compounds on mixed-mode stationary phase. *J. Chromatogr. A* 2019, 1585, 92–104.
- [145] Balkatzopoulou, P., Fasoula, S., Gika, H., Nikitas, P., Pappa-Louisi, A., Retention prediction of highly polar ionizable solutes under gradient conditions on a mixed-mode reversed-phase and weak anion-exchange stationary phase. *J. Chromatogr. A* 2015, 1396, 72–76.
- [146] Navarro-Huerta, J. A., Vargas-García, A. G., Torres-Lapasió, J. R., García-Alvarez-Coque, M. C., Interpretive search of optimal isocratic and gradient separations in micellar liquid chromatography in extended organic solvent domains. *J. Chromatogr. A* 2020, 1616, DOI: 10.1016/j.chroma.2019.460784.
- [147] Hegade, R. S., De Beer, M., Lynen, F., Chiral stationary phase optimized selectivity liquid chromatography: A strategy for the separation of chiral isomers. *J. Chromatogr. A* 2017, 1515, 109–117.
- [148] Tyteca, E., Desfontaine, V., Desmet, G., Guillaume, D., Possibilities of retention modeling and computer assisted method development in supercritical fluid chromatography. *J. Chromatogr. A* 2015, 1381, 219–228.
- [149] De Pauw, R., Shoykhet (Choikhet), K., Desmet, G., Broeckhoven, K., Effect of reference conditions on flow rate, modifier fraction and retention in supercritical fluid chromatography. *J. Chromatogr. A* 2016, 1459, 129–135.
- [150] Stankov, V., Cvetnić, M., Novak Stankov, M., Rogošić, M., Bolanča, T., Ukić, Š., Retention Modeling of Gradient Elutions: Application of Iso-to-Grad Approach for LC Systems with Dual-Species Eluent. *Chromatographia* 2019, 82, 749–755.
- [151] Tsui, H. W., Kuo, C. H., Huang, Y. C., Elucidation of retention behaviors in reversed-phase liquid chromatography as a function of mobile phase composition. *J. Chromatogr. A* 2019, 1595, 127–135.
- [152] Gritti, F., Combined solvent- and non-uniform temperature-programmed gradient liquid chromatography. I – A theoretical investigation. *J. Chromatogr. A* 2016, 1473, 38–47.
- [153] Groskreutz, S. R., Weber, S. G., Temperature-assisted solute focusing with sequential trap/release zones in isocratic and gradient capillary liquid chromatography: Simulation and experiment. *J. Chromatogr. A* 2016, 1474, 95–108.
- [154] Andrés, A., Téllez, A., Rosés, M., Bosch, E., Chromatographic models to predict the elution of ionizable analytes by organic modifier gradient in reversed phase liquid chromatography. *J. Chromatogr. A* 2012, 1247, 71–80.
- [155] Téllez, A., Rosés, M., Bosch, E., Modeling the retention of neutral compounds in gradient elution RP-HPLC by means of polarity parameter models. *Anal. Chem.* 2009, 81, 9135–9145.
- [156] Andrés, A., Rosés, M., Bosch, E., Prediction of the chromatographic retention of acid-base compounds in pH buffered methanol-water mobile phases in gradient mode by a simplified model. *J. Chromatogr. A* 2015, 1385, 42–48.

- [157] Sasaki, T., Todoroki, K., Toyóoka, T., Simultaneous optimization of pH and binary organic composition by grid form modeling of the retention behavior in reversed-phase ultra high-performance liquid chromatography. *J. Pharm. Biomed. Anal.* 2017, 146, 251–260.
- [158] Wang, F., Yang, F., Tian, Y., Liu, J., Shen, J., Bai, Q., Studies on the retention mechanism of solutes in hydrophilic interaction chromatography using stoichiometric displacement theory I. The linear relationship of $\lg k'$ vs. $\lg[H_2O]$. *Talanta* 2018, 176, 499–508.
- [159] Obradović, D., Komsta, Ł., Agbaba, D., Novel computational approaches to retention modeling in dual hydrophilic interactions/reversed phase chromatography. *J. Chromatogr. A* 2020, 1619, DOI: 10.1016/j.chroma.2020.460951.
- [160] Tyteca, E., Desmet, G., On the inherent data fitting problems encountered in modeling retention behavior of analytes with dual retention mechanism. *J. Chromatogr. A* 2015, 1403, 81–95.
- [161] Tumpa, A., Mišković, S., Stanimirović, Z., Jančić-Stojanović, B., Medenica, M., Modeling of HILIC retention behavior with theoretical models and new spline interpolation technique. *J. Chromatogr. A* 2017, 31, e2910.
- [162] Arnott, J. A., Planey, S. L., The influence of lipophilicity in drug discovery and design. *Expert Opin. Drug Discov.* 2012, 7, 863–875.
- [163] Chmiel, T., Mieszkowska, A., Kempńska-Kupczyk, D., Kot-Wasik, A., Namieśnik, J., Mazerska, Z., The impact of lipophilicity on environmental processes, drug delivery and bioavailability of food components. *Microchem. J.* 2019, 146, 393–406.
- [164] Liang, C., Lian, H. zhen, Recent advances in lipophilicity measurement by reversed-phase high-performance liquid chromatography. *TrAC - Trends Anal. Chem.* 2015, 68, 28–36.
- [165] YAMAGAMI, C., YOKOTA, M., TAKAO, N., Hydrophobicity Parameters Determined by Reversed-Phase Liquid Chromatography. IX. Relationship between Capacity Factor and Water-Octanol Partition Coefficient of Monosubstituted Pyrimidines. *Chem. Pharm. Bull. (Tokyo)*. 1994, 42, 907–912.
- [166] Giaginis, C., Tsantili-Kakoulidou, A., Current State of the Art in HPLC Methodology for Lipophilicity Assessment of Basic Drugs. A Review. *J. Liq. Chromatogr. Relat. Technol.* 2007, 31, 79–96.
- [167] Braumann, T., Determination of hydrophobic parameters by reversed-phase liquid chromatography: theory, experimental techniques, and application in studies on quantitative structure-activity relationships. *J. Chromatogr. A* 1986, 373, 191–225.
- [168] Gritti, F., Gilar, M., Walter, T. H., Wyndham, K., Retention loss of reversed-phase chromatographic columns using 100% aqueous mobile phases from fundamental insights to best practice. *J. Chromatogr. A* 2020, 1612, 460662.
- [169] Liang, C., Qiao, J. qin, Lian, H. zhen, Determination of reversed-phase high performance liquid chromatography based octanol-water partition coefficients for neutral and ionizable compounds: Methodology evaluation. *J. Chromatogr. A* 2017, 1528, 25–34.
- [170] Sobańska, A. W., Application of planar chromatographic descriptors to the prediction of physicochemical properties and biological activity of compounds. *J. Liq. Chromatogr. Relat. Technol.* 2018, 41, 255–271.
- [171] Sztanke, M., Tuzimski, T., Janicka, M., Sztanke, K., Structure-retention behaviour of biologically active fused 1,2,4-triazinones - Correlation with in silico molecular properties. *Eur. J. Pharm. Sci.* 2015, 68, 114–126.
- [172] Hawrył, A. M., Popiołek, Ł. P., Hawrył, M. A., Świeboda, R. S., Niejedli, M. A., Chromatographic and calculation methods for analysis of the lipophilicity of newly synthesized thiosemicarbazides and their cyclic analogues 1,2,4-triazol-3-thiones. *J. Braz. Chem. Soc.* 2015, 26, 1617–1624.
- [173] Klose, M. H. M., Theiner, S., Varbanov, H. P., Hoefler, D., Pichler, V., Galanski, M., Meier-Menches, S. M., Keppler, B. K., Development and validation of liquid chromatography-based methods to assess the lipophilicity of cytotoxic platinum(IV) complexes. *Inorganics* 2018, 6, DOI: 10.3390/inorganics6040130.

- [174] Malík, I., Csöllei, J., Solovič, I., Pospíšilová, S., Michnová, H., Jampílek, J., Čížek, A., Kapustíková, I., Čurillová, J., Pecháčková, M., Stolaríková, J., Pecher, D., Oravec, M., Dibasic derivatives of phenylcarbamic acid against mycobacterial strains: Old drugs and new tricks? *Molecules* 2018, 23, DOI: 10.3390/molecules23102493.
- [175] Bem, M., Radutiu, A. C., Voicescu, M., Caproiu, M. T., Draghici, C., Maganu, M., Enache, C., Constantinescu, T., Balaban, A. T., 7-Nitrobenzo[c][1,2,5]oxadiazole (nitrobenzofurazan) derivatives with a sulfide group at the 4-position. Synthesis and physical properties. *Rev. Roum. Chim.* 2018, 63, 149–155.
- [176] Gomes, J. C., Cianni, L., Ribeiro, J., dos Reis Rocho, F., da Costa Martins Silva, S., Batista, P. H. J., Moraes, C. B., Franco, C. H., Freitas-Junior, L. H. G., Kenny, P. W., Leitão, A., Burtoloso, A. C. B., de Vita, D., Montanari, C. A., Synthesis and structure-activity relationship of nitrile-based cruzain inhibitors incorporating a trifluoroethylamine-based P2 amide replacement. *Bioorganic Med. Chem.* 2019, 27, DOI: 10.1016/j.bmc.2019.115083.
- [177] Hawrył, A., Kuśmierz, E., Hawrył, M., Świeboda, R., Wujec, M., Determination of lipophilicity of new thiosemicarbazide and 1,2,4-triazole-3-thione derivatives using reversed-phase HPLC method and theoretical calculations. *J. Liq. Chromatogr. Relat. Technol.* 2015, 38, 430–437.
- [178] Pachuta-Stec, A., Hawrył, A. M., Wróbel, A., Hawrył, M. A., Pitucha, M., Chromatographic Evaluation of the Lipophilic Properties of Some 1,2,4-Triazole with Potential Antitumour Activity. *J. Liq. Chromatogr. Relat. Technol.* 2015, 38, 1199–1206.
- [179] Tosti, T., Šegan, S., Milić, D., Radoičić, A., Tešić, Ž., Milojković-Opsenica, D., Estimation of Lipophilicity of Some Polyoxygenated Steroids by the Means of Normal-Phase Thin-Layer Chromatography. *J. Liq. Chromatogr. Relat. Technol.* 2015, 38, 1097–1103.
- [180] Yükses, H., Koca, E., Gürsoy-Kol, Ö., Akyıldırım, O., Çelebier, M., Synthesis, in vitro antioxidant activity, and physicochemical properties of novel 4,5-dihydro-1H-1,2,4-triazol-5-one derivatives. *J. Mol. Liq.* 2015, 206, 359–366.
- [181] Flieger, J., Tatarczak-Michalewska, M., Kowalska, A., Rzadkowska, M., Szacoń, E., Kaczor, A. A., Matosiuk, D., Fragmental method KowWIN as the powerful tool for prediction of chromatographic behavior of novel bioactive urea derivatives. *J. Braz. Chem. Soc.* 2016, 27, 2312–2321.
- [182] Marciniec, K., Boryczka, S., Chromatographic and Computational Assessment of Lipophilicity of New Anticancer Acetylenequinoline Derivatives. *J. Chromatogr. Sci.* 2017, 55, 934–939.
- [183] Gonec, T. T., Malík, I., Csöllei, J., Jampílek, J., Stolaríková, J., Solovic, I., Miku, P., Keltoová, S., Kollár, P., O'Mahony, J., Coffey, A., Synthesis and in vitro antimycobacterial activity of novel n-arylpiperazines containing an ethane-1,2-diyl connecting chain. *Molecules* 2017, 22, DOI: 10.3390/molecules22122100.
- [184] Milosevic, N. P., Kojic, V., Curcic, J., Jakimov, D., Milic, N., Banjac, N., Uscumlic, G., Kaliszan, R., Evaluation of in silico pharmacokinetic properties and in vitro cytotoxic activity of selected newly synthesized N-succinimide derivatives. *J. Pharm. Biomed. Anal.* 2017, 137, 252–257.

CHAPTER 3

Measuring Scanning Gradients

3. Measuring and using scanning-gradient data for use in method optimization for liquid chromatography

Abstract

The use of scanning gradients can significantly reduce method-development time in reversed-phase liquid chromatography. However, there is no consensus on how they can best be used. In the present work we set out to systematically investigate various factors and to formulate guidelines. Scanning gradients are used to establish retention models for individual analytes. Different retention models were compared by computing the Akaike information criterion and the prediction accuracy. The measurement uncertainty was found to influence the optimum choice of model. The use of a third parameter to account for non-linear relationships was consistently found not to be statistically significant. The duration (slope) of the scanning gradients was not found to influence the accuracy of prediction. The prediction error may be reduced by repeating scanning experiments or – preferably – by reducing the measurement uncertainty. It is commonly assumed that the gradient-slope factor, *i.e.* the ratio between slopes of the fastest and the slowest scanning gradients, should be at least three. However, in the present work we found this factor less important than the proximity of the slope of the predicted gradient to that of the scanning gradients. Also, interpolation to a slope between that of the fastest and the slowest scanning gradient is preferable to extrapolation. For comprehensive two-dimensional liquid chromatography (LC×LC) our results suggest that data obtained from fast second-dimension gradients cannot be used to predict retention in much slower first-dimension gradients.

Publication

Measuring and using scanning-gradient data for use in method optimization for liquid chromatography

Mimi J. den Uijl, Peter J. Schoenmakers, Grace K. Schulte, Dwight R. Stoll, Maarten R. van Bommel, and Bob W.J. Pirok

J. Chromatogr. A, **2021**, 1636, 461780, DOI: 10.1016/j.chroma.2020.461780

3.1. Introduction

High-performance liquid chromatography (HPLC) is an indispensable technique in a wide variety of fields, including food science, environmental chemistry, oil analysis, forensics and (bio-)pharmaceutics. In spite of decades of research and development, the mechanisms of HPLC separation are still not fully understood [1]. Among the large number of retention mechanisms available, reversed-phase liquid chromatography (RPLC) is the most-common separation mode. In RPLC, analytes are mainly separated based on differences in partitioning between a relatively hydrophilic (aqueous/organic) mobile phase and a relatively hydrophobic stationary phase [2]. To facilitate elution of all analytes within an appropriate time window, the solvent strength of the mobile phase can be increased during the run by increasing the percentage of organic modifier in a gradient program. Despite the fact that many chromatographic methods rely on gradient-elution RPLC as an HPLC workhorse, method development can still be time consuming, since gradient method development relies on adjustment of several method parameters including gradient slope, possible steps in the gradient and the initial time associated with an isocratic hold (if not zero). Especially for challenging samples, the large number of parameters that can be adjusted requires extensive trial-and-error or design-of-experiment optimization, requiring extensive gradient training data. This is particularly true for samples of short-term interest (e.g. impurity profiling for a pharmaceutical ingredient in development) or second-dimension separations in 2DLC, where RPLC is also predominantly used [3]. Still, too often method development involves a great number of trial-and-error experiments, rendering the use of LC time-consuming and costly.

To facilitate faster method development, many groups have explored the use of computer-aided method development through retention modelling [4–15]. The aim of this approach is to predict optimal method parameters for a specific sample and a specific chromatographic system (*i.e.* stationary-phase chemistry and mobile-phase composition) through simulation of retention times. Retention modelling will result in faster method development [9], while it may also yield a better understanding of the influence of different parameters on retention, such as organic-modifier concentration, pH and the buffer concentration [8,16,17]. It is thus not surprising that modelling has been widely applied to predict retention of solutes in RPLC as a function of pH, organic-modifier concentration, charge state of the analyte and temperature [18–20]. Several strategies for retention modelling exist, but some of these require either extensive knowledge of the analytes or large quantities of input data [18,21]. One interesting approach, which does not require any *a priori* knowledge, is the use of scouting experiments. This strategy is employed in several method-optimization software tools, such as Drylab [22], PEWS² [5] and PIOTR [8,9]. Here, a very limited set of specific

pre-set gradients are employed to obtain analyte retention times [23]. A suitable retention model, designed to describe retention as a function of mobile-phase composition, is fitted to the experimental data. This yields the retention parameters for each analyte as described by the model. The model is then used to simulate the separation for all analytes under a large number of different chromatographic conditions. Each of the resulting simulated chromatograms is then evaluated against one or more desirability criteria. The most optimal separation conditions can, for example, be determined using the Pareto-optimality approach [24]. This process is described in Fig. 3.1.

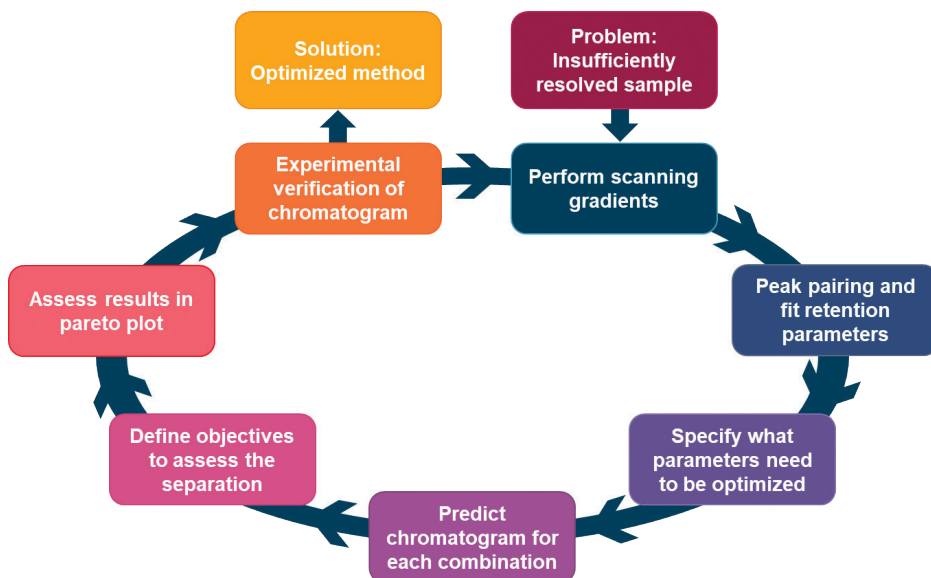


Figure 3.1. Workflow of the method optimization using scanning gradients to obtain retention-model parameters. The workflow starts at the top right with an insufficiently resolved sample, on which scanning gradients are performed. After that, the two (or more) scanning gradients are linked by peak tracking and the retention parameters are calculated. For the optimization, the different parameters that need to be optimized must be defined. The optimization program can predict outcomes for all combinations of these parameters. After that the assessment criteria must be defined and applied. The optimized separation can then be verified experimentally, which can either lead to an optimized method or trigger an additional iteration.

Retention-model parameters can either be determined from isocratic or gradient-elution retention data (or both) [5]. Isocratic measurements may yield a more accurate description of the retention as a function of mobile-phase composition, but require more tedious experimental work, whereas scanning gradients are less cumbersome. If the shape of the gradient can be accounted for then isocratic data can be used to accurately predict gradient-elution retention times [25,26], the opposite is less true [27].

Scanning experiments allow LC methods to be rapidly optimized. However, to the best of our knowledge, several factors that may influence the prediction accuracy in retention modelling have hardly been studied systematically, even though they may ultimately determine the usefulness of retention-time prediction. For RPLC, examples of such parameters include *i*) selection of the appropriate retention model and the number of parameters in the regression model, *ii*) the effect of the gradient slopes used (*e.g.* whether the use of faster gradients compromises parameter accuracy), *iii*) the minimum number of different gradient slopes required, *iv*) the minimum difference (leading to a different ratio) between these slopes, and *v*) the number of replicate measurements for each gradient elution condition.

In this work we have studied each of these aspects systematically using two sets of data having different measurement precision. For each data set by itself, each of the above-mentioned parameters is explained and investigated. Additionally, the feasibility and limitations of extrapolating (*i.e.* predicting much slower or faster gradients than those used for scanning) was investigated. Finally, the results are summarized, and guidelines are formulated for successful use of gradient-scanning techniques.

3.2. Experimental

3.2.1. Chemicals

For all measurements concerning the first dataset (Set X), the following chemicals were used. Milli-Q water (18.2 M Ω cm) was obtained from a purification system (Arium 611UV, Sartorius, Germany). Acetonitrile (ACN, LC-MS grade) and toluene (LC-MS grade) were purchased from Biosolve Chemie (Dieuze, France). Formic acid (FA, 98%) and propylparaben (propyl 4-hydroxybenzoate, \geq 99%) were purchased from Fluka (Buchs, Switzerland). Ammonium formate (AF, \geq 99%), cytosine (\geq 99%), sudan I (\geq 97%), propranolol (\geq 99%), trimethoprim (\geq 99%), uracil (\geq 99.0%), tyramine (\geq 98%) and the peptide mixture (HPLC peptide standard mixture, H2016) were obtained from Sigma Aldrich (Darmstadt, Germany). The peptides in the mixture were numbered one to five on their elution order in RPLC. The following dyes analysed in this study were authentic dyestuffs obtained from the reference collection of the Cultural Heritage Agency of the Netherlands (RCE, Amsterdam, The Netherlands): indigotin, purpurin, emodin, rutin, martius yellow, naphthol yellow S, fast red B, picric acid, flavazine L, orange IV. Stock solutions of all compounds were prepared at the concentrations and with the solvents indicated in Appendix A-1, Table A-1. From these stock solutions analytical samples were prepared by combining portions of the stock solutions in equal portions; the specific compounds that were combined into mixtures are also indicated in Table A-1.

For the second dataset (Set Y), the following chemicals were used. Milli-Q water (18.2 M Ω cm) was obtained from a purification system (Millipore, Billerica, MA) purpurin (\geq 90%), propylparaben (\geq 99%), emodin, toluene, trimethoprim, and the peptide mixture (HPLC peptide standard mixture) were obtained from Sigma Aldrich (United States). Rutin (\geq 94%) and cytosine were obtained from Sigma Aldrich (China). Berberine and naphthol yellow S were both obtained from Sigma Aldrich (India). Tyramine (\geq 98%) was obtained from Sigma Aldrich (Switzerland). Sudan I (\geq 95%) was obtained from Sigma Aldrich (United Kingdom). Propranolol (\geq 99%) was obtained from Sigma Aldrich (Belgium). Martius yellow was obtained from MP Biomedical (India). Orange IV was obtained from Eastman Chemical Company (United States). Uracil (\geq 99.85%) was obtained from US Biological. Flavazine L (Acid Yellow 11) was obtained from Matheson Coleman & Bell Chemicals. Stock solutions of individual compounds were prepared at the concentrations and with the solvents indicated in Appendix A-1, Table A-2. From these stock solutions analytical samples were prepared by combining portions of the stock solutions in equal portions; the specific compounds that were combined into mixtures are also indicated in Table A-2.

3.2.2. Instrumental

Experiments of Set X were performed on an Agilent 1290 series Infinity 2DLC system (Waldbronn, Germany) configured for one-dimensional operation. The system included a binary pump (G4220A), an autosampler (G4226A) equipped with a 20- μ L injection loop, a thermostatted column compartment (G1316C), and a diode-array detector (DAD, G4212A) with a sampling frequency of 160 Hz equipped with an Agilent Max-Light Cartridge Cell (G4212-60008, 10 mm path length, $V_{det} = 1.0 \mu\text{L}$). The dwell volume of the system was experimentally determined to be about 0.128 mL by using a linear gradient from 100% A (100% water) to 100% B (99% water with 1% acetone) and determining the delay in gradient at 50% of the gradient. The injector needle drew and injected at a speed of 10 $\mu\text{L}\cdot\text{min}^{-1}$, with a 2 s equilibration time. The system was controlled using Agilent OpenLAB CDS Chemstation Edition (Rev. C.01.10 [201]). In this study a Kinetex 1.7 m C18 100 \AA 50 \times 2.1 mm column (Phenomenex, Torrance, CA, USA) was used.

The experiments of Set Y were performed on a 2DLC system composed of modules from Agilent Technologies (Waldbronn, Germany) but configured for one-dimensional operation using the 2DLC valve to introduce samples to the column, and the 2DLC software to control mobile phase composition and switching of the 2DLC valve. This type of setup has been described previously [28,29]. The system included a binary pump (G4220A) with Jet Weaver V35 Mixer (p/n: G4220A-90123), an autosampler (G4226A), a thermostatted column compartment (G1316C), and a diode-array detector (DAD, G4212A) with a sampling frequency

of 80 Hz equipped with an Agilent Max-Light Cartridge Cell (G4212-60008, 10 mm path length, $V_{det} = 1.0 \mu\text{L}$). The 2DLC valve used in this case was a prototype (p/n: 5067-4236A-nano) that has fixed internal loops with a volume of about 150 nL. Samples were infused directly into the valve at port #3 using a 1 mL glass syringe and a Harvard Apparatus (p/n: 55-2226) syringe pump at a flow rate of $1 \mu\text{L}/\text{min}$. The dwell volume of the system was about 0.081 mL. The system was controlled using Agilent OpenLAB CDS Chemstation Edition (Rev. C.01.07 [465]). A Zorbax SB 5 m C18 80 Å $50 \times 4.6 \text{ mm}$ column (Agilent) was used.

3.2.3. Analytical methods

Set X was recorded with the following method: The mobile phase consisted of buffer/ACN [v/v, 95/5] (Mobile phase A) and ACN/buffer [v/v, 95/5] (Mobile phase B). The buffer was 5 mM ammonium formate at pH = 3 prepared by adding 0.195 g formic acid and 0.0476 g ammonium formate to 1 L of water. All gradients performed in this study started from 0 min to 0.25 min isocratic 100% A, followed by a linear gradient to 100% B in either 1.5, 3, 3.75, 4.5, 6, 7.5, 9 or 12 min. In all gradients, 100% B was maintained for 0.5 min and brought back to 100% A in 0.1 min. Mobile phase A was kept at 100% for 0.75 min before starting a new run. The flow rate was $0.5 \text{ mL} \cdot \text{min}^{-1}$ and the injection volume was $5 \mu\text{L}$. The peak tables can be found in Appendix A-2. The ten replicate measurements were recorded over a span of multiple days. The buffers used as mobile phase were refreshed several times over the duration of this study.

Set Y was recorded using the following conditions: The mobile phase consisted of buffer (Mobile phase A) and ACN (Mobile phase B), and the flow rate was $2.5 \text{ mL}/\text{min}$. The buffer was 25 mM ammonium formate at pH = 3.2. This was prepared by adding 5.98 g formic acid (98% w/w) and 2.96 mL of ammonium hydroxide (29% w/w) to 2000.0 g of water. All gradients performed in this study started at 5% B at 0 min, followed by a linear gradient to 85% B in either 1, 1.5, 3, 3.75, 4.5, 6, 7.5, 9, 12 and 18 min. In all gradients, 85% B was maintained for 0.5 min and brought back to 5% B in 0.01 min. Mobile phase B was kept at 5% for 1 min before starting a new run. Ten replicate retention measurements were made for each gradient elution condition. The entire dataset was collected using a single batch of mobile phase buffer, over a period of three days.

3.2.4. Data processing

The in-house developed data-analysis and method-optimization program MOREPEAKS (formerly known as PIOTR [9], University of Amsterdam) was used to *i*) fit the investigated retention models to the experimental data, *ii*) determine the retention parameters for each analyte from the fitted data, and *iii*) to evaluate the goodness-of-fit of the retention model. Microsoft Excel was used for further data processing.

3.3. Results & discussion

3.3.1. Design of the study

3.3.1.1. Compound selection

Compounds were selected to cover a wide range of several chemical properties, including charge, hydrophobicity and size, to increase the applicability of the results to a broad range of applications. To facilitate robust detection, UV-vis was chosen as detection method. Common small-molecule analytes were included, such as toluene, uracil and propylparaben. In addition, a number of synthetic and natural dyes were selected, which feature favourable UV-vis absorption ranges to facilitate identification. Emodin, purpurin, sudan I and rutin, were selected as neutral components. Martius yellow, naphthol yellow S, orange IV and flavazine L were included due to their (multiple) negative charges. The pharmaceutical compounds trimethoprim and propranolol were added to the set to include positively charged analytes. Metabolites, such as tyramine and cytosine, were included, but these analytes eluted around the dead time. The column dead time was determined to be 0.262 min for Setup X with a standard deviation of 0.0027 min ($V_0 = 131 \mu\text{L}$) and 0.171 min for Setup Y (determined in 50/50 ACN/buffer) ($V_0 = 428 \mu\text{L}$) with a standard deviation of 0.0005 min, which was calculated by analysing the hold-up time of uracil (non-retained analyte). A standard mixture of peptides was added yielding a final list of 18 compounds. The retention times of these compounds were measured for eight different gradient slopes for Set X and ten different gradient slopes for Set Y. Each measurement was repeated ten times over the course of several days for both sets. Set X included three extra components, viz. indigotin, picric acid, fast red B and two extra peptides, while Set Y included berberine. The analyses of Set Y were performed with a single batch of buffer, yielding highly repeatable retention times, whereas Set X was recorded over a span of a week using multiple batches of prepared buffer. This yielded a dataset with highly repeatable data (Set Y), and a set with less-repeatable data (Set X). Where relevant, the measurement precision is shown in the figures in this paper.

3.3.1.2. Decision on the model

Multiple models to describe retention in LC have been proposed [30]. For RPLC separations the most commonly used model is a linear relationship between the logarithm of the retention factor (k) and the volume fraction of organic modifier (φ). This model results in a two-parameter log-linear equation, often referred to as the “linear-solvent-strength” (LSS) model [31].

$$\ln k = \ln k_0 - S_{LSS}\varphi \quad (3.1)$$

where $\ln k$ is the natural logarithm of the retention factor at a specific modifier concentration, $\ln k_0$ refers to the isocratic retention factor of a solute in pure water, φ refers to the volume fraction of the (organic) modifier in the mobile phase, and the slope S_{LSS} is related to the interaction of the solute and the (organic) modifier. Another two-parameter (log-log) model was proposed by Snyder *et al.* to describe the adsorption behaviour in normal-phase liquid chromatography (NPLC) [32].

$$\ln k = \ln k_1 - R \ln \varphi \quad (3.2)$$

In this model, the R parameter is the so-called solvation number, which represents the ratio of surface areas occupied by adsorbed molecules of the strong eluent component and the analyte. A more extensive form of the LSS model is the quadratic model (Q), proposed by Schoenmakers *et al.*, introducing a third parameter [23].

$$\ln k = \ln k_0 + S_{1,Q}\varphi + S_{2,Q}\varphi^2 \quad (3.3)$$

In this and subsequent retention-model equations, S_1 and S_2 are empirical coefficients used to describe the influence of the organic modifier on the retention of the analyte. Other three-parameter models are also evaluated in this research, viz. the mixed-mode model (MM, Eq. 3.4), which was developed for HILIC separations [33], and the well-known Neue-Kuss model (NK, Eq. 3.5).

$$\ln k = \ln k_0 + S_{1,M}\varphi + S_{2,M} \ln \varphi \quad (3.4)$$

$$\ln k = \ln k_0 + 2 \ln(1 + S_{1,NK}\varphi) - \frac{\varphi S_{2,NK}}{1 + S_{1,NK}\varphi} \quad (3.5)$$

The latter model allowed exact integration of the retention equation, thus simplifying retention modelling in gradient-elution LC [7,34]. The above models all account only for the dependence of retention on the organic-modifier concentration. Indeed, charged compounds can also be retained through secondary interactions in RPLC, which can also depend on the organic-modifier concentration. These secondary interactions may lead to increases in prediction errors, and for that reason the results for individual compounds are shown in Figs. 3.3, 3.4, 3.6-11. In these models, the organic-modifier fraction is related to the retention factor, which can be calculated with the retention time (t_R) and the column dead time (t_0) when performing isocratic elution.

$$k = \frac{t_R - t_0}{t_0} \quad (3.6)$$

In this calculation, the obtained retention factor can directly be linked to the experimental organic-modifier concentration. When using gradient elution, the retention factor is described by the general equation of linear gradients [23].

$$\frac{1}{B} \int_{\varphi_{init}}^{\varphi_{init}+B(t_R-\tau)} \frac{d\varphi}{k(\varphi)} = t_0 - \frac{t_{init} + t_D}{k_{init}} \quad (3.7)$$

In this equation $k(\varphi)$ is the retention model, expressing the relationship between retention (k) and organic modifier fraction (φ). The slope of the gradient (B) is the change in φ as a function of time ($\varphi = \varphi_{init} + Bt$) and τ is the sum of the dwell time (t_D), the time before the start of the gradient (t_{init}) and the dead time (t_0). If the analyte does not elute during or before the gradient, the retention time is described by

$$\frac{1}{B} \int_{\varphi_{init}}^{\varphi_{final}} \frac{d\varphi}{k(\varphi)} + \frac{t_R - \tau - t_G}{k_{final}} = t_0 - \frac{t_{init} + t_D}{k_{init}} \quad (3.8)$$

in which t_G represents the gradient time.

One frequently used measure for model selection is the Akaike Information Criterion (AIC) [35]. AIC values can be calculated upon fitting a model to the data by considering the sum-of-squares error of the fit (SSE), the number of observations (*i.e.* data points, n) and the number of parameters (p). A more-negative value reflects a better description of the data by the tested model. Using more parameters generally enables more facile fitting of the data to a model, but according to Eq. 3.9 adding more model parameters is penalized by the AIC.

$$AIC = 2p + n \left[\ln \left(\frac{2\pi \cdot SSE}{n} \right) + 1 \right] \quad (3.9)$$

In Fig. 3.2A, the average AIC values are plotted for the five different models used to fit Set X (left bars) and Set Y (right bars), using all replicate measurements obtained with eight different gradient slopes (1.5, 3, 3.75, 4.5, 6, 7.5, 9, 12). The ratios between the gradient time and the dead time are comparable for the two sets, but not identical. For Set X, the plot suggests that the LSS model describes the data best, but the Neue-Kuss and the quadratic model also yield good AIC values, despite using three parameters. However, data from Set Y was best described by the log-log adsorption model rather than the log-linear LSS model. This suggests that the noise in Set X may obscure the non-linear trend and that scanning experiments are best carried out under highly repeatable conditions. The appropriateness of a non-linear model is consistent with prior observations described in the literature [20,36,37].

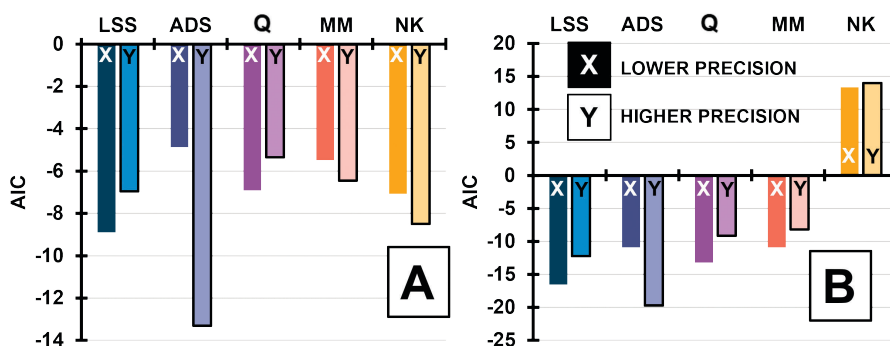


Figure 3.2. Comparison of average AIC values for all studied components for the five different models using A) all replicate measurements from eight measured gradients (1.5, 3, 3.75, 4.5, 6, 7.5, 9, 12), B) all replicate measurements from the gradients with duration of 3, 6 and 9 min. exclusively. For every pair, the first bar depicts the AIC value of Set X and the second bar represents Set Y. See Appendix A-3 for a full list of determined AIC values and Appendix A-4, Fig. A-1 for a plot of the AIC values for the complete set of gradients of Set Y.

Figure 3.2A suggests that the Neue-Kuss model describes the retention relatively well when eight different gradients are used to establish the model (supported by Fig. A-2, using the full set of all ten gradients). However, this model results in a poor description when the input data is limited to three gradient durations (Fig. 3.2B). The latter plot shows a positive average AIC value for the NK model, which indicates a poor description of the data [38].

An alternative method to assess the goodness-of-fit is to check the accuracy of predictions made using the model. When the model parameters are established using only data from three gradient programs, the retention times of the analytes for the remaining five gradient programs may in principle be predicted and used to validate the model. Models were constructed for each set (X and Y) using the data from the scanning gradients of 3, 6, and 9 min duration. These scanning gradients were selected based on the conventional wisdom that the ratio between the slopes of the two most extreme scanning gradients (the gradient slope factor or GSF, denoted by Γ) should be at least three [9,27,39]. At this point it is good to note that the effective slope of a gradient is also related to the span of the gradient ($\Delta\varphi = \varphi_{\text{final}} - \varphi_{\text{initial}}$) and to the dead time (t_0), so that changes in the gradient slope may also occur when changing the flow rate (see Eq. 3.10).

$$\Gamma_{21} = \frac{t_{G,2}\Delta\varphi_1 t_{0,1}}{t_{G,1}\Delta\varphi_2 t_{0,2}} \quad (3.10)$$

The performance of the models was assessed by predicting the retention times for gradients of 3.75, 4.5 and 7.5 min. The results are shown in Fig. 3.3 for both datasets (X and Y). The prediction errors (ε) were calculated using

$$\varepsilon = \frac{t_{R,pred} - \overline{t_{R,meas}}}{\overline{t_{R,meas}}} * 100\% \quad (3.11a)$$

$$\varepsilon = \frac{|t_{R,pred} - \overline{t_{R,meas}}|}{\overline{t_{R,meas}}} * 100\% \quad (3.11b)$$

where $t_{R,pred}$ is the predicted retention time, $\overline{t_{R,meas}}$ is the mean of all considered experimental retention times of the identical gradient. Where relevant, the following figures will indicate which equation was used, and what datapoints were included.

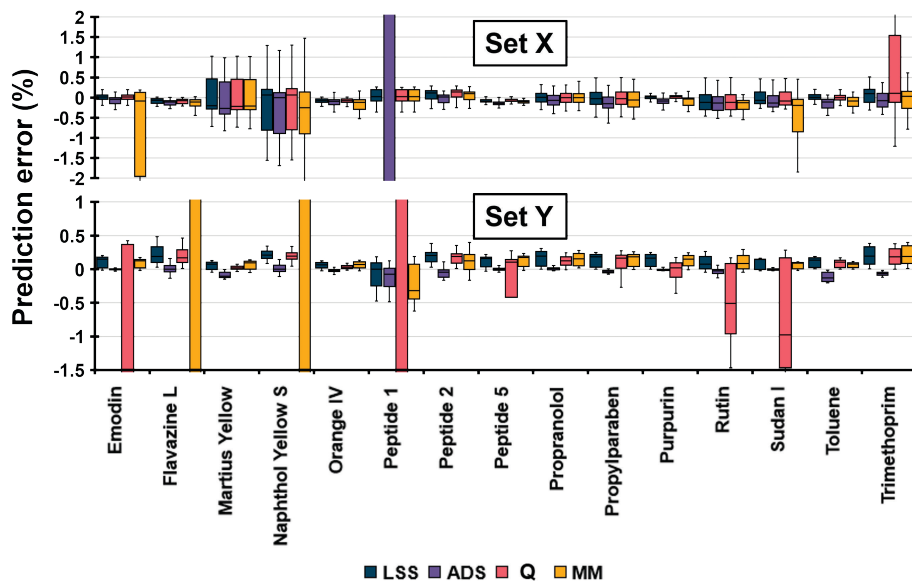


Figure 3.3. Comparison of the prediction errors (for gradient times of 3.75, 4.5, and 7.5 min) relative to the measured points for Set X (top) and Set Y (bottom) using retention parameters obtained using retention data from gradient times of 3, 6 and 9 min in the linear solvent strength (LSS, dark blue), adsorption (ADS, purple), quadratic (Q, orange) and mixed mode (MM, yellow) models, calculated using Eq. 3.11a. The box-and-whisker plots are all based on a total of 30 prediction errors, *i.e.* ten replicates for three different predicted gradients. The whiskers represent the distance from the minimum to the first quartile (0%-25%) and from the third quartile to the maximum (75%-100%) of each set of predictions. The box indicates the interquartile range between the first and third quartile (25%-75%), and the median (50%) is indicated by the horizontal line inside the box. Data are shown for a selected number of analytes. See Appendix A-5, Fig. A-2 for the results for the remainder of the compounds in this study.

The Neue-Kuss (NK) model performed poorly (see the retention plots in Appendix A-6) when using just three input gradients and, therefore, it was omitted from the figure. The results for Set X in Fig. 3.3 show that the two-parameter LSS and ADS models generally yield similar or better predictions compared to the three-parameter models. The box-and-whisker plots are based on 30 prediction errors ($n_r = 30$; 3 predicted retention times in 10 replicates). Larger

experimental variation results in a greater spread of predicted values, although the average prediction error often remains low. The narrow boxplots in the bottom half of Fig. 3.3 illustrate that a higher prediction accuracy can be obtained from more-precise data. The adsorption model (purple) yields significantly lower errors than the LSS model for almost all analytes. The predictions using the mixed-mode model, which was developed for HILIC [33], and the quadratic model exhibit relatively large deviations for Set Y. The robustness of fit was found to be better for both two-parameter models (LSS and ADS), whereas significant spread was observed for the three-parameter models (Q, MM and NK; see Appendix A-6).

3.3.2. Influences of scanning-gradient parameters

3.3.2.1. Effect of scanning speed

The total duration of the three measured scanning gradients determines the total time and resources required to obtain the retention data needed to build a retention model. Retention parameters were obtained for all analytes in Set X using three sets of gradients (Series 2 – fast, Series 3 – regular, Series 4 – slow; see Fig. 3.4, top). For Set Y an additional series (Series 1 – very fast; see Fig. 3.4, bottom) was included. The GSF (Γ) value between the slowest and fastest gradient in each series was always approximately equal to 3. Retention times were predicted for a gradient with a duration within the range of the used gradients (*i.e.* interpolation; the performance of Series 1 was assessed by predicting the retention time for a 3-min gradient and Series 2, 3 and 4 with gradients of 3.75, 7.5 and 9 min, respectively). The results are shown in Fig. 3.4.

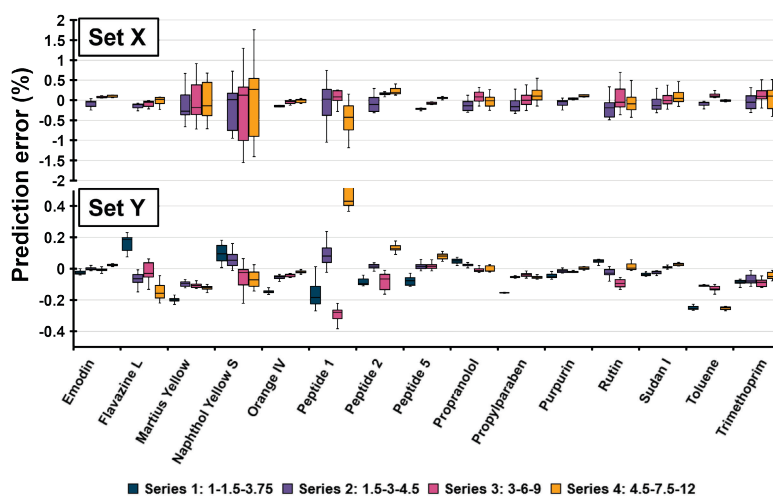


Figure 3.4. Comparison of prediction errors relative to the measured retention times using three (Set X, top) or four (Set Y, bottom) different sets of scanning gradients, with different total durations. Predictions were made with the LSS model for Set X and the ADS model for Set Y and the prediction error was calculated using Eq. 3.11a. See Appendix A-7, Fig. A-13 for the remainder of the compounds. See text for further explanation.

For the results shown in Fig. 3.4, the prediction error was calculated using Eq. 3.11a, which allowed comparison of the four series. The results in Fig. 3.4 suggest that the scanning speed (*i.e.* the different sets of scanning gradient lengths used) is insignificant relative to the measurement precision. In addition, the predicted retention times deviate mostly less than 0.5% from the measured retention times. For Set Y, almost all the prediction errors of Set Y are below 0.2%. Next to that, the prediction errors are smaller than for Set X, even when using very steep gradients (Series 1). Consequently, there is no evidence to support choosing either a fast or slow set of scanning gradients. The results suggest that relatively short scanning gradients can be used to build a reliable model. However, if the model can only be used for interpolation, the range of useful applications for a series of short gradients may be very narrow, which could be a reason to opt for a broader range of scanning gradients. This will be addressed below in Section 3.3.3.

3.3.2.2. *Effect of number of replicate measurements*

Building a model using more replicate measurements will generally decrease the influence of the measurement precision on the prediction error. This raises the question how many replicates suffice (*i.e.* yield an acceptable prediction error). To investigate this, retention times were predicted for gradient times of 4.5 and 7.5 min as a function of the number of replicate measurements used (*i.e.* the number of sampled replicates from the total of ten measurements in this study for each gradient). In all cases, the retention parameters were established for each compound using scanning gradients of 3, 6 and 9 min. The resulting prediction errors for all compounds are shown in Fig. 3.5 as a function of the number of sampled replicates. Note that the number of points used is much larger for a small number of replicates, as the total pool of experiments allows many more variations.

The trends in Fig. 3.5 suggest a small improvement in prediction accuracy for Set X (Fig. 3.5A) as more replicate measurements are sampled, whereas this is not the case for Set Y (Fig. 3.5B). This is in agreement with the fact that Set X features a larger measurement precision than Set Y. The precision of Set X only becomes similar to that of Set Y when seven or more replicate measurements are used. Although more replicates are usually thought to reduce the effect of experimental variation, Fig. 3.5B suggests that with high-precision retention-time measurements a single set of experiments may suffice. This is perhaps counterintuitive, but the model is constructed using a total of three gradients. Apparently, with high-precision measurements the model is constrained sufficiently to yield a robust prediction performance. This is also in line with the improved AIC values for the non-linear adsorption (ADS) model for Set Y (see Fig. 3.2).

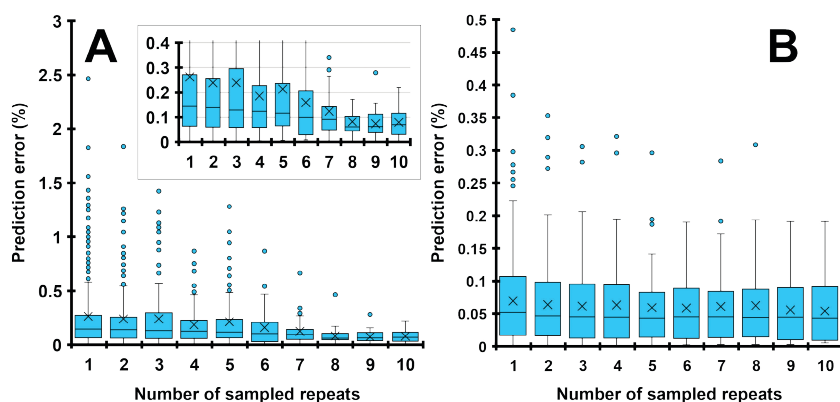


Figure 3.5. The relative prediction errors calculated using Eq. 3.11b for all compounds investigated in this study as a function of the number of sampled replicates from the total pool of experiments for Set X (A) and Set Y (B). The cross represents the mean and the points indicate outliers.

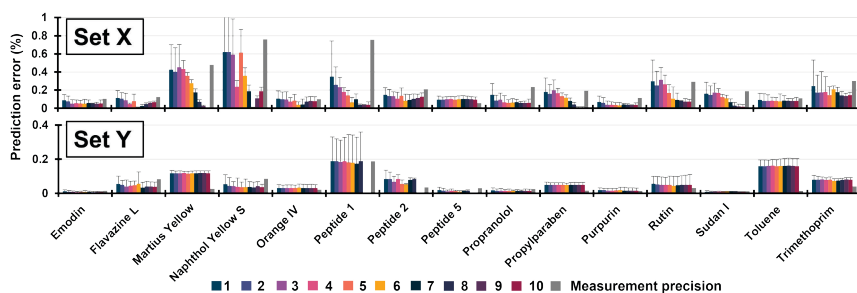


Figure 3.6. Average prediction errors relative to the measured point of the retention times of each compound for a gradient time of 4.5 and 7.5 min, using 1 to 10 replicate measurements of the experimental scanning gradients for Set X (top, using LSS model) and Set Y (bottom, using ADS model). Prediction errors calculated using Eq. 3.11b prior to averaging. The spread (standard deviation) of the predicted retention times is indicated by the error bar and the measurement precision is indicated in grey on the right of each cluster. Note that the y-axis scale is different for the two sets. See Appendix A-8, Fig. A-14 for the remainder of the compounds.

Fig. 3.6 shows the prediction error as a function of the number of replicate measurements for each compound separately for Set X (top) and Y (bottom). Generally, the results are in agreement with those of Fig. 3.5. However, for a number of compounds the influence of the number of replicates is much more profound for Set X and to a lesser extent also for Set Y. Compounds such as martius yellow, naphthol yellow S, rutin and trimethoprim feature a relatively low measurement precision in Set X. All of these compounds are charged under the mobile phase conditions, and thus their retention may be more sensitive to small changes in buffer concentration and pH. In contrast to Set Y, Set X was measured over the span of days, using several batches of buffer. Therefore, chromatographers are encouraged to take all possible measures to maximize the measurement precision, before recording scanning

gradients. Another difference between Set X and Set Y was the column used, which vary in the extent to which the stationary phases can interact with analytes through secondary interactions. This could lead to larger prediction errors for charged species.

3.3.2.3. Replicate scanning gradients or spread their duration?

Another practically relevant question is whether the accuracy of the predictions can be improved by increasing the number of different gradient times that are used, rather than repeating measurements with the same gradient time. To test this, two different sets of scanning gradients were considered, each using a total of six scanning gradients, and thus six retention times per compound for fitting the model. The first set (A) consisted of three replicate measurements each of the 3-min and the 9-min scanning gradients. The second set (B) comprised single measurements from six different scanning gradients (1.5, 3, 3.75, 6, 9, 12 min duration). The retention times from gradients (4.5 and 7.5 min) that were not used to build the model were used to test the accuracy of prediction. This process was carried out in triplicate, using three different sets of retention times. The absolute errors in the resulting replicates of predicted retention times were pooled, before conversion to relative errors and creating the plots shown in Fig. 3.7. This was performed with the LSS model for Set X (X1, top left) and the ADS model for Set Y (Y2, bottom right), indicated with the blue background. To make sure that findings were not model-dependent, the ADS model was used for Set X (X2, bottom left) and the LSS model for Set Y (Y1, top right).

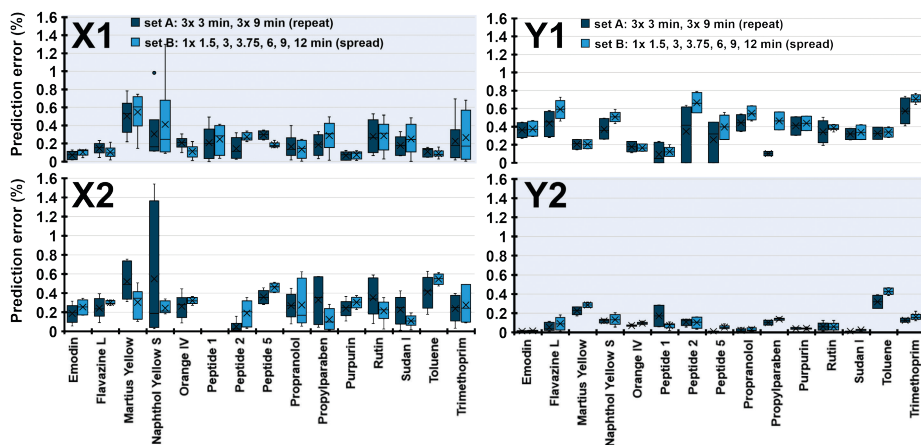


Figure 3.7. Prediction error relative to the measured retention time for two different sets of input scanning gradients, one created by repeating measurements and one by spreading measurements. Predictions performed in triplicate for 4.5-min and 7.5-min gradients, with the LSS model (X1, Y1) and the ADS model (X2, Y2) for both Set X and Set Y. Prediction errors are calculated using Eq. 3.11b. The cross represents the mean and the points indicate outlier points. See Appendix A-9, Fig. A-15 for the remainder of the compounds.

Fig. 3.7 shows that the prediction errors are similar for the set of two gradients performed in triplicate and the set of six different gradients. It is clear that using a non-optimal model (X2 and Y1) increases the prediction error, which is consistent with the results shown in Fig. 3. The difference in prediction error between Fig. 3.7-X1 and Fig. 3.7-Y2 is due to the difference in measurement precision between Set X and Set Y. For models depending on more data (e.g. Neue-Kuss) this conclusion may not be valid. Fig. 3.7 applies to two-parameter models. When the measurement precision is lower, it may be beneficial to use multiple replicates (see Fig. 3.6). For this reason, and because running fewer different methods with more replicates is easier than measuring a larger number of different gradients just once, replicate measurements may be preferred over a wider spread at the cost of a reduced interpolation range in t_g .

3.3.2.4. Effect of the gradient-slope factor of the two most extreme scanning gradients

The gradient-slope factor between the two most extreme scanning gradients (Γ , Eq. 3.10) is typically chosen around three [9]. For example, when a 3-min scanning gradient is chosen as a starting point, the other scanning gradient that needs to be measured will typically be (at least) 9 min in duration (assuming identical composition span and column dead time). The origin of the $\Gamma \geq 3$ recommendation is unclear. In this section we will investigate the effect of the magnitude of the Γ value. Combining a 3-min scanning gradient with gradients of 1.5, 3.75, 4.5, 6, 7.5, 9, or 12 min duration will result in Γ values of 0.5 (or 2), 1.25, 1.5, 2, 2.5, 3, and 4, respectively. Previously (Figs. 3.3, 3.4, 3.6, 3.7) we used the prediction accuracy for a specific gradient as a measure to assess the effects of various parameters. However, this approach cannot be used to compare the influence of the Γ value, because a specific gradient will sometimes be within and sometimes outside the range of slopes spanned by the two scanning gradients. Thus, for comparison, the retention parameters (i.e. slopes and intercepts of the retention models, $\ln k_0$ and S values for the data of Set X described by the LSS model and $\ln k_1$ and R values for the data of Set Y, described by the ADS model) were obtained for each Γ value and for each compound (with ten replicate measurements per Γ). The resulting values were then compared with the benchmark values obtained for $\Gamma = 3$. In Figs. 3.8-X1 and 3.8-X2, respectively, the $\ln k_0$ and S parameters are shown for data Set X and in Figs. 3.8-Y1 and 3.8-Y2, respectively, the $\ln k_1$ and R parameters are shown for data Set Y (all relative to the values obtained for $\Gamma = 3$). The extent of the agreement between the calculated parameters indicates a high similarity between the models.

The plots of Set X in Fig. 3.8 show that variations in the model parameters are mostly small, except for the fastest scanning gradients (1.5 and 3 minutes, $\Gamma = 0.5$, dark blue points). In that case $\ln k_0$ and S tend to covary simultaneously. The largest variations are observed for charged compounds (e.g. Fig. 3.8-X2, naphthol yellow S and orange IV) and for rutin, and

variations tend to increase with decreasing Γ . In the plots for Set Y (Figs. 3.8-Y1 and 3.8-Y2) similar trends are visible for martius yellow and toluene. The plots for Set Y include two extra Γ values (0.33 and 6, based on 1-min and 18-min gradients, respectively). The results from these two additional factors follow a similar pattern. The data for $\Gamma = 0.5$ show a larger deviation from the black line than those for $\Gamma = 2$ and the data for $\Gamma = 0.33$ deviate significantly from the black line ($\Gamma = 3$). The data in Fig. 3.8 suggests that scanning gradients of 3 and 3.75 min ($\Gamma = 1.25$) produce retention times similar to these obtained from scanning gradients of 3 and 9 min ($\Gamma = 3$). To verify this, the retention times for the 7.5-min gradient were predicted using fitting parameters obtained using various combinations of scanning gradient data (with 10 replicates). The results are shown in Fig. 3.9. Other approaches to establish the effect of Γ on the prediction error have been followed, as described in Appendix A-10, Figs. A-18-24.

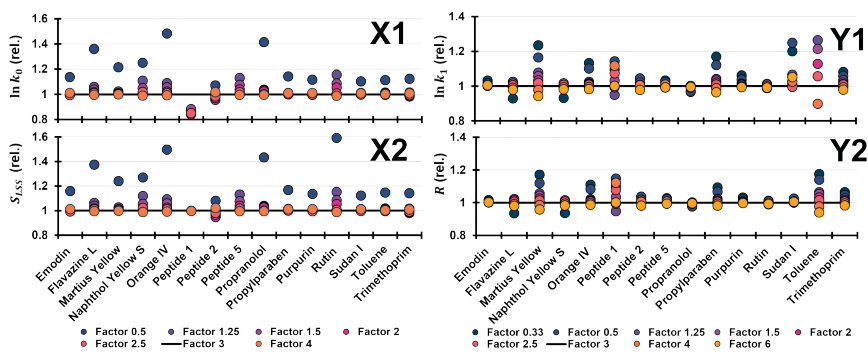


Figure 3.8. Model parameters obtained for Set X (LSS model; X1, $\ln k_0$; X2, S) and Set Y (ADS model; Y1, $\ln k_1$; Y2, R) all relative to the values obtained for $\Gamma = 3$ (black line). Data points reflect averages based on ten replicate measurements. See Appendix A-10, Fig. A-16 for the remainder of the compounds.

Fig. 3.9 shows that a value of $\Gamma > 3$ does not always result in the smallest error. A value of $\Gamma = 4$ or $\Gamma = 6$, based on longer (12 or 18 min) gradients was expected to yield the most reliable results, but greater prediction errors are typically observed than for $\Gamma = 2$ or $\Gamma = 3$. This could feasibly be explained by a lower measurement precision in longer gradient runs, but when the measurement precision is increased, as is the case for Set Y, the same trends are observed. The detrimental effect of using long gradients is more severe for $\Gamma = 6$ than for $\Gamma = 4$. All these results suggest that the prediction accuracy depends less on the gradient-slope factor (Γ) than on the proximity of the slope of the scanning gradients to that of the predicted gradient. For example, when retention for a 7.5-min gradient is predicted, the closest scanning gradients are those of 6 min ($\Gamma = 2$) and 9 min ($\Gamma = 3$). These conditions result in the lowest prediction errors in Fig. 3.9. Scanning gradients that differ more from the one that is to be predicted, for example longer gradients of 12 min ($\Gamma = 4$) or 18 min ($\Gamma = 6$), or shorter gradients of 4.5 min ($\Gamma = 1.5$) or 3.75 min ($\Gamma = 1.25$), result in increased prediction errors, independent of whether

interpolation or extrapolation is required. These effects are observed more clearly for Set Y, where the measured precision is increased. For Set X, the lowest Γ values yield the highest deviation for charged compounds, such as naphthol yellow S, orange IV and flavazine L. Low Γ values (below 1) also yield poor prediction errors using the data from Set Y. The main conclusion from Fig. 3.9 is that the proximity of the slope of the scanning gradients to that of the predicted gradient is a much more important factor than the value of Γ *per se*.

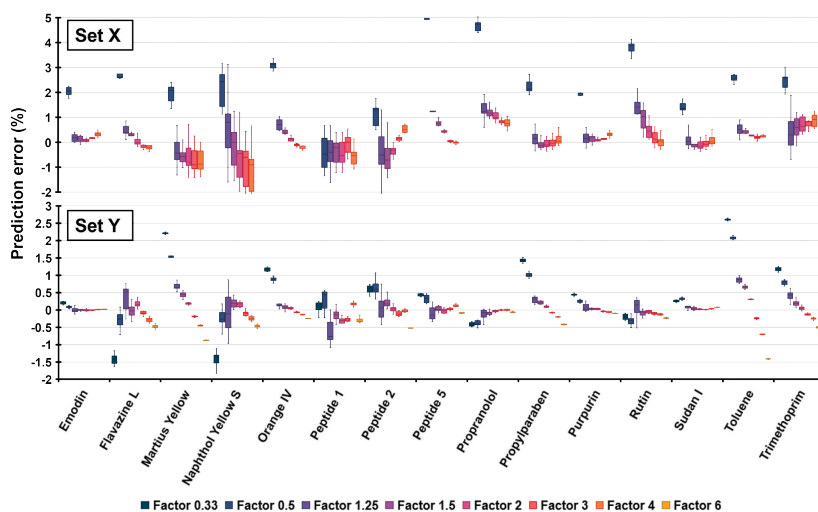


Figure 3.9. Prediction error of retention relative to the measured retention times in a 7.5-min gradient calculated with various combinations of scanning gradients (indicated by the Γ values at the bottom of the figure; one gradient is always 3 min in duration) for Set X (LSS model) and Set Y (ADS model). Prediction errors are calculated using Eq. 3.11a. Results are based on ten replicate measurements. See Appendix A-10, Fig. A-17 for the remainder of the compounds.

3.3.3. Limits of use

Generally, it is not advisable to extrapolate the retention model to predict retention times for gradients that are shorter or longer than those used for scanning. When applying scanning gradients to the development of LC \times LC methods, it is interesting to investigate whether retention times obtained using very short gradients (*i.e.* similar to conditions used for ²D separations) can be used to predict retention times under gradient conditions where shallower slopes are used (*i.e.* ¹D methods). For example, when using the reference scanning gradient set (*i.e.* 3, 6 and 9 min), it is thought to be best used to predict retention times for gradients with durations between 3 and 9 min. This conventional wisdom is tested in this section of the paper. Using the retention parameters obtained using the reference scanning gradient set to predict retention for faster gradients, such as 1.5 min, is expected to yield higher prediction errors than scanning sets that embrace this scanning gradient time (Fig. 3.9). In the top two graphs of Fig.

3.10, the prediction error for a 1.5-min gradient is shown for all compounds, calculated from a model constructed using retention times obtained from scanning gradients of 3, 6, and 9 min for different numbers of replicates (1 to 10). The prediction error for Set X remains relatively large as the number of replicates increases, irrespective of the measurement precision. This conclusion may be affected by the relatively low flow rate used for such a short gradient time. At higher flow rates, faster gradients are less affected by deformation of the gradient profile [26]. Set Y was recorded with a higher flow rate and a higher precision and, again, the prediction error does not appear to decrease with an increasing number of replicate measurements.

The same approach was used to predict retention times by extrapolation towards shallower gradients. Using the same reference gradient set, the retention times of all compounds were predicted for the 12-min gradient as a function of the number of experiments (Fig. 3.10). The prediction error decreases with increasing number of replicate measurements for compounds with a large experimental variation (naphthol yellow S, martius yellow) in Set X. The same pattern was observed for other charged compounds (see Appendix A-11, Fig. A-25). However, for all the other compounds in Set X and for all compounds in Set Y the prediction error is barely affected by the number of replicate measurements, which is consistent with our earlier conclusion regarding Set Y (see Fig. 3.6).

The prediction errors resulting from extrapolation toward either slower or faster (Fig. 3.10) gradients are higher than for gradients with a slope within the range used to establish the model parameters (Fig. 3.6), but extrapolation towards shallower gradients yields smaller errors than towards steeper gradients. Especially for highly charged compounds with low experimental precision, such as martius yellow or naphthol yellow S, multiple replicate measurements may enhance the predictive ability of the model. In the Appendix A-11 Fig. A-26 the same pattern is observed for fast red B and picric acid. However, for compounds with highly repeatable retention times the prediction error is not affected by the number of replicates.

Since gradient-scanning techniques are used for the development and optimization of 2DLC methods [3,40], prediction of first-dimension retention times (*i.e.* in slow gradients) from second-dimension retention times (*i.e.* fast gradients) is of interest. In the previous section, the retention times were predicted for a 12-min gradient using the reference set of scanning gradients (3, 6 and 9 min). The same predictions (12-min gradient) were also made using a model based on retention data from a set of faster gradients (1.5, 3 and 4.5 minutes) from Set X. For Set Y, retention times for an even slower gradient (18 min) could be predicted using a model constructed using data from an even faster set of scanning gradients (1, 1.5 and 3.75). Fig. 3.11 shows that large errors of up to 4% result from the prediction of retention times for the slow

gradient (12-min) from the model based on fast scanning gradients for Set X. In a hypothetical 20-min gradient, this amount to a difference of 48 s. For Set Y it can be seen that these errors increase when the difference between the lengths of the target and scanning gradients increases. In almost all cases the retention in slow gradients is overestimated by the model.

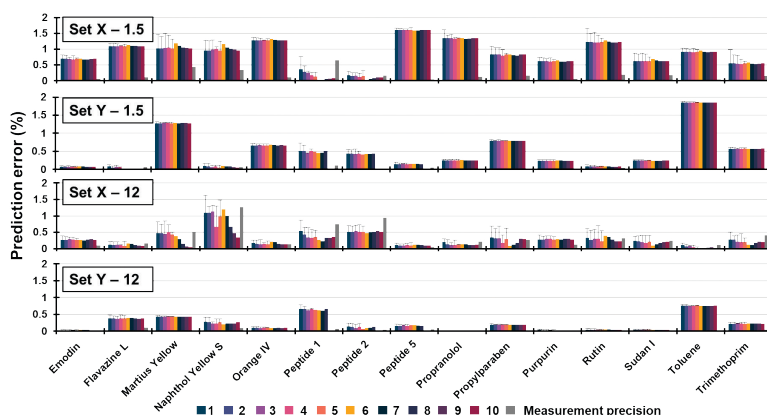


Figure 3.10. Prediction errors relative to the measured point for retention in a 1.5-min and a 12-min gradient for each compound as a function of the number of replicate experiments, using the reference set of scanning gradients (3, 6, and 9 min) for Set X (using the LSS model; 1.5, first frame; 12, third frame) and Set Y (using the ADS model; 1.5, second frame; 12, fourth frame). Prediction errors are calculated using Eq. 3.11b. The measured precision is shown in grey to the right of each cluster. See Appendix A-11, Figs. A-25 and A-26 for the remainder of the compounds.

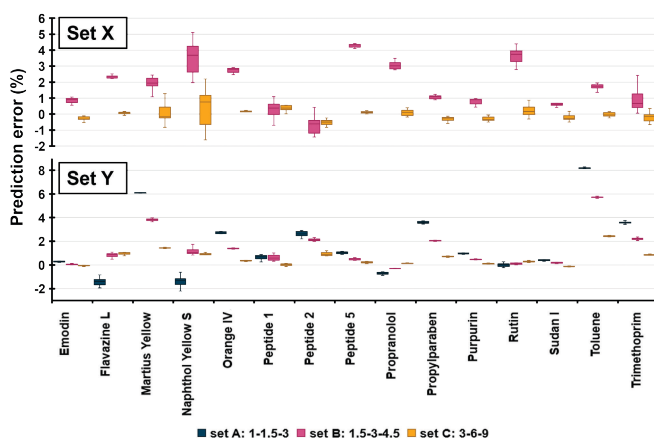


Figure 3.11. Prediction error relative to the measured point for the retention times of all compounds in a 12-min (top) and in an 18-min (bottom) gradient predicted from models constructed using two or three different sets of scanning gradients. Data based on 10 replicate measurements. Predictions are made with the LSS model for Set X and the ADS model for Set Y. Prediction errors are calculated using Eq. 3.11a. See A-11, Fig. A-27 for the remainder of the compounds.

3.4. Concluding remarks

In this paper we describe a systematic, in-depth study into the application of retention modelling for development and optimization of RPLC separations. Two data sets were recorded (X and Y), using the same analytes and similar instrumentation, but in different locations and with slightly different conditions. Set X was recorded under typical LC conditions and as such may be representative for common practice. In Set Y, conditions were chosen to minimize the experimental measurement variability, including the use of a higher flow rate (2.5 compared to 0.5 mL/min.; see ref [28]), and precise control over re-equilibration time following gradient elution [41]. This latter data set represents the highest precision achievable in our hands. Five different retention models were investigated. For Set X, a log-linear (or "linear solvent strength", LSS) model was found to provide the best fit of the data; for Set Y a log-log ("adsorption", ADS) model proved optimal. Generally, at least two scanning gradients (for a two-parameter model) that differ in their (effective) slopes by at least a factor of three are used [9,27,39]. Therefore, a benchmark set of three scanning gradients with durations of 3, 6 and 9 min was designated in this study (from 5 to 95% or 5% to 85% of strong solvent for Set X and Set Y, respectively). Fig. 3.12 was constructed by condensing the effects of the investigated parameters on the prediction accuracy of all compounds studied. We come to the following conclusions from the resulting data.

- > Whereas it is frequently recommended that the slopes of scanning gradients used to obtain retention data should vary by a factor of three or so, we do not see any evidence in our results that support this guideline. That is, similar retention prediction errors were obtained from models based on scanning gradients with slopes varying by a factor of three compared to models based on gradients with slopes varying by as little as 1.25. We also observe that the speed (*i.e.*, absolute analysis or gradient time) does not have a strong impact on prediction error. On the other hand, the data show that the proximity of the slope of a gradient, for which retention will be predicted, to one of the scanning gradients, used to build the model, is far more determinant of retention prediction error. With decreasing proximity, it is more important that the slope of the target gradient lies between the slopes of the scanning gradients (*i.e.*, interpolation is better than extrapolation, as one would expect). These findings have obvious implications for the design of experiments; using scanning gradients with a large variation in slopes is not required *per se*, but using a large range of slopes enables prediction of retention for a wider array of gradients without extrapolating.

- > When designing experiments for the purpose of building a retention model, one has to decide how to allocate instrument time and choose whether to repeat measurements for a small number of scanning gradients, or to do fewer repeat measurements for a larger set of gradient times. Using prediction error as a metric of model performance, the data do not show any general preference for sets of scanning gradients focused on replicate measurements (e.g., three replicate measurements each of two different gradients) or ones focused on using many different gradient times (e.g., one replicate each of six different gradients). However, in cases where the variability of retention measurements in scanning gradients is high, the predictive performance of models can be improved by making more repeat measurements.
- > Finally, predicting retention times for relatively slow gradients using a model constructed from data obtained from fast gradients led to relatively large prediction errors. Unfortunately, this makes it impractical to accurately predict first-dimension retention times using models constructed from second-dimension retention data for use in the development and optimization of comprehensive two-dimensional liquid chromatography.

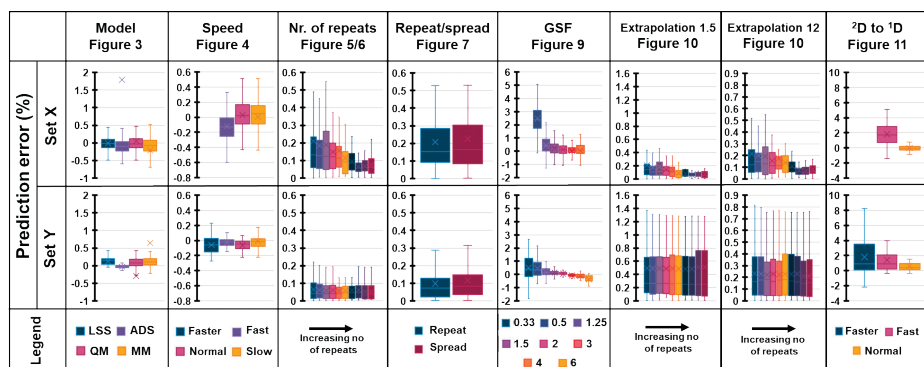


Figure 3.12. Combined results of all scanning-gradient parameters. The box-and-whisker plots represent the average prediction error of all the compounds for Set X (top) and Set Y (bottom). Predictions are made with the LSS model for Set X and the ADS model for Set Y. Prediction errors are calculated using Eq. 3.11a for columns with heading Model, Speed, GSF and 2D to 1D, and Eq. 3.11b for columns with heading Nr. of repeats, Repeat or spread, Extrapolation 1.5 and Extrapolation 12.

References

- [1] National Academies of Sciences Engineering and Mathematics, A Research Agenda for Transforming Separation Science, The National Academies Press, Washington, D. C., 2019. <https://doi.org/10.17226/25421>.
- [2] L.R. Snyder, J.W. Dolan, J.R. Gant, Gradient elution in high-performance liquid chromatography. I. Theoretical basis for reversed-phase systems, *J. Chromatogr. A.* 165 (1979) 3–30. [https://doi.org/10.1016/S0021-9673\(00\)85726-X](https://doi.org/10.1016/S0021-9673(00)85726-X).
- [3] B.W.J. Pirok, D.R. Stoll, P.J. Schoenmakers, Recent Developments in Two-Dimensional Liquid Chromatography: Fundamental Improvements for Practical Applications, *Anal. Chem.* 91 (2019) 240–263. <https://doi.org/10.1021/acs.analchem.8b04841>.
- [4] P. Česla, N. Vaňková, J. Křenková, J. Fischer, Comparison of isocratic retention models for hydrophilic interaction liquid chromatographic separation of native and fluorescently labeled oligosaccharides, *J. Chromatogr. A.* 1438 (2016) 179–188. <https://doi.org/10.1016/j.chroma.2016.02.032>.
- [5] E. Tyteca, A. Périat, S. Rudaz, G. Desmet, D. Guillaume, Retention modeling and method development in hydrophilic interaction chromatography, *J. Chromatogr. A.* 1337 (2014) 116–127. <https://doi.org/10.1016/j.chroma.2014.02.032>.
- [6] E. Tyteca, V. Desfontaine, G. Desmet, D. Guillaume, Possibilities of retention modeling and computer assisted method development in supercritical fluid chromatography, *J. Chromatogr. A.* 1381 (2015) 219–228. <https://doi.org/10.1016/j.chroma.2014.12.077>.
- [7] B.W.J. Pirok, S.R.A. Molenaar, R.E. van Outersterp, P.J. Schoenmakers, Applicability of retention modelling in hydrophilic-interaction liquid chromatography for algorithmic optimization programs with gradient-scanning techniques, *J. Chromatogr. A.* 1530 (2017) 104–111. <https://doi.org/10.1016/j.chroma.2017.11.017>.
- [8] G. van Schaick, B.W.J. Pirok, R. Haselberg, G.W. Somsen, A.F.G. Gargano, Computer-aided gradient optimization of hydrophilic interaction liquid chromatographic separations of intact proteins and protein glycoforms, *J. Chromatogr. A.* 1598 (2019) 67–76. <https://doi.org/10.1016/j.chroma.2019.03.038>.
- [9] B.W.J. Pirok, S. Pous-Torres, C. Ortiz-Bolsico, G. Vivó-Truyols, P.J. Schoenmakers, Program for the interpretive optimization of two-dimensional resolution, *J. Chromatogr. A.* 1450 (2016) 29–37. <https://doi.org/10.1016/j.chroma.2016.04.061>.
- [10] L.S. Roca, S.E. Schoemaker, B.W.J. Pirok, A.F.G. Gargano, P.J. Schoenmakers, Accurate modelling of the retention behaviour of peptides in gradient-elution hydrophilic interaction liquid chromatography, *J. Chromatogr. A.* (2019). <https://doi.org/10.1016/j.chroma.2019.460650>.
- [11] E.F. Hewitt, P. Lukulay, S. Galushko, Implementation of a rapid and automated high performance liquid chromatography method development strategy for pharmaceutical drug candidates, *J. Chromatogr. A.* 1107 (2006) 79–87. <https://doi.org/10.1016/j.chroma.2005.12.042>.
- [12] S. Fekete, V. Sadat-Noorbakhsh, C. Schelling, I. Molnár, D. Guillaume, S. Rudaz, J.L. Veuthey, Implementation of a generic liquid chromatographic method development workflow: Application to the analysis of phytocannabinoids and Cannabis sativa extracts, *J. Pharm. Biomed. Anal.* 155 (2018) 116–124. <https://doi.org/10.1016/j.jpba.2018.03.059>.
- [13] M. Taraji, P.R. Haddad, R.I.J. Amos, M. Talebi, R. Szucs, J.W. Dolan, C.A. Pohl, Prediction of retention in hydrophilic interaction liquid chromatography using solute molecular descriptors based on chemical structures, *J. Chromatogr. A.* 1486 (2017) 59–67. <https://doi.org/10.1016/j.chroma.2016.12.025>.
- [14] J.E. Madden, P.R. Haddad, Critical comparison of retention models for optimisation of the separation of anions in ion chromatography. I. Non-suppressed anion chromatography using phthalate eluents and three different stationary phases, *J. Chromatogr. A.* 829 (1998) 65–80. [https://doi.org/10.1016/S0021-9673\(98\)00775-4](https://doi.org/10.1016/S0021-9673(98)00775-4).

- [15] J. Havel, J.E. Madden, P.R. Haddad, Prediction of retention times for anions in ion chromatography using artificial neural networks, *Chromatographia*. 49 (1999) 481–488. <https://doi.org/10.1007/BF02467746>.
- [16] L.S. Roca, S.E. Schoemaker, B.W.J. Pirok, A.F.G. Gargano, P.J. Schoenmakers, Accurate modelling of the retention behaviour of peptides in gradient-elution hydrophilic interaction liquid chromatography, *J. Chromatogr. A*. 1614 (2020) 460650. <https://doi.org/10.1016/j.chroma.2019.460650>.
- [17] A. Andrés, M. Rosés, E. Bosch, Prediction of the chromatographic retention of acid-base compounds in pH buffered methanol-water mobile phases in gradient mode by a simplified model, *J. Chromatogr. A*. 1385 (2015) 42–48. <https://doi.org/10.1016/j.chroma.2015.01.062>.
- [18] P.C. Sadek, P.W. Carr, R.M. Doherty, M.J. Kamlet, R.W. Taft, M.H. Abraham, Study of retention processes in reversed-phase high-performance liquid chromatography by the use of the solvatochromic comparison method, *Anal. Chem.* 57 (1985) 2971–2978. <https://doi.org/10.1021/ac00291a049>.
- [19] R.M. Lopez Marques, P.J. Schoenmakers, Modelling retention in reversed-phase liquid chromatography as a function of pH and solvent composition, *J. Chromatogr. A*. 592 (1992) 157–182. [https://doi.org/10.1016/0021-9673\(92\)85084-7](https://doi.org/10.1016/0021-9673(92)85084-7).
- [20] E. Tyteca, J. De Vos, N. Vankova, P. Cesla, G. Desmet, S. Eeltink, Applicability of linear and nonlinear retention-time models for reversed-phase liquid chromatography separations of small molecules, peptides, and intact proteins, *J. Sep. Sci.* 39 (2016) 1249–1257. <https://doi.org/10.1002/jssc.201501395>.
- [21] J.F. Focant, A. Sjödin, D.G. Patterson, Improved separation of the 209 polychlorinated biphenyl congeners using comprehensive two-dimensional gas chromatography-time-of-flight mass spectrometry, *J. Chromatogr. A*. 1040 (2004) 227–238. <https://doi.org/10.1016/j.chroma.2004.04.003>.
- [22] J.W. Dolan, D.C. Lommen, L.R. Snyder, Drylab® computer simulation for high-performance liquid chromatographic method development, *J. Chromatogr. A*. 485 (1989) 91–112. [https://doi.org/10.1016/S0021-9673\(01\)89134-2](https://doi.org/10.1016/S0021-9673(01)89134-2).
- [23] P.J. Schoenmakers, H.A.H. Billiet, R. Tussen, L. De Galan, Gradient selection in reversed-phase liquid chromatography, *J. Chromatogr. A*. 149 (1978) 519–537. [https://doi.org/10.1016/S0021-9673\(00\)81008-0](https://doi.org/10.1016/S0021-9673(00)81008-0).
- [24] G. Vivó-Truyols, S. Van Der Wal, P.J. Schoenmakers, Comprehensive study on the optimization of online two-dimensional liquid chromatographic systems considering losses in theoretical peak capacity in first- and second-dimensions: A pareto-optimality approach, *Anal. Chem.* 82 (2010) 8525–8536. <https://doi.org/10.1021/ac101420f>.
- [25] A.P. Schellinger, P.W. Carr, A practical approach to transferring linear gradient elution methods, *J. Chromatogr. A*. 1077 (2005) 110–119. <https://doi.org/10.1016/j.chroma.2005.04.088>.
- [26] T.S. Bos, L.E. Niezen, M.J. den Uijl, S.R.A. Molenaar, S. Lege, P.J. Schoenmakers, G.W. Somsen, B.W.J. Pirok, Eliminating the influence of geometry-induced gradient deformation in liquid chromatographic retention modelling, (2020) Manuscript submitted for publication.
- [27] G. Vivó-Truyols, J.R. Torres-Lapasió, M.C. García-Alvarez-Coque, Error analysis and performance of different retention models in the transference of data from/to isocratic/gradient elution, *J. Chromatogr. A*. 1018 (2003) 169–181. <https://doi.org/10.1016/j.chroma.2003.08.044>.
- [28] C. Seidl, D.S. Bell, D.R. Stoll, A study of the re-equilibration of hydrophilic interaction columns with a focus on viability for use in two-dimensional liquid chromatography, *J. Chromatogr. A*. 1604 (2019) 460484. <https://doi.org/10.1016/j.chroma.2019.460484>.
- [29] D.R. Stoll, R.W. Sajulga, B.N. Voigt, E.J. Larson, L.N. Jeong, S.C. Rutan, Simulation of elution profiles in liquid chromatography – II: Investigation of injection volume overload under gradient elution conditions applied to second dimension separations in two-dimensional liquid chromatography, *J. Chromatogr. A*. 1523 (2017) 162–172. <https://doi.org/10.1016/j.chroma.2017.07.041>.
- [30] P. Nikitas, A. Pappa-Louisi, Retention models for isocratic and gradient elution in reversed-phase liquid chromatography, *J. Chromatogr. A*. 1216 (2009) 1737–1755. <https://doi.org/10.1016/j.chroma.2008.09.051>.

- [31] L.R. Snyder, J.W. Dolan, J.R. Gant, Gradient elution in high-performance liquid chromatography, *J. Chromatogr. A.* 165 (1979) 3–30. [https://doi.org/10.1016/S0021-9673\(00\)85726-X](https://doi.org/10.1016/S0021-9673(00)85726-X).
- [32] L.R. Snyder, H. Poppe, Mechanism of solute retention in liquid—solid chromatography and the role of the mobile phase in affecting separation, *J. Chromatogr. A.* 184 (1980) 363–413. [https://doi.org/10.1016/S0021-9673\(00\)93872-X](https://doi.org/10.1016/S0021-9673(00)93872-X).
- [33] G. Jin, Z. Guo, F. Zhang, X. Xue, Y. Jin, X. Liang, Study on the retention equation in hydrophilic interaction liquid chromatography, *Talanta.* 76 (2008) 522–527. <https://doi.org/10.1016/j.talanta.2008.03.042>.
- [34] U.D. Neue, H.J. Kuss, Improved reversed-phase gradient retention modeling, *J. Chromatogr. A.* 1217 (2010) 3794–3803. <https://doi.org/10.1016/j.chroma.2010.04.023>.
- [35] H. Akaike, A New Look at the Statistical Model Identification, *IEEE Trans. Automat. Contr.* 19 (1974) 716–723. <https://doi.org/10.1109/TAC.1974.1100705>.
- [36] M. Gilar, J. Hill, T.S. McDonald, F. Griitti, Utility of linear and nonlinear models for retention prediction in liquid chromatography, *J. Chromatogr. A.* 1613 (2020) 460690. <https://doi.org/10.1016/j.chroma.2019.460690>.
- [37] P. Jandera, T. Hájek, Possibilities of retention prediction in fast gradient liquid chromatography. Part 3: Short silica monolithic columns, *J. Chromatogr. A.* 1410 (2015) 76–89. <https://doi.org/10.1016/j.chroma.2015.07.070>.
- [38] E. Tyteca, G. Desmet, On the inherent data fitting problems encountered in modeling retention behavior of analytes with dual retention mechanism, *J. Chromatogr. A.* 1403 (2015) 81–95. <https://doi.org/10.1016/j.chroma.2015.05.031>.
- [39] M.A. Quarry, R.L. Grob, L.R. Snyder, Prediction of precise isocratic retention data from two or more gradient elution runs. Analysis of some associated errors, *Anal. Chem.* 58 (1986) 907–917. <https://doi.org/10.1021/ac00295a056>.
- [40] B.W.J. Pirok, A.F.G. Gargano, P.J. Schoenmakers, Optimizing separations in on-line comprehensive two-dimensional liquid chromatography, *J. Sep. Sci.* 41 (2018) 68–98. <https://doi.org/10.1002/jssc.201700863>.
- [41] A.P. Schellinger, D.R. Stoll, P.W. Carr, High-speed gradient elution reversed-phase liquid chromatography of bases in buffered eluents. Part I. Retention repeatability and column re-equilibration, *J. Chromatogr. A.* 1192 (2008) 41–53. <https://doi.org/10.1016/j.chroma.2008.01.062>.

CHAPTER 4

Modelling SPAM

4. Assessing the Feasibility of Stationary-Phase-Assisted Modulation for Two-Dimensional Liquid-Chromatography Separations

Abstract

Two-dimensional liquid chromatography (2DLC) offers great separation power for complex mixtures. The frequently encountered incompatibility of two orthogonal separation systems, however, makes its application complicated. Active-modulation strategies can reduce such incompatibility issues considerably. Stationary-phase-assisted modulation (SPAM) is the most-common of these techniques, but also the least robust due to the major disadvantage that analytes may elute prematurely. The range of liquid chromatography (LC) applications continues to expand towards ever more complex mixtures. Retention modelling is increasingly indispensable to comprehend and develop LC separations. In this research, a tool was designed to assess the feasibility of applying SPAM in 2DLC. Several parameters were investigated to accurately predict isocratic retention of analytes on trap columns under dilution-flow conditions. Model parameters were derived from scanning-gradient experiments performed on analytical columns. The trap-to-trap repeatability was found to be similar to the prediction error. Dead volumes for the trap columns could not be accurately determined through direct experimentation. Instead, they were extrapolated from dead-volume measurements on analytical columns. Several known retention models were evaluated. Better predictions were found using the quadratic model than with the log-linear ("linear-solvent-strength") model. Steep scanning gradients were found to result in inaccurate predictions. The impact of the dilution flow on the retention of analytes proved less straightforward than anticipated. Under certain conditions dilution with a weaker eluent was found to be counterproductive. A tool was developed to quantify the effect of the dilution flow and to predict whether SPAM could be applied in specific situations. For nine different analytes under 36 different sets of conditions and with three different modulation times, the SPAM tool yielded a correct assessment in more than 95% of all cases (less than 5% false positives plus false negatives).

Publication

Assessing the Feasibility of Stationary-Phase-Assisted Modulation for Two-Dimensional Liquid-Chromatography Separations

Mimi J. den Uijl, Tim Roeland, Tijmen S. Bos, Peter J. Schoenmakers, Maarten R. van Bommel, and Bob W.J. Pirok

J. Chromatogr. A, **2022**, 1679, 463388, DOI: 10.1016/j.chroma.2022.463388

4.1. Introduction

Liquid chromatography (LC) is one of the most important analytical techniques because of its wide range of applications, the choice of selectivity, and the possibility to couple it to many detection techniques [1]. In an LC separation, the maximum number of peaks that can be resolved is the theoretical peak capacity (n_c). While this number has been increasing in recent years by using long columns under high pressure [2], core-shell particles [3–5], monolithic stationary-phases [6], or elevated temperatures [7], it has to be accounted for that the number of peaks that are separated is far lower than the n_c [8]. Next to that, complex mixtures, like the samples from cultural heritage [9], blood analysis [10], food industry [11], and waste-water effluent [12] require unattainable peak capacities for one-dimensional liquid chromatography. In two-dimensional liquid chromatography (2DLC), more resolving power and higher peak capacities can be obtained [13]. In 2DLC, the effluent of the first-dimension column (1D) is transferred to a second-dimension column (2D), where the analytes undergo another separation. This transfer can be either performed offline, or in an online fashion by means of a valve. For comprehensive 2DLC (LC \times LC), all 1D effluent is transferred to the 2D .

The power of two-dimensional liquid chromatography (2DLC) lies in the combination of two different retention mechanisms, which are carefully chosen by *i*) the sample dimensionality, *ii*) the compatibility with the detector, *iii*) their duration (*i.e.* one needs to be fast), and, of course, *iv*) the compatibility of the two dimensions with each other. Although 2DLC has been developing in the last years, with 160 applications from 2016 to 2018 [14], this latter compatibility issue significantly complicates its implementation [15].

The employed modulation strategy plays a key role to improve the compatibility of the two dimensions within a 2DLC method. Unmodified transfer of the 1D effluent to the 2D through an 8- or 10-port valve equipped with empty loops is referred to as passive modulation [14]. For this to succeed, the two separation techniques should be compatible to prevent miscibility and adsorption issues such as breakthrough, peak deformation, and peak splitting [16,17]. Another issue is the loss of sensitivity due to the additional dilution induced by a second dimension [18–20]. Driven to combine organic-based separations with aqueous based, these compatibility challenges defined the fundamental work of many groups worldwide in the past decades. These efforts culminated into the development of active modulation techniques: active-solvent modulation (ASM) [21,22], stationary-phase-assisted modulation (SPAM) [9,23–25], thermal modulation [26–29], evaporative membrane modulation [30], vacuum evaporation modulation [31,32], and cold trapping [33]. While the latter four techniques have seen relatively few applications thus far, the former two are considered established in academia [14].

In SPAM, the analytes in the ^1D effluent are trapped on a small guard column, which is connected similarly like the loops in passive modulation. In this method, the total volume of the SPAM column, and thus the injection volume of the ^2D , is small. Another advantage of this modulation technique is that the modulation volume is not restricted to a loop volume. However, where ASM has been demonstrated to be a robust technique, for SPAM *i*) guard columns do not feature the same quality and robustness standards as normal columns, rendering reproducibility of the method difficult, *ii*) pressure pulses on the guard column are expected to reduce its lifetime, and *iii*) when the analyte retention is too low in the effluent of the ^1D , the compounds will elute prematurely from the guard column and be lost. While the first two challenges can be addressed technically, the latter describes a discriminatory attribute that is intrinsically fatal to a method. While premature elution can be detected by installing a ^1D detector post-valve to monitor the ^1D waste, this is not practical for complex samples of unknown composition.

To prevent premature elution, methods that use SPAM often feature an active dilution flow to the ^1D effluent to reduce the elution strength, however these dilution flows are often chosen rather randomly [9]. Moreover, the improved retention factor by the weaker elution strength is countered by the additional elution volume induced by the additional flow. For users it is thus difficult to gauge whether SPAM could be applied for a sample of interest and, if so, what conditions should be used. Unknown loss of analytes to the lack of retention renders SPAM unreliable, yet some applications do rely on complete removal of the ^1D eluent and thus this problem must be addressed.

One potential solution may be found in empirical retention modelling. Here, retention parameters are established that relate analyte retention as a function of mobile-phase composition [34]. These parameters are obtained by fitting an empirical model to retention data for each analyte. This data is obtained by measuring analyte retention at several mobile-phase compositions which is often used to develop optimal gradient conditions [35]. For SPAM, there is an opportunity to employ retention modelling since the guard columns used typically feature an identical or similar stationary phase relative to the analytical ^2D column. This suggests that retention parameters obtained from analytical ^2D columns can be extrapolated to the shorter guard columns to predict retention on SPAM columns, a concept that has recently also been used [36], is particularly attractive because the ^2D is often reversed-phase liquid chromatography (RPLC) [37] and often a 1DLC starting point for any 2DLC method. If successful, retention modelling could be used to estimate the success rate of the implementation of SPAM for all analytes, without trial-and-error 2DLC experiments.

In this work we aim to develop a tool to quickly assess the feasibility of using SPAM in 2DLC. We evaluate retention prediction on SPAM (trap) columns with sufficient accuracy to decide on *i*) the feasibility of SPAM and *ii*) the desired dilution flow rate. We aim to use empirical retention models constructed using data obtained from scanning gradients on analytical columns. Various factors need to be controlled to achieve this goal. System parameters, such as the extra-column residence times and column dead time, and the trap-to-trap repeatability must be controlled. We aim to establish an optimal set of gradient-scanning experiments and an optimal retention model to predict isocratic retention factors on SPAM columns. The obtained models will be used to predict the minimal dilution flow needed to achieve sufficient retention on the trap columns. We finally aim to use all this information to decide whether a SPAM process can be used successfully within certain boundaries, such as (minimum and maximum) modulation time, dilution flow, ¹D flow rate, and ¹D modifier composition.

4.2. Experimental

4.2.1. Chemicals

Milli-Q water ($R = 18.2 \text{ M}\Omega \text{ cm}$) was obtained from a purification system (Arium 611UV, Sartorius, Germany). Acetonitrile (ACN, HPLC grade), Acetone (HPLC grade) and Toluene (LC-MS grade) were purchased from Biosolve Chemie (Valkenswaard, The Netherlands). Formic acid (98%) was purchased from Fluka (Buchs, Switzerland). Riboflavin ($\geq 99\%$), crystal violet ($\geq 90\%$), Ammonium formate ($\geq 99\%$), phenol ($\sim 99\%$), orange G, 4-hydroxybenzoic acid ($\geq 99\%$), propranolol ($\geq 99\%$), trimethoprim ($\geq 99\%$), uracil ($\geq 99\%$), and acetaminophen ($\geq 99\%$) were purchased from Sigma Aldrich (Darmstadt, Germany).

Stock solutions were made in $\text{H}_2\text{O}/\text{ACN}$ (50/50, [v/v]) of 500 ppm (riboflavin, toluene, phenol, uracil, acetaminophen, propranolol, trimethoprim, and 4-hydroxy benzoic acid) and 1000 ppm (crystal violet and orange G). Two solutions were made from these separate stock solutions, each containing five compounds, which were further diluted with $\text{H}_2\text{O}/\text{ACN}$ (50:50, [v/v]). The final concentrations can be found in Appendix B-1, Table B-1.

4.2.2. Instrumental

All experiments were carried out on an Agilent 1290 series Infinity 2DLC system (Agilent, Waldbronn, Germany), which was configured for one-dimensional operation. This system was equipped with a binary pump (G7120A) equipped with a 35- μL JetWeaver mixer, an autosampler (G7129B), column oven (G7116B) and a diode-array detector (DAD, G7117B).

For all measurements on the analytical column, a Zorbax RRHD Eclipse Plus C18 column with dimensions 50 × 2.1 mm, 1.8 μm (Agilent) was used. For the measurements on the trapping column the Zorbax RRHD Eclipse plus C18 guard column with dimensions 5 × 2.1 mm, 1.8 μm UHPLC guard (Agilent) was used. The temperature was not controlled. A DAD detector was equipped at several wavelengths, depending on the absorption spectrum of the compound. The detection wavelength for phenol, trimethoprim, propranolol, and toluene was 214 nm, for uracil, 4-hydroxy benzoic acid and acetaminophen it was 254 nm, 590 nm was used for crystal violet, 492 nm for orange G, and 450 nm for riboflavin. The slit size was set to 4 nm and the sampling rate to 240 Hz.

4.2.3. Analytical methods

The following mobile phases were used for all experiments in this project unless stated otherwise. Mobile phase A consisted of a 5 mM ammonium formate buffer targeted to a pH of 3. To prepare 1 L of buffer 0.0476 grams of ammonium formate and 0.195 grams (\pm 160 μL) formic acid were mixed with 1 L of water. The pH of the buffer was verified using a pH-meter (Metrohm, Herisau, Switzerland) and adjusted to pH = 3.00 using additional formic acid and a glass Pasteur pipette. Mobile phase B consisted of ACN.

The dwell volume of the system was determined to be about 0.1775 mL, which was experimentally determined using acetone as modifier. Solvent A was water and solvent B was water with 0.1% [v/v] acetone. An initial time of 4 min was used followed by a gradient from 0 to 100% B in 8 min. These were performed in triplicate and 210 nm was used as detection wavelength. The gradient delay was determined at 50% of the gradient.

The dead volume (V_0) of the analytical column and the guard column was determined by injecting uracil ($V_{inj} = 2 \mu\text{L}$) on the column at a 50/50 [v/v] composition of mobile-phase components A and B and at a flow rate of 0.5 mL/min. The extra-column volume (V_{ex}) was determined by repeating the previous experiments while replacing the column with a union.

4.2.2.1. Isocratic measurements

Isocratic measurements were performed on an analytical column and two trapping columns (trap A and B). Seven different organic-modifier fractions (ϕ) were performed at a flow rate of 0.5 mL·min⁻¹ with an injection volume of 2 μL. The chosen ϕ levels were 0.025, 0.05, 0.075, 0.1, 0.2, 0.3, and 0.4. The analysis time of the isocratic measurements was 10 min. After this period, mobile phase B was increased to 95% in 1 min and maintained for 0.5 min to elute potentially retained compounds. Afterwards, the mobile phase was brought back to the starting conditions of the subsequent method in 0.01 min and maintained for 1.49 min for

re-equilibration. All measurements for both stock solutions with all three columns (*i.e.* one analytical column and two trapping columns) were repeated 5 times using a single batch of buffer.

4.2.2.2. Scanning-gradient experiments

For the scanning gradients on the analytical column, the following gradients were performed. All gradients started with an initial time of 0.25 min at 1% B, followed by a linear gradient to 95% B in either 1, 2, 3, 6, 9, 12, 15, 24, or 48 min. 95% B was maintained for 0.5 min and brought back to 1% B in 0.01 min, followed by a 1.24-min re-equilibration step at 1% B. These scanning gradients were performed at a flow rate of 0.5 mL·min⁻¹. All measurements were performed in triplicate.

4.2.2.3. Dilution-flow experiments

Four different dilution-flow series (DF 1, 2, 3, and 4) were applied on the trap columns. Here, the initial ϕ of the ¹D was varied between the four DF series. The initial ¹D ϕ for DF 1, 2, 3 and 4 were 0.75, 0.5, 0.25, and 0.1, respectively. The initial ¹D flow rate remained the same (50 μ L·min⁻¹), which was diluted 1:0, 1:1, 1:2, 1:3, 1:4, 1:6.5, 1:9, 14:1 and 19:1, corresponding to total flow rates of 50, 100, 150, 200, 250, 375, 500, 750 and 1000 L·min⁻¹, respectively. This yielded 36 different methods, with varying flow rate and ϕ , as can be seen in Appendix B-2. Every measurement was performed in triplicate.

Each of these 36 methods is essentially a 10-min isocratic measurement. For these measurements, the first 10 min consisted of the isocratic part at the described ϕ level and corresponding flow rate. After this part, the flow rate and %B were adjusted to quickly elute potentially retained compounds and re-equilibrate the trapping column.

4.2.4 Data processing

The in-house built MATLAB-based user interface MOREPEAKS [38,39] was used to fit the retention models and determine the retention parameters from the experimental data. The boundaries for the LSS model were -10 to 50 for $\ln k_0$ and 0 to 100 for S_{LSS} . For the QUA model the boundaries were -10 to 50 for $\ln k_0$ and 0 to 100 for S_{1r} and 0 to 100 for S_2 . Expert fitting was used and the multistart function was used at 40 for both models, unless stated otherwise. Microsoft Excel and MATLAB R2020b were used for all other data processing.

4.3. Results & discussion

The goal of this work was to develop a tool to assess the feasibility of using SPAM in 2DLC by predicting retention on SPAM (trap) columns with sufficient accuracy using scanning-gradient experiments on analytical columns. This concept essentially comprised method transfer from one column (analytical) to another (trap) and prediction of isocratic retention at variable flow rate with data from gradient-elution experiments. To achieve this, three steps were outlined, namely *i*) establishing correct system parameters, such as V_0 and V_{ex} , *ii*) selection of appropriate method parameters, such as the number of scanning gradients, the retention model, and the gradient steepness, and *iii*) the accurate description of the effect of a dilution flow on retention. These points were envisaged to predict SPAM retention with a new tool developed in this work. This workflow is shown in Fig. 4.1. These three steps will be covered in Sections 4.3.1, 4.3.2, and 4.3.3, respectively

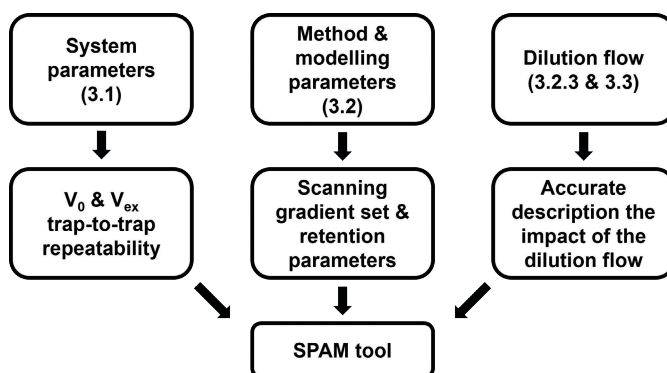


Figure 4.1. Workflow for the development of a retention-prediction tool on trap columns with retention data from analytical columns. Every step corresponds to a result section.

4.3.1. Matching system parameters between analytical columns and trap columns

In order to assess the feasibility of using retention data from analytical columns to predict those on trap columns, it is necessary to compare isocratic retention factors obtained from both columns individually. To compare retention between columns with different dimensions, the dead volume (V_0) of the columns should be determined. Values for V_0 were experimentally determined by injection of a V_0 marker (*i.e.* uracil) in a mobile-phase composition of 50/50 buffer/ACN. Values of 12 μL and 88 μL were obtained for the trap- and analytical columns, respectively. Next to that, the extra-column volume between the injector and the detector (V_{ex}) needs to be determined. By replacing the column with a union, V_{ex} was determined to be 29 μL . The retention factor can then be calculated with Eq. 4.1.

$$k = \frac{V_R - V_0}{V_0 - V_{ex}} \quad (4.1)$$

In Fig. 4.2A, the logarithm of the retention factor is shown for nine compounds at different ϕ for the analytical column and the trap column using the two experimentally determined values for V_0 .

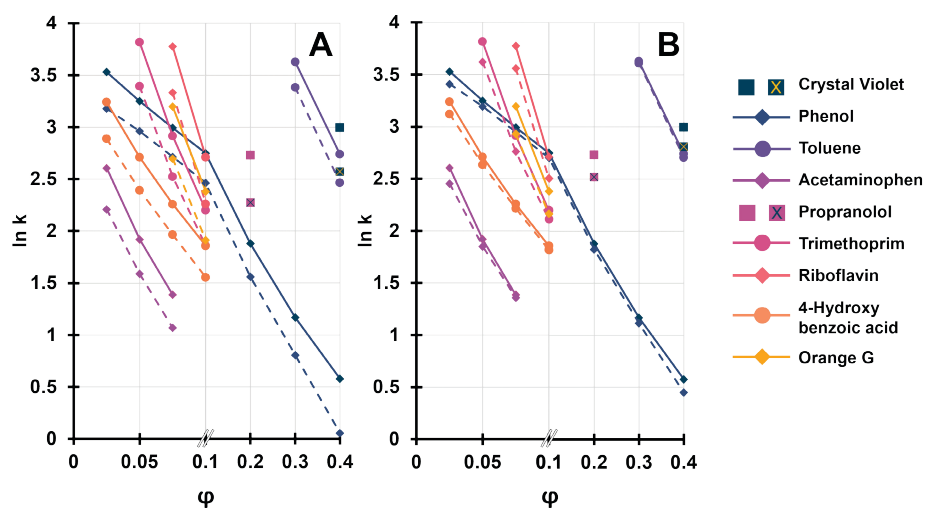


Figure 4.2. Comparison of retention factors of nine compounds on a trap column and an analytical column at different ϕ . The dashed lines depict trap data, whereas the solid lines depict analytical columns. Lines are drawn for visualization purposes if more than one data point is found (*i.e.* not for crystal violet and propranolol). A) retention factors calculated using experimental V_0 values for both the trap and the analytical column; B, retention factors calculated using experimental V_0 value for the analytical column and a proportional V_0 value for the trap. Note the non-continuous x-axis.

The retention factors at different ϕ are seen to deviate systematically between the trap and analytical columns. A possible explanation may be found in the values used for calculating the retention factors. The experimental dead volumes (12 μL and 88 μL) do not seem to vary in proportional to the empty column volumes (17.3 μL and 173 μL , respectively). The columns are packed with a similar stationary phase and have an identical internal diameter. It is reasonable to assume the packing and the resulting porosity to be similar. Thus, the actual dead volume of the trap is expected to be one-tenth of that of the analytical column (8.8 μL). A possible explanation of the higher measured dead volume of the trap could be that there is a significant volume in the trap hardware that is not filled with stationary phase, such as the frit volume. While this is only 3 μL , it amounts to more than 30% of the actual V_0 .

The corrected dead volume shows better agreement (Fig. 4.2B), with the retention factors from the trap overlaying almost exactly with the retention on the column. This demonstrates that if traps and columns are packed with identical stationary phases, there is no need to measure neither analyte retention factors, nor the dead volume on the trap. This is in agreement with our other work [40]. From measurements performed on the column, retention on the trap can be accurately predicted.

SPAM trap columns are typically employed in pairs in fast-paced LC×LC experiments. Consequently, for our protocol to be applicable, good trap-to-trap repeatability is required. To investigate this, retention data was predicted from and for different column-trap or trap-trap combinations. The results are shown in Fig. 4.3. On the left in Fig. 4.3, the experimental values for V_0 are used for each column. There are large deviations when comparing retention values on either of the traps with those obtained on the column (compare Fig. 4.2A). The trap-to-trap repeatability is good, but extrapolation to column retention factors is error prone. Much smaller errors are observed when the corrected dead volume is used for the traps (Fig. 4.3, right).

Only at the extremes of the composition range studied (scarce data with very high or very low retention factors), the errors are seen to be significant. Deviations can be seen between trap A and trap B, likely due to the fact that a somewhat different dead volume (12 and 11 μL) was measured, respectively, while after correction an identical value of 8.8 μL was used.

After correction, the average deviations in retention factors between the column and trap are similar to the deviations between traps. In general, using uncorrected values yields significantly larger errors.

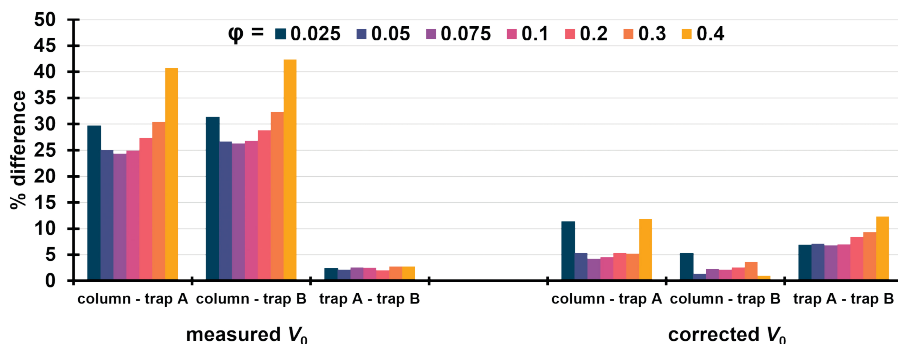


Figure 4.3. Percentual difference in retention between traps and columns at different organic-modifier concentrations with the measured V_0 and the corrected V_0 .

4.3.2. Establishing parameters for retention prediction on trap columns

4.3.2.1. Model selection

Retention modelling can be used to predict isocratic retention on trap columns based on scanning gradients conducted on analytical columns. In principle, models constructed using gradient data can be used to predict isocratic retention times, although significant errors may be obtained [41]. Our earlier work suggested that the most-useful models to fit scanning-gradient data for RPLC were the log-linear or linear-solvent strength (LSS) model and the adsorption (ADS) model. Also, we concluded that the range of slopes of the scanning-gradients set should encompass or approach that of the optimized gradient [35]. The previous research, however, focused on method optimization for gradients on the same column, while in the present study we attempt to predict isocratic retention on much shorter columns than that used to construct the model.

To explain the relevance of any prediction errors, Fig. 4.4 shows the isocratic retention of acetaminophen on a trap column plotted with both the LSS and ADS model fitted to the data.

Overestimation of the retention, *i.e.* predicting that the analyte is retained whereas it is not, is a *false positive* in the context of the present study, as it results in a loss of analyte. This is visualized in Fig. 4.4 by the ADS model, which predicts an $\ln k$ of about 5 for $\varphi = 0$, whereas the actual retention factor may be much lower. In contrast, underestimation of retention, *i.e.* predicting that the analyte is not retained, whereas in fact it is, can be regarded as a *false negative*. This would not lead to a loss of analyte since it is trapped better than anticipated.

The LSS model, however, cannot deal with any curvature in the data. For this reason, the quadratic model (QUA)¹ was also investigated. For the obtained fitting parameters, Fig. 4.4 shows that the QUA model yields similar retention factors at $\varphi = 0$ as the LSS model, while accounting for some curvature across the range of φ . For this reason, both the LSS and the QUA model were investigated in the remainder of this research. The appropriate equations for these two models are

$$\ln k = \ln k_0 - S_{\text{LSS}}\varphi \quad (4.2)$$

$$\ln k = \ln k_0 - S_1\varphi + S_2\varphi^2 \quad (4.3)$$

1 Model described as Q model in Chapter 2 and 3. To be consistent in this chapter, three-letter abbreviations were chosen for all models.

where $\ln k_0$ represents the logarithm of the retention factor at an imaginary organic-modifier concentration of 0, the S_{LSS} value or the S_1 and S_2 values describe how the retention changes with changing modifier concentration for the LSS model and QUA model, respectively.²

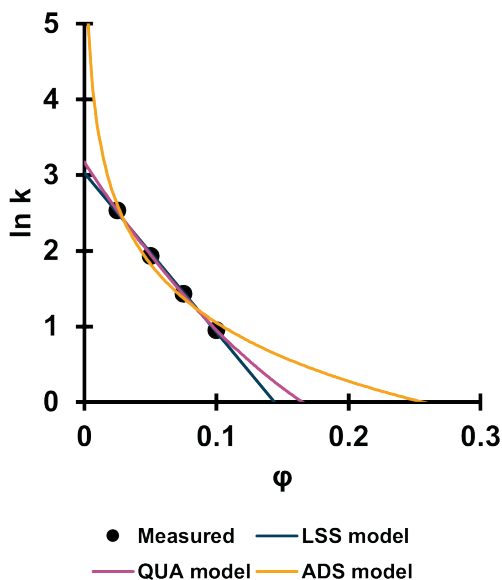


Figure 4.4. Fit of the LSS (blue), QUA (violet), and ADS (yellow) models to the isocratic retention data of acetaminophen on a C18 trap column against the volume fraction of ACN.

When coefficients in the retention equation (“retention parameters”) are to be obtained from gradient-elution data, we cannot directly fit the retention model. Instead, we have to use the more-complex equations that relate the retention time under gradient conditions to the retention parameters and the parameters that describe the gradient program. There is no analytical solution for these equations and an iterative numerical approach must be followed, starting from an initial estimate of the retention parameters. Such an approach may lead to a local optimum and multiple combinations of model coefficients can yield similar sum-of-squares errors [40]. For that reason, the model fit was optimized with a “multistart” function, *i.e.* multiple starting points in the parameter space are used to find a global optimum of the fit. The number of multistart positions was examined. With a lower and upper boundary of 0 and 100, respectively, for both the S_{LSS} , S_1 and S_2 parameters of the model and a -10 to 50 range for the value of $\ln k_0$, multistarts with 20, 40, and 100 positions were investigated.

2 Both S_1 and S_2 parameters are described as $S_{1,0}$ and $S_{2,0}$ parameter in Chapter 2 and 3. Since QUA is the only 3-parameter models in this chapter, both parameters are described as S_1 and S_2 .

The model was fitted five times and the standard deviation in the AIC value was used as indication of the correct number of starting points. The results are summarized in Fig. 4.5. For some compounds, such as crystal violet, phenol, toluene, and trimethoprim, the multistart function does not seem to have an effect on the deviation. However, for other compounds the multistart 20 gives rise to a higher AIC value (*i.e.* a worse fit). There is very little difference between 40 and 100, although the latter requires significant computational resources. Thus, a multistart with 40 positions was selected.

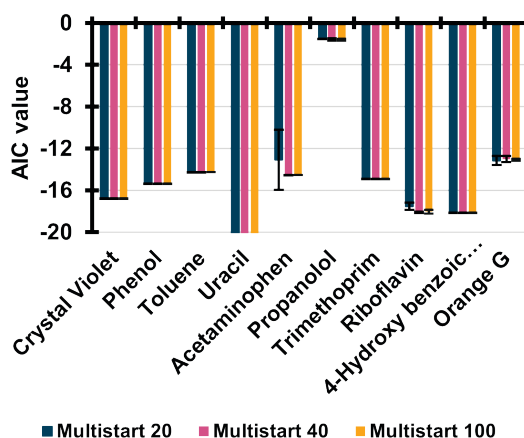


Figure 4.5. Average AIC values for multistart 20 (blue), 40 (violet), and 100 (yellow) for all analysed compounds. Note that the AIC values for uracil exceed the y-axis.

4.3.2.2. Validity of using gradient data to predict isocratic retention

To assess the validity of using gradient data to predict isocratic retention, isocratic retention was predicted from gradient data on an analytical column. Five different sets of gradient-scanning experiments were used throughout this study, as specified in Appendix B-3. Nine data points were used, comprising of either *i*) 3 repeat experiments of 3-, 6- and 9-min gradients (set 2), or *ii*) one of each 1-, 2-, 3-, 6-, 9-, 12-, 15-, 24-, and 48-min gradients (set 5). The prediction error ($\varepsilon_{\text{pred}}$) was calculated from

$$\varepsilon_{\text{pred}} = t_{\text{R,pred}} - \overline{t_{\text{R,exp}}} \quad (4.4)$$

where $t_{\text{R,pred}}$ is the predicted retention time and $\overline{t_{\text{R,exp}}}$ is the measured retention time (average of triplicate measurements). The resulting values are plotted for all compounds and a series of ϕ values in Fig. 4.6A.

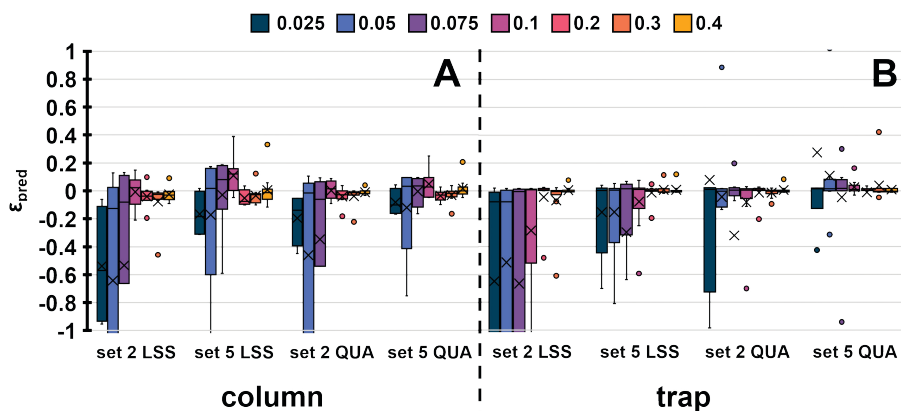


Figure 4.6. Prediction error for the LSS and QUA model with gradient sets of 3, 6, and 9 min (set 2) or all gradients (1, 2, 3, 6, 9, 12, 15, 24, and 48 min; set 5) on the analytical column (A) and trap column (B). The colours indicate the different ϕ levels (increasing from left to right within each cluster). The crosses indicate the average, while the points indicate outliers. The complete graph with all outliers is shown in Appendix B-4, Fig. B-2.

In Fig. 4.6A, all models and sets consistently show underestimation ($t_{R,pred} < \overline{t_{R,exp}}$) for the lowest ϕ values. This error is more severe for set 2 and slightly larger for the LSS model. When results for set 5 are compared, a better prediction is obtained using the QUA model. This confirms the impression of Fig. 4.4 that the QUA model yields better predictions in the low- ϕ range. When the same experiment was repeated for retention prediction on trap columns, slightly larger prediction errors were observed (Fig. 4.6B). The quadratic model seems to yield more-useful predictions relative to the LSS model.

4.3.2.3. Effect of the dilution flow

The experimental setup used to record the data of Fig. 4.6B resembles that encountered with SPAM experiments in two-dimensional liquid chromatography, but it does not account for a possible dilution flow, which would result in altered flow rates and mobile-phase compositions. The purpose of diluting the 1D effluent is a reduction of the organic-modifier fraction (ϕ) at the cost of an increase in flow rate (F). Both parameters exert opposite effects on the retention volume. By decreasing ϕ in RPLC the retention is increased, as prescribed by the S_{LSS} parameter in the LSS model, whereas the increasing flow rate results in a reduced t_0 and thus a reduced t_R . This net result of the two effects is displayed in Fig. 4.7.

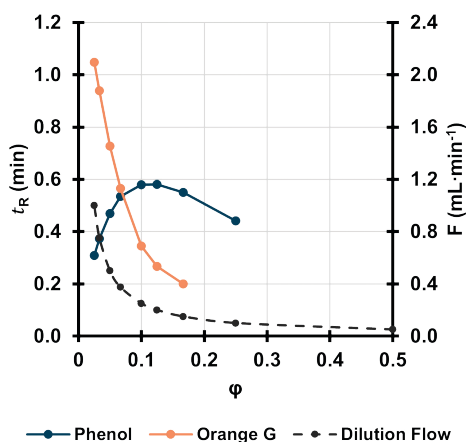


Figure 4.7. Experimental retention times of phenol (blue line, left axis) and orange G (orange line, left axis) at various organic modifier concentrations. Each organic-modifier concentration corresponds with a specific flow rate. The correlation is shown by the grey dashed line (right axis). Experimental details correspond to dilution-flow series 2 (DF2, starting value for ${}^1\varphi = 0.5$) (see Appendix B-2).

In Fig. 4.7 the retention time is depicted along the φ range for phenol and orange G. While the retention time of orange G increases with decreasing φ (corresponding with an increasing F), phenol shows a maximum in retention time. When the flow surpasses $0.250 \text{ mL}\cdot\text{min}^{-1}$ retention starts to decrease with increasing flow, even though φ is still decreasing. Clearly, a dilution flow can have a counter-intuitive effect on the retention of an analyte on a SPAM trap. Therefore, it is dangerous to dilute samples limitlessly. In the LSS and QUA model, the parameters that describe the effect of the organic modifier are S_{LSS} and the S_1 and S_2 , respectively. When the retention parameters of these two compounds, calculated from the scanning-gradient data of the analytical column, are compared, they are found to be much lower for phenol (S_{LSS} , 8.60, S_1 , 11.42, S_2 , 8.53) than for orange G (S_{LSS} , 28.90, S_1 , 41.47, S_2 , 48.31). This result indicates that the effect of the dilution flow is related to the magnitude of the retention parameters. Compounds with high S-values will benefit from higher dilution flows, whereas for those with low S-values the effect may be opposite. The effects of a dilution flow can be described by the following formulae for the LSS model (Eq. 4.5) and the QUA model (Eq. 4.6).

$$\frac{t_{R,q}}{t_{R,p}} = \frac{1 + \exp\left(\ln k_0 - S_{LSS} \cdot \frac{\varphi}{1+q}\right)}{1 + \exp\left(\ln k_0 - S_{LSS} \cdot \frac{\varphi}{1+p}\right)} \cdot \frac{1+p}{1+q} \quad (4.5)$$

$$\frac{t_{R,q}}{t_{R,p}} = \frac{1 + \exp\left(\ln k_0 - S_1 \cdot \frac{\varphi}{1+q} + S_2 \cdot \left(\frac{\varphi}{1+q}\right)^2\right)}{1 + \exp\left(\ln k_0 - S_1 \cdot \frac{\varphi}{1+p} + S_2 \cdot \left(\frac{\varphi}{1+p}\right)^2\right)} \cdot \frac{1+p}{1+q} \quad (4.6)$$

Where $t_{R,p}$ and $t_{R,q}$ are the retention times of an analyte at dimensionless dilution flows (actual flow divided by 1F) p and q . At a p value of zero the dilution factor $(1+p)$ equals 1 and the 1D effluent is not diluted. Eqs. 4.5 and 4.6 are derived in Appendix B-5. The first (large) factor on the right-hand side of Eqs. 4.5 and 4.6 represents the effect of the mobile-phase composition on the retention time, whereas the factor $(1+p)/(1+q)$ represents the effect of the flow rate.

4.3.2.4. Model evaluation and comparison

Now that the effect of the dilution flow has been described, scanning gradients will be used to predict retention for four series of dilution-flow experiments. These series started with ${}^1F = 50 \mu\text{L}\cdot\text{min}^{-1}$ and ${}^1\phi$ values of 0.75, 0.5, 0.25, and 0.1. All effluents were diluted 1:0, 1:1, 1:2, 1:3, 1:4, 1:6.5, 1:9, 1:14 and 1:19 (${}^1F:p$), corresponding to total flow rates through the trap column of 50, 100, 150, 200, 250, 375, 500, 750 and 1000 $\mu\text{L}\cdot\text{min}^{-1}$. The results for all compounds are shown in Fig. 4.8A. Similar results are found regarding underestimation of retention at low ϕ values with the LSS model and gradient set 2. The smallest errors were again found for set 5 in combination with the QUA model. The latter was thus selected for the remaining studies. It should be noted here that underestimation of retention (a negative value of ϵ_{pred}) at low ϕ values may have no consequences for the SPAM process, since retention at these values is already much higher than the minimum value needed for successful trapping. In Figs. 4.8B and 4.8C, the predicted and measured retention factors for series DF2 are shown for riboflavin and toluene, respectively. Riboflavin was hard to model (*i.e.* high AIC values). It can be seen in Fig. 4.8B that set 2 led to underestimation of the retention with both models. The most-accurate retention prediction was found for set 5 with the QUA model. In Fig. 4.8C the underestimation of the LSS model with set 2 is also evident for toluene, while the other predictions seem to be close to the measured values.

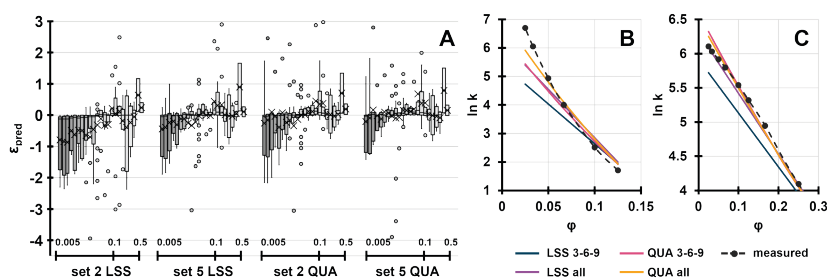


Figure 4.8. A) Prediction errors for all compounds calculated with the LSS and QUA models with a gradient set of 3, 6, and 9 min or with all gradients (1, 2, 3, 6, 9, 12, 15, 24, and 48 min); C18 trap column; four dilution-flow series (overlapping in the figure). The final composition is depicted on the horizontal axis for each cluster; the darkness of the bars also decreases with increasing ϕ values. The crosses indicate the average, the points indicate outliers. Fig. B-3 in Appendix B-6 shows the complete y-axis. B-C) Retention curves for riboflavin and toluene, respectively, in the DF2 series (starting value for ${}^1\phi = 0.5$).

4.3.2.5. Optimal gradient set

Now that the most-accurate model has been established, we focus on the selection of the most-accurate gradient set. Five sets were designed, that either consisted of three repeats of three gradients (1, 2, and 3 min, set 1; 3, 6, and 9 min, set 2; 9, 12, and 15 min, set 3; and 15, 24, and 48 min, set 4) or one repeat of nine different gradients (1, 2, 3, 6, 9, 12, 15, 24, and 48 min, set 5), always yielding a total input of nine datapoints. The retention was predicted for all analytes for all four dilution-flow series and the results are shown in Fig. 4.9A.

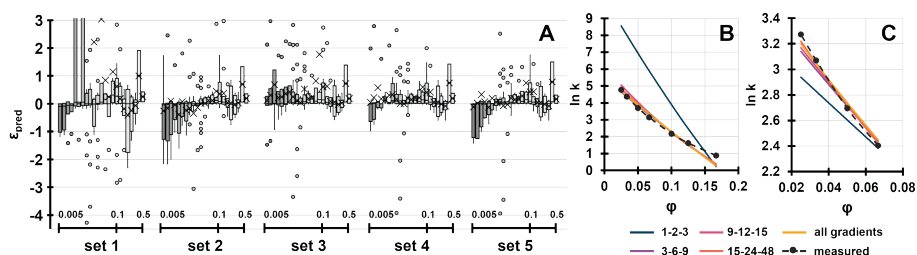


Figure 4.9. A) Prediction error for all compounds calculated with five different gradient sets (three repeats of 1-, 2-, and 3-min; 3-, 6-, and 9-min; 9-, 12-, and 15-min; and 15-, 24-, and 48-min gradients or a single repeat of all nine gradients, set 1-5 respectively) for the trap columns subjected to four different dilution-flow series. The final composition is depicted on the horizontal axis for each cluster; the darkness of the bars also decreases with increasing ϕ values. The crosses indicate the average, the points indicate outliers. Fig. B-4 in Appendix B-7 shows the complete y-axis. B-C) Retention curves for orange G and 4-hydroxy benzoic acid, respectively, in the DF2 series (starting value for $\phi = 0.5$).

The results show that the steep gradients (set 1) yield unstable predictions. Furthermore, both set 2 and 5 yield underestimations of retention in the low- ϕ range (*i.e.* $\phi < 0.02$). Set 3 and 4 both seem to mainly overpredict retention on trap columns. It is possible that the underestimation in the low- ϕ range with set 5 is due to the inclusion of the steep gradients, which are not part of set 3. The inaccurate prediction from the steep-gradient set (set 1, 1, 2, 3 min) is confirmed by the compound-specific retention plots shown for orange G and 4-hydroxy benzoic acid in Fig. 4.9B and Fig. 4.9C, respectively. Using the steep-gradient set, the retention is either overestimated (Fig. 4.9B) or underestimated (Fig. 4.9C), while the other gradient sets all seem to yield a similar and more accurate prediction of the retention.

4.3.3. Development of a SPAM-prediction tool

Prediction of successful trapping on SPAM columns requires calculation of the minimal retention factor needed. Suppose we have a trap that, for a given modulation time and at a given flow rate, must retain an analyte. The retention factor (k) is related to the void volume (V_p) and the retention volume (V_R) as shown by Eq. 4.7.

$$V_R = V_0(1 + k) \quad (4.7)$$

For our trap, there will be a maximum volume (V_{\max} ; or time t_{\max} at a given flow rate) for which the analyte can be retained. There is a corresponding minimal retention factor (k_{\min}).

However, V_{\max} represents the apex of the analyte band or the chromatographic peak. We want the front section of the peak to not prematurely elute either. By taking into account the efficiency of the trap (standard deviation σ), this can be corrected for (Eqs. 4.8-4.10).

$$k_{\min} = \frac{V_{\max}}{V_0} + 2\sigma - 1 \quad (4.8)$$

If the peak is Gaussian, this leads to

$$k_{\min} = \frac{V_{\max}}{V_0} + \frac{2V_{\max}}{\sqrt{N}} - 1 \quad (4.9)$$

$$k_{\min} = \frac{V_{\max}}{V_0} \left(1 + \frac{2V_0}{\sqrt{N}} \right) - 1 \quad (4.10)$$

where N is the plate number. With a given modulation time (t_{mod}) and total flow rate (F_{tot}), defined as the sum of the 1D flow rate (1F), and a dilution flow rate, ($^D F = p^1 F$), Eq. 4.11 is obtained.

$$k_{\min} = \frac{t_{\text{mod}} \cdot (^1 F + p \cdot ^1 F)}{V_0} \left(1 + \frac{2V_0}{\sqrt{N}} \right) - 1 \quad (4.11)$$

Depending on which model is used, the retention of a compound can be described according to the LSS model (Eq. 4.12A) or the QUA model (Eq. 4.13A) if the dilution flow is 100% aqueous ($^D \varphi = 0$) or for a different composition ($\varphi \neq 0$, Eq. 4.12B and 4.13B).

$$k_{\text{LSS},p} = \exp \left(\ln k_0 - S_{\text{LSS}} \cdot \frac{^1 \varphi}{p+1} \right) \quad (4.12A)$$

$$k_{\text{LSS},p} = \exp \left(\ln k_0 - S_{\text{LSS}} \cdot \frac{^1 \varphi + p^D \varphi}{p+1} \right) \quad (4.12B)$$

$$k_{\text{QUA},p} = \exp \left(\ln k_0 + S_1 \cdot \left(\frac{^1 \varphi}{p+1} \right) + S_2 \left(\frac{^1 \varphi}{p+1} \right)^2 \right) \quad (4.13A)$$

$$k_{\text{QUA},p} = \exp \left(\ln k_0 + S_1 \cdot \left(\frac{^1 \varphi + p^D \varphi}{p+1} \right) + S_2 \left(\frac{^1 \varphi + p^D \varphi}{p+1} \right)^2 \right) \quad (4.13B)$$

We developed a tool to determine whether SPAM can be applied to a sample and what would be the optimal dilution flow ($^D F$) and modulation time (t_{mod}) [42]. For this tool both

the equation for the minimal k is used, as well as the formula for the compound-specific retention (Eqs. 4.11-4.13). The user is asked to provide a list of compounds with corresponding retention parameters. Next to that, the user is asked to provide values for 1F , ${}^1\phi$, $F_{\text{tot,min}}$, $F_{\text{tot,max}}$, $t_{\text{mod,min}}$, and $t_{\text{mod,max}}$. Besides these parameters, the user needs to estimate the plate number (N) and the V_0 of the trap column. This volume should be estimated from the V_0 of the analytical column, as described in Section 4.3.1. The ϕ of the dilution flow can be adjusted by the user. The user is advised to use scanning gradients that cover a wide range of scanning gradients without using very steep gradients (see Section 4.3.2.5).

To test the effectiveness of this tool, the retention was predicted for four dilution flow series, all starting with a flow rate of $50 \mu\text{L}\cdot\text{min}^{-1}$ and with ϕ values of 0.75, 0.5, 0.25, and 0.1. All effluents were diluted 1:0, 1:1, 1:2, 1:3, 1:4, 1:6.5, 1:9, 1:14, and 1:19, corresponding to total flow rates of 50, 100, 150, 200, 250, 375, 500, 750, and $1000 \mu\text{L}\cdot\text{min}^{-1}$. The modulation time was set to 0.5, 1, and 2 min, and the retention of all compounds was predicted with the QUA model. Sets 1 to 5 were used to estimate the coefficients (retention parameters) of this model. Four possible outcomes were distinguished.

- > predicted and measured retention above the modulation time (true positive)
- > predicted and measured retention below the modulation time (true negative)
- > predicted retention above the modulation time and measured retention below the modulation time (false positive)
- > predicted retention below the modulation time and the measured retention above the modulation time (false negative).

For this tool to work, the ratios of the numbers of false positives and false negatives to the total number of measurements should be as low as possible. Both types of errors are undesirable. Therefore, the total fraction of false positives plus false negatives was considered in this work. This ratio was found to be 8.64%, 4.01%, 3.24%, 3.10%, and 2.94% for set 1, set 2, set 3, set 4, and set 5, respectively. However, it was found that much of the error was due to the compounds that were harder to fit the models to. This is illustrated in Fig. 4.10. There were no false positives or false negatives observed for phenol, toluene, uracil, and acetaminophen. Also, for crystal violet, only one false positive was found. However, because of the total number of measurements (6), this contributed significantly to the total percentage of false positives. There is no clear link between the goodness-of-fit and the rate

of false positive plus false negatives. The error rate along the different sets is similar for all compounds, except for those of set 1. This set consists of very steep scanning gradients. Set 2 yields better results than set 1, but the other three sets all perform better. It is surprising that set 5, with a single run of all nine gradients, yields the lowest error percentage on average. This could be because many points are available along the ϕ axis, so that the QUA model can fit the curve better, even though somewhat worse AIC values were observed than for all but the fastest gradient set (Fig. 4.10, right-hand scale).

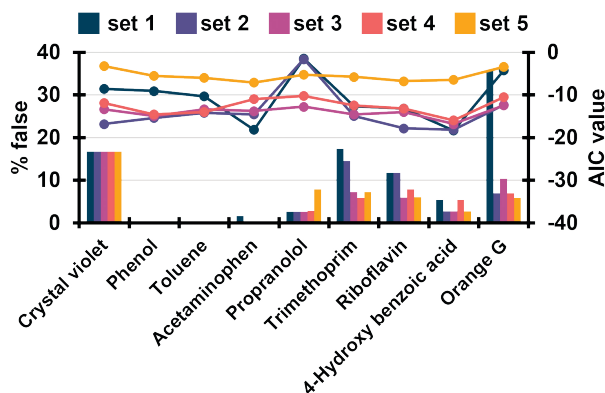


Figure 4.10. Percentage of false positives plus false negatives relative to the total number of measurements (bars). Retention times are predicted on the trap for four dilution-flow series at three modulation times, using retention parameters established from five different gradient sets (three repeats of 1-, 2- and 3- min, set 1; 3-, 6- and 9-min, set 2; 9-, 12-, and 15-min, set 3; and 15-, 24-, and 48-min gradients, set 4; or a single repeat of all nine gradients, set 5). The lines indicate the AIC values (right axis) for the specific compounds with the different gradient sets. Connecting lines between points are for visualization purposes only.

In the present version of our tool, the composition of the ^1D effluent is assumed constant during the run. In some LC \times LC setups, for example with ion exchange or size-exclusion in the first dimension, this may be realistic [9,43]. However, in the more-common case where the ^1D separation is a reversed-phase or hydrophilic-interaction liquid chromatography (HILIC) gradient, the organic-modifier concentration will vary with time. In that case, the correct ^1D -effluent composition to use in Eqs. 4.12 and 4.13 is the elution composition of the specific analyte, which can readily be determined from the retention parameters of the analyte on the ^1D column. A final difference between our current experimental setup and contemporary implementation of comprehensive two-dimensional liquid chromatography may be the possible incorporation of a mixer. A mixer may promote effective retention of the analyte on the trap, but it will contribute to the band broadening. Some of the experiments reported in this paper were repeated with a mixer incorporated. The results are documented in Appendix B-8, Fig. B-5. The early eluting peaks experience additional band broadening,

but the retention volumes are essentially unaffected. The additional band broadening can be accounted for in the model through the experimental value of σ or N . For later eluting compounds, the effects were more severe, but the consequences for predicting the success of trapping were minimal, because these compounds typically eluted much later than the modulation time.

4.4. Concluding remarks

In this research, a tool was developed that allows chromatographers to rapidly develop two-dimensional liquid chromatography methods with stationary-phase-assisted modulation (SPAM). The tool is publicly available on-line [42]. Retention modelling was applied to predict the feasibility of SPAM for a variety of analytes under a range of conditions. Experimentally obtained values for the dead volume of very small (trap) columns showed large errors. More-accurate values were obtained by extrapolating the values obtained on larger (analytical) columns. Among the retention models studied, the quadratic model yielded better predictions than the log-linear ("linear-solvent-strength") model. Guidelines were formulated for scanning gradients. Short gradients gave rise to large prediction errors. Introducing variations in both flow rate and organic-modifier concentration, *i.e.* simulating dilution flows, caused a significant increase in prediction errors for all models and gradient sets analysed. Dilution with a weaker eluent is usually assumed to promote trapping, but it was shown that dilution may have an adverse effect for compounds that show modest retention. A tool was developed to help the analyst decide whether a specific analyte can or cannot be trapped. The tool yielded correct decisions in more than 95% of cases, for each set of gradients with either the quadratic or log-linear model.

References

- [1] B.W.J. Pirok, A.F.G. Gargano, P.J. Schoenmakers, Optimizing separations in on-line comprehensive two-dimensional liquid chromatography, *J. Sep. Sci.* 41 (2018) 68–98. <https://doi.org/10.1002/jssc.201700863>.
- [2] J. De Vos, K. Broeckhoven, S. Eeltink, Advances in Ultrahigh-Pressure Liquid Chromatography Technology and System Design, *Anal. Chem.* 88 (2015) 262–278. <https://doi.org/10.1021/ACS.ANALCHEM.5B04381>.
- [3] V. González-Ruiz, A.I. Olives, M.A. Martín, Core-shell particles lead the way to renewing high-performance liquid chromatography, *TrAC Trends Anal. Chem.* 64 (2015) 17–28. <https://doi.org/10.1016/J.TRAC.2014.08.008>.
- [4] T.H. Walter, R.W. Andrews, Recent innovations in UHPLC columns and instrumentation, *TrAC Trends Anal. Chem.* 63 (2014) 14–20. <https://doi.org/10.1016/J.TRAC.2014.07.016>.
- [5] S. Fekete, J. Schappler, J.L. Veuthey, D. Guillaume, Current and future trends in UHPLC, *TrAC Trends Anal. Chem.* 63 (2014) 2–13. <https://doi.org/10.1016/J.TRAC.2014.08.007>.
- [6] N. Tanaka, D. V. McCalley, Core-Shell, Ultrasmall Particles, Monoliths, and Other Support Materials in High-Performance Liquid Chromatography, *Anal. Chem.* 88 (2015) 279–298. <https://doi.org/10.1021/ACS.ANALCHEM.5B04093>.
- [7] C.V. McNeff, B. Yan, D.R. Stoll, R.A. Henry, Practice and theory of high temperature liquid chromatography, *J. Sep. Sci.* 30 (2007) 1672–1685. <https://doi.org/10.1002/JSSC.200600526>.
- [8] J.M. Davis, J.C. Giddings, Statistical theory of component overlap in multicomponent chromatograms, *Anal. Chem.* 55 (2002) 418–424. <https://doi.org/10.1021/AC00254A003>.
- [9] B.W.J. Pirok, M.J. Den Uijl, G. Moro, S.V.J. Berbers, C.J.M. Croes, M.R. Van Bommel, P.J. Schoenmakers, Characterization of Dye Extracts from Historical Cultural-Heritage Objects Using State-of-the-Art Comprehensive Two-Dimensional Liquid Chromatography and Mass Spectrometry with Active Modulation and Optimized Shifting Gradients, *Anal. Chem.* (2019). <https://doi.org/10.1021/acs.analchem.8b05469>.
- [10] M. Iguiniz, S. Heinisch, Two-dimensional liquid chromatography in pharmaceutical analysis. Instrumental aspects, trends and applications, *J. Pharm. Biomed. Anal.* 145 (2017) 482–503. <https://doi.org/10.1016/J.JPBA.2017.07.009>.
- [11] F. Cacciola, F. Rigano, P. Dugo, L. Mondello, Comprehensive two-dimensional liquid chromatography as a powerful tool for the analysis of food and food products, *TrAC Trends Anal. Chem.* 127 (2020) 115894. <https://doi.org/10.1016/J.TRAC.2020.115894>.
- [12] X. Ouyang, P. Leonards, J. Legler, R. van der Oost, J. de Boer, M. Lamoree, Comprehensive two-dimensional liquid chromatography coupled to high resolution time of flight mass spectrometry for chemical characterization of sewage treatment plant effluents, *J. Chromatogr. A.* 1380 (2015) 139–145. <https://doi.org/10.1016/J.CHROMA.2014.12.075>.
- [13] N. Abdulhussain, S. Nawada, P. Schoenmakers, Latest Trends on the Future of Three-Dimensional Separations in Chromatography, *Chem. Rev.* (2021). <https://doi.org/10.1021/ACS.CHEMREV.0C01244>.
- [14] B.W.J. Pirok, D.R. Stoll, P.J. Schoenmakers, Recent Developments in Two-Dimensional Liquid Chromatography: Fundamental Improvements for Practical Applications, *Anal. Chem.* 91 (2019) 240–263. <https://doi.org/10.1021/acs.analchem.8b04841>.
- [15] J. De Vos, D. Stoll, S. Buckenmaier, S. Eeltink, J.P. Grinias, Advances in ultra-high-pressure and multi-dimensional liquid chromatography instrumentation and workflows, *Anal. Sci. Adv.* 2 (2021) 171–192. <https://doi.org/10.1002/ANSA.202100007>.
- [16] P. Dugo, F. Cacciola, T. Kumm, G. Dugo, L. Mondello, Comprehensive multidimensional liquid chromatography: Theory and applications, *J. Chromatogr. A.* 1184 (2008) 353–368. <https://doi.org/10.1016/J.CHROMA.2007.06.074>.

- [17] A. Moussa, T. Lauer, D. Stoll, G. Desmet, K. Broeckhoven, Numerical and experimental investigation of analyte breakthrough from sampling loops used for multi-dimensional liquid chromatography, *J. Chromatogr. A*. 1626 (2020) 461283. <https://doi.org/10.1016/j.chroma.2020.461283>.
- [18] L. Mondello, M. Herrero, T. Kumm, P. Dugo, H. Cortes, G. Dugo, Quantification in Comprehensive Two-Dimensional Liquid Chromatography, *Anal. Chem.* 80 (2008) 5418–5424. <https://doi.org/10.1021/AC800484Y>.
- [19] D.R. Stoll, R.W. Sajulga, B.N. Voigt, E.J. Larson, L.N. Jeong, S.C. Rutan, Simulation of elution profiles in liquid chromatography – II: Investigation of injection volume overload under gradient elution conditions applied to second dimension separations in two-dimensional liquid chromatography, *J. Chromatogr. A*. 1523 (2017) 162–172. <https://doi.org/10.1016/j.chroma.2017.07.041>.
- [20] L.N. Jeong, R. Sajulga, S.G. Forte, D.R. Stoll, S.C. Rutan, Simulation of elution profiles in liquid chromatography—I: Gradient elution conditions, and with mismatched injection and mobile phase solvents, *J. Chromatogr. A*. 1457 (2016) 41–49. <https://doi.org/10.1016/j.chroma.2016.06.016>.
- [21] D.R. Stoll, K. Shoykhet, P. Petersson, S. Buckenmaier, Active Solvent Modulation: A Valve-Based Approach To Improve Separation Compatibility in Two-Dimensional Liquid Chromatography, *Anal. Chem.* 89 (2017) 9260–9267. <https://doi.org/10.1021/ACS.ANALCHEM.7B02046>.
- [22] D.R. Stoll, H.R. Lhotka, D.C. Harmes, B. Madigan, J.J. Hsiao, G.O. Staples, High resolution two-dimensional liquid chromatography coupled with mass spectrometry for robust and sensitive characterization of therapeutic antibodies at the peptide level, *J. Chromatogr. B Anal. Technol. Biomed. Life Sci.* 1134–1135 (2019). <https://doi.org/10.1016/j.jchromb.2019.121832>.
- [23] M. Sun, M. Sandahl, C. Turner, Comprehensive on-line two-dimensional liquid chromatography × supercritical fluid chromatography with trapping column-assisted modulation for depolymerised lignin analysis, *J. Chromatogr. A*. 1541 (2018) 21–30. <https://doi.org/10.1016/J.CHROMA.2018.02.008>.
- [24] R.J. Vonk, A.F.G. Gargano, E. Davydova, H.L. Dekker, S. Eeltink, L.J. de Koning, P.J. Schoenmakers, Comprehensive Two-Dimensional Liquid Chromatography with Stationary-Phase-Assisted Modulation Coupled to High-Resolution Mass Spectrometry Applied to Proteome Analysis of *Saccharomyces cerevisiae*, *Anal. Chem.* 87 (2015) 5387–5394. <https://doi.org/10.1021/ACS.ANALCHEM.5B00708>.
- [25] B.W.J. Pirok, N. Abdullhussain, T. Brooijmans, T. Nabuurs, J. de Bont, M.A.J. Schellekens, R.A.H. Peters, P.J. Schoenmakers, Analysis of charged acrylic particles by on-line comprehensive two-dimensional liquid chromatography and automated data-processing, *Anal. Chim. Acta.* 1054 (2019) 184–192. <https://doi.org/10.1016/J.ACA.2018.12.059>.
- [26] S.R. Groskreutz, S.G. Weber, Temperature-assisted solute focusing with sequential trap/release zones in isocratic and gradient capillary liquid chromatography: Simulation and experiment, *J. Chromatogr. A*. 1474 (2016) 95–108. <https://doi.org/10.1016/j.chroma.2016.10.062>.
- [27] M.E. Creese, M.J. Creese, J.P. Foley, H.J. Cortes, E.F. Hilder, R.A. Shellie, M.C. Breadmore, Longitudinal On-Column Thermal Modulation for Comprehensive Two-Dimensional Liquid Chromatography, *Anal. Chem.* 89 (2016) 1123–1130. <https://doi.org/10.1021/ACS.ANALCHEM.6B03279>.
- [28] S.R. Groskreutz, A.R. Horner, S.G. Weber, Temperature-based on-column solute focusing in capillary liquid chromatography reduces peak broadening from pre-column dispersion and volume overload when used alone or with solvent-based focusing, *J. Chromatogr. A*. 1405 (2015) 133–139. <https://doi.org/10.1016/J.CHROMA.2015.05.071>.
- [29] H.C. Van de Ven, A.F.G. Gargano, S.J. Van der Wal, P.J. Schoenmakers, Switching solvent and enhancing analyte concentrations in small effluent fractions using in-column focusing, *J. Chromatogr. A*. 1427 (2016) 90–95. <https://doi.org/10.1016/J.CHROMA.2015.11.082>.
- [30] E. Fornells, B. Barnett, M. Bailey, E.F. Hilder, R.A. Shellie, M.C. Breadmore, Evaporative membrane modulation for comprehensive two-dimensional liquid chromatography, *Anal. Chim. Acta.* 1000 (2018) 303–309. <https://doi.org/10.1016/J.ACA.2017.11.053>.

- [31] H. Tian, J. Xu, Y. Guan, Comprehensive two-dimensional liquid chromatography (NPLC×RPLC) with vacuum-evaporation interface, *J. Sep. Sci.* 31 (2008) 1677–1685. <https://doi.org/10.1002/JSSC.200700559>.
- [32] H. Tian, J. Xu, Y. Xu, Y. Guan, Multidimensional liquid chromatography system with an innovative solvent evaporation interface, *J. Chromatogr. A* 1137 (2006) 42–48. <https://doi.org/10.1016/J.CHROMA.2006.10.005>.
- [33] L.E. Niezen, B.B.P. Staal, C. Lang, B.W.J. Pirok, P.J. Schoenmakers, Thermal Modulation To Enhance Two-Dimensional Liquid Chromatography Separations of Polymers, *J. Chromatogr. A* 1653 (2021) 462429. <https://doi.org/10.1016/J.CHROMA.2021.462429>.
- [34] M.J. den Uijl, P.J. Schoenmakers, B.W.J. Pirok, M.R. van Bommel, Recent applications of retention modelling in liquid chromatography, *J. Sep. Sci.* 44 (2021) 88–114. <https://doi.org/10.1002/JSSC.202000905>.
- [35] M.J. den Uijl, P.J. Schoenmakers, G.K. Schulte, D.R. Stoll, M.R. van Bommel, B.W.J. Pirok, Measuring and using scanning-gradient data for use in method optimization for liquid chromatography, *J. Chromatogr. A* 1636 (2021) 461780. <https://doi.org/10.1016/J.CHROMA.2020.461780>.
- [36] D.R. Stoll, G. Kainz, T.A. Dahlseid, T. Kempen, T. Brau, B. 4 Pirok, An Approach to High Throughput Measurement of Accurate Retention Data in Liquid Chromatography, (2022). <https://doi.org/10.26434/CHEMRXIV-2022-PKQS1>.
- [37] B.W.J. Pirok, D.R. Stoll, P.J. Schoenmakers, Recent Developments in Two-Dimensional Liquid Chromatography: Fundamental Improvements for Practical Applications, *Anal. Chem.* 91 (2018) 240–263. <https://doi.org/10.1021/ACS.ANALCHEM.8B04841>.
- [38] S.R.A. Molenaar, P.J. Schoenmakers, B.W.J. Pirok, MOREPEAKS, (2021). <https://doi.org/10.5281/ZENODO.6375413>.
- [39] B.W.J. Pirok, S. Pous-Torres, C. Ortiz-Bolsico, G. Vivó-Truyols, P.J. Schoenmakers, Program for the interpretive optimization of two-dimensional resolution, *J. Chromatogr. A* 1450 (2016) 29–37. <https://doi.org/10.1016/j.chroma.2016.04.061>.
- [40] T. Brau, B. Pirok, S. Rutan, D. Stoll, Accuracy of retention model parameters obtained from retention data in liquid chromatography, *J. Sep. Sci.* (2022). <https://doi.org/10.1002/JSSC.202100911>.
- [41] G. Vivó-Truyols, J.R. Torres-Lapasió, M.C. García-Alvarez-Coque, Error analysis and performance of different retention models in the transference of data from/to isocratic/gradient elution, *J. Chromatogr. A* 1018 (2003) 169–181. <https://doi.org/10.1016/j.chroma.2003.08.044>.
- [42] M.J. den Uijl, T. Roeland, T.S. Bos, P.J. Schoenmakers, M.R. van Bommel, B.W.J. Pirok, Tool for Assessing the Feasibility of Stationary-Phase-Assisted Modulation for Two-Dimensional Liquid-Chromatography Separations, (2022). <https://doi.org/10.5281/ZENODO.6538470>.
- [43] B.W.J. Pirok, N. Abdulhussain, T. Aalbers, B. Wouters, R.A.H. Peters, P.J. Schoenmakers, Nanoparticle Analysis by Online Comprehensive Two-Dimensional Liquid Chromatography combining Hydrodynamic Chromatography and Size-Exclusion Chromatography with Intermediate Sample Transformation, *Anal. Chem.* 89 (2017) 9167–9174. <https://doi.org/10.1021/ACS.ANALCHEM.7B01906>.

PART III

Photodegradation research

CHAPTER 5

Comparing Photodegradation Techniques

5. Comparing different light-degradation approaches for the degradation of Crystal Violet and Eosin Y

Abstract

Organic colourants have important applications in many fields. Their photostability is an important characteristic. Several methods to study photodegradation were compared in this work. Eosin Y (C.I. Generic name: Acid Red 87, EY) and crystal violet (C.I. Generic Name: Basic Violet 3, CV) were used as test compounds, both in solution and dyed on silk. Commonly applied methods were included, viz. Xenotest, Microfading-Tester, and light-box (Spectrolinker) experiments. A novel method was based on a liquid-core-waveguide (LCW) cell. After photodegradation on textile, extraction was performed using dimethyl sulfoxide (DMSO). The degraded solutions and extracts were analysed with liquid chromatography combined with diode-array detection and mass spectrometry. The degradation products were compared between techniques. Degradation in the LCW cell progressed much faster than in standard tests (Xenotest and Spectrolinker) and could be performed online, without a need for extraction or sample transfer. The degradation of CV in the LCW was comparable to its degradation in standard tests. For EY, there was a clear difference in degradation mechanisms between in-solution and on-textile samples. This could be due to the matrix or to incomplete extraction. Because the light sources used in the different experiments differed in energy and spectral emission, the results could not be quantitatively compared. However, the degradation products formed were shown to be independent of the light source. Therefore, the LCW is an attractive method for rapid and efficient studies into the chemistry of photodegradation.

Publication

Comparing different light-degradation approaches for the degradation of Crystal Violet and Eosin Y

Mimi J. den Uijl, Anika Lokker, Bob van Dooren, Peter J. Schoenmakers, Bob W.J. Pirok, and Maarten R. van Bommel

Dye. Pigment., **2022**, 197, 109882, DOI: 10.1016/j.dyepig.2021.109882.

5.1. Introduction

Organic colourants are important components in many products within fields such as food production, forensic science, cultural heritage, and the paint industry [1–5]. The stability of these colourants depends on many external stress factors, such as temperature and moisture and, most importantly, light [1,6]. The photostability of a colourant determines its applicability (e.g. in food or paint industry). Also, it may reveal information about the object it was applied to (e.g. in the field of forensics or conservation). Thus, there is significant interest in the photostability of colourants and a growing interest in degradation pathways and products [7–9]. In food science, a better understanding of the photodegradation pathway may lead to better products with longer shelf life [10]. Wastewater treatment may be improved if the influence of key parameters on the degradation of contaminants is known [11,12]. In cultural-heritage research, a better understanding of degradation processes of colourants can aid in dating the object, generating historical context, and developing mitigation strategies [8,13].

Techniques currently used in photodegradation research have serious limitations and tend to be very laborious. Many techniques investigate only the loss of colour and do not provide understanding of the chemical degradation process, or they focus solely on the degradation of the main compound [14,15]. Within the field of cultural heritage, photodegradation research is performed using many different techniques. The most commonly used setup is the Xenotest (XT), which is a standardized method, widely used in the textile-manufacturing industry [16]. It has been developed to measure lightfastness of a wide range of materials, but not necessarily to study degradation pathways. When used in conservation science, model samples (mock-ups) are studied, which are freshly dyed samples that resemble an (often paper- or textile-based) original art object as closely as possible. The instrument consists of a casing with a xenon-arc lamp in the centre, surrounded by several sample holders, which rotate around their own axis and around the lamp to ensure a homogeneous light exposure of all the samples throughout. It is possible to selectively cover parts of a sample to conduct time-series experiments. Additionally, the humidity, temperature, emitted energy, and the illuminance can be controlled. After the desired exposure time, colour measurements can be performed. To study degradation pathways, the sample needs to be extracted and the degradation products must be analysed. The XT has several advantages in comparison with other photodegradation techniques, viz. *i*) the test is standardized, *ii*) it allows measurement of time series, *iii*) it works automatically, and *iv*) the effects of the substrate can be studied. The disadvantages of the technique are *i*) an extraction step is needed prior to analysis, *ii*) the duration of experiments (full degradation can take up to several weeks), *iii*) degradation can only be applied to mock-ups, and *iv*) relatively large surfaces are needed.

Another technique used for measuring the light stability is the MicroFading Tester (MFT) [15]. The MFT was developed to investigate colour fading directly on objects of cultural heritage that can be mounted under a microscope, such as paintings and fabrics. It measures the reflectance of radiation. Since the aim of the MFT is to study light ageing directly on objects, the sample spot is relatively small (0.3 – 0.4 mm) [17]. In MFTs, the light source is often a xenon-arc lamp equipped with UV-IR filters that eliminate light below 400 and above 700 nm, so as to mimic the light encountered in museums. The advantages of the MFT are the following: *i*) a small spot size, making it applicable to small sample areas of historical objects, *ii*) direct degradation of the colorant on the substrate, and *iii*) measurement of the colour change in real-time. To study degradation mechanisms and kinetics, the MFT has several disadvantages, *viz.* *i*) an extraction step is needed before analysis, *ii*) the small spot size yields small amount of degraded sample, and *iii*) time series are difficult to perform.

A third and simpler technique is a light box. In a light-box setup, a sample can be placed in a contained space, which is illuminated from the top with a selected light source. An example is a UV crosslinker (such as the Spectrolinker, SL), which is intended for polymerization and light-induced cross-linking of polymers [7]. In the SL a detector monitors the total light dosage. The benefits of this setup include *i*) the possibility to degrade colourants on a substrate or in solution for comparison studies, *ii*) the option to measure time series, *iii*) the possibility to perform many (different) degradations in parallel, and *iv*) the ease of use. The drawbacks of this approach include that it *i*) is time consuming, *ii*) needs relatively large samples to allow off-line analysis, and *iii*) employs a different light source than established methods. Care should be taken when comparing photodegradation in different matrices, since different sample pre-treatment, *i.e.* no sample pre-treatment for solutions but an extraction step for dyes applied on a solid matrix, can affect the composition of the components measured.

Recently, a new photodegradation cell based on liquid-core-waveguide techniques (LCW) was introduced [18]. These LCW cells are made of amorphous-Teflon tubing, the refractive index of which is lower (RI = 1.29-1.31) than that of the liquid inside, resulting in total internal reflection, *i.e.* the light can be coupled in under a specific angle and remains within the liquid core until leaving the tubing at the other side [19]. Because of this, LCWs can be used as elements in photodetection systems, especially in the ultraviolet and visible ranges (UV-vis) [20,21]. Both absorption and Raman spectroscopic detection [22,23] have been documented with the use of LCWs. When using a strong irradiation source, LCWs can be used to study photo-degradation processes, and when using gas-permeable Teflon tubing, it is possible to carry out such studies in an aerobic or anaerobic environment. The setup also allows studying the effects of solvents and of the addition of components which can affect the

degradation mechanisms, such as catalysts or inhibitors [18,19]. Depending on the objectives of the study, the light spectrum can be changed by selecting different lamps and/or by incorporating filters. The recently developed cell allows studying light degradation online in a (multi-dimensional) liquid chromatography setup, as opposed to the offline techniques described above [7,18,24,25]. The LCW cell offers several potential benefits compared to other photodegradation techniques, viz. *i*) faster degradation, *ii*) analysis of the entire sample, *iii*) no need for sample preparation (eliminating sources of error), *iv*) degradation in solution, and *v*) small samples volumes (< 60 μ L) [18]. Potential disadvantages are the absence of a substrate, which can result in less-representative and less-realistic degradation pathways, and the fact that recording a time series requires a series of separate experiments.

	XENON LAMP	MERCURY LAMP
ON TEXTILE	<div style="border: 1px solid black; padding: 5px; margin: 5px;">XENOTEST</div> <div style="border: 1px solid black; padding: 5px; margin: 5px;">MICROFADING TESTER</div>	<div style="border: 1px solid black; padding: 5px; margin: 5px;">SPECTROLINKER TEXTILE</div>
IN SOLUTION	<div style="border: 1px solid black; padding: 5px; margin: 5px;">LCW CELL</div>	<div style="border: 1px solid black; padding: 5px; margin: 5px;">SPECTROLINKER SOLUTION</div>

Figure 5.1. Scheme of different photodegradation techniques, classified in terms of the type of lamp used and the degradation matrix.

Many of the current photodegradation approaches have not been developed with the intention to study degradation pathways. Currently, there is no consensus on the effects of the various techniques on the observed degradation pathways. The LCW technique is very attractive to study degradation pathways in solution, thanks to much greater versatility. However, for it to be accepted in the field of photodegradation research, the differences between this method and the other available techniques must be documented. This work aims to show how these photodegradation techniques can be compared and whether they can be used to analyse photodegradation mechanisms rather than just the main compound or the colour. Fig. 5.1 shows a classification of the different techniques used in this study. The techniques on the left illuminate the sample with a xenon lamp, while the right techniques consist of a mercury lamp. The techniques above degrade a sample on a substrate, while the techniques on the bottom degrade the sample in solution. Two techniques in diagonally opposed boxes cannot easily be compared. Observed (quantitative) differences between such techniques

could be the result of different lamp spectra and intensities, different extraction efficiencies (e.g. in case of textile) or dyeing inconsistencies. Hence, the current study focusses on the practical aspects of different light degradation system and a qualitative comparison.

The current research focusses on the photodegradation of crystal violet (CV) and eosin Y (EY) as model components, both with a poor light fastness (ISO 2 and ISO 1, respectively) [26]. These two components are early synthetic organic dyes, both widely used towards the end of the 19th century, but with many recent applications [9,24,27–32]. Presently, EY is applied in cell staining, as pH indicator, as pigment in for example lipstick, and as a visible-light photocatalyst in organic synthesis [33,34]. CV is nowadays used as a pigment in inks (e.g. in inkjet printers) and as a histological staining agent [5,29]. Additionally, it has antibacterial properties and it is used as an alternative to penicillin [35]. Much is already known about the degradation pathways of EY and CV, but differences have been observed in degradation mechanisms, depending on many factors, such as the lamp spectrum and intensity, the availability of oxygen, and the matrix, *i.e.* whether the compound was in solution, on textile, or in oil [7,9,36,37].

The objective of the present work is to qualitatively compare degradation studies in the new LCW cell with those in other degradation systems, *i.e.* the Xenotest (XT), Microfading tester (MFT), and more-basic lightbox degradations in a Spectrolinker device (SL). The degradation of two popular colorants, crystal violet (CV) and eosin Y (EY), will be used for this comparison in two different matrices, *i.e.* in-solution and on textile. Finally, we aim to provide recommendations on how to implement the LCW in the field of light-degradation research.

5.2. Materials and Methods

5.2.1. Chemicals

Milli-Q water (18.2 M Ω cm) was obtained from a purification system (Arium 611UV, Sartorius, Germany). Methanol (MeOH, ULC/MS grade) was obtained from Biosolve (Valkenswaard, The Netherlands). Acetonitrile (ACN, LC-MS) was purchased from Biosolve (Dieuze, France). Eosin Y (C.I. Generic name: Acid Red 87, EY) (99%), crystal violet (C.I. Generic Name: Basic Violet 3, CV) (\geq 90%), ammonium formate (Fluka, BioUltra \geq 99.0%) and dimethyl sulfoxide (DMSO, Chromasolv (\geq 99.0%)) were purchased from Sigma Aldrich (Zwijndrecht, The Netherlands). Sulphuric acid (95-97%) and sodium sulphate (anhydrous for synthesis \geq 99.0%) were obtained from Merck (Darmstadt, Germany). Formic acid (98%) was purchased from AnalaR (Poole, UK). All chemicals were used as purchased. The blue-wool standards used for the Xenotest and the Microfading tester that satisfied the BS EN ISO 105 B08 requirements were purchased from SDC Enterprises (Bradford, UK).

5.2.2. Instrumentation

5.2.2.1. Xenotest

Photodegradation of dyed silk was performed using a Xenotest 440 (Atlas, Ametek, Mount Prospect, IL, USA) instrument, including two 2200-W xenon-arc lamps, room for 15 sample holders, and a black standard thermometer. After degradation, the colour change was measured with a Minolta MC-2600d spectrometer (Konica Minolta, Nieuwegein, The Netherlands). The degradation was performed at black standard temperature (BST, 47 °C). Further information about the Xenotest procedure can be found in Appendix C-1.

5.2.2.2. Microfading tester

The microfading tester (MFT) was used to investigate photofading on silk. The instrument consisted of an HPX-2000 xenon-arc lamp (Ocean Optics, Duiven, The Netherlands), a microscope (Stemi SV 11, Zeiss, Breda, The Netherlands), a camera (DFK 41AU02, The Imaging Source, Bremen, Germany) and a detector which was connected using fibre guides to a spectrophotometer (Tidas S 300 MMS Vis/NIR 3011, J&M, Essingen, Germany). The sample was placed under the microscope and the detector was placed at a 45° angle. The light of the xenon lamp was directed through the objective of the microscope to the sample underneath. A removable UV-IR filter was placed between the xenon lamp and the objective of the microscope to filter out all the light below 400 nm. An external power meter (Thorlabs, PM100usb, Newton, NJ, USA) was used to estimate the energy of the lamp and to check its stability. The degradation was performed at room temperature. Further information about the Microfading Tester procedure can be found in Appendix C-2.

5.2.2.3. Spectrolinker

Both the in-solution and on-silk degradation studies were performed in a UV-light box Spectrolinker XL-1500 UV crosslinker (Spectronics, Westbury, NY; maximum wavelength 254 nm). The degradation was performed at room temperature. The degradation procedure is described in Appendix C-3.1 for in-solution degradation and in Appendix C-3.2 for the on-silk degradation.

5.2.2.4. Online liquid-core waveguide cell

Degradation in solution was performed with a prototype instrument, incorporating a Teflon AF liquid core waveguide exposure cell (Vrije Universiteit, Amsterdam, The Netherlands). An Argos 250b FL-Detector (Flux instruments, Basel Switzerland) xenon-arc lamp was used for irradiation. The light was directed into the exposure cell via a glass optical fibre. The degradation was performed at room temperature. Further details on the setup can be found in [18] and Appendix C-4.

5.2.2.5. *Liquid chromatography coupled to diode array detector and mass spectrometry*

All liquid-chromatographic (LC) analyses, besides the online LCW degradations, were performed on an Agilent Infinity 1290 2DLC system (Agilent, Waldbronn, Germany) configured for one-dimensional operation. The system included an Infinity 1290 binary pump (G4220A), an Infinity 1290 diode-array detector (DAD; G4212A), an Infinity 1290 autosampler (G4226A) and an Infinity 1290 column compartment. An Agilent ZORBAX eclipse plus C18 column was used (150 mm length × 2.1 mm ID, 3.5 µm particles, part nr. 959763-902). For the LC-DAD-MS measurements an LTQ Velos mass spectrometer (Thermo Scientific, Waltham, MA, USA) was coupled in series after the DAD with electrospray ionization. The precursor and product ions are enlisted in Appendix C-5.

For online degradation studies, the LCW was coupled with a Shimadzu HPLC system (Shimadzu, Kyoto, Japan), consisting of an LC-20AT vp binary pump (L20224708228), an SPD-M20A diode array detector (228-45005-38), an CBM-20A column module (L20234370270 US L) and a manual 6-port injection valve with a 50 µL injection loop. An Agilent ZORBAX eclipse plus C18 column was used (same as for the 1D-LC experiments), coupled to the LTQ Velos mass spectrometer with electrospray ionization.

5.2.3. Methods

5.2.3.1. *Dyeing and Extraction Method*

The dyeing and extraction process of the silk samples in this research is described in Appendix C-6.

5.2.3.2. *Analytical Methods*

For the LC analysis of both dyes, mobile phase A and B consisted of mixtures of aqueous buffer and MeOH in ratios of 95/5 [v/v] for mobile phase A and mobile phase B consisted of MeOH/buffer [v/v, 95/5]. The buffer was 10 mM ammonium formate at pH = 3 prepared by adding 0.390 g formic acid and 0.0952 g ammonium formate to 1 L of water. The flow rate is set at 0.2 ml/min. For the analysis of EY samples, the gradient program started isocratically at 100% A from 0 min to 1 min, followed by a linear gradient to 50% B in 1 min and then to 100% B in 4 min. For 3 min the composition was maintained at 100% B, and finally brought back to 100% A in 1 min. The mobile phase was kept at 100% A for 2 min before starting a new run. For the analysis of the CV samples, the gradient program started with an isocratic hold of 100% A from 0 min to 1 min, followed by a linear gradient to 80% B in 2 min. Until 7 min, the organic modifier concentration was kept at 80% B, followed by a linear gradient to 100% B in 1 min. Until 10 min the composition was maintained at 100% B, before it was brought back to 100% A in 1 min. The mobile phase was kept at 100% A for 2 min before starting a new run.

The temperature of the injection chamber was 6 °C, the analyses were performed at room temperature, which was about 295 K. The injection volume for studying the degradation in solution was set at 10 µL for EY and 1 µL for CV (3 µL injection volume was used for trace degradation products). For the extracted XT samples, the injection volume was 20 µL and for the extracted samples irradiated using the MFT it was 10 µL. The solution subjected to online LCW degradation (60 µL) was transported to a 50 µL loop, which was coupled to the analytical system. Every sample was measured in duplicate.

For the online coupling of the LCW, it was coupled to a 6-port injection valve, which was positioned in-line in an LC-DAD-MS system between the pump and the column. Prior to irradiation, 60 µL of sample was injected into the LCW. After irradiation, the sample was transferred from the LCW to the injection loop by injecting 60 µL of elution solvent into the LCW cell. See Appendix C-4 for a schematic setup. The gradient used for chromatographic analysis was similar as previously described, but the total analysis time was increased, because of the increased dwell volume of the system.

5.2.4. Data processing

The chromatograms and UV/vis spectra obtained on the Agilent LC system were processed with Agilent OpenLAB CDS software. The chromatograms and UV/vis spectra obtained on the Shimadzu system were processed with LabSolutions CS, version 5.42 (Shimadzu corporations, Kyoto, Japan). The mass-spectral data were processed with XCalibur, version 2.2 (Thermo Fisher Scientific, Waltham, MA, USA). Calculations performed using in-house routines written in MATLAB R2018b (Mathworks, Natick, MA, USA). Microsoft Excel was used for further data processing.

5.3. Results & Discussion

Five different photodegradation techniques were tested with EY and CV as test analytes, varying the illumination source and the matrix of the dye, *i.e.* textile or solution. The extracted samples irradiated using the MFT turned out to be not very reliable, probably due to very small size of the actually degraded sample. This resulted in very low amounts of dye and degradation products extracted. Although the technique may be suitable to study the photostability, it cannot be used to study chemical degradation mechanisms. The photodegradation results obtained by the other four techniques are summarized in Fig. 5.2 and Fig. 5.3 for EY and CV, respectively.

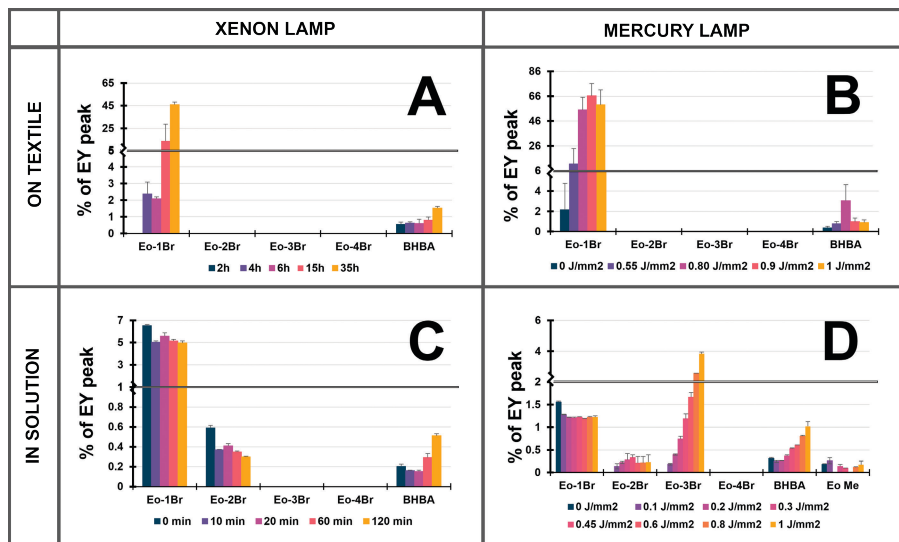


Figure 5.2. Degradation of eosin Y (EY). The ratio of the areas of the degradation product peaks and the EY peak is shown for various light doses or illumination times, as indicated on the y-axis. The relative areas of the four debrominated products and the oxidation product BHBA are shown. Experiments with the Xenon lamp were performed using the Xenotest instrument on textile (Fig. 5.2A) or the LCW cell for solutions (Fig. 5.2C). Experiments with the mercury lamp were performed using the Spectrolinker instrument (Figs. 5.2B and 5.2D for textile and solutions, respectively). The thick horizontal line indicates a change in the vertical axis.

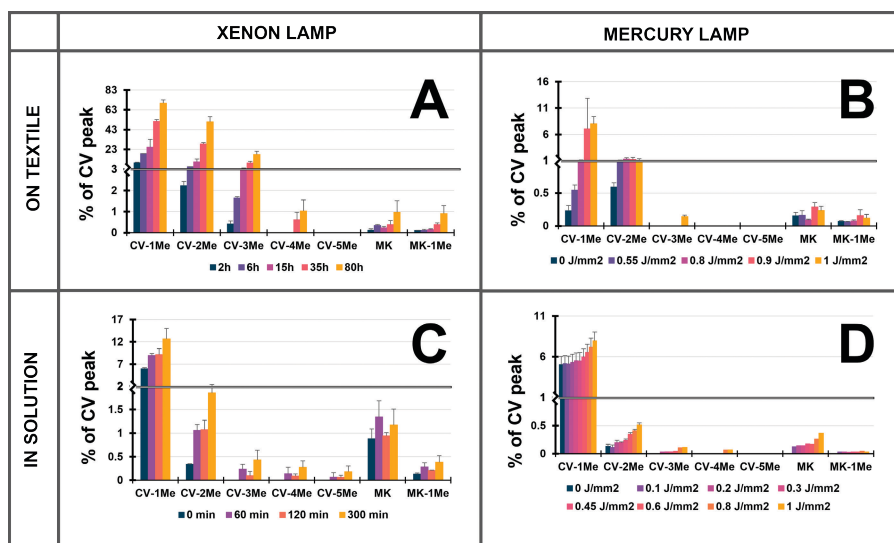


Figure 5.3. Degradation of crystal violet (CV). The ratio of the areas of the degradation product peaks and the CV peak is shown for various light doses or illumination times, as indicated on the y-axis. Peak areas relative to that of CV are shown for the five demethylation products (CV-1Me through CV-5Me), the oxidation product MK, and its demethylated form (MK-1Me). The thick horizontal line indicates a change in the vertical axis.

5.3.1. Degradation in the Xenotest

The Xenotest (XT) is mostly used in the textile industry. It provides a standardized method for testing the light stability of colourants on a solid matrix. The large surface area of textile illuminated in the XT (e.g. 200 × 200 mm) allows performing time series and repeats on a single sample. A degradation series was created with a maximum duration of 35 h for EY (Fig. 5.2A) and 80 h for CV (Fig. 5.3A). This yielded a total light dose of 57 J/mm² and 129 J/mm², respectively. In the degradation of EY (Fig. 5.2A) the only debrominated product observed is the first debrominated species. The photo-oxidation product 2-(3,5-dibromo-2,4-dihydroxybenzoyl)benzoic acid (BHBA) was also observed. This product was recently identified by Chieli *et al.*, who characterized it in both samples irradiated with visible light and with a combination of visible and UV light [38]. Since there is no further debromination of the first debromination product, its peak area can increase to more than 50% of that of EY. The degradation of EY in the XT test was stopped after 35 h (vs. 80 h for the degradation of CV), because the dyed textile was already completely faded at this time. This observation is not in line with the LC results, which show that the peak area of EY is still double that of the first debrominated product. The latter is also not colourless, while the other observed degradation product (BHBA) has a yellowish colour. One of the reasons for this discrepancy may be that the photodegradation of textile mainly affects the outside of the fibres, while the colorants present inside the fibre or fabric are less exposed. This is the main difference from in-solution degradation, where the sample is homogenized during fading. In addition, part of the EY may possibly be degraded to other (colourless) compounds that were not recorded during analysis.

In Fig. 5.3A, the degradation over time (up to 80 hours) of CV in the XT experiment is shown. As can be seen in the figure, four demethylated products of CV are present in high concentrations relative to CV. A gradual increase in concentration of all these degradation products is visible and, since all these degradation products are formed sequentially (*i.e.* the second demethylated product can only be formed from the first demethylated crystal violet, the third from the second, and so on), greater amounts of the daughter compounds are formed than are being consumed. Next to the coloured demethylated products, Michler's ketone (MK), which is the product of oxidation of the central carbon atom [31], and the demethylated MK, which is the oxidation product after the first demethylation reaction, are both formed.

While degradation of EY and CV in the XT instrument is time-consuming, it is an easy-to-use technique and time series can be generated relatively easily. The downside is that the sample needs to be extracted prior to analysis, which is quite time-consuming, easily

doubling the total experiment time. Furthermore, it is clear the EY sample is not degraded homogeneously and likely the same is true for CV. Besides the possible introduction of error, the extraction method can be analyte dependent and exhibit different specificity for the different degradation products, leading to possible invalid conclusions about the degradation mechanism.

5.3.2. Degradation in the Microfading Tester

Another technique that is used to test the photostability of colourants in the field of cultural heritage is the Microfading Tester (MFT) [15]. This technique performs the degradation on a solid sample, for example a textile or a painting, similar to the XT experiment, but on a smaller area. In the MFT, the goal is to test the light stability of an art object with minimal damage. For the current research, the spot size of the MFT experiment was increased to enlarge the area of the illuminated sample, which was later extracted. Because the spot size exceeded the range of the microscope, the total dose of this degradation could only be estimated (130 J/mm^2), a dose comparable with 80 hours exposure in the XT. For the degradation of EY-dyed textile no degradation products were found, probably due to the small sample area. In addition, we noticed variations in the concentrations of EY in different samples, indicating that the dyeing process was not very homogeneous. Since the same sample spot of the textile cannot both serve as starting point ($t = 0$) and as degraded sample, and since the EY peak area found in the analysis is susceptible to variations, the MFT instrument cannot be used reliably to perform quantitative degradation-mechanism studies for EY. For the CV degradation using the MFT slightly better results were obtained. The degradation was performed during 20 minutes in threefold, after which the samples were extracted, and analysed. The results are presented in Fig. 5.4.

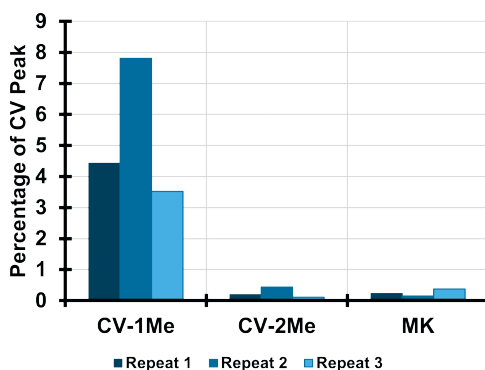


Figure 5.4. Degradation of CV on textile using the MFT instrument (triplicate results).

The first demethylated product yielded an average percentage peak area of 5.3% relative to CV. The average relative peak area of the second degradation product (CV-2Me) was 0.24%. The average percentage peak area of Michler's ketone (MK) relative to CV was 0.25%. However, a large variation in response was observed, which could be due to inhomogeneous dyeing, incomplete fading (*i.e.* only the top surface), or the low amount of sample extracted.

When comparing these results to those in Fig. 5.3, the total degradation of CV is seen to be very limited, despite the high total dose (estimated at 130 J/mm²). Similar to the XT experiment, fading occurs superficially and the core of the fabric may be degraded less. The small spot size results in a low amount of sample extracted. The present results suggest that the contemporary MFT setups, such as the one used in this study, cannot be used as a tool for studying chemical photodegradation mechanisms. However, reflectance measurements of the extent of discolouration (Appendix C-7) can accurately be used to confirm the photodegradation of the dye on the surface of the object.

5.3.3. Degradation in the Spectrolinker

In this research, degradation of EY and CV was performed in the Spectrolinker, which is a controlled light box, designed for photopolymerization. The main reason to include this light box in this research is that it allows both in-solution and in on-textile degradation. Therefore, recommendations can possibly be made by comparing degradation of dyes in different matrices. The instrument was previously used to study the effect of the solvent on the degradation of EY [7]. The degradation of EY in DMSO was found to yield one additional degradation product than in water. In the present work a broad-spectrum mercury lamp was used as irradiation source, with the lower UV range (< 300 nm) being blocked with a glass sheet. The degradation of EY is compared in Fig. 5.2B (on textile) and in Fig. 5.2D (in solution). The first clear difference is that on textile the debromination reaction only results in the mono-debromination product, while EY debrominates further in solution. The absence of further degradation products of EY is analogous to the results of XT degradation seen in Fig. 5.2A, confirming the hypothesis that further debromination is not favoured on a textile matrix. The difference in relative peak areas between Fig. 5.2A and Fig. 5.2B may be due to different illumination spectra or to the total dose, which differs by a factor of 50. Comparing the degradation of EY in the SL (Fig. 5.2B) and in the XT (Fig. 5.2A), the debromination of EY seems to progress much faster in the former. These two techniques cannot directly be compared, because the SL has a lower dose and employs a lower-wavelength spectrum, while the XT produces a higher dose at higher wavelengths during a longer period of time. The faster formation of the debromination products in the SL, despite the lower overall dose, indicates that the photodegradation proceeds much faster at lower wavelengths. The ratio

of the first debrominated product of EY to EY on exposed textile is higher than in solution, which can be explained by the observation that debromination continues in the latter case. The amount of BHBA (the oxidation product of EY) formed is similar in both matrices. When examining the degradation in solution (Fig. 5.2D) a plateau can be observed in the relative concentration of the first debromination product. This indicates that the singly debrominated product is formed about as fast as it degrades, since there is a clear increase in the thrice debrominated product.

The degradation of CV in the Spectrolinker for two different matrices is compared in Fig. 5.3B (on textile) and in Fig. 5.3D (in solution). There are no large differences between the degradation mechanisms when comparing on-textile to in-solution degradation. The degradation seems to progress slightly faster in solution, but the differences are small. However, when the degradation in the SL on textile (Fig. 5.3B) is compared to that in the XT experiment (Fig. 5.3A), the degradation in the latter is more severe. The demethylation products are formed until four methyl groups have been lost, while the SL degradation only progresses through three demethylation steps after a total dose of 1 J/mm^2 . The two degradation systems (SL and XT) contain different light sources. The emission spectrum of the XT lamp resembles the absorption spectrum of CV, while this is not the case of the emission spectrum of the SL lamp. Moreover, the difference in dose, which is 1 J/mm^2 in the SL and 129 J/mm^2 in the XT, differs by more than a factor 100, which could explain why the degradation in the SL does not progress quite as far as that in the XT. Smaller differences in degradation rates are observed when observing the formation of MK and demethylated MK (Fig. 5.3A and Fig. 5.3B). This may be due to the differences in initiation wavelength for the photo-oxidation and demethylation reactions. The ratio of MK-1Me relatively to MK is higher in the degradation of CV in XT (Fig. 5.3A) since there is more demethylated product. In future research this hypothesis could be tested with similar setups with a Xenon lamp, such as the Solarbox device [39]. The sample throughput of the SL is lower than that of the XT, because for every 0.01 J/mm^2 in the SL the instrument needs to be started manually. It must be noted that the SL was designed for other purposes than photodegradation. The XT is computer controlled and can be programmed according to the requirements. The main advantages of the SL are that it can accommodate both solutions and solid matrices and that the total dose can be closely monitored.

5.3.4. Degradation in the liquid-core waveguide

5.3.4.1. Online coupling of the liquid-core waveguide to LC-DAD-MS

In this research, the LCW cell has been applied for the first time as a device for online degradation coupled to LC-DAD-MS. By coupling the LCW cell to a six-port valve equipped

with a 50- μL loop, the degraded solution can be transferred to the LC column. This analysis was performed on a different LC-DAD-MS system than the off-line measurements of the XT, MFT, and SL. Since the degraded sample is transferred completely to the LC system, time series can only be obtained by repeating the experiment with different irradiation times. Prior to performing degradation studies on EY and CV, the coupling of the LCW cell to LC had to be validated. To confirm that the sample is transferred from the LCW cell to the LC system completely, a manual injection in the loop of the six-port injection valve was compared to a manual injection from the LCW cell. These experiments were performed for both EY and CV. To investigate the adsorption of CV on the Teflon wall, CV was dissolved in either 100% H_2O or 50%/50% $\text{H}_2\text{O}/\text{MeOH}$ (by volume).

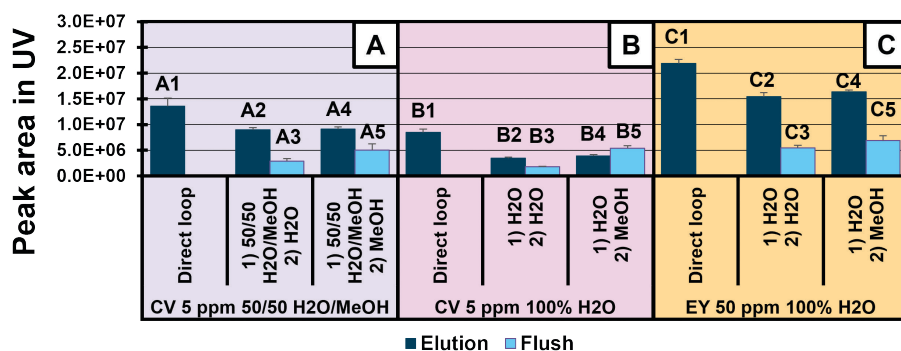


Figure 5.5. Sample transfer directly from the six-port injection valve (“Direct loop”) or from the LCW. The experiments in box A show the injection of a 5 ppm CV solution in 50/50 $\text{H}_2\text{O}/\text{MeOH}$, the experiments in box B show the injection of a 5 ppm CV solution in 100% H_2O and the experiments in box C show the injection of a 50 ppm EY solution in 100% H_2O . Within each box the first bar (A1, B1, and C1) shows the peak area obtained from the direct loop injection of the sample. The second experiment in each box shows the elution of the sample (A2, B2 and C2) and a flush with water (A3, B3, and C3). The last experiment shows the elution of the sample (A4, B4, C4) and a flush with MeOH (A5, B5 and C5). Standard deviations are indicated with an error bar ($n = 3$).

In Fig. 5.5 the results are shown for an injection of 5 ppm CV solution in either 100% H_2O or 50/50 $\text{H}_2\text{O}/\text{MeOH}$ in the LCW cell and for an injection of 50 ppm EY in H_2O . Each sample was either directly injected in the loop or transferred from the LCW to the LC system with a flush of H_2O or transferred with a flush of MeOH. From the latter two experiments, the first bar indicates the total area of CV or EY in the transferred sample (in the sample solvent), while the second bar indicates the total area of CV or EY in the flush solvent, *i.e.* H_2O or MeOH. For all three samples, a direct injection of sample yields a higher response compared than an LCW transfer. For EY, the signal from direct injection (C1) is 37% higher (average of C2 and C4). For CV, this is 50% (A1 compared to A2 and A4) for the 50/50 MeOH/ H_2O sample and 130% (B1 compared to B2 and B4) for the H_2O sample. The difference between the latter

two numbers indicates the higher adsorption of CV to the Teflon wall from a fully aqueous solution. A similar trend is visible in the flush with water compared to the flush with MeOH, *i.e.* a flush with water yields smaller areas than a MeOH flush. From the results for CV, 50/50 H₂O/MeOH was chosen as the degradation solvent in further experiments. For EY, the differences between the H₂O flush and the MeOH flush were smaller, indicating that EY is less prone to adsorb to the cell wall. No second flush was performed in further experiments for either dye, since the yield of the first flush (70%) and the repeatability (RSD < 5%) were found to be acceptable.

5.3.4.2. Degradation in the liquid-core waveguide coupled to LC-DAD-MS

The experiments with the online LCW coupling were performed on a different system than the offline analyses. The online system featured a different UV detector, which showed higher limits of detection, so that not all degradation products could be observed. Therefore, MS detection was used. In Fig. 5.2C and Fig. 5.3C, the results of the degradation of both dyes in the LCW cell are shown, based on the mass spectra instead of the DAD results. The ionization efficiencies of the debromination products of EY are expected to be similar to that of EY, as well as the demethylation products of CV to CV, because the ionized groups are the same. Recording a time series using the LCW required a series of independent experiments, resulting in somewhat higher standard deviations. When comparing online degradation in the LCW cell to in-solution degradation using the SL, there were some specific differences that could affect the degradation. First, the dye solution was illuminated with a different light source. In the LCW cell a xenon lamp was used with a glass optic fibre, blocking the lower UV (< 300 nm) from the spectrum. The SL contained a mercury lamp in combination with a glass sheet, also blocking the lower UV range. This resulted in different irradiation spectra, which might affect the degradation of the two target compounds absorbing at higher wavelengths. This could potentially lead to different reaction mechanisms or reaction kinetics. Another difference was the introduction of the sample. The LCW cell was coupled online to an LC-DAD-MS system. Since the degradation in the SL was performed offline, there is a greater chance of introducing errors in the handling of the sample or because of evaporation of the solution during degradation. For the degradation of EY, a similar plateau is seen for the first debrominated product degraded in the LCW (Fig. 5.2C) and the SL (Fig. 5.2D). Thrice and fully debrominated products were not found within 120 min of degradation. The formation of BHBA followed similar pattern in the two systems, but the %-area was lower in the SL. This difference could be due to the detection method (MS in the LCW degradation and UV in the SL degradation). Since BHBA was an oxidation product, photo-oxidation could be observed in the LCW, presumably due to its gas permeability.

The degradation of CV during 5 h in the LCW (Fig. 5.3C) is seen to progress to the fifth demethylation product, which is not observed during the 80-h degradation in the XT system (Fig. 5.3A) and the SL experiments (Fig. 5.3B and Fig. 5.3D). Michler's ketone was detected in the LCW system, again confirming that photo-oxidation occurred. Longer degradation times could lead to more adsorption of CV to the Teflon tubing or to a loss of light due to the formation of air bubbles. This is reflected in Fig. 5.3C by an increase in the standard deviations at longer irradiation times. Since the volume of the LCW is fixed, the absolute peak areas of EY and CV can be compared over time. This is shown in Fig. 5.6.

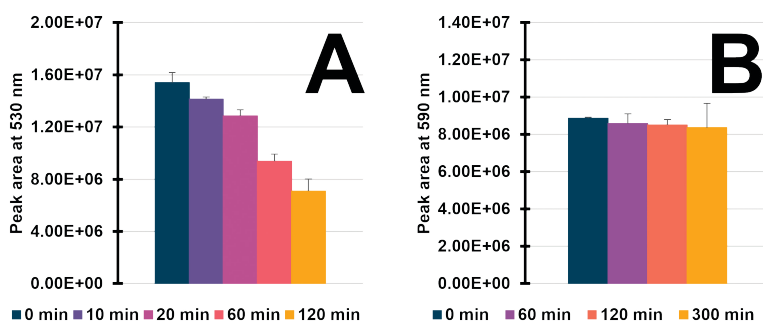


Figure 5.6. Total area of EY (left, 530 nm) and CV (right, 590 nm) in the DAD signal over time in the LCW cell degradation.

From the error bars in Fig. 5.6A, the decrease in EY is seen to be precise. For the degradation of CV (Fig. 5.6B) the standard deviation seems to increase with increasing degradation time. Possible explanations include an increase of adsorption to the fibre or a memory effect. When implementing this system in further degradation studies, care should be taken to minimize the effects of adsorption of apolar compounds on the interpretation of the data, by following cleaning procedures between degradations.

The LCW cell has proven to be a good alternative to off-line degradations in the SL instrument. The difference between in-solution and on-textile degradation has been shown to depend on the dye examined. The LCW cell promises to provide fast and accurate degradation experiments.

5.4. Concluding remarks

In this study, a newly developed on-line photo-degradation system using a liquid-core-waveguide (LCW) cell was implemented. Its performance was compared with that of other photodegradation techniques used in the field of cultural heritage (Spectrolinker, SL; Xenotest, XT; Microfading Tester, MFT). The degradation of two dyes was studied, *i.e.* eosin Y and crystal violet, on two different matrices (in-solution and on-textile) and the advantages and disadvantages of each technique were established. Degradation in the LCW cell progressed much faster than in standard tests (XT and SL) and was performed online, *i.e.* without a need for extraction or sample transfer.

While the degradation in the XT system was slower, it was an easy-to-use technique, although it needed relatively large samples. The required extraction step made the process more difficult and potentially more error prone. The SL method was more labour intensive, since the system had to be started many times. The main advantage of this technique was that it could be applied to both solid and liquid matrices. For the MFT experiment the extraction results showed that the current setup could not be used for the analysis of the chemical photodegradation mechanisms. The XT, MFT, and the SL setups were used to degrade solid matrices, while the SL system could also degrade other matrices, such as solutions. The LCW could only be used to degrade liquid samples. The light source of the SL was a mercury lamp, while the other techniques all employed a Xenon lamp. While the degradation of CV in the LCW was comparable to its degradation in standard tests, this was not true for the degradation of EY. In the latter case, there was a clear difference in degradation mechanisms between in-solution and on-textile samples. Indeed, photodegradation can depend on the matrix and some degradation routes may be more-or-less favourable in paper, textile, oil, aqueous solution, etc. Difference in the apparent degradation on textile vs. that in solution may also result from incomplete extraction, since only the compounds that are extracted from the textile are analysed.

The light sources used differ in energy and spectral emission. Therefore, the results of degradation studied cannot be directly compared. Obviously, a higher light intensity leads to increased degradation. In addition, for EY clear effects were observed of the wavelength on the degradation kinetics. However, in the present study the degradation products formed did not depend on the light source. The LCW is good candidate technique for studying the chemistry of photodegradation, especially for small samples. In future experiments the effect of oxygen, the illumination wavelength, and the solution composition (solvent, pH, presence of additives, such as inhibitors or catalysts) on the photodegradation will be studied.

References

- [1] Verduin J, Den Uijl MJ, Peters RJ, Van Bommel MR. Photodegradation Products and their Analysis in Food. *J Food Sci Nutr* 2020;6. <https://doi.org/10.24966/FSN-1076/100067>.
- [2] Nigel Corns S, Partington SM, Towns AD. Industrial organic photochromic dyes. *Color Technol* 2009;125:249–61. <https://doi.org/10.1111/j.1478-4408.2009.00204.x>.
- [3] Goodpaster J V., Liszewski EA. Forensic analysis of dyed textile fibers. *Anal Bioanal Chem* 2009;394:2009–18. <https://doi.org/10.1007/s00216-009-2885-7>.
- [4] Terán JE, Millbern Z, Shao D, Sui X, Liu Y, Demmler M, et al. Characterization of synthetic dyes for environmental and forensic assessments: A chromatography and mass spectrometry approach. *J Sep Sci* 2021;44:387–402. <https://doi.org/10.1002/jssc.202000836>.
- [5] Weyermann C, Kirsch D, Costa Vera C, Spengler B. Evaluation of the Photodegradation of Crystal Violet upon Light Exposure by Mass Spectrometric and Spectroscopic Methods. *J Forensic Sci* 2009;54:339–45. <https://doi.org/10.1111/j.1556-4029.2008.00975.x>.
- [6] Hao Z, Iqbal A. Some aspects of organic pigments. *Chem Soc Rev* 1997;26:203. <https://doi.org/10.1039/cs9972600203>.
- [7] Pirok BWJ, Moro G, Meekel N, Berbers SVJ, Schoenmakers PJ, van Bommel MR. Mapping degradation pathways of natural and synthetic dyes with LC-MS: Influence of solvent on degradation mechanisms. *J Cult Herit* 2019;38:29–36. <https://doi.org/10.1016/j.culher.2019.01.003>.
- [8] Pérez-Alonso M, Castro K, Madariaga JM. Investigation of degradation mechanisms by portable Raman spectroscopy and thermodynamic speciation: The wall painting of Santa María de Lemoniz (Basque Country, North of Spain). *Anal Chim Acta* 2006;571:121–8. <https://doi.org/10.1016/j.aca.2006.04.049>.
- [9] Alvarez-Martin A, Trashin S, Cuykx M, Covaci A, De Wael K, Janssens K. Photodegradation mechanisms and kinetics of Eosin-Y in oxic and anoxic conditions. *Dye Pigment* 2017;145:376–84. <https://doi.org/10.1016/j.dyepig.2017.06.031>.
- [10] Duncan SE, Chang HH. Implications of Light Energy on Food Quality and Packaging Selection. *Adv. Food Nutr. Res.*, vol. 67, Academic Press Inc.; 2012, p. 25–73. <https://doi.org/10.1016/B978-0-12-394598-3.00002-2>.
- [11] Hisaindee S, Meetani MA, Rauf MA. Application of LC-MS to the analysis of advanced oxidation process (AOP) degradation of dye products and reaction mechanisms. *TrAC - Trends Anal Chem* 2013;49:31–44. <https://doi.org/10.1016/j.trac.2013.03.011>.
- [12] Kolkman A, Martijn BJ, Vughs D, Baken KA, van Wezel AP. Tracing Nitrogenous Disinfection Byproducts after Medium Pressure UV Water Treatment by Stable Isotope Labeling and High Resolution Mass Spectrometry. *Environ Sci Technol* 2015;49:4458–65. <https://doi.org/10.1021/es506063h>.
- [13] Degano I, Ribechini E, Modugno F, Colombini MP. Analytical Methods for the Characterization of Organic Dyes in Artworks and in Historical Textiles. *Appl Spectrosc Rev* 2009;44:363–410. <https://doi.org/10.1080/05704920902937876>.
- [14] Kansal SK, Singh M, Sud D. Studies on photodegradation of two commercial dyes in aqueous phase using different photocatalysts. *J Hazard Mater* 2007;141:581–90. <https://doi.org/10.1016/j.jhazmat.2006.07.035>.
- [15] Whitmore PM, Pan X, Bailie C. Predicting the fading of objects: Identification of fugitive colorants through direct nondestructive lightfastness measurements. *J Am Inst Conserv* 1999;38:395–409. <https://doi.org/10.1179/019713699806113420>.
- [16] Friele LFC. A Comparative Study of Natural and Xenotest Exposure Condition: for Measuring Fading and Degradation. *J Soc Dye Colour* 2008;79:623–31. <https://doi.org/10.1111/j.1478-4408.1963.tb02522.x>.
- [17] Whitmore PM, Bailie C, Connors SA. Micro-fading tests to predict the result of exhibition: progress and prospects. *Stud Conserv* 2000;45:200–5. <https://doi.org/10.1179/sic.2000.45.supplement-1.200>.

- [18] Groeneveld I, Schoemaker SE, Somsen GW, Ariese F, van Bommel MR. Characterization of a liquid-core waveguide cell for studying the chemistry of light-induced degradation. *Analyst* 2021. <https://doi.org/10.1039/D1AN00272D>.
- [19] Altkorn R, Koev I, Van Duyne RP, Litorja M. Low-loss liquid-core optical fiber for low-refractive-index liquids: fabrication, characterization, and application in Raman spectroscopy. *Appl Opt* 1997;36:8992. <https://doi.org/10.1364/ao.36.008992>.
- [20] Beschere K, Barnes JA, Loock HP. Absorption measurements in liquid core waveguides using cavity ring-down spectroscopy. *Anal Chem* 2013;85:4328–34. <https://doi.org/10.1021/ac4007073>.
- [21] Rubles T, Paige D, Anastasio C. Lens-coupled liquid core waveguide for ultraviolet-visible absorption spectroscopy. *Rev Sci Instrum* 2006;77:073103. <https://doi.org/10.1063/1.2219973>.
- [22] Marquardt BJ, Vahey PG, Synovec RE, Burgess LW. A Raman waveguide detector for liquid chromatography. *Anal Chem* 1999;71:4808–14. <https://doi.org/10.1021/ac9907336>.
- [23] Dijkstra RJ, Bader AN, Hoornweg GP, Brinkman UAT, Gooijer C. On-line coupling of column liquid chromatography and Raman spectroscopy using a liquid core waveguide. *Anal Chem* 1999;71:4575–9. <https://doi.org/10.1021/ac9902648>.
- [24] Confortin D, Neevel H, van Bommel MR, Reissland B. Study of the degradation of an early synthetic dye (crystal violet) on cotton linters, lignin and printing paper by the action of UV-Vis and Vis light and evaluation of the effect of gum arabic on degradation products and on colour change. *Creat 2010 Conf Proc - 'Colour Coded'* 2010:81–5.
- [25] Sabatini F, Degano I, Bommel M van. Investigating the in-solution photodegradation pathway of Diamond Green G by chromatography and mass spectrometry. *Color Technol* 2021. <https://doi.org/10.1111/COTE.12538>.
- [26] Society of Dyers and Colourists (Great Britain), American Association of Textile Chemists and Colorists. *Colour Index*. vol. third edition. Bradford, Yorkshire: 1974.
- [27] Sabatini F, Giugliano R, Degano I, Lluveras-Tenorio A, Sokolová R, Thoury M, et al. Development of a multi-analytical approach to investigate the fading of eosin in painting matrices. *IOP Conf. Ser. Mater. Sci. Eng.*, vol. 364, Institute of Physics Publishing; 2018, p. 012066. <https://doi.org/10.1088/1757-899X/364/1/012066>.
- [28] Alvarez-Martin A, Cleland TP, Kavich GM, Janssens K, Newsome GA. Rapid evaluation of the debromination mechanism of eosin in oil paint by direct analysis in real time and direct infusion-electrospray ionization mass spectrometry. *Anal Chem* 2019;91:10856–63. <https://doi.org/10.1021/acs.analchem.9b02568>.
- [29] Cooksey C. Quirks of dye nomenclature. 10. Eosin Y and its close relatives. *Biotech Histochem* 2018;93:211–9. <https://doi.org/10.1080/10520295.2017.1413207>.
- [30] Anselmi C, Capitani D, Tintaru A, Doherty B, Sgamellotti A, Miliani C. Beyond the color: A structural insight to eosin-based lakes. *Dye Pigment* 2017;140:297–311. <https://doi.org/10.1016/j.dyepig.2017.01.046>.
- [31] Favaro G, Confortin D, Pastore P, Brustolon M. Application of LC-MS and LC-MS-MS to the analysis of photo-decomposed crystal violet in the investigation of cultural heritage materials aging. *J Mass Spectrom* 2012;47:1660–70. <https://doi.org/10.1002/jms.3110>.
- [32] Cesaratto A, Lombardi JR, Leona M. Tracking photo-degradation of triarylmethane dyes with surface-enhanced Raman spectroscopy. *J Raman Spectrosc* 2017;48:418–24. <https://doi.org/10.1002/jrs.5056>.
- [33] Haria DP, König B. Synthetic applications of eosin Y in photoredox catalysis. *Chem Commun* 2014;50:6688–99. <https://doi.org/10.1039/c4cc00751d>.
- [34] Derayea SM, Nagy DM. Application of a xanthene dye, eosin y, as spectroscopic probe in chemical and pharmaceutical analysis; A review. *Rev Anal Chem* 2018;37. <https://doi.org/10.1515/revac-2017-0020>.
- [35] Ozkan E, Allan E, Parkin IP. The antibacterial properties of light-activated polydimethylsiloxane containing crystal violet. *RSC Adv* 2014;4:51711–5. <https://doi.org/10.1039/c4ra08503e>.

- [36] Confortin D, Neevel H, Brustolon M, Franco L, Kettelarij AJ, Williams RM, et al. Crystal violet: Study of the photo-fading of an early synthetic dye in aqueous solution and on paper with HPLC-PDA, LC-MS and FORS. *J. Phys. Conf. Ser.*, vol. 231, Institute of Physics Publishing; 2010, p. 012011. <https://doi.org/10.1088/1742-6596/231/1/012011>.
- [37] Huang YR, Kong Y, Li HZ, Wei XM. Removal of crystal violet by ultraviolet/persulfate: Effects, kinetics and degradation pathways. *Environ Technol Innov* 2020;18:100780. <https://doi.org/10.1016/j.eti.2020.100780>.
- [38] Chieli A, Miliani C, Degano I, Sabatini F, Tognotti P, Romani A. New insights into the fading mechanism of Geranium lake in painting matrix". *Dye Pigment* 2020;181:108600. <https://doi.org/10.1016/j.dyepig.2020.108600>.
- [39] Aguirre M, Goikoetxea M, Otero LA, Paulis M, Leiza JR. Accelerated ageing of hybrid acrylic waterborne coatings containing metal oxide nanoparticles: Effect on the microstructure. *Surf Coatings Technol* 2017;321:484–90. <https://doi.org/10.1016/J.SURFCOAT.2017.05.013>.

CHAPTER 6

LCW Cell in 2DLC

6. Combining photodegradation in a liquid-core-waveguide cell with multiple-heart-cut two-dimensional liquid chromatography

Abstract

Photodegradation greatly affects everyday life. It poses challenges when food deteriorates or when objects of cultural-heritage fade, but it can also create opportunities applied in advanced oxidation processes in water purification. Studying photodegradation, however, can be difficult, because of the time needed for degradation, the inaccessibility of pure compounds, and the need to handle samples manually. A novel light exposure cell, based on liquid-core-waveguide (LCW) technology, was embedded in a multiple-heart-cut two-dimensional liquid chromatography system, by coupling the LCW cell to the multiple-heart-cut valve. The sample was flushed from the heart-cut loops into the cell by an isocratic pump. Samples were then irradiated using different time intervals and subsequently transferred by the same isocratic pump to a second-dimension sample loop. The mixture containing the transformation products was then subjected to the second-dimension separation. In the current setup, about 30% to 40% of the selected fraction was transferred. Multiple degradation products could be monitored. Degradation was found to be faster when a smaller sample amount was introduced (0.3 μg as compared to 1.5 μg). The system was tested with three applications, *i.e.* fuchsin, a 19th-century synthetic-organic colorant, annatto, a lipophilic food dye, and vitamin B complex.

Publication

Combining photodegradation in a liquid-core-waveguide cell with multiple-heart-cut two-dimensional liquid chromatography

Mimi J. den Uijl, Yorn J.H.L. van der Wijst, Iris Groeneveld, Peter J. Schoenmakers, Bob W.J. Pirok, and Maarten R. van Bommel

Anal. Chem., **2022**, *94*, 11055-11061, DOI: 10.1021/acs.analchem.2c01928

6.1. Introduction

Photodegradation is the process in which molecules undergo a change due to UV/Vis irradiation. It poses challenges in many different fields, but also some opportunities. Food products, especially those stored over time, can be susceptible to light, which affect their shelf-life time. For other products pulsed-light processing is used as disinfection technique [1–4]. Light may affect healthy food ingredients, *e.g.* vitamins, to degrade and thus lose their nutritional value [5]. The problem becomes even larger when food ingredients are transformed into products that can be harmful [6]. Understanding photodegradation and its pathways can help prevent food spoilage and aid in the development of packaging materials that reduce light-induced transformation. Another field in which light degradation poses serious problems is cultural heritage. Organic colorants applied as dyes degrade over time, resulting in art objects, such as textiles, furniture, drawings, and paintings, changing colour and losing their historical value [7–11]. Knowledge about the degradation pathways and the influence of other parameters on light degradation can help us preserve valuable objects for future generations and understand the original appearance of objects of art.

Conversely, there are fields that exploit photodegradation advantageously. For example, in water-purification systems, advanced oxidation processes are applied to reduce the concentration of organic matter [12,13]. In such processes, hydrogen peroxide can be used in combination with UV light to eradicate toxic compounds in drinking water. The photodegradation reactions occurring in such systems (*i.e.* radical reactions) require further study, since the by-products formed could possibly be harmful [14].

To study photodegradation several methods exist [7,15–17]. The simplest method is to illuminate a solution of a single dissolved compound with a lamp. Unfortunately, degradation studies often report exclusively on the degradation of the starting compound, rather than studying the pathways and concentrations of all different degradation products [5,18]. Introducing more compounds and parameters inevitably leads to a tangle of different degradation pathways that occur simultaneously. To establish unambiguous links between a compound and its degradation products, it is preferable to isolate it prior to degradation, so as to circumvent tedious (or even impossible) measurements and data analysis. Unfortunately, few compounds are available in pure form or are very difficult and/or expensive to obtain. To determine the reaction rates different time points should be recorded, so sufficient material must be available.

Photodegradation techniques generally require time and manual handling (*e.g.* degradation during a week) [7]. Often a subsequent manual extraction is needed, introducing more sources of error. If more compounds and/or more parameters (*e.g.* time, catalysts, oxygen supply) are studied, the experimental procedure becomes very cumbersome and lengthy.

An alternative method to perform photodegradation research more efficiently was recently published [7,19,20]. In this study a liquid-core-waveguide (LCW) photodegradation cell was developed. This LCW cell comprises of an amorphous-Teflon (AF2400) tubing, which has a lower refractive index ($RI = 1.29$) than typical solvents. When the LCW cell is filled, the light is guided through the cell by total internal reflection, irradiating the sample inside [21]. However, just as with conventional techniques, this approach focused on solutions of pure compounds [7,19]. Investigating mixtures is feasible with this system, however, complicated since the link between parent molecules and their degradation products will be difficult. One way to reduce the complexity of the sample undergoing degradation is to separate the compound of interest from the mixture with liquid chromatography (LC) separation. If the reaction products are to be characterized with the aid of LC, the resulting setup would be akin to a two-dimensional liquid chromatography (2DLC) system with a light cell implemented as the modulator [22]. Photodegradation is then a specific form of reaction modulation or transformative modulation [23–25]. To our knowledge such a 2DLC system with light modulation has never been realized before. Normally, in 2DLC, a high orthogonality should be achieved between the two different (first-dimension, 1D , and second-dimension, 2D) separation systems [26]. However, in reaction modulation, the situation might be opposite. The difference between the two separations is due to the sample being transformed and the separation systems do not need to be different.

In this work an on-line photodegradation system was developed that allows fast and efficient study of solutions of a number of individual compounds from a complex mixture. This approach is based on an (LCW) reactor embedded in a multiple-heart-cut 2DLC with reversed-phase liquid chromatography (RPLC) in the 1D and 2D separation. The aim was to investigate the effects of a number of 2DLC method parameters and the concentration of compounds on the design and application of the LCW reactor and to evaluate its performance by comparing the products obtained at varying residence times with control samples. Finally, it was aspired to demonstrate the versatility of the new approach by applying it to examples from cultural heritage and food ingredients. These include fuchsin [27–29], which is a mixture of organic colorants that was extensively used in the late 1900s as dye for textile, food, and wine, but is now used as a biological staining agent, annatto-seeds extract [30,31], used widely in the food industry to colour hydrophobic products, such as cheese and butter, and a vitamin-B-complex formulation [32], a mixture of essential vitamins.

6.2. Materials and Methods

6.2.1. Chemicals

HPLC-quality water was obtained from a purification system ($R=18.2\text{ M}\Omega\text{ cm}$; Arium 611UV, Sartorius, Göttingen, Germany). Methanol (MeOH, LC-MS grade) was obtained from Biosolve (Valkenswaard, The Netherlands). Crystal violet (CV; $\geq 90\%$), eosin Y (EY; 99%), riboflavin (RF; $\geq 98\%$), ammonium formate (AF; $\geq 99.0\%$) and formic acid (FA, $\geq 95\%$) were purchased from Sigma Aldrich (Zwijndrecht, The Netherlands).

Fuchsin was a gift from the Cultural Heritage Agency of The Netherlands (RCE, Amsterdam, The Netherlands). Annatto seeds were purchased from De Peperbol (Amsterdam, The Netherlands) and the Davitamon vitamin-B pills were purchased from Etos (RF concentration 2.8 mg per pill, Amsterdam, The Netherlands).

6.2.2. Instrumentation

6.2.2.1. LC-LCW-LC-DAD

An Agilent 1290 Infinity 2DLC system (Agilent, Waldbronn, Germany) was used for all experiments in this study. The system was comprised of two binary pumps (G4220A), two diode-array detectors (DAD, G4212A) equipped with Agilent Max-Light Cartridge Cells (G4212-6008, $V_0 = 1.0\ \mu\text{L}$), and a G4226A autosampler as injector. A 2-position 10-port valve configured as an 8-port valve (G4243A) was used with two multiple-heart-cut (mHC) valves (G64242-64000) with 40- μL loops installed. Two reversed-phase liquid chromatography (RPLC) Zorbax Eclipse Plus C18 (Agilent) were used, with dimensions of 150 \times 2.1 mm (3.5 μm particle size) and 50 \times 4.6 mm (1.8 μm) in the first- and second-dimension, respectively. An 1100 Agilent isocratic pump (G1310A) was used to transfer the sample from the mHC valve to the LCW cell and eventually to the loop.

The LCW cell (ID 800 μm , OD. 1000 μm , length 12 cm, volume 60 μL , pressure limit 0.5 MPa) was placed in a light box created by DaVinci Laboratory Solutions (Rotterdam, The Netherlands), which is described and validated in previous research [19,20] and shown in Appendix D-1. The light source for degradation was a cold-white (400-700 nm) LED lamp (MCWHF2, Thorlabs, Newton, NJ, United States), which was coupled to a light fiber cable (M113L01, Thorlabs) with a 400 m core diameter, a UV/Vis collimator from Avantes (COL-UV/VIS, Apeldoorn, The Netherlands) and a plano-convex lens ($f=35\text{ mm}$, Thorlabs, LA4052-ML) to couple the light from the source into the LCW cell. The LED was controlled by a LED driver (LEDD1B, Thorlabs). The lightbox was also equipped with a 6-port switching valve to transfer the sample from the light box to the ²D separation. The 6-port switching valve was equipped with a loop of 20 μL .

6.2.3. Methods

6.2.3.1. Analytical Methods

In this work a multiple-heart-cut two-dimensional liquid-chromatography setup is developed and expanded to allow photodegradation in an LCW cell between the two separation dimensions. A binary pump, autosampler, ¹D column, the ¹D DAD and 10-port valve were connected in series. This latter valve was equipped with two multiple-heart-cut (mHC) valves. An isocratic pump was used to transfer the ¹D fractions stored in the loops of the mHC valves to the LCW cell. This latter cell was coupled to a 6-port valve, equipped with a 20 μ L loop, which connected the ²D binary pump to the ²D column. A schematic overview of the setup is shown in Fig. 6.1.

For the LC analysis of all samples, mobile-phase components A and B consisted of mixtures of aqueous buffer and MeOH in ratios of 95/5 [v/v] for mobile phase A and 5/95 [v/v] for mobile phase B. The aqueous buffer contained 10 mM ammonium formate at pH = 3, prepared by adding 0.390 g formic acid and 0.095 g ammonium formate to 1 L of water. Mobile-phase components A and B were used for both the ¹D and ²D separation. The ¹D flow rate was set to 0.4 mL/min. The ¹D gradient program started isocratically at 100% A from 0 min to 1 min, followed by a linear gradient to 100% B in 7 min, maintained for 2 min at 100% B, and finally returned to 100% A in 2 min. The composition was kept at 100% A for the remainder of time before starting a new run. The ²D flow rate was set to 0.3 mL/min. The ²D gradient program started isocratically at 100% A from 0 min to 1 min, followed by a linear gradient to 100% B in 7 min, 100% B for 1 min, and back to 100% A in 0.01 min. The mobile phase was kept at 100% A for at least 12 min, depending on the degradation time. The isocratic pump delivered a 50/50 [v/v] mixture of A and B at a flow rate of 0.05 mL/min when in operation.

In the multiple-heart-cut method, a ²D gradient stop time of 11.95 min and a cycle time of 12.00 min were used for both the 0-min (10 min residence time, no illumination) and 10-min (10 min residence time with illumination) degradations. In general, the total duration of the ²D method was 2 min longer than the residence time. For example, for a 30-min degradation the ²D cycle time was 32 min and the gradient stop time 31.95 min. The time-based heart-cut method was used and the cut times for all compounds studied in this work can be found in Appendix D-2. In all cases, an extra blank cut was taken before the elution of the first peak.

The isocratic pump (^{iso}P, Fig. 6.1) was used to transfer the sample from the mHC loop (indicated in Fig. 6.1) to the LCW cell and to transfer the degraded sample from the cell to the ²D injection loop (see Fig. 6.1). When the ²D method was started, the ^{iso}P was operated

for 1 min (50 μ L) to bring the sample from the mHC loop to the LCW cell. The flow rate of the ^{iso}P was then set to zero to degrade the sample until 1.6 min (80 μ L) before the start of the next modulation, where the sample was flushed to the 2D injection loop. For example, in a method where the sample was degraded for 10 minutes and the heart-cut of the last peak ended at 8.81 min, the isocratic pump was operated at a flow rate of 0.05 mL/min from 8.81 till 9.81 min, 0 mL/min from 9.82 min till 19.20 min, and 0.05 mL/min from 19.21 till 20.81 min. This 12-min cycle was then repeated for the number of cuts taken.

6.2.3.2. Sample preparation

A test mixture was used of riboflavin (RF, 25 ppm), eosin Y (EY, 20 ppm) and crystal violet (CV, 5 ppm) in a $H_2O/MeOH$ (70/30%) solution. Fuchsin was dissolved in $H_2O/MeOH$ (50/50%) with a concentration of 50 ppm.

Five annatto seeds (0.1620 grams) were extracted in 5 mL of $MeOH/H_2O$ (75/25%) and sonicated for 20 min in an ultrasonic bath. After sonicating, the solution was passed through a PTFE filter (0.45 μ m) [33].

Two pills of vitamin B (0.8820 grams) were grinded, dissolved in 20 mL of $MeOH$ and sonicated in an ultrasonic bath for 20 min. After this, the liquid was passed through a PTFE filter (0.45 μ m) and then diluted in a vial to reach a $H_2O/MeOH$ ratio of 50/50% [34].

6.2.4. Data processing

The chromatograms were processed with Agilent OpenLAB CDS software (Agilent, Santa Clara, CA, USA). Calculations and figures were performed with MATLAB R2018a (Mathworks, Woodshole, MA, USA) and Microsoft Excel.

6.3. Results & Discussion

In this research, an on-line system was developed that allowed fast and efficient study of the in-solution photodegradation of a number of individual compounds obtained from the separation of a mixture. The system was based on a liquid-core-waveguide (LCW) reactor embedded in a multiple-heart-cut 2DLC (mHC-2DLC) setup. In this Section, the setup and optimizable parameters will first be discussed (Section 6.3.1). The degradation efficiency will be evaluated (Section 6.3.2). To demonstrate the potential of the system three applications will be described (Section 6.3.3-6.3.5).

6.3.1. Design of the System

To facilitate quick and efficient light degradation, an LCW cell was incorporated in a mHC-2DLC setup. This LCW cell was previously coupled to an LC-DAD for studying degradation products [7,19]. In those studies, the sample was directly introduced into the light cell either manually [7,19] or by automated sampling with a multipurpose sampler [20]. In the setup used in the present research, however, the sample was automatically transferred to the LCW from the ¹D separation (Fig. 6.1). In the so-called time-based-sampling method, the timeframe of the eluting compounds must be inserted in the method. Therefore, the retention times of the targeted analytes in the ¹D system had to be determined first. The cut times for all compounds studied in this work can be found in Appendix D-2. After the cut times were established, a sample was injected by an autosampler into the ¹D column. The components of interest were transferred to loops in the mHC valve. In this work the number of peaks collected did not exceed the capacity of a single “deck” (multi-loop valve) and the first ²D method only started after the last fraction was stored.

When the mHC is used to store the separated components prior to exposure in the LCW, an additional loop is required to transfer the last exposed component to the ²D separation. Normally in mHC-2DLC, the ²D pump is directly connected to the heart-cut valve. In the present setup an additional pump (^{iso}P in Fig. 6.1) was inserted to transfer the component of interest from the mHC valve to the LCW cell. The outlet of the LCW was connected to a six-port valve that served as modulation valve and injection valve for the ²D system. The storage loops were eluted one by one to the LCW cell, where they were either stored or degraded for a selected time interval. The exact timing had to be adapted, depending on the degradation time. When the sample was injected to the ²D separation, the next component in a storage loop was transferred to the LCW and the cycle repeats. To ensure the start of the last ²D separation, an extra ¹D cut was required, since the presence of the additional flow path and the light cell could not be detected by the software. In the present setup, a blank ²D run was performed before the components of interest were transferred to the second dimension, since all stored analyte peaks were first transferred to the LCW cell before being transported to the ²D system. This extra cut was always taken in the method between 5 and 5.1 min. The timings established for the different degradation times are listed in Appendix D-3, Table D-2-4.

Because the LCW cell has a pressure limit of 0.5 MPa, the flow rates used in the ¹D and ²D LC cannot be used to fill and empty the light cell. This is circumvented by using wider tubing (between the LCW and the six-port valve and for the loop in this valve) and a low operating flow rate for the isocratic pump (see Fig. 6.1). The volume of the mHC storage loops (40 μ L) is smaller than that of the LCW cell (60 μ L), which in turn is larger than the injection loop of the

^2D system (20 μL). This will result in an inevitable loss of sample when a peak is transferred from the ^1D column to the ^2D system. The highest yields were observed with a flush volume of either 80 or 85 μL (pump operating at 1.6 min or 1.7 min at 50 $\mu\text{L}/\text{min}$). The ratio of ^2D peak area to ^1D peak area for an 80 μL flush volume was found to be 36% for RF, 42% for CV, and 30% for EY. For an 85 μL flush volume, the ratios were 34% for RF, 37% for CV, and 26% for EY. These ratios are seen to be significantly different for the different compounds. This is due to the limited size of the storage loops in the mHC valve (40 μL , corresponding to an elution window of 0.1 min at a ^1D flow rate of 400 $\mu\text{L}/\text{min}$). A smaller fraction of the sample is transferred when the ^1D peak is broader. This can be corrected for, resulting in a reduction of the variation between the different analytes. The corrected ratios for an 80 μL flush volume were found to be 39% for RF, 45% for CV, and 43% for EY. For the 85 μL flush volume, the ratios were found to be 37% for RF, 39% for CV, and 36% for EY. Slightly higher ratios were observed for a transfer volume of 80 μL . For riboflavin the effect of the transfer time is seen to be small, whereas it is larger for the later-eluting compounds.

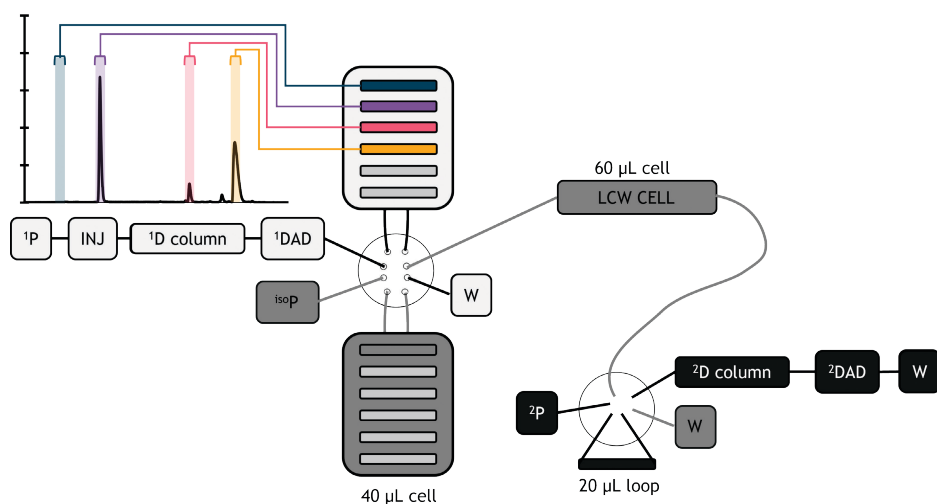


Figure 6.1. Schematic illustration of liquid chromatography – liquid-core-waveguide cell – liquid chromatography setup. The three different flow paths are indicated with a different shade of grey (white, grey, and black). On the top left the ^1D chromatogram of the test mix is shown with the peak cuts for the blank, riboflavin, crystal violet, and eosin Y (semi-transparent rectangles).

It may be argued that peak-based cutting (based on a detection threshold) is less prone to variations in chromatographic conditions than time-based cutting. However, in the present setup peak-based cutting was only possible with one specific wavelength. Moreover, a blank (first) cut should be additionally programmed (time-based) and the entire program of the isocratic pump must be anchored on the peak-based cutting times. This was not possible with the present setup.

6.3.2. Feasibility of the system

To assess the system, three compounds in a mixture were studied, *i.e.* riboflavin, crystal violet, and eosin Y. The first step in this process was to explore how the analytes behave in the cell, with and without irradiation. The results are shown in Fig. 6.2.

These data were obtained with a modulation time of 12 min, leading to a residence time in the LCW cell of about 10 min. The sample was irradiated with an LED ‘white’ spectrum, including wavelengths ranging from 400 nm to 800 nm. This illumination source was chosen to mimic indoor conditions without UV light. Clear degradation can be seen for riboflavin (Fig. 6.2A). For crystal violet and eosin Y no degradation products are observed (Figs. 6.2B and 6.2C). Some variations are observed in the peak area of the main compounds, but this is likely due to slight variations in the ^1D retention times between runs, leading to variations in sample transfer. For riboflavin, a number of different degradation products are formed after 10 min. The most intense peak (eluting at 51 min) corresponds to lumichrome, as confirmed by its UV-absorbance spectrum. The complete identification of the degradation products of riboflavin is beyond the scope of this research.

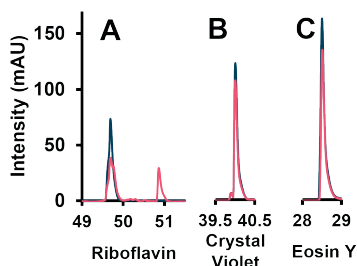


Figure 6.2. Overlay of chromatograms obtained after 10-min residence time of a fraction cut from the ^1D effluent in the LCW cell with the light off (blue) and the light on (pink). A, riboflavin (254 nm), B, crystal violet (590 nm), C, eosin Y (520 nm). Note that the x-axis is following the ^1D separation order.

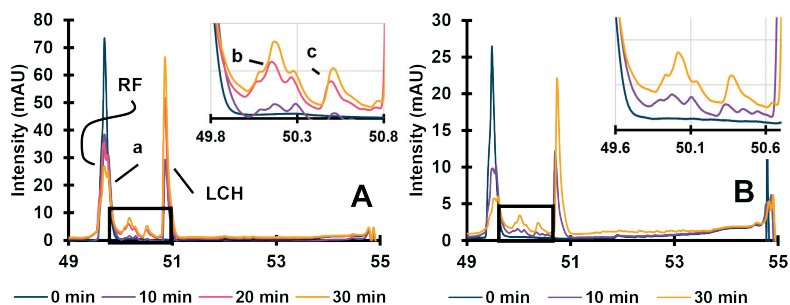


Figure 6.3. Timeseries of riboflavin (RF) degradation in the LCW cell for ^1D injection volumes of 15 μL (A) and 3 L (B). 0 min (10 min with lamp off, blue) 10 min (purple), 20 min (pink, Fig. 6.3A only), 30 min (yellow).

To study the effect of the degradation time, a time series was recorded with irradiation ranging from 0 to 30 min (Fig. 6.3A). Longer residence times in the LCW result in a further degradation. Besides the increase in peak area for the lumichrome (LCH in Fig. 6.3) and other degradation products, a peak arose for the RF peak for longer irradiation times, indicating the formation of a product with a nearly identical ^2D retention time. For quantitative interpretation (*vide infra*) the two compounds were sufficiently separated and treated independently.

The results presented in Fig. 6.3A were obtained by using a ^1D injection volume of 15 μL , which leads to large sample amounts and, therefore, possible “saturation” of the LCW cell. The intention is to irradiate the collected fraction along the entire length of the cell. However, when saturated, a significant fraction of the light may be absorbed by the sample at the front of the LCW cell, leading to an axial illumination gradient. To test this hypothesis, the ^1D injection volume of the same sample was reduced by 80% to 3 μL . The results are shown in Fig. 6.3B. While the two sets of overlaid chromatograms in Fig. 6.3 are seemingly similar, the areas of the degradation products are much larger relative to the RF peak in Fig. 6.3B. Clearly, the lower amount of sample introduced into the LCW leads to faster degradation. However, smaller amounts of degradation product are formed, and identification of minor products may be more difficult in the current setup. In Fig. 6.4 the area of the degradation products relative to the total peak area of RF is shown for both the 15 μL and 3 μL ^1D injection volumes. Degradation product A is formed in the first 10 min, but its relative concentration stays similar thereafter. Hence, its absolute concentration passes through a maximum. The relative peak areas of the other three degradation products all increase over time. Products B and C were only detected after 30 min degradation at the lower injected concentration. However, for LCH, there is a clear increase visible. The results confirm that a lower analyte concentration results in faster degradation. The injection volume or the absolute amount of sample introduced, should be optimized, so as to avoid saturation of the LCW cell, while exceeding the limits of detection for the degradation products. A more-sensitive detector shifts the optimum towards lower injected amounts.

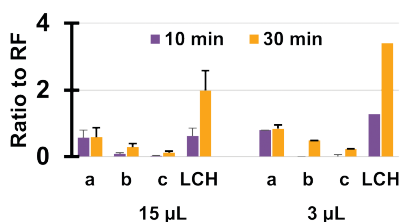


Figure 6.4. Ratios of peak areas relative to riboflavin for the various degradation products (a, b, c, and lumichrome, L) for ^1D injection volumes of 15 μL (bottom) and 3 μL (top) and different irradiation times as indicated in the figure.

6.3.3. Application to fuchsin

To demonstrate the versatility of the LC-LCW-LC system several different applications were studied. The first of these concerned fuchsin, which is one of the earliest synthetic organic colorants from the 19th century. It was used to dye textile and as a food colorant in the beginning of the 20th century. Nowadays it is used as a biological staining agent for bacteria, and sometimes as a disinfectant [30,31]. The structure of fuchsin is shown in Appendix D-4, Fig. D-3. It is sold as a mixture of four compounds, which are the triply, doubly, and singly methylated derivatives (known as Magenta III, M3, Magenta II, M2, and Magenta I, M1, respectively) and pararosaniline (M0), which is not methylated (see Figs. D-2-5). The chromatogram of the mixture (detection wavelength 555 nm) is shown in Fig. 6.5A. The four main compounds can clearly be seen, but impurities are also present. Out of the four main compounds, M0 and M3 are commercially available as pure components, allowing their degradation pathways to be studied individually [35,36]. In contrast, it has not been possible so far to study the degradation of M1 and M2, which are not available as (more or less) pure compounds. The present LC-LCW-LC setup offers a unique possibility for degradation studies of such individual compounds. Separating the fuchsin mixture prior to compound degradation is essential for this purpose. Fig. 6.5B illustrates the successful degradation of M1.

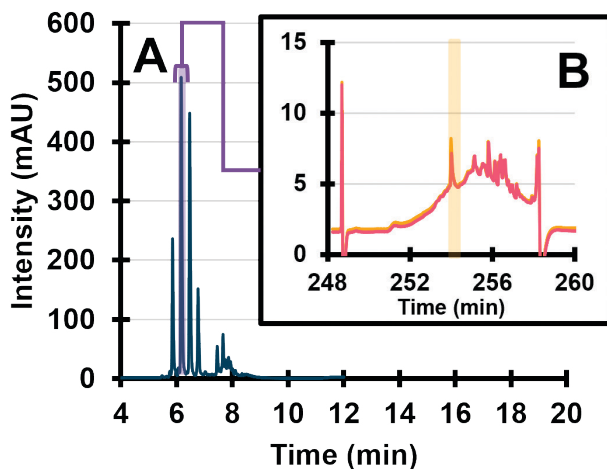


Figure 6.5. A) RPLC chromatogram of a fuchsin sample. ¹D detection wavelength 555 nm. The shaded fraction (M1) is transferred to the LCW and degraded for 4 h. B) second-dimension chromatograms of the M1 fraction after 4 h degradation shown in yellow and pink (overlay of two repeat experiments). M1 in ²D indicated by the yellow shaded bar. ²D detection wavelength 254 nm.

After one hour no degradation products were observed. The present setup readily allows more extensive degradation studies. For that reason, it was chosen to degrade fuchsin (M1) for a longer period. After 4 h, at a wavelength of 254 nm, a number of degradation products

were detected (Fig. 6.5B). The present system creates opportunities to study these products in detail, for example by attaching the setup to a mass spectrometer. However, this is beyond the scope of the present study. The entire experiment (^1D separation, 4 h degradation, ^2D separation) was repeated and the ^2D chromatograms are overlaid in Fig. 6.5B. Excellent repeatability of the entire process is demonstrated, despite the long degradation times. Slight variations in peak areas (e.g. for M1) can be explained from minor variations in the ^1D retention times.

6.3.4. Application to annatto

Annatto is a natural food-colouring agent. It is obtained from the seeds of the Achiote tree and used for colouring many different lipophilic products, such as cheese, ice cream, and margarin. The main colouring compound in the annatto extract is bixin, an apocarotenoid, but there are many other colouring compounds in the extract, as can be seen in the two chromatograms of Fig. 6.6A (recorded at 254 nm and 450 nm). Studying the photodegradation pathways of bixin can help the food industry prevent food spoilage and improve food packaging. Bixin is one of many compounds present and it is difficult and expensive to obtain it in a purified form. Therefore, degradation studies of bixin have been only been performed on bixin from the annatto extract instead on the pure form [37,38].

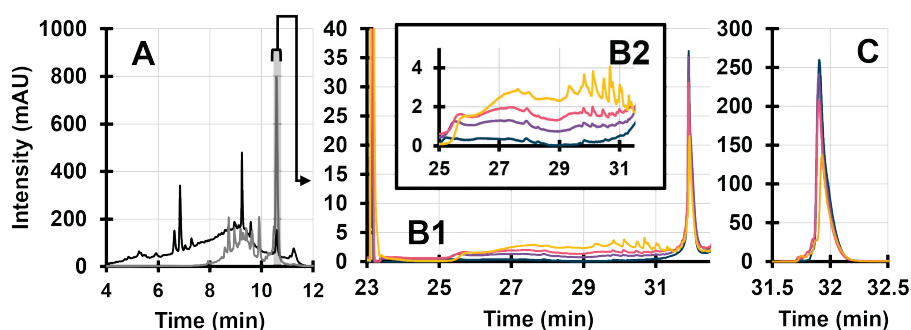


Figure 6.6. A) RPLC chromatogram of an annatto seed extract. Detection wavelength 254 nm (black) and 450 nm (grey). The shaded blue fraction is transferred to the LCW and degraded using different time intervals. B1 and B2) ^2D chromatograms representing a timeseries of bixin during 0 (blue), 30 (purple), 60 (pink) and 120 min (yellow), recorded at 254 nm. C, as B, except recorded at 450 nm.

Figs. 6.6B and 6.6C show a series of overlaid ^2D chromatograms of degraded bixin (0, 30, 60 and 120 min), recorded at 254 and 450 nm, respectively. At 450 nm a small shoulder peak starts to appear before the bixin peak after 30 min exposure. After 60 min, a number of small peaks are visible at 254 nm. This shows the complexity of the degradation of a single compound, and it underlines the value of the current LC-LCW-LC setup. Without the prior

separation it would be impossible to deduce which degradation products arise from bixin. This shows how important a pre-separation to the photodegradation reaction can be. Again, adding a mass spectrometer to the system will allow detailed interpretation of the structures and pathways.

6.3.5. Application to vitamin B

Vitamin B is a group of eight essential vitamins, including thiamine (B_1), riboflavin (B_2), niacin (B_3), pantothenic acid (B_5), pyridoxine (B_6), biotin (B_7), folic acid (B_{11}), and cobalamins (B_{12}), with all kinds of health benefits. Many different vitamin-B products are available on the market. As already described in Section 6.3.2, riboflavin is susceptible to light. The riboflavin for the study described in Section 6.3.2 was obtained as a chemical standard which can be studied without prior separation. The LC-LCW-LC setup allows study of riboflavin, and all other compounds present in a vitamin B complex. In Fig. 6.7A the 1D chromatogram is shown for a vitamin-B formulation. Many compounds with vastly different peak areas are observed. The chromatographic behaviour of the molecules with many acid groups is poor under these chromatographic conditions.

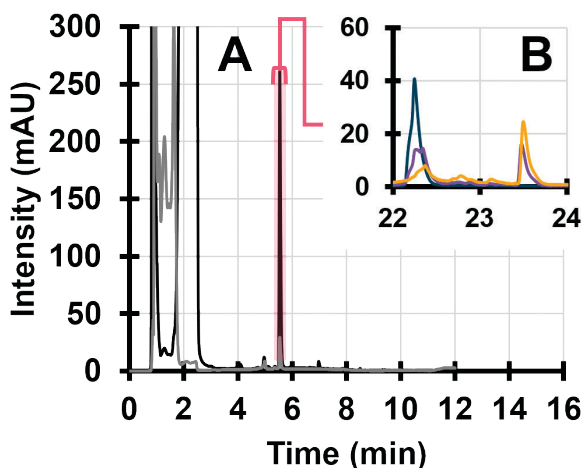


Figure 6.7. A) RPLC chromatogram of a vitamin-B-complex formulations, recorded at 254 nm (black) and 300 nm (grey). B) 2D chromatograms corresponding to a timeseries of degradations of RF recorded at 254nm (0 min, blue, 10 min, purple, 30 min, yellow).

RF was isolated from the mixture using the 1D separation, introduced into the LCW and irradiated using different time intervals. The 2D chromatograms after degradation of RF are shown in Fig. 6.7B. This illustrates that RF (or, indeed, any compound) can be studied from complex mixtures, yielding results that are comparable to those obtained with pure standards (see Section 6.3.2, Fig. 6.3). It should be noted, however, that the conditions in the

light cell are different from the conditions experienced in a real-world situation. This matrix is acidified and has MeOH present as organic modifier. It is possible that these reaction conditions could lead to different reaction kinetics than present in real world degradations. It is of importance to compare these degradation studies to the literature present on these subjects. As such this system should not be considered as a replacement of other ageing techniques, but rather as a new tool providing information about degradation mechanisms in a much faster manner. However, comparing these different matrices is from a fundamental point of view also interesting to understand the effect of the matrix, as is shown previously [7,8,39].

6.4. Concluding remarks

In this work, a 2DLC-based photodegradation workflow was developed to study isolated compounds from mixtures using a liquid-core-waveguide cell as reactor. This allowed rapid and efficient studies of components of interest isolated from mixtures. Fractions of the first-dimension effluent were collected by a multiple-heart-cut valve, specifically targeting compounds of interest. A method was developed to transfer the analyte fractions from the first-dimension separation to the light exposure cell and subsequently to the second-dimension separation. About 30% to 40% of the isolated and degraded fraction was transferred. The fastest degradations could be performed with low concentrations of sample (total amount of analyte approximately 0.3 μg) and care should be taken to avoid saturation of the LCW, which can result in an inhomogeneous irradiation. The system allows us to generate degradation profiles by irradiation of the sample using different time intervals. To our knowledge, this is the first time light-induced reaction modulation has been employed. The method proved to be stable over longer degradation times (up to 4 hours). To demonstrate the versatility of the system several samples that contained compounds of interest, as well as many other components, were studied by selecting one of the components present in the mixture. This illustrates the relevance of a pre-separation having the advantage that the first separation, the exposure inside the LCW and the second separation can be carried out online and fully automated. As example, according to our knowledge this was the first time a degradation profile of magenta I isolated from fuchsin was demonstrated.

References

- [1] Verduin J, Den Uijl MJ, Peters RJ, Van Bommel MR. Photodegradation Products and their Analysis in Food. *J Food Sci Nutr* 2020;6. <https://doi.org/10.24966/FSN-1076/100067>.
- [2] Ignat A, Manzocco L, Maifreni M, Bartolomeoli I, Nicoli MC. Surface decontamination of fresh-cut apple by pulsed light: Effects on structure, colour and sensory properties. *Postharvest Biol Technol* 2014;91:122–7. <https://doi.org/10.1016/J.POSTHARVBIO.2014.01.005>.
- [3] Bosset JO, Gallmann PU, Sieber R. Influence of light transmittance of packaging materials on the shelf-life of milk and dairy products — a review. *Food Packag Preserv* 1994;222–68. https://doi.org/10.1007/978-1-4615-2173-0_13.
- [4] Thu Trang V, Kurogi Y, Katsuno S, Shimamura T, Ukeda H. Protective effect of aminoreductone on photo-degradation of riboflavin. *Int Dairy J* 2008;18:344–8. <https://doi.org/10.1016/J.IDAIRYJ.2007.10.001>.
- [5] Allwood MC, Martin HJ. The photodegradation of vitamins A and E in parenteral nutrition mixtures during infusion. *Clin Nutr* 2000;19:339–42. <https://doi.org/10.1054/CLNU.2000.0109>.
- [6] He J, Evans NM, Liu H, Zhu Y, Zhou T, Shao S. UV treatment for degradation of chemical contaminants in food: A review. *Compr Rev Food Sci Food Saf* 2021;20:1857–86. <https://doi.org/10.1111/1541-4337.12698>.
- [7] den Uijl MJ, Lokker A, van Dooren B, Schoenmakers PJ, Pirok BWJ, van Bommel MR. Comparing different light-degradation approaches for the degradation of crystal violet and eosin Y. *Dye Pigment* 2022;197:109882. <https://doi.org/10.1016/J.DYEPIG.2021.109882>.
- [8] Alvarez-Martin A, Trashin S, Cuykx M, Covaci A, De Wael K, Janssens K. Photodegradation mechanisms and kinetics of Eosin-Y in oxic and anoxic conditions. *Dye Pigment* 2017;145:376–84. <https://doi.org/10.1016/j.dyepig.2017.06.031>.
- [9] Pirok BWJ, Den Uijl MJ, Moro G, Berbers SVJ, Croes CJM, Van Bommel MR, et al. Characterization of Dye Extracts from Historical Cultural-Heritage Objects Using State-of-the-Art Comprehensive Two-Dimensional Liquid Chromatography and Mass Spectrometry with Active Modulation and Optimized Shifting Gradients. *Anal Chem* 2019. <https://doi.org/10.1021/acs.analchem.8b05469>.
- [10] Pérez-Alonso M, Castro K, Madariaga JM. Investigation of degradation mechanisms by portable Raman spectroscopy and thermodynamic speciation: The wall painting of Santa María de Lemoniz (Basque Country, North of Spain). *Anal Chim Acta* 2006;571:121–8. <https://doi.org/10.1016/j.aca.2006.04.049>.
- [11] Degano I, Ribechini E, Modugno F, Colombini MP. Analytical Methods for the Characterization of Organic Dyes in Artworks and in Historical Textiles. *Appl Spectrosc Rev* 2009;44:363–410. <https://doi.org/10.1080/05704920902937876>.
- [12] Kolkman A, Martijn BJ, Vughes D, Baken KA, van Wezel AP. Tracing Nitrogenous Disinfection Byproducts after Medium Pressure UV Water Treatment by Stable Isotope Labeling and High Resolution Mass Spectrometry. *Environ Sci Technol* 2015;49:4458–65. <https://doi.org/10.1021/es506063h>.
- [13] Hisaindee S, Meetani MA, Rauf MA. Application of LC-MS to the analysis of advanced oxidation process (AOP) degradation of dye products and reaction mechanisms. *TrAC - Trends Anal Chem* 2013;49:31–44. <https://doi.org/10.1016/j.trac.2013.03.011>.
- [14] Brunner AM, Bertelkamp C, Dingemans MML, Kolkman A, Wols B, Harmsen D, et al. Integration of target analyses, non-target screening and effect-based monitoring to assess OMP related water quality changes in drinking water treatment. *Sci Total Environ* 2020;705:135779. <https://doi.org/10.1016/J.SCITOTENV.2019.135779>.
- [15] Confortin D, Neevel H, Brustolon M, Franco L, Kettelarij AJ, Williams RM, et al. Crystal violet: Study of the photo-fading of an early synthetic dye in aqueous solution and on paper with HPLC-PDA, LC-MS and FORS. *J. Phys. Conf. Ser.*, vol. 231, Institute of Physics Publishing; 2010, p. 012011. <https://doi.org/10.1088/1742-6596/231/1/012011>.

- [16] Whitmore PM, Pan X, Bailie C. Predicting the fading of objects: Identification of fugitive colorants through direct nondestructive lightfastness measurements. *J Am Inst Conserv* 1999;38:395–409. <https://doi.org/10.1179/019713699806113420>.
- [17] Friele LFC. A Comparative Study of Natural and Xenotest Exposure Condition: for Measuring Fading and Degradation. *J Soc Dye Colour* 2008;79:623–31. <https://doi.org/10.1111/j.1478-4408.1963.tb02522.x>.
- [18] Kansal SK, Singh M, Sud D. Studies on photodegradation of two commercial dyes in aqueous phase using different photocatalysts. *J Hazard Mater* 2007;141:581–90. <https://doi.org/10.1016/j.jhazmat.2006.07.035>.
- [19] Groeneveld I, Schoemaker SE, Somsen GW, Ariese F, van Bommel MR. Characterization of a liquid-core waveguide cell for studying the chemistry of light-induced degradation. *Analyst* 2021. <https://doi.org/10.1039/D1AN00272D>.
- [20] Groeneveld I, Bagdonaite I, Beekwilder E, Ariese F, Somsen GW, Bommel MR van. Liquid Core Waveguide Cell with In Situ Absorbance Spectroscopy and Coupled to Liquid Chromatography for Studying Light-Induced Degradation. *Anal Chem* 2022;94:7647–54. <https://doi.org/10.1021/ACS.ANALCHEM.2C00886>.
- [21] Altkorn R, Koev I, Van Duyn RP, Litorja M. Low-loss liquid-core optical fiber for low-refractive-index liquids: fabrication, characterization, and application in Raman spectroscopy. *Appl Opt* 1997;36:8992. <https://doi.org/10.1364/ao.36.008992>.
- [22] Pirok BWJ, Stoll DR, Schoenmakers PJ. Recent Developments in Two-Dimensional Liquid Chromatography: Fundamental Improvements for Practical Applications. *Anal Chem* 2018;91:240–63. <https://doi.org/10.1021/ACS.ANALCHEM.8B04841>.
- [23] Wouters B, Pirok BWJ, Soulis D, Garmendia Perticarini RC, Fokker S, van den Hurk RS, et al. On-line microfluidic immobilized-enzyme reactors: A new tool for characterizing synthetic polymers. *Anal Chim Acta* 2019;1053:62–9. <https://doi.org/10.1016/J.ACA.2018.12.002>.
- [24] Pirok BWJ, Abdullhussain N, Aalbers T, Wouters B, Peters RAH, Schoenmakers PJ. Nanoparticle Analysis by Online Comprehensive Two-Dimensional Liquid Chromatography combining Hydrodynamic Chromatography and Size-Exclusion Chromatography with Intermediate Sample Transformation. *Anal Chem* 2017;89:9167–74. <https://doi.org/10.1021/ACS.ANALCHEM.7B01906>.
- [25] Groeneveld G, Pirok BWJ, Schoenmakers PJ. Perspectives on the future of multi-dimensional platforms. *Faraday Discuss* 2019;218:72–100. <https://doi.org/10.1039/C8FD00233A>.
- [26] Cacciola F, Rigano F, Dugo P, Mondello L. Comprehensive two-dimensional liquid chromatography as a powerful tool for the analysis of food and food products. *TrAC Trends Anal Chem* 2020;127:115894. <https://doi.org/10.1016/J.TRAC.2020.115894>.
- [27] Degano I, Sabatini F, Braccini C, Colombini MP. Triarylmethine dyes: Characterization of isomers using integrated mass spectrometry. *Dye Pigment* 2019;160:587–96. <https://doi.org/10.1016/J.DYEPIG.2018.08.046>.
- [28] Cooksey C, Dronsfield A. Fuchsine or magenta: the second most famous aniline dye. A short memoir on the 150th anniversary of the first commercial production of this well known dye. <http://DxDoiOrg/101080/10520290903081401> 2009;84:179–83. <https://doi.org/10.1080/10520290903081401>.
- [29] Tamburini D, Breitung E, Mori C, Kotajima T, Clarke ML, McCarthy B. Exploring the transition from natural to synthetic dyes in the production of 19th-century Central Asian ikat textiles. *Herit Sci* 2020;8:1–27. <https://doi.org/10.1186/S40494-020-00441-9/FIGURES/8>.
- [30] Kapoor L, Ramamoorthy S. Strategies to meet the global demand for natural food colorant bixin: A multidisciplinary approach. *J Biotechnol* 2021;338:40–51. <https://doi.org/10.1016/J.JBIOTEC.2021.07.007>.
- [31] Tennant DR, O'Callaghan M. Survey of usage and estimated intakes of annatto extracts. *Food Res Int* 2005;38:911–7. <https://doi.org/10.1016/J.FOODRES.2005.01.013>.
- [32] Powers HJ. Riboflavin (vitamin B-2) and health. *Am J Clin Nutr* 2003;77:1352–60. <https://doi.org/10.1093/AJCN/77.6.1352>.

- [33] Rodrigues LM, Alcázar-Alay SC, Petenate AJ, Meireles MAA. Bixin extraction from defatted annatto seeds. *Comptes Rendus Chim* 2014;17:268–83. <https://doi.org/10.1016/J.CRCI.2013.10.010>.
- [34] Jin P, Xia L, Li Z, Che N, Zou D, Hu X. Rapid determination of thiamine, riboflavin, niacinamide, pantothenic acid, pyridoxine, folic acid and ascorbic acid in Vitamins with Minerals Tablets by high-performance liquid chromatography with diode array detector. *J Pharm Biomed Anal* 2012;70:151–7. <https://doi.org/10.1016/J.JPBA.2012.06.020>.
- [35] Kosanić MM, Tričković JS. Degradation of pararosaniline dye photoassisted by visible light. *J Photochem Photobiol A Chem* 2002;149:247–51. [https://doi.org/10.1016/S1010-6030\(02\)00007-2](https://doi.org/10.1016/S1010-6030(02)00007-2).
- [36] Cesaratto A, Lombardi JR, Leona M. Tracking photo-degradation of triarylmethane dyes with surface-enhanced Raman spectroscopy. *J Raman Spectrosc* 2017;48:418–24. <https://doi.org/10.1002/jrs.5056>.
- [37] Alwis DDDH, Chandrika UG, Jayaweera PM. Photostability of apocarotenoids on surface of TiO₂ semiconductor nanoparticles. *J Photochem Photobiol A Chem* 2021;407:113061. <https://doi.org/10.1016/J.JPHOTOCHEM.2020.113061>.
- [38] Lobato KB de S, Paese K, Forgearini JC, Guterres SS, Jablonski A, Rios A de O. Evaluation of stability of bixin in nanocapsules in model systems of photosensitization and heating. *LWT - Food Sci Technol* 2015;60:8–14. <https://doi.org/10.1016/J.LWT.2014.09.044>.
- [39] Pirok BWJ, Moro G, Meekel N, Berbers SVJ, Schoenmakers PJ, van Bommel MR. Mapping degradation pathways of natural and synthetic dyes with LC-MS: Influence of solvent on degradation mechanisms. *J Cult Herit* 2019;38:29–36. <https://doi.org/10.1016/j.culher.2019.01.003>.

CHAPTER 7

LCW Cell in Recycling LC

7. Incorporating a liquid-core-waveguide cell in recycling liquid chromatography for detailed studies of photodegradation reactions

Abstract

In this work, a microfluidic photoreactor was embedded in a liquid-chromatography system. Mixtures were separated on an analytical column and compounds of interest were subsequently introduced into the light-reactor cell. After degradation, the content of the light-reactor cell was reinjected onto the same column, to separate the compound of interest from its degradation products. Because the separation was performed on the same column, degradation products could be linked to the components in the original mixture. The present system allowed further degradation cycles. A separated degradation product can be re-introduced into the photoreactor and irradiated again. The next generation of degradation products can again be separated on the same analytical column. This cycling procedure is an excellent tool to elucidate degradation pathways. This was demonstrated using riboflavin, better known as vitamin B2. By degrading it in the first cycle, its degradation products were isolated and subjected to a second degradation in the light-reactor cell. This allowed us to pinpoint secondary products and connect these with primary degradation products. The peak transfer between the first and second cycles and between the second and third cycles were optimized to provide recycling yields of 81% ($\pm 2.3\%$) and 73% ($\pm 5\%$), respectively, with the current setup.

Publication

Incorporating a liquid-core-waveguide cell in recycling liquid chromatography for detailed studies of photodegradation reactions

Mimi J. den Uijl, Ingrida Bagdonaite, Peter J. Schoenmakers, Bob W.J. Pirok, and Maarten R. van Bommel

J. Chromatogr. A, **2022**, accepted with major revisions

7.1. Introduction

Many organic compounds can change under the influence of light. This process is called photodegradation. In food science, it is usually seen as undesirable, when healthy food ingredients, such as vitamins, degrade or when products lose their colour when stored over time [1–3]. In other fields, such as cultural heritage, photodegradation can lead to a loss of value, due to the fading of art objects, such as paintings and tapestries [4–6]. There are fields where photodegradation can be used advantageously, for example in advanced oxidation processes for water purification, where ultraviolet (UV) light is used in conjunction with hydrogen peroxide to reduce the organic-matter concentration [7,8].

Photodegradation, whether intentional or unwanted, is difficult to study. If a target molecule is degraded, many structurally related degradation products can be formed, which makes it hard to distinguish clear degradation pathways [9]. Moreover, degradation studies are often performed in simple setups, such as a solution in a beaker irradiated with a lamp. This requires a great deal of manual sample handling and makes it difficult to control factors, such as evaporation and the light dose [7,10]. Another disadvantage of simple setups is their inability to deal with complex matrices [11,12]. When food ingredients are degraded in pure-component aqueous solutions, degradation pathways may be different from those occurring in complex food or paint matrices [12,13]. Established methods to study photodegradation, such as the Microfading tester (MFT) and the Xenotest (XT) allow degradation of colorants applied directly on a solid matrix, while light-exposure rooms exist, for example to accelerate studies into the shelf lives of food products [14–16].

Recently, a new light-exposure cell was developed by our group, based on a liquid-core-waveguide (LCW) principle [17]. This light cell is made from Teflon-AF2400, a material with a lower refractive index than most liquids. In this way, the light can be captured within the cell and guided along its axis [18]. Photodegradation is performed in solution, making it compatible with liquid chromatography (LC). The degradation products formed in the LCW cell can be transferred to an on-line LC system, eliminating all manual sample handling [19]. Such photodegradation research can be completely automated by integrating the photoreactor with a multi-purpose sampler (MPS), which can inject samples into the cell and, after degradation through light irradiation, flush the degraded sample to the injection loop of the LC. The MPS can be programmed to start the LC run, clean the LCW cell, and prepare the system for another injection.

One problem that is not solved in any of the above techniques, is that very few compounds are available for study in their pure form. To circumvent this problem, an LC separation can

also be performed prior to degradation. To realize a system with separation stages both before and after photodegradation (*i.e.* LC-LCW-LC), an LCW cell was installed in a multiple-heart-cut two-dimensional LC system [20]. Using LC-LCW-LC, a sample could be separated on a first-dimension (¹D) column and several fractions of the effluent could be stored in the multiple-heart-cut loops. These purified fractions (ideally pure-component peaks) were transferred to the LCW cell one by one and degraded, after which the reaction products were transferred to the second-dimension (²D) separation. This LC-LCW-LC system allowed studying the degradation of many (possibly unknown) compounds from a complex mixture in a light-exposure cell in an on-line, automated fashion for the first time. The setup was easy to use and yielded repeatable results. It was also the first time that photodegradation was employed as reaction modulation in two-dimensional LC (2D-LC) [21–23].

This LC-LCW-LC did have its limitations [20]. First of all, reversed-phase LC (RPLC) was used in both the ¹D and ²D separations with similar mobile phases. The columns, however, were not identical, neither in terms of the stationary phase, nor in their dimensions. As a result, the ¹D and ²D chromatograms were quite different, making it difficult to connect degradation products observed in the ²D chromatogram to impurities observed in the ¹D chromatogram. Moreover, many of the compounds from a mixture selected for degradation yielded multiple degradation products, all of which inviting further study. The complex LC-LCW-LC setup did not allow performing such follow-up degradations on-line. Time profiles could be generated for each selected compound, but without further information it is nearly impossible to establish the complete network of structurally related degradation products. Lastly, although the LC-LCW-LC system was based on commercial 2D-LC hardware, it was complex and not straightforward to reproduce elsewhere [23,24]. Also, both the MPS-LCW-LC and LC-LCW-LC carry costs that prohibit their routine use in many laboratories.

One way to alleviate some of these issues is to use identical columns and conditions in the ¹D and ²D separations. This would make it easier to track degradation products across chromatograms, but it does not remove the limitation of a single degradation step per compound. An elegant way to circumvent the latter problem is to redirect the effluent from the LCW cell back to the ¹D column, *i.e.* LC followed by the LCW and back to the same LC, in short LC-LCW \cup LC. This operation can be repeated to create an LC-(LCW \cup LC)^{*n*} system that allows several (*n*) generations of photodegradation products to be studied for a single small sample in an automated fashion. Potentially, LC-(LCW \cup LC)^{*n*} experiments allow highly detailed degradation studies, providing a path to improved understanding of degradation pathways. This new setup is experimentally much simpler than the LC-LCW-LC system, since no multiple-heart-cut valves and no ²D LC system (solvent-delivery system and column) are

needed. Also, the detector monitoring the ^1D effluent can be eliminated from the setup. It is also considerably more simple and less expensive than an MPS-LCW-LC setup.

The objective of the present research is to create an automated on-line system that facilitates extensive photodegradation studies on small samples. We aim to generate information on the degradation of individual, potentially unknown components in complex matrices and to elucidate degradation pathways by tracing multiple generations of degradation products. To develop and demonstrate such a system we set out to study three samples, viz. an annatto extract (used as a food colorant), fuchsine (used as a textile dye), and vitamin B2.

7.2. Materials and Methods

7.2.1. Chemicals

Milli-Q water was obtained from a purification system (Arium 611UV, Sartorius, Goettingen, Germany; $R=18.2 \text{ M}\Omega\cdot\text{cm}$). Methanol (MeOH, ULC/MS grade) was obtained from Biosolve (Valkenswaard, The Netherlands). Riboflavin (RF, $\geq 98\%$) was purchased from Sigma Aldrich (Zwijndrecht, The Netherlands). Acetic acid ($\geq 95\%$) was purchased from Acros Organics (Geel, Belgium). All chemicals were used as purchased, except for RF which was used in a H_2O solution. Fuchsin was a gift from the Cultural Heritage Agency of The Netherlands (RCE, Amsterdam, The Netherlands). Annatto seeds were purchased from De Peperbol (Amsterdam, The Netherlands).

7.2.2. Instrumentation

7.2.2.1. Liquid Chromatography

All experiments were performed on an Agilent 1290 Infinity 2D-LC system (Agilent, Waldbronn, Germany) configured for one-dimensional operation. The system was comprised of a binary pump (G4220A), a diode-array detector (DAD, G4212A) equipped with an Agilent Max-Light Cartridge Cell (G4212-6008, $V_{\text{cell}} = 1.0 \mu\text{L}$), and an autosampler (G4226A). A 2-position 8-port valve (G4236A) was used with 40- μL loops installed. A reversed-phase liquid chromatography (RPLC) Zorbax Eclipse Plus C18 column (Agilent) was used with dimensions of $150 \times 2.1 \text{ mm ID}$, 3.5 μm particle size. An 1100 Agilent isocratic pump (G1310A) was used to transfer the sample from the loops to the LCW cell and eventually to the injection loop.

7.2.2.2. Liquid-Core-Waveguide Cell

The LCW cell (ID 800 μm , OD 1000 μm , length 120 mm, volume 60 μL , pressure limit 0.5 MPa) was placed in a light box created by DaVinci Laboratory Solutions (Rotterdam, The Netherlands), which has been developed and validated in previous research, as described

in [19,20,25] and shown in Appendix D-1. The light source for degradation was a cold-white (400-700 nm) LED lamp (MCWHF2, Thorlabs, Newton, NJ, United States), which was coupled to a light fibre cable (M113L01, Thorlabs) with a core diameter of 400 μm , a UV/Vis collimator from Avantes (COL-UV/VIS, Apeldoorn, The Netherlands) and a plano-convex lens ($f=35$ mm, Thorlabs, LA4052-ML) to couple the light from the source into the LCW cell. The LED lamp was controlled by a LED driver (LEDD1B, Thorlabs). The lightbox was also equipped with a 6-port switching valve (EUHA, Vici, Houston, TX) to transfer the sample from the light box to the ^2D separation. The 6-port switching valve was equipped with a loop of 100 μL .

7.2.3. Methods

7.2.3.1. Analytical Methods

In this work, an LC-(LCW \cup LC) n setup is developed to perform photodegradation. The binary pump, autosampler, 6-port injection valve, column, DAD, and 8-port valve described in the previous sections were connected in series. This latter valve was equipped with two 40 μL loops. An isocratic pump was used to transfer the ^1D fractions stored in the loops to the LCW cell. This latter cell was coupled to the 6-port valve, equipped with a 100 μL loop, which was connected in between the autosampler and the column. A schematic overview of the setup is shown in Fig. 7.1.

For the LC analysis of all samples, mobile-phase components A and B consisted of mixtures of acidified water and MeOH in ratios of 99/1 [v/v] for mobile phase A and 1/99 [v/v] for mobile phase B. Mobile-phase component A contained 0.05% acetic acid (by volume). The flow rate of the binary pump was set to 0.4 mL/min. The gradient program started isocratically at 100% A from 0 min to 1 min, followed by a linear gradient to 100% B in 9 min, maintained for 1 min at 100% B, and finally returned to 100% A in 0.01 min. The composition was kept at 100% A for the remainder of time before the degraded mixture was re-injected onto the column. When the degraded sample was injected again, the same gradient program was started. The isocratic pump delivered a flow rate of 0.05 mL/min of mobile phase A when in operation. When the compound of interest eluted from the column, the 8-port valve was switched, and the compound was transferred to the LCW cell. After degradation it was transferred to the injection loop, after which it was re-injected onto the column. The specific time schedules are supplied in Appendix E-1. Depending on the application, this cycle was repeated either once or twice *i.e.* LC-(LCW \cup LC) n with $n = 1$ or 2. The injection volume in all experiments was 5 μL .

7.2.3.2. Sample Preparation

A test mixture of riboflavin (RF, 100 mg/L) in H₂O was used. Fuchsin was dissolved in H₂O at a concentration of 100 mg/L.

Five annatto seeds (0.1620 grams) were extracted in 5 mL of MeOH/H₂O (75/25%) and sonicated for 20 min in an ultrasonic bath. After sonicating, the solution was passed through a PTFE filter (0.45 μm).

7.2.4. Data processing

The chromatograms were processed with Agilent OpenLAB CDS (Agilent, Santa Clara, CA, USA) software. Calculations were performed and figures were created with MATLAB R2020a (Mathworks, Woodshole, MA, USA) and Microsoft Excel.

7.3. Results & Discussion

In this research an online setup was developed to establish firm connections between sample components and their degradation products and to elucidate photodegradation mechanisms by repeated degradation of specific components. This system was built around a liquid-core-waveguide (LCW) cell, which was embedded in an LC setup with an extra 8-port valve and isocratic pump. The system is displayed in Fig. 7.1. One of the loops in the 8-port valve is coupled to the separating dimension, while the other is coupled to the degradation dimension.

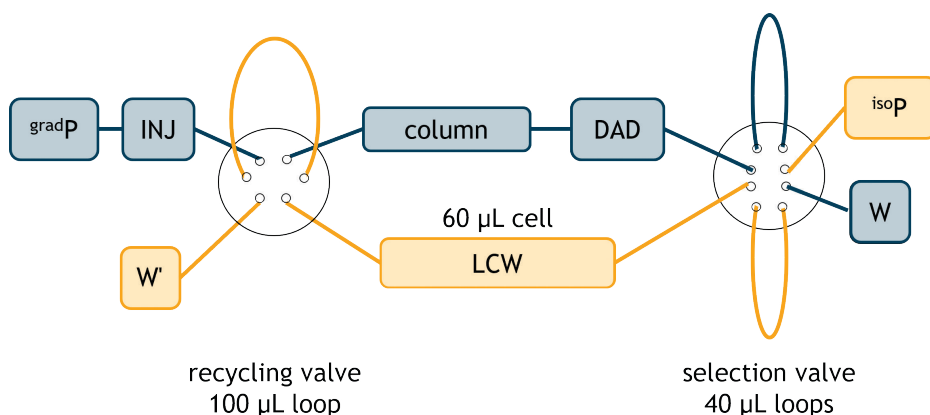


Figure 7.1. Schematic setup of the cyclic separation setup. Blue and yellow indicate the two flow paths, i.e. blue is the separation dimension and yellow is the degradation dimension. *gradP* is the gradient pump, INJ the injector, DAD the diode-array detector, *isoP* the isocratic pump, LCW the liquid-core-waveguide cell, and W and W' the waste bins. The left valve is indicated as recycling valve and the right valve as selection valve.

To test the transfer of a peak from the first separation to the next cycle, riboflavin was injected. The valve-switching times were optimized to facilitate efficient peak transfer. The time schedule of the method is provided in Appendix E-1. The fraction of the riboflavin peak transferred was determined with the light in the LCW cell off. It was found to be 81% ($\pm 2.3\%$) and 73% ($\pm 5\%$) between the first and the second separation, and between the second and third separation, respectively. A possible explanation of the difference in peak transfer and repeatability between the first and second transfer could be the slight shift in retention time in the second separation, because of the high injection volume. The fact that the sample transfer is not approaching 100% is probably due to the volume of the sample-transfer loops (40 μL), which is slightly smaller than the peak volume established using the DAD. Moreover, since these loops are placed behind the DAD in the streamline, the peak has probably experienced additional band broadening before it arrives at the loop, resulting in incomplete sample transfer. This effect is much smaller in the recycling valve, since the loop used for re-injection is much larger than the LCW cell (100 μL and 60 μL , respectively). Nevertheless, the experiments clearly showed that we can transfer the vast majority of a selected component to the LCW cell and subsequently reinject the degraded fraction in the column. In future work, the 40- μL loops may be larger to increase the sample transfer. Finally, it should be noted that in the present set up, the injection loop of 100 μL was not inserted in the flow line during the initial injection. This resulted in a peak shift of 0.25 min for compounds in the second or third separation. This can be remedied by modifying the setup such that the loop is inserted in the flow stream also during the initial injection.

7.3.1. Relating degraded fraction to initial separation

To demonstrate the versatility of the new setup we studied the degradation of fuchsin. Fuchsin is a synthetic organic colorant that was one of the most-important dyes for textile colouring in the 19th and 20th centuries [26–29]. Later it was applied in food, for example in wine and in sausages [26]. In more recent years, it has been used as biological staining agent and as a model compound for benchmarking waste-water-treatment facilities [30,31]. Fuchsin is a triarylmethane dye, with a methyl group at the meta position on one of the aromatic rings (see Appendix D-4). It is a starting material for the entire class of triarylmethane dyes. However, fuchsin is only available as a mixture of four compounds that differ in their degrees of methylation, *i.e.* not methylated (a, known as pararosaniline and as Magenta 0), singly methylated (b, known as fuchsin and as Magenta I), doubly methylated (c, known as Magenta II) and triply methylated (d, known as new fuchsin or Magenta III). The lower-case letters a-d refer to the initial chromatogram (blue line) in Fig. 7.2 (see Appendix D-4). While Magenta 0 and Magenta III are available as pure compounds, the other ones are not. Studying photodegradation of Magenta I or Magenta II is not possible in a mixture, since all four

components will likely yield comparable degradation products. This renders it impossible to link the degradation products to a specific parent molecule. Using the present setup, Magenta I was isolated from the fuchsin mixture and transferred to the light cell. It was either transferred through the light-exposure cell with the light off (purple line) or degraded for four hours (yellow line). The results of these experiments are shown in Fig. 7.2.

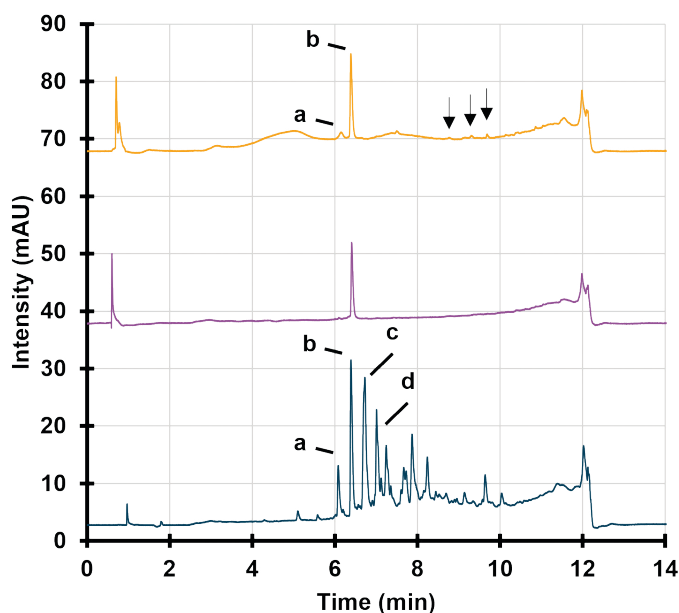


Figure 7.2. Chromatograms of fuchsin after the first separation (blue trace), after the second separation, without intermediate irradiation (purple trace) and after 4-h irradiation (yellow trace). All chromatograms were recorded at 254 nm. Note that the time axis is corresponding to the initial separation. The other two chromatograms were aligned to the initial time axis.

The figure shows the three separations overlaid. The fuchsin can be largely separated from all other peaks and reinjected in the system, without any other products in the chromatogram, as is evident from the purple trace in Fig. 7.2. In the degraded fraction (yellow trace) the original fuchsin peak is still visible, but some degradation products have formed. First of all, the demethylated product has been formed, which was already present in the first mixture (peak a). This confirms the hypothesis that one pathway in fuchsin photodegradation is the loss of methyl groups, leading to pararosaniline. Next to that, some very small peaks appear in the range from 8 min to 10 min (indicated by arrows). These small peaks are also present in the ^1D chromatogram but have not been identified in this study. A next step in our work will be to couple the setup to a mass spectrometer to try and identify these products and to propose degradation pathways.

Next, a more-complex sample was analysed, *i.e.* an extract of annatto seeds. These seeds, originating from the achiote tree, are often used to produce a lipophilic natural food dye for products such as butter, cheese, and ice cream [32,33]. Its main compound is bixin, a carotenoid, with a yellow to orange colour. In Fig. 7.3, the chromatogram is shown of an extract of the annatto seeds (MeOH/H₂O, 75/25 [v/v]) at 450 nm. Bixin is clearly identified as the most lipophilic component in the mixture. The other (colouring) compounds found in the mixture elute before this main product. Since many of these components showed similar DAD spectra, we expect that they have structures similar to bixin with some slight modifications. When degrading annatto-seed extracts, degradation products cannot be distinguished from the minor components already present in the mixture. Therefore, bixin should be first isolated from the mixture. After isolation and reinjection (but without intermediate irradiation), the chromatogram consists only of bixin, meaning it was successfully isolated (see Fig. 7.3, purple trace). The chromatogram of the degraded fraction (irradiated for 2 h) is shown as the yellow trace in Fig. 7.3. Beside the bixin peak, which has clearly decreased in area, indicating degradation, some degradation products are seen in the chromatogram, the peaks of which correspond with those of components that were present in the starting mixture (see insert in Fig. 7.3). This suggests that bixin had already degraded to some extent prior to analysis.

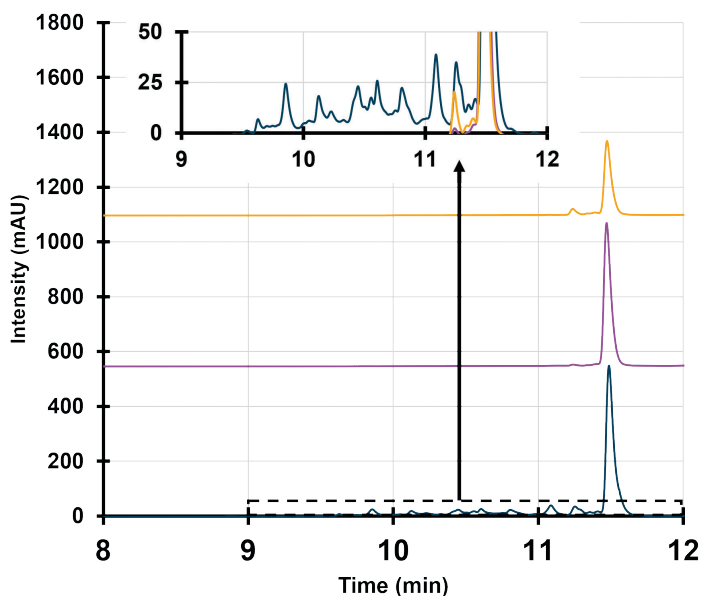


Figure 7.3. Chromatograms of the initial annatto extract (blue trace), the reinjected fraction containing bixin without irradiation (purple trace) and after irradiation during 2 h (yellow trace). All chromatograms were recorded at 450 nm. Note that the time axis is corresponding to the initial separation. The other two chromatograms were aligned. Expansions of parts of the three chromatograms are plotted in the insert.

Caution should be taken in connecting degradation products with peaks present in the starting extract before confirmation experiments have been performed, for example with mass spectrometry. Moreover, the chromatograms shown were recorded at a wavelength of 450 nm, which implies that any products that do not absorb at this wavelength could not be observed.

7.3.2. Elucidation of degradation mechanisms

The current setup allows connecting degradation products to compounds in a mixture, as shown in section 7.3.1. It also makes it possible to study the degradation (and degradation mechanisms) of compounds that are not – or not easily – available in their pure form. This is a massive advantage for compounds that are prone to degradation. One example is riboflavin, known as vitamin B2, shown in Fig. 7.4A. Riboflavin is known to be very susceptible to light, which reduces its health effects in food or in supplements. When riboflavin is degraded, a mixture results that consists of (at least) seven different degradation products, as illustrated in Fig. 7.4B. The relation between these degradation products is hard to establish, since they could not be isolated previously.

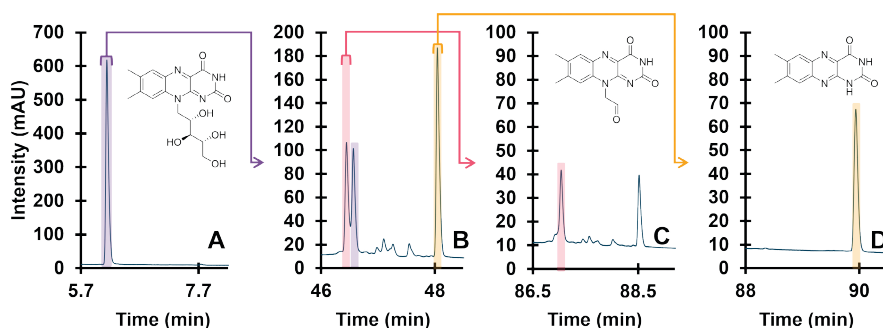


Figure 7.4. Repeated injection of riboflavin and its degradation products in the LCW light cell. Detection wavelength 254 nm. A: undegraded riboflavin, B: degraded riboflavin, C: FMF isolated from RF degradation mixture and degraded further, D: LCH isolated from RF degradation and degraded further. All degradations were performed for 30 min.

Using the present setup both formyl-methyl flavin (FMF, Fig. 7.4C) and lumichrome (LCH, Fig. 7.4D) could be effectively isolated from the degradation mixture and subsequently subjected to a second degradation cycle with a similar dose and duration (30 min) as the initial degradation of the riboflavin mixture. In case of FMF it can be seen that a small amount of riboflavin is transferred to the second degradation cycle. This is probably due to the band broadening and incomplete chromatographic resolution (see also the beginning of Section 7.3). The degradation pattern looks similar to that in Fig. 7.4B, indicating that all these peaks may represent secondary degradation products of FMF. This is supported by literature [34,35],

indicating that previously proposed degradation mechanisms can be verified using our developed system. Besides FMF, LCH was isolated and degraded yielding no new degradation products (Fig. 7.4D). This shows that LCH is much more stable under these conditions than RF. Since the absorption spectrum of LCH is also shifted to slightly lower wavelengths than that of RF, changing the irradiation source may result in more degradation of LCH.

7.4. Concluding remarks

In this paper, a novel setup was described featuring a liquid-core-waveguide light-exposure cell that allows online photodegradation. The fraction of the peak that was transferred was optimized to 81% (\pm 2.3%) and 73% (\pm 5%) between the first and the second separation, and the second and third separation, respectively. This system allows the user to readily connect degradation products to compounds present in the starting mixture. This was demonstrated with a degradation of fuchsin and of an annatto extract. In both these cases, the major degradation product was already found to be present at a significant level prior to degradation. The new setup also facilitates the elucidation of degradation mechanism, which was confirmed by performing applying it to riboflavin, a compound for which many photodegradation pathways had been proposed. The setup required fewer liquid-chromatography (LC) modules, making it less complex, cheaper, and more user-friendly than a previously proposed setup based on two-dimensional LC. The new system can operate with a basic injection device; it does not require a multi-purpose sampling system. The only additions to a standard LC instrument are the liquid-core-waveguide-cell box, an 8-port or 6-port valve, and a (low-pressure) isocratic pump.

References

- [1] Verduin J, Den Uijl MJ, Peters RJ, Van Bommel MR. Photodegradation Products and their Analysis in Food. *J Food Sci Nutr* 2020;6. <https://doi.org/10.24966/FSN-1076/100067>.
- [2] Lu LX, Xu F. Effect of light-barrier property of packaging film on the photo-oxidation and shelf life of cookies based on accelerated tests. *Packag Technol Sci* 2009;22:107–13. <https://doi.org/10.1002/PTS.838>.
- [3] He J, Evans NM, Liu H, Zhu Y, Zhou T, Shao S. UV treatment for degradation of chemical contaminants in food: A review. *Compr Rev Food Sci Food Saf* 2021;20:1857–86. <https://doi.org/10.1111/1541-4337.12698>.
- [4] Manhita A, Balcaen L, Vanhaecke F, Ferreira T, Candeias A, Dias CB. Unveiling the colour palette of Arraiolos carpets: Material study of carpets from the 17th to 19th century period by HPLC-DAD-MS and ICP-MS. *J Cult Herit* 2014;15:292–9. <https://doi.org/10.1016/J.CULHER.2013.04.005>.
- [5] Pirok BWJ, Den Uijl MJ, Moro G, Berbers SVJ, Croes CJM, Van Bommel MR, et al. Characterization of Dye Extracts from Historical Cultural-Heritage Objects Using State-of-the-Art Comprehensive Two-Dimensional Liquid Chromatography and Mass Spectrometry with Active Modulation and Optimized Shifting Gradients. *Anal Chem* 2019. <https://doi.org/10.1021/acs.analchem.8b05469>.
- [6] Tang Y, Smith GJ, Weston RJ, Kong X. Chinese handmade mulberry paper: Generation of reactive oxygen species and sensitivity to photodegradation. *J Cult Herit* 2017;28:82–9. <https://doi.org/10.1016/J.CULHER.2017.06.004>.
- [7] Kolkman A, Martijn BJ, Vughs D, Baken KA, van Wezel AP. Tracing Nitrogenous Disinfection Byproducts after Medium Pressure UV Water Treatment by Stable Isotope Labeling and High Resolution Mass Spectrometry. *Environ Sci Technol* 2015;49:4458–65. <https://doi.org/10.1021/es506063h>.
- [8] Vughs D, Baken KA, Kolkman A, Martijn AJ, de Voogt P. Application of effect-directed analysis to identify mutagenic nitrogenous disinfection by-products of advanced oxidation drinking water treatment. *Environ Sci Pollut Res* 2018;25:3951–64. <https://doi.org/10.1007/s11356-016-7252-6>.
- [9] Confortin D, Neevel H, Brustolon M, Franco L, Kettelarij AJ, Williams RM, et al. Crystal violet: Study of the photo-fading of an early synthetic dye in aqueous solution and on paper with HPLC-PDA, LC-MS and FORS. *J. Phys. Conf. Ser.*, vol. 231, Institute of Physics Publishing; 2010, p. 012011. <https://doi.org/10.1088/1742-6596/231/1/012011>.
- [10] Confortin D, Neevel H, van Bommel MR, Reissland B. Study of the degradation of an early synthetic dye (crystal violet) on cotton linters, lignin and printing paper by the action of UV-Vis and Vis light and evaluation of the effect of gum arabic on degradation products and on colour change. *Creat 2010 Conf Proc - 'Colour Coded'* 2010:81–5.
- [11] Giri RR, Ozaki H, Okada T, Takikita S, Taniguchi S, Takanami R. Water matrix effect on UV photodegradation of perfluorooctanoic acid. *Water Sci Technol* 2011;64:1980–6. <https://doi.org/10.2166/WST.2011.825>.
- [12] den Uijl MJ, Lokker A, van Dooren B, Schoenmakers PJ, Pirok BWJ, van Bommel MR. Comparing different light-degradation approaches for the degradation of crystal violet and eosin Y. *Dye Pigment* 2022;197:109882. <https://doi.org/10.1016/J.DYEPIG.2021.109882>.
- [13] Fernández-Alba AR, García-Reyes JF. Large-scale multi-residue methods for pesticides and their degradation products in food by advanced LC-MS. *TrAC Trends Anal Chem* 2008;27:973–90. <https://doi.org/10.1016/J.TRAC.2008.09.009>.
- [14] Friele LFC. A Comparative Study of Natural and Xenotest Exposure Condition: for Measuring Fading and Degradation. *J Soc Dye Colour* 2008;79:623–31. <https://doi.org/10.1111/j.1478-4408.1963.tb02522.x>.
- [15] Whitmore PM, Pan X, Bailie C. Predicting the fading of objects: Identification of fugitive colorants through direct nondestructive lightfastness measurements. *J Am Inst Conserv* 1999;38:395–409. <https://doi.org/10.1179/019713699806113420>.

- [16] Verardo V, Ferioli F, Riciputi Y, Iafelice G, Marconi E, Caboni MF. Evaluation of lipid oxidation in spaghetti pasta enriched with long chain n-3 polyunsaturated fatty acids under different storage conditions. *Food Chem* 2009;114:472–7. <https://doi.org/10.1016/J.FOODCHEM.2008.09.074>.
- [17] Groeneveld I, Schoemaker SE, Somsen GW, Ariese F, Van Bommel MR. Characterization of a liquid-core waveguide cell for studying the chemistry of light-induced degradation. *Analyst* 2021;146:3197–207. <https://doi.org/10.1039/D1AN00272D>.
- [18] Altkorn R, Koev I, Van Duyne RP, Litorja M. Low-loss liquid-core optical fiber for low-refractive-index liquids: fabrication, characterization, and application in Raman spectroscopy. *Appl Opt* 1997;36:8992. <https://doi.org/10.1364/ao.36.008992>.
- [19] Groeneveld I, Bagdonaite I, Beekwilder E, Ariese F, Somsen GW, Bommel MR van. Liquid Core Waveguide Cell with In Situ Absorbance Spectroscopy and Coupled to Liquid Chromatography for Studying Light-Induced Degradation. *Anal Chem* 2022;94:7647–54. <https://doi.org/10.1021/ACS.ANALCHEM.2C00886>.
- [20] Uijl MJ den, Wijst YJHL van der, Groeneveld I, Schoenmakers PJ, Pirok BWJ, Bommel MR van. Combining Photodegradation in a Liquid-Core-Waveguide Cell with Multiple-Heart-Cut Two-Dimensional Liquid Chromatography. *Anal Chem* 2022;94:11055–61. <https://doi.org/10.1021/ACS.ANALCHEM.2C01928>.
- [21] Wouters B, Pirok BWJ, Soulis D, Garmendia Perticarini RC, Fokker S, van den Hurk RS, et al. On-line microfluidic immobilized-enzyme reactors: A new tool for characterizing synthetic polymers. *Anal Chim Acta* 2019;1053:62–9. <https://doi.org/10.1016/J.ACA.2018.12.002>.
- [22] Pirok BWJ, Abdhussain N, Aalbers T, Wouters B, Peters RAH, Schoenmakers PJ. Nanoparticle Analysis by Online Comprehensive Two-Dimensional Liquid Chromatography combining Hydrodynamic Chromatography and Size-Exclusion Chromatography with Intermediate Sample Transformation. *Anal Chem* 2017;89:9167–74. <https://doi.org/10.1021/ACS.ANALCHEM.7B01906>.
- [23] Groeneveld G, Pirok BWJ, Schoenmakers PJ. Perspectives on the future of multi-dimensional platforms. *Faraday Discuss* 2019;218:72–100. <https://doi.org/10.1039/C8FD00233A>.
- [24] Pirok BWJ, Stoll DR, Schoenmakers PJ. Recent Developments in Two-Dimensional Liquid Chromatography: Fundamental Improvements for Practical Applications. *Anal Chem* 2019;91:240–63. <https://doi.org/10.1021/acs.analchem.8b04841>.
- [25] Groeneveld I, Schoemaker SE, Somsen GW, Ariese F, van Bommel MR. Characterization of a liquid-core waveguide cell for studying the chemistry of light-induced degradation. *Analyst* 2021. <https://doi.org/10.1039/D1AN00272D>.
- [26] Cooksey CJ, Dronsfield AT. Quirks of dye nomenclature. 4. Fuchsin: Four shades of magenta. *Biotech Histochem* 2015;90:288–93. <https://doi.org/10.3109/10520295.2014.989543>.
- [27] Cooksey C, Dronsfield A. Fuchsin or magenta: the second most famous aniline dye. A short memoir on the 150th anniversary of the first commercial production of this well known dye. <http://DxDoiOrg/101080/10520290903081401> 2009;84:179–83. <https://doi.org/10.1080/10520290903081401>.
- [28] Liu J, Zhou Y, Zhao F, Peng Z, Wang S. Identification of early synthetic dyes in historical Chinese textiles of the late nineteenth century by high-performance liquid chromatography coupled with diode array detection and mass spectrometry. *Color Technol* 2016;132:177–85. <https://doi.org/10.1111/COTE.12205>.
- [29] Mantzouris D, Karapanagiotis I, Valianou L, Panayiotou C. HPLC-DAD-MS analysis of dyes identified in textiles from Mount Athos. *Anal Bioanal Chem* 2011;399:3065–79. <https://doi.org/10.1007/S00216-011-4665-4/FIGURES/6>.
- [30] Ba Mohammed B, Hsini A, Abdellaoui Y, Abou Oualid H, Laabd M, El Ouardi M, et al. Fe-ZSM-5 zeolite for efficient removal of basic Fuchsin dye from aqueous solutions: Synthesis, characterization and adsorption process optimization using BBD-RSM modeling. *J Environ Chem Eng* 2020;8:104419. <https://doi.org/10.1016/J.JECE.2020.104419>.

- [31] Churukian CJ, Schenk EA. Staining With Basic Fuchsin. *Lab Med* 1983;14:431–4. <https://doi.org/10.1093/LABMED/14.7.431>.
- [32] Tennant DR, O'Callaghan M. Survey of usage and estimated intakes of annatto extracts. *Food Res Int* 2005;38:911–7. <https://doi.org/10.1016/J.FOODRES.2005.01.013>.
- [33] Kapoor L, Ramamoorthy S. Strategies to meet the global demand for natural food colorant bixin: A multidisciplinary approach. *J Biotechnol* 2021;338:40–51. <https://doi.org/10.1016/J.JBIOTEC.2021.07.007>.
- [34] Insińska-Rak M, Prukała D, Golczak A, Fornal E, Sikorski M. Riboflavin degradation products; combined photochemical and mass spectrometry approach. *J Photochem Photobiol A Chem* 2020;403:112837. <https://doi.org/10.1016/J.JPHOTOCHEM.2020.112837>.
- [35] Ahmad I, Fasihullah Q, Vaid FHM. Effect of light intensity and wavelengths on photodegradation reactions of riboflavin in aqueous solution. *J Photochem Photobiol B Biol* 2006;82:21–7. <https://doi.org/10.1016/J.JPHOTOBIO.2005.08.004>.

PART IV

Evaluation

CHAPTER 8

Conclusions and Future Perspectives

All of the research presented in this thesis was performed within the framework of the TooCOLD project (Toolbox for studying the Chemistry Of Light-induced Degradation). The main goal of TooCOLD was to develop an “innovative, high-resolution, and fully orthogonal system to study the degradation of a wide range of components, either present as pure components or in mixtures, under the influence of light”. Groeneveld *et al.* developed a light-exposure cell, referred to as light cell, using a liquid-core-waveguide (LCW) technique [1].

This new LCW cell was compared to other photodegradation techniques in the field of cultural heritage. Our work showed that the degradation in the LCW cell progressed much faster than in the more-established techniques and that the degraded sample could be analysed online, *i.e.* without a need for extractions. We found that degradation mechanisms could be different when dyes were degraded on textile or in solution and that the irradiation spectrum influenced the degradation kinetics and the products formed. To demonstrate the power of reaction modulation, the LCW cell was installed in a two-dimensional-liquid-chromatography (2DLC) setup. By doing so, compounds in mixtures could be separated, degraded, and analysed, leading to better understanding of degradation pathways of specific compounds isolated from mixtures. This work was later developed into a conceptually more-advanced, but experimentally more-simple setup that facilitated easier comparison of degradation products and allowed multi-step degradation to elucidate degradation mechanisms.

Another part of this research has been the use of retention modelling in method optimization. After an extensive literature study into the different ways of retention modelling, the concept was applied to both method optimization for one-dimensional LC (1DLC), as well as stationary-phase-assisted modulation (SPAM). While this work is of interest for the entire field of LC and 2DLC, it is of specific interest for the TooCOLD project, since the relatively large volume of the LCW can lead to loss of resolution, *i.e.* through band broadening, or even breakthrough when the entire volume of the cell is injected in LC. In the research performed, we identified several fields where retention modelling plays a role, *viz.* *i*) method transfer, *ii*) method optimization, *iii*) stationary-phase characterization, *iv*) understanding retention mechanisms, and *v*) lipophilicity determination. We established specific rules for performing the scanning-gradient experiments needed for any of the above purposes. Lastly, we developed a tool to predict retention on SPAM columns to aid in the application of the techniques in the field of 2DLC.

Unfortunately, time is limited, and with time the number of ideas that can be explored. Initially within TooCOLD, it was planned to degrade several compounds in parallel by creating a so-called multicell. This could facilitate illumination of, ideally, the complete chromatogram, *i.e.*

comprehensive-photodegradation 2DLC, or could reduce the time needed for creating time series. Up to this point the improvements in retention modelling were not combined with the developments in photodegradation research, which would be an obvious next step. Lastly, the development of the online light cell has opened a path for many different applications to benefit from the research performed within TooCOLD. This chapter will describe some preliminary experiments and future perspectives and this will culminate in some general recommendations concerning the field of multidimensional LC (mDLC).

8.1. Towards comprehensive photodegradation in two-dimensional liquid chromatography

The ultimate goal of the implementation of reaction modulation in mDLC is to isolate each individual component from a complex mixture from the effluent of the ¹D, subject this compound to the reaction, and then separate the degradation products using a second-dimension (²D) LC separation. This can be called comprehensive reaction modulation. In the development of the liquid-core-waveguide cell (LCW), much attention was paid to other important parameters, such as gas permeability, real-time absorption spectroscopy during the degradation, and the effect of different solvents that can be used. Although this resulted in a flexible system in which many parameters of photodegradation can be studied, comprehensive photodegradation in 2DLC is complicated, especially by the limited pressure resistance of the LCW cell (maximum pressure 0.5 MPa) and the relatively long residence times. In a typical 2DLC system pressures up to 130 MPa are encountered in the modulator loops, due to the high flow rates required for fast ²D separations. When two light cells replace the loops or the trap columns at the modulation stage in LC×LC, the degradation time is limited to the modulation time, which is typically shorter than 2 min. In the LCW cell degradation times used have typically been 10 and 30 min for light-sensitive compounds, while much longer times were needed for more-light-stable compounds. One solution for this problem may be to create a number of exposure cells that are operated in parallel, allowing the analytes to be degraded for longer times (t_{deg}), *i.e.* $t_{deg} = n_{parch} \times t_{mod}$, where n_{parch} is the number of parallel channels and t_{mod} is the modulation time. A way to achieve this is to replace the loops on a multiple-heart-cut (mHC) deck with LCW cells. This would bring a similar gain as above in case of operation in comprehensive mode, *i.e.* $t_{deg} = n_{LCW} \times t_{mod}$, where n_{LCW} is the number of LCW cells installed on the mHC deck. Such a system would also allow longer degradation times for selected fractions, but this would jeopardize comprehensive operation and increase the total duration of the experiment. Although in principle the LCW cell could function as a light modulator in a mHC-2DLC setup, a redesign of the cell may be needed to increase its pressure limit.

These considerations ignited a new direction of research. Requirements were formulated for creating and optimizing a new cell. A comprehensive light cell would need to have multiple parallel channels or at least the option to easily extend this number. Another requirement was a possibility to easily change the volume of the cell.

8.1.1. Designing a 3D-printed multichannel light cell

In this process we resorted to 3D printing to easily construct and test different cell designs. The 3D-printing technique used was stereolithography, a process in which a liquid resin (in our case Durable Resin from Formlabs, Somerville, MA, USA) is photopolymerized by a laser, crosslinking the polymer in a point-by-point manner. This process is repeated in a number of layers, until the desired solid object is formed. After the process, the object needs to be rinsed with isopropanol (IPA) to remove all the non-reacted resin, followed by a final photopolymerization (UV-curing, 1 hour, 254 nm) step to harden the object. In our design the bottom half of the cell was 3D-printed and this was later covered by a glass sheet, which was glued to the cell. In the first design, four separate cells were created with cylindrical inlets and outlets. Ridges were implemented in the cells, shown in Fig. 8.1, to facilitate mixing of the top and bottom layer, so as to prevent inhomogeneous illumination. To connect a cell in a flow path, polyether ether ketone (PEEK) tubing was glued to its inlet and outlet. The outer diameter of the tubing was measured and this was taken into account in the design in- and outlets, so as to make the connections leak tight. However, the variation in outer diameter of this type of tubing was found to be extensive, which led in some cases to adhesive migrating from the sides of the tubing into the flow path, and eventually to clogging of the cells. The adhesive used (Norland Optical Adhesive 63, Norland Products, Jamesburg, USA) was photo-initiated and it may have been susceptible to the light applied in degradation studies. This effect can be reduced by UV-curing after the application of adhesive. To circumvent the glue from entering the flow path, the cylindrical entrance and exit were combined with a squared section, indicated by the 1 in Fig. 8.1B.

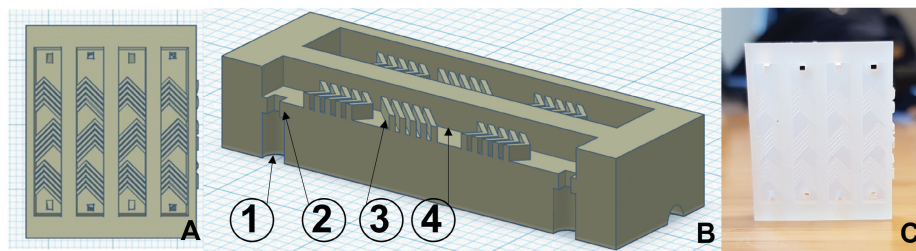


Figure 8.1. A) Design of the first multicell for 3D printing; B) Cross section of the design with 1) tubing inlet, 2) constriction for the tubing, 3) ridges, 4) channel; C) Printed version of the multicell.

The complete design is illustrated in Figs. 8.1A-C. After closing these light cells by gluing on a glass cover, it was possible to fill and empty them, providing us with a cell ready for the photodegradation study described below.

The cell was filled with a riboflavin solution and placed in a light box (Spectrolinker XL-1500 UV crosslinker; Spectronics, Westbury, NY, USA; most-intense wavelength 254 nm) to perform photodegradation. This light box was similar to the one used in Chapter 5. The cell was exposed with 0, 15 (30 min to 1 h, depending on the condition of the light source), and 30 J·cm⁻¹ (1 to 2 h) doses of light. The chromatograms of the degraded samples and the undegraded sample are shown in Fig. 8.2. It can be seen this “perpendicular” way of illumination can yield high amounts of degradation products.

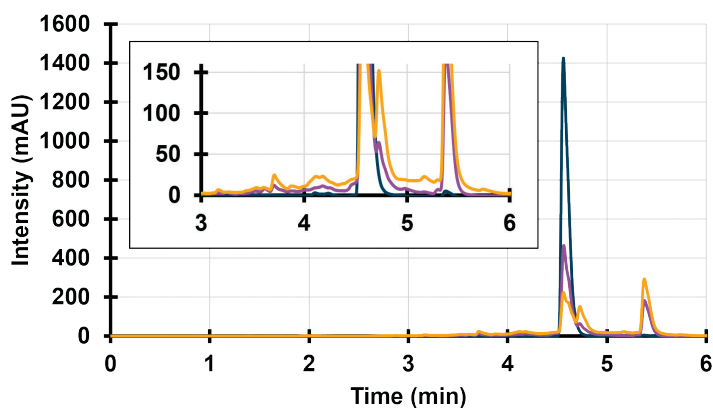


Figure 8.2. Degradation of riboflavin in the 3D-printed cell with 0 J·cm⁻¹ (blue), 15 J·cm⁻¹ (purple) and 30 J·cm⁻¹ (yellow) doses of light. The insert shows the low-abundant compounds.

While the cell could be used to perform light-induced degradation studies, we observed that during the experiment the glass sheet and the 3D-printed cell started to detach. The top of the cell slowly started to warp, and the glass sheet and cell started to disconnect. This was probably due to incomplete photopolymerization of the polymer during the UV-treatment step in the fabrication process and to the fact that the adhesive also functions after photopolymerization. If polymerization and cross-linking continue during the degradation experiment this will cause contraction of the material. Steps were taken to prevent this from happening, such as very extensive polymerization of the cell and then “face-milling” the top, but this did not result in a good product, since the polymer was still affected by UV radiation. Moreover, the material started to change colour, as shown in Fig. 8.3A. In Fig. 8.3B the previous version is displayed for comparison. This effect may be less serious if different irradiation spectra are used, but this would limit our flexibility in selecting light sources.

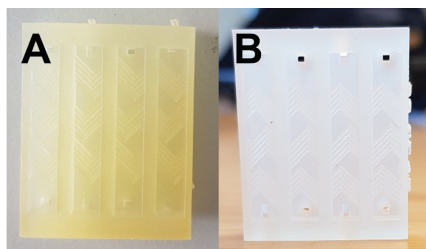


Figure 8.3. Photodegradation cell after 24 h (A) and 1 h (B) of UV curing.

8.1.2. Multichannel light cell made of PEEK

To circumvent the use of materials that photopolymerize, a photostable material was selected. Polyether ether ketone (PEEK) is not susceptible to light and is inert to solvents typically used in liquid chromatography. The fabrication process for this cell differed from that of the 3D-printing process, because PEEK cannot be produced by photolithography and because alternative 3D-printing methods, such as fused-deposition modelling cannot produce pieces with sufficient strength and spatial resolution [2]. Micro-milling was used to create the different channels and connections in PEEK. The adhesive used for attaching the cell to the glass cover had also been identified as a potential risk to the sealing of the cell, since the adhesive was also affected by the irradiation. Sealing of the cell is key to prevent air from leaking in and to obtain sufficient resistance to pressure. The glass sheet was fastened to the PEEK cell with bolts and nuts to close the channels. To prevent the glass cover from breaking and to avoid leakage from the cells, a silicone spacer (“gasket”) was implemented between the cell and the cover. In addition, a glass sheet of 8-mm thickness was chosen instead of one of 3 mm to prevent the sheet from breaking. Another improvement implemented in this cell was the ability to attach tubing using nuts instead of an adhesive. This cell and the respective parts are shown in Fig. 8.4.

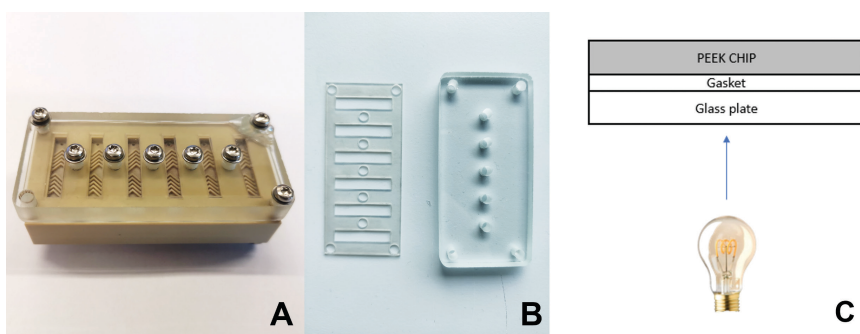


Figure 8.4. A) First PEEK multicell, B) Picture of gasket and glass plate, C) schematic overview of the operation of the multicell.

This cell performed much better than the 3D-printed cell. The material was found to be stable during the degradation experiments performed and, at low pressure, the spacer yielded no leakage. To determine the operating limit of this design a pressure test was performed by connecting the multichannel cell to a pump. Different flow rates were used and tubes with different inner diameters were connected to the outlet of the cells, resulting in different pressures in the multichannel cell. The PEEK multicell proved to be resistant to leakage at pressures up to 0.6 MPa. It proved possible to operate the cell with relatively high flows if the exit tubing has a relatively large internal diameter (e.g. 0.762 mm). In the event of a leak, we observed liquid flowing from one cell towards the other cells. To avoid this, it is recommended to tighten the nuts in the centre of the multichannel cell. Moreover, it was found that to avoid air bubbles in the cell, it could be filled best with liquid flowing upwards.

To test whether a sample of riboflavin could be degraded in the cell, it was illuminated in the light box previously described in Chapter 5. After 5 h of degradation, the cell was found to be filled with bubbles, while visual inspection did show fading of riboflavin and thus photodegradation. The bubbles were likely due to the cell being heated in the Spectrolinker without it being completely closed. In addition, the same cell was illuminated by a 3D photopolymerization printer that contained a 365 nm lamp (Asiga Pico 2 HD 3D-printer, Erfurt, Germany). The light source was thought to be more stable and consistent in its emission spectrum. Some air bubbles were still formed, but to a lesser extent than with the low-wavelength UV lamp. This lamp, however, did not provide homogeneous illumination across all the channels, which is why it was not used in further research.

O-rings were explored instead of the silicone spacer as an alternative method to seal the PEEK multicell. This would allow the nuts to be fastened more strongly, which would make the cells more resistant to pressure when filling and emptying. The cells in the first design were relatively close to each other. With the new way of closing the cell, *i.e.* with bolts and nuts, the illumination along the channel might be compromised, since the nuts and bolts partly blocked the irradiation. For that reason, the channels were placed at a greater distance from each other and the channel volume was reduced to 100 μL . The resulting cell is shown in Fig. 8.5.

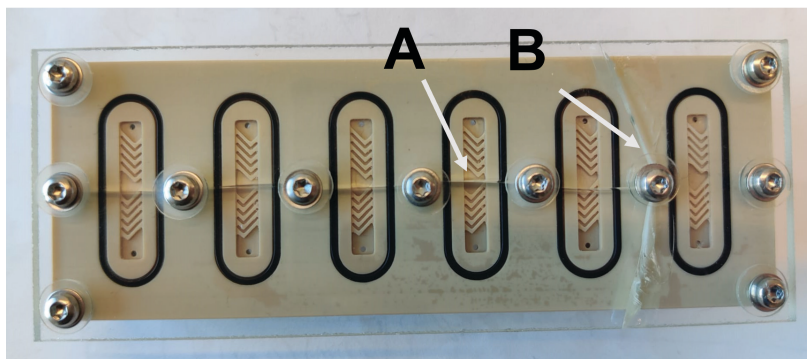


Figure 8.5. Second PEEK-cell design with O-rings. A indicates the breaking of the glass due to point pressure of the nuts and B indicates the breaking of glass because of pressure inside the cell.

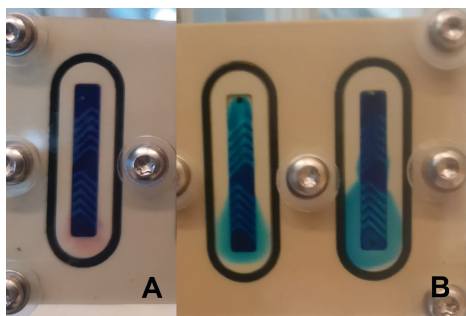


Figure 8.6. Pressure effect on the cells demonstrated with methylene-blue solution. A) low-pressure filling. B) high-pressure filling.

When these cells were tightened with the nuts, the point load on the glass proved too high and, as a result, the glass sheet broke in the horizontal direction, as indicated by A in Fig. 8.5. When the cell was closed carefully, the multicell breakage could be circumvented and the cells could be filled and emptied in a correct way at low pressure (see Fig. 8.6A). However, when the cell was filled using a higher pressure, we noticed that it started leaking and that the solvent reached the O-ring, as shown in Fig. 8.6B. When the pressure was too high, the glass sheet broke in a vertical direction, as indicated by B in Fig. 8.5. The main disadvantages of this design were that when relatively high pressures were required *i*) it was hard to clean the cell, especially when the sample had migrated to tight places and *ii*) the photodegradation became inhomogeneous across the cell when part of the sample moved out of the channel, *iii*) air bubbles formed got stuck between the ridges in the cell, *iv*) the ridges gave rise to increased carryover. Since these ridges were designed to instigate lateral mixing during filling and because the degradation was eventually performed during standstill, the ridges were deemed unnecessary and removed at a later stage.

8.1.3. Perpendicular-illumination (PI) light cell

At this stage, it was decided that the way of securing the glass sheet to the cell described in second 8.1.2 would not result in the desired outcome. In addition, since the LCW cell offers the possibility to monitor the photoreaction in the cell through *in-situ* absorption measurements, ways of monitoring the degradation in the PI cell were investigated. The cell as such could facilitate *in-situ* surface enhanced Raman spectroscopy (SERS) alongside the photodegradation. SERS can be performed using either a probe or a Raman microscope, which irradiates the sample with a laser and measures the light scattered by the sample. The focal distance between the sample and the microscope used is quite restricted (between 5 and 7 mm) and this Raman-microscope objective has a diameter of about 32 mm. If one channel were to be illuminated, the bolts would prevent the objective of the microscope to get sufficiently close to the cell. For this reason, a completely new design was made. To make space for the microscope the cell was closed using a metal clamping ring to press the glass sheet to the PEEK body. Next to that, it was decided to reduce the number of cells from six to one, since the breaking of the glass sheet around one cell would result in discarding the complete multicell. This new cell is named the perpendicular-illumination cell (PI cell) and its design is shown in Fig. 8.7.

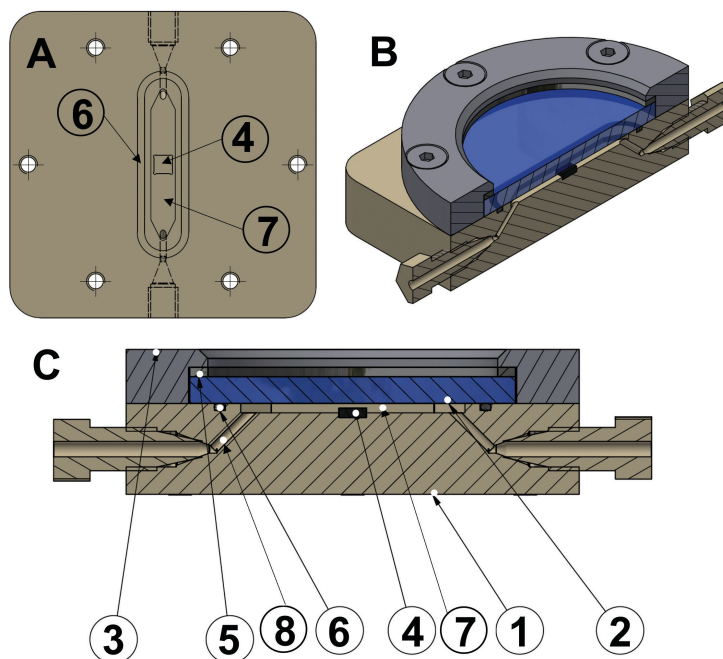


Figure 8.7. Design of a single cell with in-situ monitoring. A) top view of PEEK piece; B) complete cell cross section; C) side view with 1) PEEK piece, 2) glass sheet (blue), 3) stainless-steel clamping ring, 4) SERS-substrate notch, 5) nitrile-butadiene-rubber (NBR) ring, 6) O-ring, 7) channel, 8) flow path to the cell.

In Fig. 8.7, different views of the cell are shown. First, a channel with a volume of 100 μL was drilled without ridges. The angles of entrances were set at 53.13 degrees, following the theory of field-flow fractionation (FFF) [3]. Next, a small rectangle was cut out in the middle of the cell, to accommodate a possible SERS substrate. To close the cell, an O-ring was placed much closer to the channel than in the previous design. A circular glass window, with a thickness of either 3 or 4 mm, was placed on top of the O-ring. Between the glass sheet and the stainless-steel clamping ring, a rubber ring was placed to compensate for variations in the thickness of the glass and to spread the pressure evenly over the channel. The arrangement was tightened by six screws that were screwed into the PEEK piece, rather than with bolts and nuts. The screws connected the stainless-steel ring to the PEEK without touching the glass. This meant that there was no need for perforating the glass, making it much less prone to breaking. As can be seen in Figs. 8.7B and 8.7C, the flow path is connected with two nuts and a channel leads the flow to the cell at a 45-degree angle (see '8' in Fig. 8.7C). To test whether this cell could be used for photodegradation, it was connected between an autosampler and an 8-port valve configured as injection valve as shown in Fig. 8.8. This latter valve was connected to a one-dimensional LC system with a DAD. To illuminate the sample, a Amaran P60x bi-color lamp was used (Aputure, Los Angeles, CA, USA). Such a lamp is normally used for illumination at photo or film sets and provides different lamp temperatures. The spectrum ranges from about 400 nm to 800 nm and varies with the light temperature, as shown in Fig. 8.9. It consists of an array of LED lamps.

As shown in the figure, a sample is injected using an autosampler (INJ) and transferred to the light cell by the first pump (P). After illumination, during which the flow is set to zero, 'P is used to transfer the sample to the injection loop. After injection, the PI cell can be cleaned using 'P. When 'P is a binary pump, multiple solvents can be applied to rinse the light cell. This provides ample opportunities to thoroughly clean the cell prior to a next injection. To test the repeatability of the system, RF was degraded for 2 min in the light cell at a light temperature for the lamp of 5500 K. As can be seen in the left-hand part of Fig. 8.10, the degradation of RF seems to be accelerated in successive repeats, even though the illumination time was the same. An explanation could be that the cell heats up during degradation and that part of the degradation is thermally induced instead of light induced. To alleviate this issue, an active air flow was introduced to cool the light cell during degradation and a longer waiting period was obeyed prior to the first measurement. These conditions led to the results shown in the right-hand part in Fig. 8.10, which were much-more repeatable than those without air flow, with relative standard deviations between 2.5 and 5.5%. The degradation progressed further during the first degradation than in the experiments without air flow, suggesting that that the cell needs to heat up and reach a steady-state temperature before starting degradation experiments.

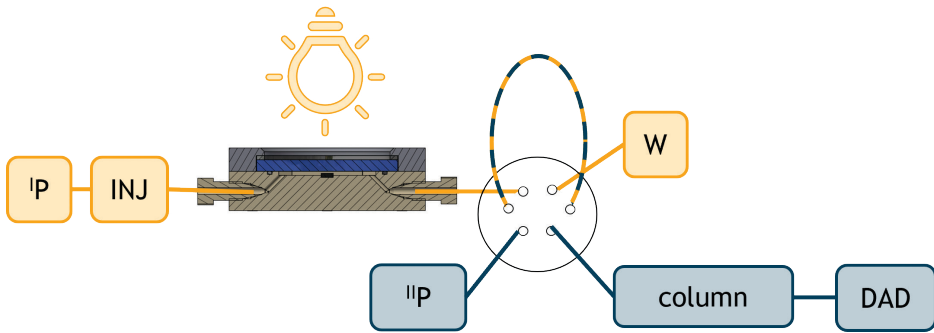


Figure 8.8. Schematic overview of the online implementation of the light cell. IP is the pump used to transfer the sample to and from the light cell, INJ is the autosampler, IP is the gradient pump, column is the analytical column and DAD is the diode-array detector. The sample-introduction flow path is depicted in yellow; the sample flow path is depicted in blue.

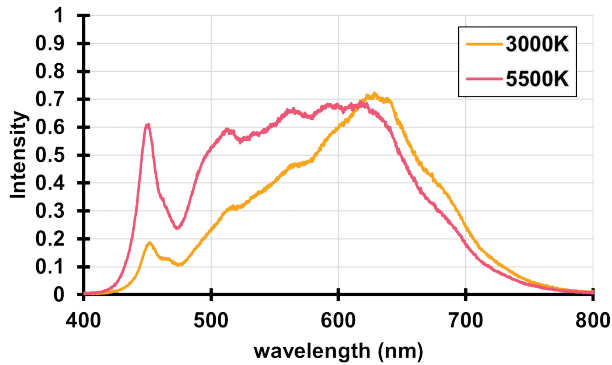


Figure 8.9. Spectrum of the Amaran P60x bi-color lamp at 3000 K (orange) and 5500 K (pink).

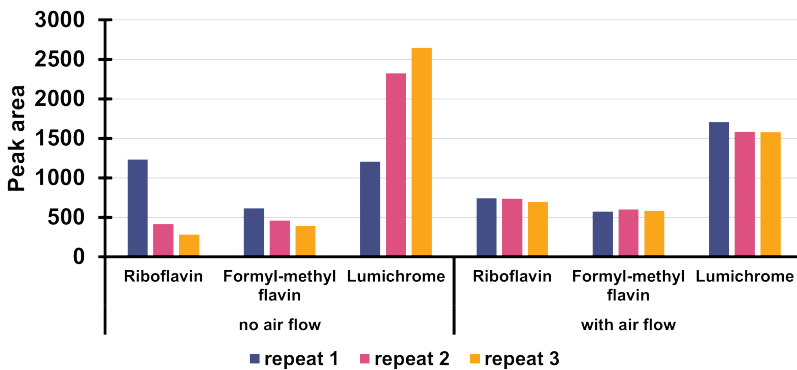


Figure 8.10. Repeats of a 2-min degradation of riboflavin with A) no active air flow along the light cell and B) with an active air flow. Peak areas at 254 nm shown for riboflavin and two degradation products, formyl-methyl flavin and lumichrome.

The active air flow was applied during subsequent experiments. A time series was recorded for RF, with degradation times ranging from 0 to 5 min. The resulting chromatograms are shown in Fig. 8.11.

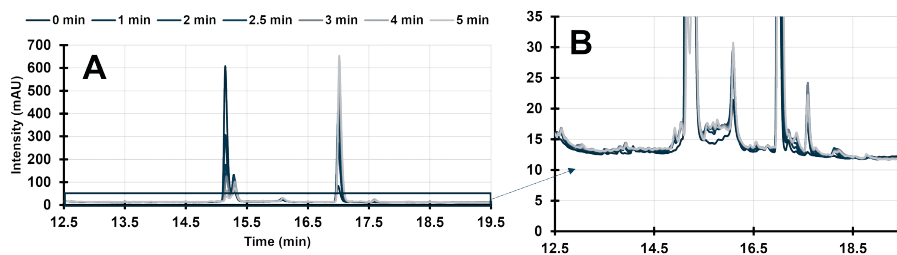


Figure 8.11. A) Degradation profile of riboflavin from 0 min stand still in PI cell (dark blue) to 5 min stop-flow in the PI cell (light blue) at 254 nm. B) close-up of part of the chromatograms.

The results in Fig. 8.11 show that an extensive degradation of riboflavin can be achieved within 5 min. Besides the degradation products that were already identified in Chapters 6 and 7, many more components present at low concentrations can be seen when zooming in on the chromatogram (Fig. 8.11B). This confirms the high speed of degradation in this setup. Since there was no possibility in this automated experiment to shield of the light in the light cell, it was not feasible to perform the same experiment without exposure of the sample to the irradiation source. To achieve a true-zero measurement the lamp should be manually shut off and the 0-min experiment should be repeated. However, we performed an experiment in which the flow was not set to zero, so the sample moved through the cell during about 30 s while the lamp was on. This extra illumination occurred in all experiments, but it meant that the first point in the time series did not depict zero illumination. This explains the presence of lumichrome in the first experiment. In future work this should be corrected. However, it is interesting to note that even at very short exposure times degradation occurred. Another factor that may have contributed to the fast degradation may be the temperature in the cell in this specific setup. However, there is a high probability that the nature of the products formed in the two processes are the same.

For the PI cell to be implemented in a two-dimensional LC system, its pressure resistance should be tested. Depending on how exactly the cell is incorporated, the pressure to which it is exposed will differ. Four situations are depicted in Figs. 8.12A-D. For example, when the cell is placed in series after the first-dimension separation and loops are implemented in the 8-port valve, the pressure experienced by the cell will be lowest (about 0.1 to 0.4 MPa, Fig. 8.12A). If these loops were to be replaced with traps, the pressure would increase (to about 1 MPa to 5 MPa, Fig. 8.12B), especially if a dilution flow is required (DFP in Fig. 8.12B). The

highest pressure would be encountered if the light cell would be implemented in the 8-port valve, since the 2D gradient (or at least the early part of the solvent program) would pass through the multicell and the pressure drop across the 2D column would be experienced by the cell (up to 130 MPa, Fig. 8.12C). This latter is most akin to an active-modulation interface for LC \times LC, there are two downsides to this approach. To reduce the pressure exerted on the light cells, an extra 8-port valve equipped with loops may be implemented, as shown in Fig. 8.12D, but this would complicate the system. Another disadvantage of this approach is that the illumination time in the light cell will not be equal for all molecules. This is because the cell is filled much-more slowly than it is emptied. The molecules that enter the cell when the fraction starts to be collected will be illuminated immediately since the lamp is on and exposed longer than the molecules entering the light cell towards the end of the modulation time, *i.e.* at the back of the fraction. This could be circumvented by emptying the light cell at the same pace at which it is filled. However, because of the significant axial dispersion in the cell caused by the parabolic profile of the laminar (Poiseuille) flow, the exposure-time differences cannot be eliminated completely. A final disadvantage of the setups shown in Figs. 8.12C and 8.12D is that two – ideally identical – light cells are needed. The simple setups shown in Figs. 8.12A and 8.12B are expected to yield the best results. If the pressure resistance of the light cell is adequate, the setup of Fig. 8.12B may be preferred.

To test the pressure resistance of the PI cell, a trap column was installed directly after it and the flow was increased up to 100 $\mu\text{L}/\text{min}$. Such a flow may, for example, be encountered with a 1D flow of 40 $\mu\text{L}/\text{min}$ and a dilution factor of 2.5. The pressure was tested with 100% H_2O and with a 50/50 $\text{H}_2\text{O}/\text{methanol}$ (MeOH) mixture, the viscosity of which is known to be almost double that of pure water. The pressure with 100% water was found to be about 0.96 MPa, while the pressure increased to 1.25 MPa at the 50/50 composition. Under these conditions no leakage was observed, confirming that the PI cell could be used in the configuration of Fig. 8.12B.

Safety factors were calculated for the PI cell at an applied pressure of 3 MPa. The results are shown in Fig. 8.13. The safety factor can be calculated by dividing the ultimate load on a material by the applied load. The ultimate load can be calculated from the material properties. In Fig. 8.13 the safety factor of the glass is seen to be lower (between 2 and 3) above the channel (orange spot in the middle) than it is in areas next to the channel. The lowest safety factors are found in the ring around the cell, but because of the NBR ring between the glass sheet and the clamping ring, the chances of the sheet breaking at these points were thought to be small. For these designs a safety factor of 3 is usually taken as the minimum, which implies that the maximum operating pressure in this cell is lower than 3 MPa. To stay on the safe side, the PI cell was operated below pressures of 2 MPa.

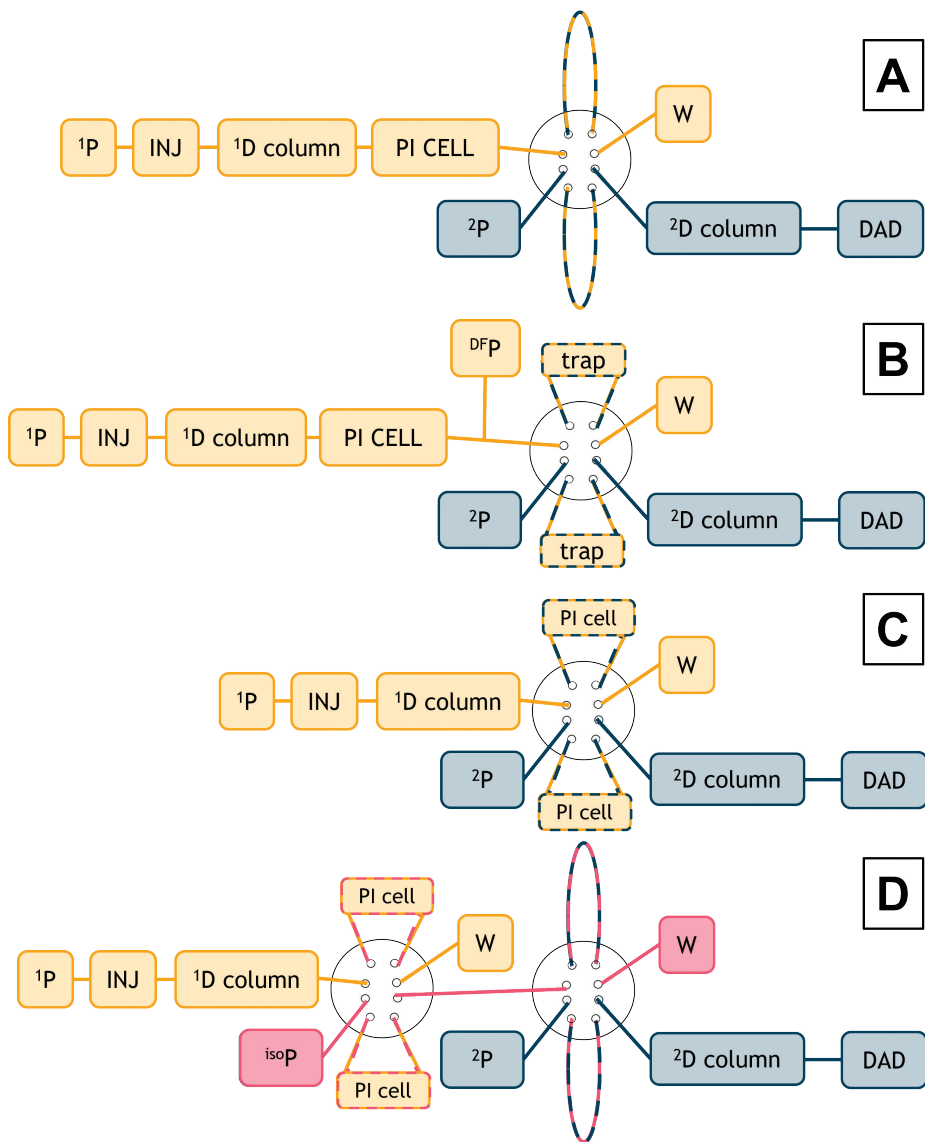


Figure 8.12. Four possible configurations with the PI cell incorporated in two-dimensional LC. 1P is the 1D pump, INJ the autosampler, 2P the 2D pump, isoP the isocratic pump, W is waste, DAD is diode-array detector. The 1D flow path is indicated in yellow and the 2D flow path in blue in 12A-D, whereas the transfer-flow path in 12D is indicated in pink.

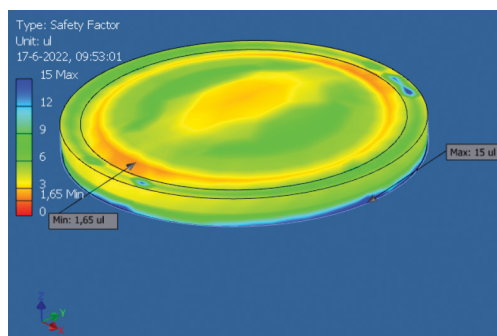


Figure 8.13. Safety factors (ratio the maximal load not leading breakage and the maximal load that is expected to be applied) calculated for the PI cell at an internal pressure of 3 MPa. The scale is indicated on the left.

8.1.4. Comprehensive photodegradation in two-dimensional liquid chromatography

To demonstrate whether the PI cell can be used for light-induced-reaction modulation in comprehensive 2DLC, both setups 12A and 12B were tested. A sample was created by combining a solution of RF, which was degraded in a vial for 1 h at a relative lamp intensity of 100%, and an undegraded solution of RF in a 50/50 ratio. The reason why this sample was chosen was because we wanted to elucidate the degradation mechanism by degrading both the main compound and the degradation products and connecting degradation products to their precursor molecules.

In both setups 1F was $40 \mu\text{L}\cdot\text{min}^{-1}$, which corresponded to a degradation time of 2.5 min. The relative lamp intensity was 50% at a light temperature of 5500 K. In the comprehensive setup with loops ($40 \mu\text{L}$), a 54 s modulation time was chosen with a 2F of $950 \text{ L}\cdot\text{min}^{-1}$. In setup 12B, the modulation time was set to 75 s with a 2F of $800 \text{ L}\cdot\text{min}^{-1}$. The traps used were Zorbax RRHD Eclipse plus C18 guard columns, with dimensions $5 \times 2.1 \text{ mm}$, particle size $1.8 \mu\text{m}$ (Agilent) and the 1D effluent was diluted 1:1 with a 99/1 [v/v] solution of H_2O and MeOH. Both columns were C18 columns (1D , Zorbax Eclipse Plus, $150 \times 2.1 \text{ mm}$ ($3.5 \mu\text{m}$ particle size), Agilent; 1D , Zorbax RRHD, $50 \times 2.1 \text{ mm}$ ($1.8 \mu\text{m}$ particle size), Agilent) and the same mobile phases were used for both dimensions. Mobile-phase components A and B consisted of mixtures of acidified water and MeOH in ratios of 99/1 [v/v] for mobile phase A and 1/99 [v/v] for mobile phase B. Mobile-phase component A contained 0.05% acetic acid (by volume). The full spectrum was recorded in both setups and yielded the 2D plots shown in Fig. 8.14. In Figs. 8.14A and 8.14B the results are shown obtained with the setup with loops, while the results obtained with the traps installed are displayed in Figs. 8.14C-8.14H. Fig. 8.14A-D show the results of degradation at 100% lamp intensity, and Fig. 8.14E-F at 75% lamp intensity, Fig. 8.14G is the dark control, and Fig. 8.14H is the result at 50% lamp intensity. The first noticeable difference is that the trap setup shows many more degradation products than the loop setup. Also, the total

area of all peaks in the chromatogram in the setup with loops (8.14A-B) is smaller than that in the setup with traps (8.14C-H), while the same amount was injected onto the ^1D column. A possible explanation may be that sample was lost by inefficient filling of the loops. In the current experiment the loops were 90% filled, which was previously reported to be too high [4]. In the setup with loops, breakthrough of the RF peak can be observed in the ^2D separation, indicated by the arrow in Fig. 8.14A (BT), which can be explained by the high organic-modifier concentration at the time of elution from the ^1D separation and insufficient dilution prior to injection in the ^2D separation. The peak width in the ^2D separation is smaller in the setup with traps, which indicates that a reduction of the ^2D injection volume is achieved, as intended.

In all plots in Fig. 8.14, the undegraded compounds can be found along the diagonal of the plot. The degradation products formed are found at off-diagonal locations in the vertical direction. Compounds that appear multiple times are both present in the starting mixture and newly formed degradation products. The dashed lines in Figs. 8.14B and 8.14D-H indicate the diagonal. Especially the degradation pathway of the compounds eluting between RF (8.14B, 48 min; 8.14D-H, 50 min) and LCH (72 min) can now be elucidated. A clear decrease in the extent of degradation of the RF can be observed at decreasing lamp intensities, which means that we are able to deliver variable doses to the sample. In Figs. 8.14D-F and 8.14H, six peaks are indicated by letters *a-f*. Peaks *a* and *c* are still present on the diagonal of the chromatogram, which implies that these products formed in the prior degradation have not yet been fully degraded. However, at both horizontal locations of these peaks a small LCH peak can be observed at the appropriate vertical position, suggesting that LCH is the photodegradation product of these compounds. Product *b* deviates from the diagonal and has a similar ^2D retention time as product *c*. This could mean that the original compound entering the light cell was fully degraded, forming both compound *c* and LCH. However, in the dark control (Fig. 8.14G), the same behaviour is observed to a lesser extent. Product *d* is only present as a degradation product of RF and not in the ^1D chromatogram. This may possibly be due to the limited sensitivity of the ^1D method, since the design of the light cell was not yet optimized from a chromatographic perspective. In future research, this channel may be designed such as to minimize band broadening. In the high-dose experiments (Fig. 8.14C-F), more polar degradation products (*e* and *f*) can be identified both in the sample and among the degradation products of RF. In the highest-dose experiments, breakthrough can be observed. A possible explanation is that the amount of polar degradation product has increased during the degradation and it cannot be retained on the column.

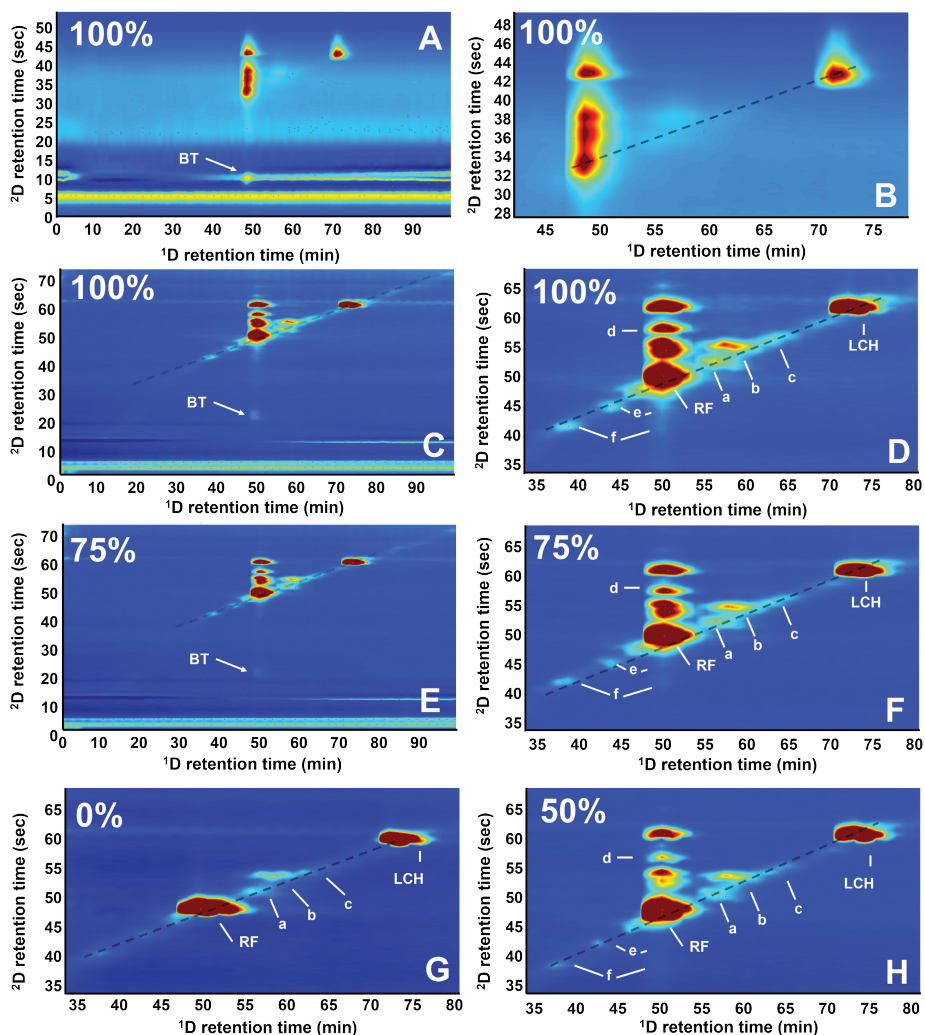


Figure 8.14. Photodegradation LCxLC of a partially degraded RF sample. A) LCxLC with loops at 100% lamp intensity, B) close up of A, C) LCxLC with traps at 100% lamp intensity, D) close up of C, E) LCxLC with traps at 75% lamp intensity, F) close up of E, G) LCxLC with traps with lamp off, H) close up of LCxLC with traps at 50% lamp intensity. Detection wavelength 270 nm. Dashed lines in B,D-H indicate the diagonal.

8.1.5. Comparing the light cells

In the previous sections we have shown that an alternative type of light cell (perpendicular illumination, PI) may harbour different strengths than the LCW cell used in the research described in Chapters 5 to 7, when applied to obtain diverse information on the photodegradation of compounds. In Table 8.1 the two light cells are compared based on several features. The greatest advantages of the LCW cell are that i) the degradation can

be monitored through absorption measurements, *ii*) there is a possibility to adjust the flow of specific gases (e.g. oxygen or nitrogen) in the outer tubing during degradation, which can, for example, be used to study photodegradation in an oxygen-rich or anoxic environment, and *iii*) multiple illumination sources can be coupled to the system, making it versatile to accommodate many different applications. The main disadvantages are that the cell is *i*) not pressure resistant, *ii*) relatively expensive to make and hard to repair, and that *iii*) the illumination can be affected by the concentration, *i.e.* when the concentration is too high, the irradiation through the cell will be inhomogeneous, since much of the radiation will be absorbed in the first part of the exposure cell. In addition, the LCW is susceptible to air bubbles which can interrupt the irradiation. The main advantages of the PI cell are *i*) the speed of degradation, *ii*) the pressure resistance, and *iii*) the low costs of both its fabrication and the required lamp. Its disadvantages are that *i*) there are not many light-emitting-diode (LED) arrays available with different illumination spectra, *ii*) there is no gas permeability, *iii*) air bubbles may disturb the illumination (but not to the same extent as for the LCW) and *iv*) there is currently no possibility to obtain information during degradation in the cell.

Both types of light cells require an external sampler. Injection can be performed manually, by injecting the sample and closing the cell prior to degradation. Care must be taken that no air is introduced in the light cell, especially in the LCW, where an air bubble can block the passage of light. Better results have been obtained when the injection is controlled by a sampling device. Within the TooCOLD project, quite some research was performed using a Multi-Purpose Solvent handler, a so-called MPS (MPS 2L, Gerstel, Mülheim an der Ruhr, Germany). Such instruments have a wide range of possibilities, besides sampling and injection, such as solvent transfer, mixing different solutions prior to sample introduction, and the opportunity to apply different cleaning procedures. The MPS systems used in TooCOLD were found to introduce less air than manual injectors, but the procedure was not completely closed to air. In Chapter 5 to 7 research was described in which the LCW cell was implemented within the LC system and this setup proved consistently airtight. The PI cell was not connected to an MPS but incorporated in an LC system. The sample was injected by an autosampler, and later transferred to an injection loop using a separate pump. This method did not allow for extensive cleaning procedures besides the solvents used in the (binary) pump. However, since the system was completely closed, no air bubbles were introduced. The two methods of sample introduction are compared in Table 8.2.

Table 8.1. Comparison of the LCW cell (second column) and the PI cell (third column) on different features. The fourth column list any eventual remarks and the fifth column refers to chapters in this thesis or to specific publications.

	LCW cell	PI cell	Remarks	Refs
<i>Volume</i>	60 μL	100 μL	May be optimized	[1], Ch. 8
<i>Degradation speed</i>	Medium ¹	High	Both methods are faster than offline degradation setups	[1], Ch. 8
<i>Effect of gas bubbles on degradation</i>	High	Medium to low	Both are affected differently ²	
<i>Concentration range</i>	Low concentrations	Wide range of concentrations	Path length differs (Lambert Beer)	[1,5], Ch. 6,7,8
<i>Gas Permeability</i>	Yes	No		[1], Ch. 8
<i>Maximum pressure</i>	ca. 0.5 MPa	ca. 2 MPa		Ch. 8
<i>Light-filter application</i>	Easy	Easy		[5]
<i>Replaceable parts</i>	No ³	Yes	The PI cell is a modular system, consisting of several replaceable parts	Ch. 8
<i>Illumination sources</i>	Many	Some	For the PI cell the source has to illuminate a large area; different sources need to be evaluated	
<i>Real time reaction monitoring</i>	Yes	No		[5]
<i>Real time monitoring of light dose</i>	Yes	Possible		[5]
<i>Temperature stability</i>	Yes	No ⁴	Increase of temperature in PI cell due to light source	Ch. 8
<i>Possibility for parallel cells</i>	Possible	Yes	It would require complex optics to irradiate and monitor several parallel LCW cells	Ch. 8
<i>Validated system</i>	Yes	Partially		[1,5]
<i>Raman spectroscopy</i>	Yes	No		[6]
<i>SERS possibility</i>	No	Yes ⁵		
<i>Connection 2DLC</i>	Yes	Yes		[7]
<i>Comprehensive LC\timesLC</i>	No	Yes ⁶		Ch. 8
<i>Costs of the cell</i>	Medium	Low		
<i>Sample throughput</i>	Medium	High		Ch. 8

1. Because of the coupling of the light into the LCW cell.
2. In the PI cell degradation ratios will be similar with and without air bubbles, whereas in the LCW cell no degradation takes place downstream from the air bubble.
3. The LCW cell may be repaired, but this requires a high skill level.
4. Unless forced-air flow is applied.
5. The PI cell provides a possibility, but this is still work in progress.
6. Work in progress.

Table 8.2. Comparison of the multi-purpose-sampling device (MPS) and a liquid-chromatography (LC) autosampler as sample introduction for the light cell. Both setups are connected to an LC separation after degradation.

	MPS	LC
<i>Airtight</i>	No	Yes
<i>Cleaning possibilities</i>	Extensive	Limited
<i>Injection volume range</i>	Broad	Narrow
<i>Reagent addition</i>	Possible	Not Possible
<i>Costs</i>	High	High
<i>Pressure range</i>	Narrow	Broad
<i>Automated</i>	Yes	Yes

Concerning the future of photodegradation research in liquid chromatography, I think these two light cells both have their merits, depending on the questions of the user. If the user is interested in a specific compound that is available in its pure form, the LCW cell will provide more information on its degradation pathways. The matrix can easily be adjusted to the liking of the user (using the MPS) and the wavelength range of illumination can be varied through the light source, or even more specifically by using bandpass filters. Moreover, the presence or absence of oxygen can be controlled. Detailed information can be obtained if the cell is coupled to LC with mass-spectrometric detection (LC-MS). If the compound under study is not pure, for example because it derives from a natural source or because it contains impurities from its fabrication process, then a separation prior to the LCW cell becomes worthwhile. We have shown that by coupling the LCW in a cyclic way to the separation, one can even isolate the degradation products and degrade these further by re-injection. This has the advantage that just one LC system is required with one extra pump and one valve to study photodegradation in detail, obviating the need for an extra autoinjector such as the MPS.

Although the degradation time using an LCW decreased dramatically in comparison with off-line exposure [1,8,9], it is not sufficiently fast to perform reaction modulation in LC×LC. If the user wants to use an LED source and does not need to record spectra during degradation the PI cell becomes more attractive. If very fast degradation is required, as in LC×LC with reaction modulation, the PI is currently the only viable option. Due to the greater exposure to irradiation, LC×LC with online photodegradation has become possible and this can be very interesting for elucidating degradation mechanisms. Even though the current PI cell has proven its value, further adaptations of the geometry of the cell may still lead to improved performance. The PI cell is a fast, no-frills alternative without minimal instrumental complexity.

Looking back at the developments during the TooCOLD project, we started at a point where only discoloration or diminishing of the main compound could be studied. The systems available were not suitable to rapidly study chemical degradation. Testing for the effects of the matrix, oxygen present, or illumination spectra could hardly be performed, since few if any techniques were available for the purpose. The PI cell provide an “entry-level model” for performing photodegradation studies, while the LCW cell provide more tuning options and can be seen as a more-advanced model. For the implementation in (comprehensive) 2DLC, however, I think that the pressure resistance of the PI cell allows greater possibilities. This simple light cell opens up the entire field of comprehensive reaction modulation to photodegradation studies. This may be very exciting for science, especially for studying components with a poor light fastness.

8.2. Photo-reaction applications that will benefit from TooCOLD

When the idea of TooCOLD was conceived, some applications fields were already envisioned. Understanding photodegradation pathways of dyes in cultural-heritage objects was one of the reasons the project was initiated, but researchers from other areas also had strong incentives to study photodegradation. In the food industry, for example, there is an urge for more transparent and recyclable packaging materials, while still maintaining a long product shelf life. A different approach is sought within the water-purification industry, where methods are used that employ UV light. This creates a strong interest in studying the photodegradation of contaminants. In all these fields the developed cells can be used to elucidate the degradation pathways. In food science, for example, the filter wheel that is incorporated in the prototype system developed in the TooCOLD project can be used to install different (new) packaging material to test their light-blocking ability and their effects on the photodegradation of the compounds of interest. With the MPS and the LCW cell, researchers in the field of water purification may mix their samples with, for example, hydrogen peroxide and/or natural organic matter prior to photodegradation. In such studies the irradiation source may be replaced by a high- or low-pressure mercury UV lamp.

These anticipated users, however, are not alone in their need for a new photodegradation method. Possible other fields where the TooCOLD cells could facilitate research include extending the shelf-life of pharmaceutical products, developing sunscreen formulations that are better for the environment, or studying the stability of specific polymers in the environment. While the former two may be addressed directly using the systems we have developed, the latter field is slightly more difficult. When the molar masses of the analytes

increase, for example in microplastics, the separation techniques should be adapted. In that case, the light cell may be coupled to size-exclusion chromatography (SEC) or, less conveniently, to field-flow fractionation (FFF). Microplastics would be a field of great interest, since we have learned a great deal about their properties and the ways in which they end up in our environment and in our bodies [10,11], but much still remains unknown about degradation processes and how these may be accelerated.

Lastly, while the TooCOLD project has focused exclusively on photodegradation, it can also lead to new methods to characterize the products of photo-initiated reactions. Reactions that need a certain gas to be present in the cell could benefit from the LCW cell [12,13]. While many synthesis or catalysis groups resort to analytical techniques such as nuclear-magnetic-resonance (NMR) spectroscopy, coupling photo-reactors to separation and detection techniques, such as LC and MS, can provide a great deal of information rapidly and automatically.

8.3. Developments in photodegradation research

An interesting question which remains open is whether the degradation research performed within the TooCOLD project can be compared to the photoreactions occurring in our daily life. Matrix effect of solvents, such as water or methanol, or additives such as buffers or salts, may influence degradation pathways or degradation kinetics. Such effects can be readily studied using the systems described. However, the research in TooCOLD has focused on components in solution. Chapter 5 describes the work performed to compare degradation in solution with degradation on textile. It was found that photodegradation pathways can be similar, as for crystal violet, but can also be different, as for degradation of eosin Y. This means that a liquid-based photodegradation will never completely replace degradation studies performed on solid matrices.

The main bottleneck in photodegradation research on solid matrices currently is the time and labour required. Studies can take up to weeks of degradation time and extractions are performed manually. Apart from the time and work needed, the manual steps can introduce errors and the extraction process can be analyte specific. Degradation may even be caused by the extraction, rather than by irradiation. The in-solution-degradation cells developed in this work allow degradations to be performed faster, simpler and without manual sample handling. The information obtained can then be used to design a smaller number of photodegradation studies using other matrices.

Considering the future of photodegradation research, there are two main routes that can be developed. The first one would be parallel studies of dye degradation in many matrices. Comparison studies like the one described in Chapter 5 can be of great help in understanding mechanisms and how they are affected by the matrix. The LCW cell provides a method to quickly investigate the photostability and the degradation products of a compound. Moreover, the influence of oxygen or that of other solvents can be studied. These results of such experiments can then be compared to studies performed on, for example, textile. It should be noted that, as long as the analyte specificity of extraction methods is not fully understood, the results of experiments performed on solid matrices should be treated with care. Other analytical techniques that can be applied directly on the degraded objects without extraction will play a crucial role comparing the different techniques and their outcomes. The development of the Microfading Tester (MFT) is an example of this.

The other route would be the development of a “TooCOLD-like” system that can perform degradation studies on solid samples. In such a system, the compound of interest would be either dissolved or extracted after the degradation. A versatile sampling device, such as the multi-purpose sample handler (MPS) could possibly be used for this purpose. The proposed method would be akin to head-space extractions performed with gas chromatography, but the extraction fluid would be a liquid rather than a gas. Such a system would significantly reduce the labour needed to perform degradation studies on solid matrices and would make the extraction step more repeatable between analyses and between analysts. It would, however, take many years to realize and validate such a system.

As has already been discussed, within the framework of TooCOLD many significant strides forward have been taken in the development of new systems that facilitate gaining a better understanding of photodegradation mechanisms. When the project started the state-of-the-art approach was to focus solely on the degradation of the main compound, rather than on the products formed. I believe in that the developed systems provide an easier and more-comprehensive method to perform degradation studies and that they will spur developments in many fields.

8.4. Connecting TooCOLD to retention modelling

While the first and second part of this thesis may seem to exist on their own, they are in fact connected. In standard LC and 2DLC, method optimization is a crucial and difficult aspect. Without optimized separations, sample information can be lost because of overlapping peaks. In the current setup, in which a light cell is coupled to an LC separation, the optimization of

the second separation gets even more complicated since the sample is 'created' within the method. Moreover, the degradation products formed can have very similar structures since they all originate from the same parent compound. Various reaction products may therefore exhibit very similar retention behaviour. The work we have performed on retention modelling with semi-empirical models has led to clear guidelines for optimizing separations. Since photodegradation degradation can now be performed online and in automated fashion, scanning-gradient experiments can be performed on a degraded sample and the optimal separation conditions may be established. The calculated retention parameters may also serve to predict the retention on SPAM columns, which can be used if the ¹D effluent is incompatible with the ²D column or if the sensitivity of the method is too low. In the latter case, preconcentration on a SPAM column may increase the sensitivity compared to injection loops and decrease the injection volume on the ²D column from, say, 100 μ L to a few μ L of (potentially) a better-compatible solvent, so as to greatly improve the ²D efficiency and resolution and the detection sensitivity.

Another way to use retention modelling in the current setup would be to rely on quantitative-structure retention relationships (QSRRs). In this technique, the retention of a compound is computed using (potentially many) structural parameters. Since the formed products are typically unknown, such a retention-modelling method does not seem to hold any advantages in comparison with the method based on semi-empirical models, which does not need any prior knowledge. However, in the field of environmental chemistry progress has been made in predicting transformation products [14]. When combined these developments may hypothetically result in a method to optimize the separation of a sample that has not yet been created. The only information needed in such a system would be the structure of the starting compound.

8.5. Future of 2DLC

Much of the work described in this thesis underlines the versatility of LC. It is an immensely flexible technique, thanks to its wide variety of separation modes and its ability to handle complex samples, especially if one embraces 2DLC. While many groups in academia use LC \times LC for their separations, it is still not yet widespread in industry. The most obvious reason for this is that there are so many parameters to optimize in LC \times LC that the time and effort needed for method development currently does not outweigh the benefits [15]. Using active-modulation strategies, such as active-solvent modulation (ASM) or stationary-phase-assisted modulation (SPAM), makes method development and optimization even harder. With programs such as MOREPEAKS [16] and the SPAM tool developed in Chapter 4,

great steps are taken to reduce the optimization time. Such tools may eventually enhance the proliferation of 2DLC in many fields in which the technique is not currently applied. In combination with improved modulation strategies and reliable hardware that can withstand high pressures, 2DLC is about to change the world.

Retention modelling will play a big role in these developments. Predicting retention from a small number of experiments or eventually from analyte data is key to facilitate efficient method development and optimization. It can lead to a better understanding of retention. Interesting aspects that still need further investigation include modelling the effect of pressure and pH on the retention of compounds in RPLC and modelling separation modes that are less-commonly used, such as (hydrophilic-interaction liquid chromatography) HILIC or (ion-exchange chromatography) IEX. As to performing scanning experiments, one could try to perform experiments at higher flow rates instead of with longer gradient times. In this way the gradient volume increases, but the total time required for the scanning experiments is reduced. The main difference between these two ways of scanning gradients would be a difference in pressure, which may lead to differences compounds of which the retention is pressure dependent. While the effects of pH, pressure, and organic-modifier concentration have been extensively studied since the beginning of RPLC, their combined effects are still not completely understood [17–20]. Such a comprehensive understanding would potentially lead to greatly improved retention predictions.

In the present thesis, another aspect of 2DLC has been touched upon, *i.e.* reaction modulation. The work presented in this thesis has shown this to be a viable technique for light-induced (degradation) reactions. I expect future work that involves reaction modulation will benefit from the work we have published in this field. Incorporating the reactors developed in the current project in a 2DLC setup implies that pressure-sensitive parts (< 2MPa) are installed in the flow stream of a setup operating at high pressures (> 40 MPa), which forces the analyst to find creative solutions. Reaction modulation shines a different light on the term orthogonality. The two separation mechanisms in a 2DLC method are considered to be orthogonal when the retention times in the two separation systems are completely independent. This concept changes when a reaction is implemented. When a ¹D fraction undergoes a reaction, its composition changes. If the changes are significant the samples before and after the reaction may themselves be “orthogonal”. An orthogonal separation mechanism in the ²D separation would complicate the method, since two processes are happening at the same time. Normally, an orthogonal separation reveals the properties of the sample components being transferred. For example, when an IEX separation and an RPLC separation are combined, the retention in the two dimensions is

indicative of the charge on the molecule and its hydrophobicity. However, when these two separation modes are used while reaction modulation is applied, it will be hard to attribute these properties to a certain compound, since some compounds will disappear from the chromatogram while other ones appear. The assignment of sample properties will only be of interest when a sample has been completely altered and the ²D separation is used to separate the degradation product. For example, in the work of Pirok *et al.* nanoparticles were separated by hydrodynamic chromatography, after which these particles were dissolved, and size-exclusion chromatography was used in the ²D separation to show the composition of these nanoparticles. With the increased use of reaction modulation in 2DLC, there will be a shift in how we perceive orthogonality.

References

- [1] Groeneveld I, Schoemaker SE, Somsen GW, Ariese F, van Bommel MR. Characterization of a liquid-core waveguide cell for studying the chemistry of light-induced degradation. *Analyst* 2021. <https://doi.org/10.1039/D1AN00272D>.
- [2] Abdullhussain N. Towards microfluidic devices for multi-dimensional separations - PhD Thesis. University of Amsterdam, 2022.
- [3] Wahlund KG, Nilsson L. Flow FFF – basics and key applications. *Field-Flow Fractionation Biopolym Anal* 2012;1–22. https://doi.org/10.1007/978-3-7091-0154-4_1/COVER/.
- [4] Moussa A, Lauer T, Stoll D, Desmet G, Broeckhoven K. Numerical and experimental investigation of analyte breakthrough from sampling loops used for multi-dimensional liquid chromatography. *J Chromatogr A* 2020;1626:461283. <https://doi.org/10.1016/j.chroma.2020.461283>.
- [5] Groeneveld I, Bagdonaite I, Beekwilder E, Ariese F, Somsen GW, Bommel MR van. Liquid Core Waveguide Cell with In Situ Absorbance Spectroscopy and Coupled to Liquid Chromatography for Studying Light-Induced Degradation. *Anal Chem* 2022;94:7647–54. <https://doi.org/10.1021/ACS.ANALCHEM.2C00886>.
- [6] Dijkstra RJ, Bader AN, Hoornweg GP, Brinkman UAT, Gooijer C. On-line coupling of column liquid chromatography and Raman spectroscopy using a liquid core waveguide. *Anal Chem* 1999;71:4575–9. <https://doi.org/10.1021/ac9902648>.
- [7] den Uijl MJ, van der Wijst Y, Groeneveld I, Schoenmakers PJ, Pirok BWJ, van Bommel MR. Combining photodegradation in a liquid-core-waveguide cell with multiple-heart-cut two-dimensional liquid chromatography. *Anal Chem* 2022:under revision.
- [8] Groeneveld I, Bagdonaite I, Beekwilder E, Ariese F, Somsen GW, Bommel MR van. Liquid Core Waveguide Cell with In Situ Absorbance Spectroscopy and Coupled to Liquid Chromatography for Studying Light-Induced Degradation. *Anal Chem* 2022;94:7647–54. <https://doi.org/10.1021/ACS.ANALCHEM.2C00886>.
- [9] Confortin D, Neevel H, Brustolon M, Franco L, Kettelarij AJ, Williams RM, et al. Crystal violet: Study of the photo-fading of an early synthetic dye in aqueous solution and on paper with HPLC-PDA, LC-MS and FORS. *J. Phys. Conf. Ser.*, vol. 231, Institute of Physics Publishing; 2010, p. 012011. <https://doi.org/10.1088/1742-6596/231/1/012011>.
- [10] Leslie HA, van Velzen MJM, Brandsma SH, Vethaak AD, Garcia-Vallejo JJ, Lamoree MH. Discovery and quantification of plastic particle pollution in human blood. *Environ Int* 2022;163:107199. <https://doi.org/10.1016/J.ENVINT.2022.107199>.
- [11] Perez CN, Carré F, Hoarau-Belkhir A, Joris A, Leonards PEG, Lamoree MH. Innovations in analytical methods to assess the occurrence of microplastics in soil. *J Environ Chem Eng* 2022;10:107421. <https://doi.org/10.1016/J.JECE.2022.107421>.
- [12] Noël T, Hessel V. Membrane Microreactors: Gas–Liquid Reactions Made Easy. *ChemSusChem* 2013;6:405–7. <https://doi.org/10.1002/SSC.201200913>.
- [13] Noël T, Cao Y, Laudadio G. The Fundamentals behind the Use of Flow Reactors in Electrochemistry. *Acc Chem Res* 2019;52:2858–69. https://doi.org/10.1021/ACS.ACCOUNTS.9B00412/ASSET/IMAGES/LARGE/AR9B00412_0010.JPEG.
- [14] Helmus R, van de Velde B, Brunner AM, ter Laak TL, van Wezel AP, Schymanski EL. patRoon 2.0: Improved non-target analysis workflows including automated transformation product screening. *J Open Source Softw* 2022;7:4029. <https://doi.org/10.21105/JOSS.04029>.
- [15] Schoenmakers PJ, Vivó-Truyols G, Decrop WMC. A protocol for designing comprehensive two-dimensional liquid chromatography separation systems. *J Chromatogr A* 2006;1120:282–90. <https://doi.org/10.1016/j.chroma.2005.11.039>.

- [16] Molenaar SRA, Schoenmakers PJ, Pirok BWJ. MOREPEAKS 2021. <https://doi.org/10.5281/ZENODO.6375413>.
- [17] Schoenmakers PJ, Billiet HAH, de Galan L. Description of solute retention over the full range of mobile phase compositions in reversed-phase liquid chromatography. *J Chromatogr A* 1983;282:107–21. [https://doi.org/10.1016/S0021-9673\(00\)91596-6](https://doi.org/10.1016/S0021-9673(00)91596-6).
- [18] Schoenmakers PJ, Billiet HAH, Tussen R, De Galan L. Gradient selection in reversed-phase liquid chromatography. *J Chromatogr A* 1978;149:519–37. [https://doi.org/10.1016/S0021-9673\(00\)81008-0](https://doi.org/10.1016/S0021-9673(00)81008-0).
- [19] Lopez Marques RM, Schoenmakers PJ. Modelling retention in reversed-phase liquid chromatography as a function of pH and solvent composition. *J Chromatogr A* 1992;592:157–82. [https://doi.org/10.1016/0021-9673\(92\)85084-7](https://doi.org/10.1016/0021-9673(92)85084-7).
- [20] Schoenmakers PJ, Tijssen R. Modelling retention of ionogenic solutes in liquid chromatography as a function of pH for optimization purposes. *J Chromatogr A* 1993;656:577–90. [https://doi.org/10.1016/0021-9673\(93\)80820-X](https://doi.org/10.1016/0021-9673(93)80820-X).

CHAPTER 9

Epilogue

If you can't communicate your science, is it even science?

The scientific community uses rather traditional ways of communicating, such as presentations and posters, and still do not use the full potential of the tools unleashed by the digital revolution. While to-the-point, application-based videos have become the norm rather than the exception in our digital society, most communication performed within academia is lengthy and theory-based. This shows the somewhat rigid character of academia. For academia to stay connected to science performed in industry, for example, new ways of science communication should be explored. Examples are pitches, videos, or even podcasts about scientific subjects. Luckily, conferences create more and more room for these kinds of communication, through video contests, pitch competitions, or even an open assignment where the candidate is completely free to share their science story in their own way.

While these competitions are very stimulating, there are only few students that commit to these assignments compared to, for example, poster presentations. You might argue that the new generation of scientists is, apparently, not ready for this revolution, but I think this is untrue for four reasons, *i.e.* *i)* early-career scientists are stimulated by their supervisors to present their work as poster or as presentation, *ii)* they have limited knowledge about the possibilities concerning new competitions, *iii)* it will take a lot of time to prepare both a poster and a pitch or video, and *iv)* the present generation of students was barely stimulated during their studies to use new media. In my 10 years at the University of Amsterdam I was never challenged during my courses to think outside the box when it comes to communicating science within the field. Implementing new ways of communication in bachelor or master courses could stimulate creativity, which can then lead to scientific innovation.

For an enthusiastic student there are possibilities to develop and challenge themselves. Pitch competitions, such as FameLab and the 3-minute thesis competition (3MT) are contests for students around the world to tell the story of their PhD in only three minutes and. Such competitions are often accompanied with pitch training. On a national level, similar pitch competitions exist, such as the Spotlight prize of the Royal Dutch Chemical Society (KNCV) in The Netherlands. An enthusiastic student could also apply for actual science-communication summer schools, such as the one organized at Leiden University, or even choose to pursue a science-communication major in an MSc program. If you are interested in communicating your scientific research, reach out to the press office of the university, who may help you with presenting your science to a new audience.

In March 2020 we all experienced a seismic shift in science communication due to the Covid-19 pandemic. With the science communication migrating to completely online, new methods suddenly became more accepted and used more than before. Such methods are here to stay, although they will not fully replace the commonly used methods of communication. Also, online platforms, such as LinkedIn, started to play a bigger role in connecting scientists with colleagues in the field. Fast forward to 2022, we can still see the remains of this sudden shift, which has made many scientists realize that new ways of science communication need a place in the scientific world

While the previous part of this section concerned communication within academia or between academia and industry, I also want to touch upon science communication to another audience: the general public. Better communication about science and about the scientific field could help in various areas, such as *i)* the distrust of the public towards science, *ii)* the stereotypes about scientists, and *iii)* the number of students choosing a natural-science degree. I will discuss these areas separately, but as you will see, they are interconnected.

During the covid-19 pandemic we saw an increasing distrust of the public towards science, which could be attributed to, among other things, the communication from academia to the public. Without any interaction, scientists are often seen as privileged people in their 'ivory' tower, without any human characteristics. Giving scientist a seat at the table during talk shows or creating more in-depth items on the news may reduce this distrust. An alternative way to reach the public would be through social media, such as Instagram, TikTok, or YouTube. The age group using those channels does not watch television as much (if at all), which means that they are normally not reached at all.

Then the stereotypes about scientists. The idea that scientists generally are old, white, and male is toxic for the work environment at the university. It reduces diversity in all layers (future students, students, PhD candidates, middle-career staff, and professors) since the 'perfect' scientist is always portrayed in this way. The feeling of not belonging can be a reason to overlook the field or a reason to decide that it is just not for you. The problem is that once we let people outside science create communication about science, for example a tv show or a movie, the stereotypes will appear. Think about children shows where the evil scientist has crazy grey hair, or the Big Bang Theory, where the scientists all seem to have social difficulties and are dressed in a hysterical way. Because we let this happen, new generations are exposed to the same stereotypes, which makes those stereotypes very persistent.

Lastly, the next generation of students often think that studies such as chemistry have poor career perspectives. I remember very well when I was a high-school student that we used to say that with a bachelor's in law or economics we could 'still become anything'. In retrospect, I could not agree less. Where is the logic in that? And why could you not still be anything if you were to go for chemistry or physics. I personally think you can do much more with these natural sciences. By communicating about science and showing the extent of the influence that science has on our economy, future students will see that you can become more than only a science teacher.

Because the world is not equally exposed to role models from all fields, we as scientists have the duty to spread the story of science to the general audience. With new developments in The Netherlands concerning science-communication centres, I believe that the government is starting to realize this as well. Science communication should be a crucial part of being a scientist and in my opinion, we should enhance the skills of communicating about science on the bachelor, master, and PhD levels. If science communication receives greater recognition, it can also play an important part in the selection process of candidates at the tenure-track or professor level. In this way we will slowly start to step down from the idea that a professor is only good with 'male qualities', such as leadership and dominance, instead of 'female qualities', such as communication and teamwork.

During my PhD, I was looking for (new) ways to communicate my science. It started with some videos and pitches, but it *really* started around October 2020. I was discussing many of the problems described in this chapter with my dear colleagues Noor Abdhussain and Lotte Schreuders. Before then, Noor and I had already tried to film our daily life at university, but this unfortunately came with an incredible workload. Together with Lotte we decided to create an Instagram channel about our life at university and we named it *Sisters in Science NL*. On this channel we created many posts about our science, our life at university, and about the stereotypes. Our slogan eventually became: *if you can see it, you can be it*.

One thing led to another. Since then, we appeared on national television twice, starred on the radio a couple of times, did many presentations, performed in a theatre show, and shared our story in different interviews and podcasts. We found a new way of communicating science in a fun, exciting and fast way, which fitted our creative style. I think my research benefitted from the creative endeavours we engaged in with *Sisters in Science*, since it made me use a completely different way of thinking that I could also implement in my scientific work.

With *Sisters in Science*, we hope to make an impact on three different levels. Firstly, by making ourselves visible to the public, we hope to battle stereotypes and to break the vicious cycle of scientist stereotyping. Secondly, we aim to show the current generation of students that they can become a scientist, even if they think that they do not belong in the scientific world because of the stereotypes. We hope to make the university a more diverse place on all levels. Lastly, we hope to show the future generation of scientists that they, too, can be a scientist. We need to be aware that academia is a privileged place that many people have no connection to. With our initiative we hope to remove these barriers.

When starting this new type of science communication, we were unsure whether the scientific community would appreciate it. We do not shy away for difficult subjects, such as the enormous number of burnouts in the field. However, in December 2021 we were granted the Diversity Initiative Award (50 k€) of the Dutch Research Council, which confirmed that what we are doing is benefitting the science community in general.

Still not convinced? Think about this.

A brilliant scientist may perform fantastic research, publish very important papers, and maybe even win a Nobel prize. A brilliant science communicator, however, may inspire thousands of children, motivate many early-career scientists, and create an army of change.

In the end, you can do so much more together than alone.

PART V

Summary

CHAPTER 10

Summary

10. Summary

In photodegradation a molecule is excited by light, which causes it to degrade. It happens in many fields around us. Cultural-heritage objects slowly fade and lose their esthetical value. Understanding the photodegradation processes can aid in preserving and conserving these objects for future generations. In food science, packaging materials need to protect the products from photodegradation, but these materials need to fulfill many requirements. Improved knowledge will yield better storage possibilities. Lastly, in water-purification systems, ultraviolet (UV) light in combination with hydrogen peroxide can be used to reduce the concentrations of potentially harmful substances in the water. These processes, however, yield many degradation products in low concentrations that cannot be identified with current methods. To conduct photodegradation research, the possibilities are limited. Many methods only study the degradation of the compound of interest and not the products formed. Within the TooCOLD project (‘Toolbox for studying the Chemistry Of Light-induced Degradation’), a light-exposure cell was developed to more-efficiently degrade samples. One way to use this light cell is to couple it with liquid chromatography (LC). Another possibility is to couple the light cell within two-dimensional liquid chromatography (2DLC) as a type of reaction modulator. To optimize the separations in LC and the sensitive measurement of reaction products, retention modelling can be used. **Chapter 1** consists of an overview of photodegradation and its application, LC and 2DLC, different types of modulation, and an introduction into the use of retention modelling in method optimization.

In **Chapter 2** we present an overview of the research performed on modelling with semi-empirical retention models in the period 2015-2020. Additionally, we aimed to describe the general theory on the subject, including the origin of the models used, a guideline on how to perform the scanning experiments needed, and possibilities to evaluate the data. In this review, five workflows were established in which retention modelling is used. These included method optimization, method transfer, stationary-phase characterization, understanding retention, and lipophilicity determination. The review culminated in recommendations for future work on retention modelling. The most important advice was that researchers should provide more data on the outcome of their retention modelling research for comparison with other work. Moreover, there is currently no consensus on what is determined to be “accurate”.

In **Chapter 3** guidelines are formulated for the best set of scanning experiments for retention modelling. Two data sets of scanning-gradient experiments with different measurement precision were used for this research. It was found that these two sets of data yielded different optimal models. The gradient duration did not affect the accuracy of the retention prediction.

Another parameter investigated was the gradient-slope factor, *i.e.* the ratio between slopes of the fastest and the slowest scanning gradients, which researchers thought needed to be at least three. We found this factor to be less important than the proximity of the slope of the scanning gradients to that of the predicted gradient. Additionally, it was found that very fast gradients, like those encountered in the second dimension (²D) of comprehensive two-dimensional liquid chromatography (LC×LC), cannot be used to predict the slower, first-dimension (¹D) gradients.

Complex samples can be separated by 2DLC. However, incompatibility between dimensions is often encountered when coupling two orthogonal, *i.e.* very different, separation systems. Active modulation (AM) can be used to circumvent this problem. One AM technique is stationary-phase-assisted modulation (SPAM), described in **Chapter 4**. SPAM is thought to be the least robust AM technique, due to possible premature elution of analytes. In this chapter a retention-modelling tool is described to predict retention on SPAM columns for their implementation in 2DLC. It was found that the dead-volume determination of trap columns did not yield accurate results and that a better value could be obtained by extrapolation of analytical-column data. Moreover, the dilution-flow strategy often employed in 2DLC was found to work counterproductively for some analytes. The tool was tested for nine analytes under 36 sets of conditions with three modulation times and yielded a correct assessment in more than 95% of all cases (less than 5% false positives plus false negatives).

The next part of the thesis revolved around photodegradation. In **Chapter 5**, a study is described of the photodegradation of eosin Y and crystal violet in the liquid-core-waveguide (LCW) cell developed by Groeneveld *et al.* The results were compared with those obtained with several other methods used to study photodegradation, such as a light box (Spectrolinker), a Xenotester, and a MicroFading tester. The dyes were degraded in solution, as well as on textile. It was found that the degradation in the LCW cell progressed much faster than in the Xenotester and the Spectrolinker. Because the LCW system works online, there is no need for a sample transfer or an extraction. While the degradation of crystal violet was comparable in all systems, a difference was found for the debromination reaction of eosin Y. The degradation products formed in this test proved to be independent of the light source.

While the LCW cell has proven to be a good alternative to other photodegradation methods, it can only degrade compounds that are available in their pure form. To circumvent this, the LCW cell was incorporated in a multiple-heart-cut (mHC) 2DLC system, which is described in **Chapter 6**. In this setup, several fractions from the ¹D separation were isolated from the effluent in a mHC valve, after which these fractions were degraded one by one during different

periods of time. By coupling a 2D separation to the exit of the LCW cell, the degradation products could be measured. The degradation proved to be faster when smaller amounts of sample were introduced, which was ascribed to the fact that at high concentrations too much light absorbance occurs, resulting in an inhomogeneous irradiation of the sample in the axial direction of the LCW. The setup was tested with three applications, *i.e.* fuchsin, annatto, and a vitamin-B complex.

While the mHC-2DLC system worked as planned, it was rather complex and it was hard to compare degradation products found in the 2D separation and impurities detected in the 1D separation. In **Chapter 7** a new system is described, using which a mixture can be separated on an analytical column. A fraction of the effluent can be selected and transferred to the LCW cell to be degraded. Thereafter, the degraded fraction was reinjected onto the same column to separate the compound of interest from its degradation products. This system allowed a direct comparison of the degradation products and the contaminants in the 1D separation. This created an opportunity to allow further degradation cycles to elucidate degradation pathways. This new TooCOLD setup requires just a single LC system to study either pure samples or components isolated from complex mixtures. This makes the technique much more accessible and applicable.

Finally, **Chapter 8** culminates in conclusions on the work described in Chapter 2 to 7. The development of a new perpendicular-illumination light-exposure cell is described. Moreover, perspectives on the future of photodegradation research, retention modelling and two-dimensional liquid chromatography are discussed.

10. Samenvatting

Wanneer een molecuul wordt aangeslagen door licht, kan er lichtdegradatie plaatsvinden. Dit proces doet zich voor in verschillende materialen. Kunstobjecten kunnen langzaam vervagen en hun esthetische waarde verliezen. Wanneer we lichtdegradatie beter begrijpen kunnen we deze objecten beter bewaren en conserveren voor toekomstige generaties. Een ander veld is voedingsmiddelentechnologie, waar (transparante) verpakkingsmaterialen worden gebruikt om producten deels af te schermen van licht. Betere kennis over het degradatieproces kan de houdbaarheid verlengen. Als laatste voorbeeld wordt er in waterzuiveringsinstallaties ultraviolet (UV) licht gebruikt in combinatie met waterstofperoxide om de concentratie organisch componenten in het water te verlagen. Tijdens deze processen kunnen helaas ook ongewilde, en wellicht toxische, producten worden gevormd. Er zijn echter beperkte mogelijkheden om geavanceerd onderzoek te doen naar lichtdegradatie. Veel methodes bestuderen alleen een kleurverandering of de afname van een hoofdcomponent en niet de producten die gevormd worden. Binnen het TooCOLD project (*'Toolbox for studying the Chemistry Of Light-induced Degradation'*) is er een belichting cel ontwikkeld om monsters heel efficiënte wijze te belichten. Een manier om deze licht cel te gebruiken is door deze te koppelen met vloeistofchromatografie (LC) of door deze in een tweedimensionaal vloeistofchromatografie (2DLC) systeem te installeren, als een vorm van reactie modulatie. Om betere en meer sensitieve scheidingen te ontwikkelen in LC, zou je retentie modellering kunnen gebruiken. **Hoofdstuk 1** omvat een overzicht van lichtdegradatie en haar toepassingen, LC en 2DLC, verschillende vormen van modulatie, en een introductie voor het gebruik van retentie modellering in methode optimalisering.

In **Hoofdstuk 2** presenteren we een overzicht van het uitgevoerde onderzoek over retentie modellering met semi-empirische modellen in de periode van 2015 tot 2020. Daarnaast wordt de algemene theorie over dit onderwerp beschreven, inclusief de oorsprong van de gebruikte modellen, een richtlijn over de uitvoering van de experimenten en de mogelijkheden om data te evalueren. In dit review artikel zijn vijf werkprocessen vastgesteld binnen de onderzochte literatuur, waaronder methode optimalisering, methode overdracht, stationaire fase karakterisering, retentie begrip, en lipofiliciteit bepaling. Dit hoofdstuk eindigt met aanbevelingen voor toekomstige onderzoek naar retentie modellering. Het belangrijkste advies was om meer experimentele gegevens te delen, zodat de verschillende resultaten makkelijker met elkaar vergeleken kunnen worden. Daarnaast bleek er geen consensus over wat beschouwd wordt als accuraat is en wat niet.

In **Hoofdstuk 3** worden er richtlijnen geformuleerd om de beste set aan gradiëntscans voor gebruik met retentie modellering te meten. Twee gradiënt datasets met verschillende precisie werden hiervoor gebruikt. Deze twee sets bleken elk een eigen optimaal model te hebben. De duur van de gradiënt beïnvloedde de nauwkeurigheid van de voorspelling niet. Een andere onderzochte parameter was gradiënt-helling factor, wat kan worden beschreven als de ratio tussen de helling van de snelste en de langzaamste gradiënt uit de sets. Voorafgaand aan dit onderzoek werd deze factor vaak op drie gezet, maar uit het onderzoek blijkt dat deze factor minder belangrijk is dan de nabijheid van de helling van de gradiënt uit de scanning set tot de uiteindelijke voorspelde gradiënt. Daarnaast bleken hele snelle gradiënten, zoals de gradiënten die gebruikt worden in de tweede dimensie (²D) van *comprehensive* (alomvattende) 2DLC (LC×LC), niet gebruikt te kunnen worden om de langzamere, eerste dimensie (¹D) gradiënten te voorspellen.

Complexe monsters kunnen gescheiden worden met 2DLC. In 2DLC worden twee zo verschillend mogelijke, ofwel orthogonale, retentiemechanismen aan elkaar gekoppeld. De condities tussen deze methodes kunnen incompatibel zijn. Active modulatie (AM) kan dienen als oplossing. Een AM-techniek is *stationary-phase-assisted* modulatie (SPAM), wat in **Hoofdstuk 4** wordt beschreven. Door mogelijke premature elutie is SPAM de minst robuuste techniek. In dit hoofdstuk wordt een retentie modellering programma beschreven, die de retentie op de SPAM kolommen in een 2DLC setup kan voorspellen. Het bleek dat de bepaling van het dode volume van de SPAM kolommen geen accurate waardes gaf en dat deze waarde beter kon worden bepaald door extrapolatie van het dode volume van de analytische kolom. Er wordt vaak een verdunning toegepast bij de implementatie van SPAM in 2DLC, maar deze verdunning bleek voor sommige stoffen een tegengesteld effect te hebben. Het programma werd getest door negen stoffen onder 36 condities en 3 verschillende modulatie tijden te meten en gaf een correcte voorspelling in meer dan 95% van alle gevallen (minder dan 5% vals positieven plus valse negatieven).

Het tweede deel van dit proefschrift richt zich op lichtdegradatie. **Hoofdstuk 5** beschrijft een studie naar de lichtdegradatie van eosine Y en kristalviolet in de *liquid-core-waveguide* (LCW) cel, ontwikkeld door Groeneveld *et al.* Deze resultaten werden vergeleken met andere soortgelijke degradatie methodes, zoals een licht box (Spectrolinker), een Xenotester en een MicroFading tester. De kleurstoffen werden zowel in oplossing gedegradieerd, als op textiel. Het bleek dat de degradatie in de LCW-cel veel sneller verliep dan in de Xenotester, de microfading tester of de Spectrolinker. Omdat het LCW-systeem *online* is, is er geen monsteroverdracht of extractie nodig wat niet alleen de analyse sneller maakt, maar ook voorkomt dat het monster verandert tijdens de monstervoorbewerking. Hoewel de degradatie van kristalviolet vergelijkbaar in alle

matrices, werd er een verschil gevonden in de debrominatie reactie van eosine Y. De gevormde degradatieproducten in dit onderzoek bleken onafhankelijk van de belichtingsbron, wel is de intensiteit van de lichtbron van grote invloed op de degradatiesnelheid.

Ondanks dat de LCW-cel een goed alternatief is ten opzichte van andere lichtdegradatie technieken, kan het alleen worden toegepast op stoffen in pure vorm. Om ook mengsels te kunnen onderzoeken, werd de LCW-cel in een *multiple-heart-cut* (mHC) 2DLC systeem gekoppeld. Dit systeem wordt beschreven in **Hoofdstuk 6**. In deze methode werden meerdere fracties uit de ¹D scheiding geïsoleerd in de mHC kraan, waarna deze fracties één voor één werden belicht in de LCW cel. Door het uiteinde van de belichting cel aan een ²D scheiding te koppelen, konden de degradatieproducten worden gemeten. De degradatie bleek sneller te verlopen wanneer de concentratie lager was. Dit kon worden verklaard doordat er te veel absorptie plaatsvindt bij hogere concentraties, waardoor er een belichtingsgradiënt ontstond in de axiale richting van de licht cel. Deze opstelling werd getest met drie verschillende monsters, waaronder fuchsine, een anatto extract en een vitamine B complex. Hiermee is aangetoond dat componenten geselecteerd kunnen worden uit een mengsel en afzonderlijk van elkaar verouderd kunnen worden, waardoor een eenduidig beeld ontstaat van de degradatieproducten van specifieke componenten,

Hoewel het mHC-2DLC systeem werkte naar behoren, is het een vrij complex systeem en is het moeilijk om gedetecteerde degradatieproducten in de ²D scheiding te vergelijken met de componenten gevonden in de ¹D scheiding. In **Hoofdstuk 7** wordt een nieuw systeem beschreven, waar een monster wordt gescheiden op een analytische kolom. Een fractie van het effluent kon worden geselecteerd en worden overgebracht naar de LCW-cel, waar het kon worden belicht. Hierna wordt het gedegradeerde sample opnieuw geïnjecteerd op hetzelfde analytische systeem om de hoofdcomponent te scheiden van de degradatieproducten. Door tweemaal exact dezelfde condities te gebruiken konden de ¹D en de ²D scheiding direct worden vergeleken. Ook werd het mogelijk om een meerstaps degradatie te doen om het degradatieverloop op te helderen. Om deze nieuwe opstelling te bouwen is maar één LC systeem nodig om zowel pure stoffen als componenten uit mengsels te bestuderen. Dit maakt de licht cel breder toepasbaar.

Tenslotte eindigt dit proefschrift in **Hoofdstuk 8** met conclusies over het werk uit Hoofdstuk 2 tot en met 7. Daarnaast wordt de ontwikkeling van een nieuwe *perpendicular-illumination* belichting cel beschreven. Als laatste wordt er vooruitgekeken naar de toekomst van lichtdegradatie onderzoek, retentie modellering en tweedimensionale vloeistofchromatografie.

PART VI

Supporting Information

CHAPTER 11

Sundries

11.1. List of Publications

- 1. Recent applications of retention modelling in liquid chromatography**
Mimi J. den Uijl, Peter J. Schoenmakers, Bob W.J. Pirok, and Maarten R. van Bommel.
J. Sep. Sci., **2021**, 44, 88–114, DOI: 10.1002/jssc.202000905
Covered by Chapter 2
- 2. Measuring and using scanning-gradient data for use in method optimization for liquid chromatography**
Mimi J. den Uijl, Peter J. Schoenmakers, Grace K. Schulte, Dwight R. Stoll, Maarten R. van Bommel, and Bob W.J. Pirok.
J. Chromatogr. A, **2021**, 1636, 461780, DOI: 10.1016/j.chroma.2020.461780
Covered by Chapter 3
- 3. Comparing different light-degradation approaches for the degradation of Crystal Violet and Eosin Y**
Mimi J. den Uijl, Anika Lokker, Bob van Dooren, Peter J. Schoenmakers, Bob W.J. Pirok, and Maarten R. van Bommel.
Dye. Pigment., **2022**, 197, 109882, DOI: 10.1016/j.dyepig.2021.109882.
Covered by Chapter 5
- 4. Combining photodegradation in a liquid-core-waveguide cell with multiple-heart-cut two-dimensional liquid chromatography**
Mimi J. den Uijl, Yorn J.H.L. van der Wijst, Iris Groeneveld, Peter J. Schoenmakers, Bob W.J. Pirok, and Maarten R. van Bommel.
Anal. Chem., **2022**, 94, 11055-11061, DOI: 10.1021/acs.analchem.2c01928
Covered by Chapter 6
- 5. Assessing the Feasibility of Stationary-Phase-Assisted Modulation for Two-Dimensional Liquid-Chromatography Separations**
Mimi J. den Uijl, Tim Roeland, Tijmen S. Bos, Peter J. Schoenmakers, Maarten R. van Bommel, and Bob W.J. Pirok.
J. Chromatogr. A, **2022**, 1679, 463388, DOI: 10.1016/j.chroma.2022.463388
Covered by Chapter 4

6. **Incorporating a liquid-core-waveguide cell in recycling liquid chromatography for detailed studies of photodegradation reactions**
Mimi J. den Uijl, Ingrida Bagdonaite, Peter J. Schoenmakers, Bob W.J. Pirok, and Maarten R. van Bommel.
J. Chromatogr. A, **2022**, *accepted with major revisions*
Covered by Chapter 7
7. **The enigmatic structure of the crenarchaeol isomer.**
Jaap S. Sinninghe Damsté, W. Irene C. Rijpstra, Ellen C. Hopmans, Mimi J. den Uijl, Johan W.J. Weijers, Stefan Schouten
Org. Geochem., **2018**, *124*, 22-28, DOI: 10.1016/j.orggeochem.2018.06.005
8. **Photodegradation products and their analysis in food**
J. Verduin, Mimi J. den Uijl, Ruud J.B. Peters, and Maarten R. van Bommel.
J. Food Sci. Nutr., **2020**, *6.3*, 067-083, DOI: 10.24966/fsn-1076/100067
9. **Characterization of dye extracts from historical cultural-heritage objects using state-of-the-art comprehensive two-dimensional liquid chromatography and mass spectrometry with active modulation and optimized shifting gradients.**
Bob W.J. Pirok, Mimi J. den Uijl, Giacomo G. Moro, Sanne V. Berbers, Charlotte J.M. Croes, Maarten R. van Bommel, and Peter J. Schoenmakers.
Anal. Chem., **2022**, *91*, DOI: 10.1021/acs.analchem.8b05469
10. **Reducing the influence of geometry-induced gradient deformation in liquid chromatographic retention modelling**
Tijmen S. Bos, Leon E. Niezen, Mimi J. den Uijl, Stef R.A. Molenaar, Sascha Lege, Peter J. Schoenmakers, Govert W. Somsen, Bob W.J. Pirok.
J. Chromatogr. A, **2021**, *1635*, 461714, DOI: 10.1016/j.chroma.2020.461714

11.2. Overview of co-authors' contribution

Chapter 1

Introduction

Mimi J. den Uijl	Wrote the chapter
Bob W.J. Pirok	Reviewed the manuscript and provided feedback for improvements
Peter J. Schoenmakers	Reviewed the manuscript and provided feedback for improvements
Maarten R. van Bommel	Reviewed the manuscript and provided feedback for improvements

Chapter 2

Recent applications of retention modelling in liquid chromatography

J. Sep. Sci., **2021**, 44, 88–114, DOI: 10.1002/JSSC.202000905

Mimi J. den Uijl	Wrote the introduction of the chapter. Wrote the theory section. Organised the literature of the last five years and subdivided the literature in the five sections. Wrote the discussion and co-authored the recommendations in the concluding remarks. Developed the overview table of how to perform retention modelling and graded the different types of retention modelling (Fig. 2.9).
Peter J. Schoenmakers	Co-authored the recommendations in the concluding remarks. Reviewed the manuscript and provided feedback for improvements. Overall supervisor of the project.
Bob W.J. Pirok	Reviewed the manuscript and provided feedback for improvements. Overall supervisor of the project.
Maarten R. van Bommel	Reviewed the manuscript and provided feedback for improvements. Overall supervisor of the project.

Chapter 3

Measuring and using scanning-gradient data for use in method optimization for liquid chromatography

J. Chromatogr. A, **2021**, 1636, 461780, DOI: 10.1016/J.CHROMA.2020.461780

Mimi J. den Uijl	Co-developed the idea for this work. Designed the experimental setup and performed the experiments of Set X. Performed the data analysis. Wrote the manuscript, designed all the figures.
Peter J. Schoenmakers	Reviewed the manuscript and provided feedback for improvements. Overall supervisor of the project.
Grace K Schulte	Performed the experiments of Set Y.
Dwight R. Stoll	Co-developed the idea for this work. Reviewed the manuscript and provided feedback for improvements. Overall supervisor of the project.
Maarten R. van Bommel	Reviewed the manuscript and provided feedback for improvements.
Bob W.J. Pirok	Co-developed the idea for this work. Reviewed the manuscript and provided feedback for improvements. Overall supervisor of the project.

Chapter 4

Assessing the Feasibility of Stationary-Phase-Assisted Modulation for Two-Dimensional Liquid-Chromatography Separations

J. Chromatogr. A, **2022**, 1679, 463388, DOI: 10.1016/j.chroma.2022.463388

Mimi J. den Uijl	Co-developed the idea for this work, including the new theory on dilution flows in SPAM. Designed the experimental setup. Performed the data analysis. Supervised the project. Wrote the manuscript, designed all the figures.
Tim Roeland	Performed all experiments. Performed preliminary data analysis.
Tijmen S. Bos	Developed the SPAM-tool.
Peter J. Schoenmakers	Reviewed the manuscript and provided feedback for improvements. Overall supervisor of the project.
Maarten R. van Bommel	Reviewed the manuscript and provided feedback for improvements.
Bob W.J. Pirok	Co-developed the idea for this work. Reviewed the manuscript and provided feedback for improvements. Overall supervisor of the project.

Chapter 5

Comparing different light-degradation approaches for the degradation of Crystal Violet and Eosin Y

Dye. Pigment., **2022**, 197, 109882, DOI: 10.1016/J.DYEPIG.2021.109882

Mimi J. den Uijl	Co-developed the idea for this work. Designed the experimental setup. Performed the data analysis. Supervised the project. Wrote the manuscript, designed all the figures.
Anika Lokker	Performed experiments on the XenoTester, Microfading Tester, and the Spectrolinker. Optimized the LC-MS method.
Bob van Dooren	Performed experiments on the liquid-core-waveguide cell.
Peter J. Schoenmakers	Reviewed the manuscript and provided feedback for improvements.
Bob W.J. Pirok	Reviewed the manuscript and provided feedback for improvements.
Maarten R. van Bommel	Co-developed the idea for this work. Reviewed the manuscript and provided feedback for improvements. Overall supervisor of the project.

Chapter 6

Combining photodegradation in a liquid-core-waveguide cell with multiple-heart-cut two-dimensional liquid chromatography

Anal. Chem., **2022**, 94, 11055-11061, DOI: 10.1021/acs.analchem.2c01928

Mimi J. den Uijl	Developed the idea for this work. Designed the experimental setup. Performed the data analysis. Supervised the project. Wrote the manuscript, designed all the figures. Performed the mHC-2DLC experiments.
Yorn J.H.L. van der Wijst	Optimized the ¹ D and ² D separations. Performed the mHC-2DLC experiments. Prepared the samples.
Iris Groeneveld	Developed the LCW cell.
Peter J. Schoenmakers	Reviewed the manuscript and provided feedback for improvements. Overall supervisor of the project.
Bob W.J. Pirok	Reviewed the manuscript and provided feedback for improvements. Overall supervisor of the project.
Maarten R. van Bommel	Reviewed the manuscript and provided feedback for improvements. Overall supervisor of the project.

Chapter 7

Incorporating a liquid-core-waveguide cell in recycling liquid chromatography for detailed studies of photodegradation reactions

J. Chromatogr. A, 2022, accepted with major revisions

Mimi J. den Uijl	Co-developed the idea for this work. Designed the experimental setup. Performed the data analysis. Supervised the project. Wrote the manuscript, designed all the figures. Performed the mHC-2DLC experiments.
Ingrida Bagdonaite	Performed all experiments. Prepared the samples.
Peter J. Schoenmakers	Reviewed the manuscript and provided feedback for improvements. Overall supervisor of the project.
Bob W.J. Pirok	Reviewed the manuscript and provided feedback for improvements.
Maarten R. van Bommel	Co-developed the idea for this work. Reviewed the manuscript and provided feedback for improvements. Overall supervisor of the project.

Chapter 8

Conclusions & Future Perspectives

Mimi J. den Uijl	Co-developed the idea of a multicell and PI cell. Wrote the conclusions and the future perspectives. Wrote the section about the development of a new light cell. Performed the data analysis of the section of the light cell. Designed all the figures.
Jasper P.H. Smeets	Performed the comprehensive reaction modulation experiments. Developed the PI cell.
Yorn J.H.L. van der Wijst	Performed the experiments with the first PEEK light cell
Nienke C. Schut	Printed and tested the 3D-printed cells.
Suhas H. Nawada	Designed the 3D-printed cells and the first PEEK light cell. Co-developed the idea of a multicell.
Hans J. Ellermeijer	Designed the PI cell. Performed the safety test.
Sven Koot	Created the parts of the PI cell.
Peter J. Schoenmakers	Reviewed the manuscript and provided feedback for improvements. Overall supervisor of the project.
Bob W.J. Pirok	Reviewed the manuscript and provided feedback for improvements.
Maarten R. van Bommel	Co-developed the idea of a multicell and PI cell. Reviewed the manuscript and provided feedback for improvements. Overall supervisor of the project. Co-developed the idea of a multicell.

Prologue & Epilogue

Introduction

Mimi J. den Uijl	Wrote both chapters.
Bob W.J. Pirok	Reviewed the chapters and provided feedback for improvements.
Peter J. Schoenmakers	Reviewed the chapters and provided feedback for improvements.
Maarten R. van Bommel	Reviewed the chapters and provided feedback for improvements.

11.3. List of abbreviations⁷

¹ D	First-dimension
1DLC	One-dimensional liquid chromatography
² D	Second-dimension
2DLC	Two-dimensional liquid chromatography
ACD	At-column dilution
ACN	Acetonitrile
ADS	Adsorption
AIC	Akaike Information criterion
AM	Active modulation
ANN	Artificial neural network
AOP	Advanced oxidation process
ASM	Active-solvent modulation
BHBA	2-(3,5-dibromo-2,4-dihydroxybenzoyl)benzoic acid
CV	Crystal violet
DAD	diode-array detector
DF	Dilution flow
DMSO	Dimethyl sulfoxide
EY	Eosin Y
FFF	Field-flow fractionation
FMF	Formyl-methyl flavin
GA	Genetic algorithm
GSF	Gradient-slope factor
H ₂ O	Water
HILIC	Hydrophilic interaction liquid chromatography
HPLC	High-performance liquid chromatography
HSM	Hydrophobic-subtraction model
ID	Internal diameter
IEX	Ion-exchange chromatography
IPA	Isopropanol
IR	infrared light
^{ISO} P	Isocratic pump
LC	liquid chromatography
LC×LC	Comprehensive two-dimensional liquid chromatography
LCH	Lumichrome
LCW	liquid-core waveguide
LED	Light-emitting diode

⁷ This list only includes the abbreviations that are used throughout the manuscript. Singly used abbreviations from Chapter 2 are omitted from the table.

Chapter 11

LFER	Linear-free-energy relationships
LSS	Linear-solvent-strength
mDLC	Multi-dimensional liquid chromatography
MeOH	Methanol
MFT	MicroFading Tester
mHC	Multiple-heart-cut
mHC-2DLC	Multiple-heart-cut two-dimensional liquid chromatography
MK	Michler's ketone
MM	Mixed-mode
MPS	Multi-purpose sampler
MS	Mass spectrometry
NK	Neue-Kuss
NMR	Nuclear-magnetic resonance
NPLC	Normal-phase liquid chromatography
OD	Outer diameter
PAH	Polycyclic aromatic hydrocarbon
PEEK	Polyether ether ketone
PI	Perpendicular-illumination
Q / QUA	Quadratic model
QSRR	Quantitative Structure-Retention Relationships
RF	Riboflavin
RI	Refractive index
RP	Reversed phase
RPLC	Reversed-phase liquid chromatography
RSD	Relative standard deviation
SEC	Size-exclusion chromatography
SERS	Surface enhanced Raman Spectroscopy
SFC	Supercritical-fluid chromatography
SL	Spectrolinker
sLC×LC	Selective comprehensive two-dimensional liquid chromatography
SPAM	Stationary-phase-assisted modulation
THF	Tetrahydrofuran
TLC	Thin-layer chromatography
TooCOLD	Toolbox for studying the Chemistry Of Light-induced Degradation
UV	Ultraviolet light
Vis	Visible light
XT	Xenotester

11.4. List of symbols⁸

1t_R	First-dimension retention time
1F	First-dimension flow rate
${}^1\varphi$	First-dimension organic-modifier concentration
2t_R	Second-dimension retention time
${}^D F$	Dilution-flow flow rate
${}^D \varphi$	Dilution-flow organic-modifier concentration
k_{ow}	Octanol-water partition coefficient
$\overline{t_{R,exp}}$	Average experimental retention time
$\ln k_0$	Logarithm of the retention factor at $\varphi = 0$
$\ln k$	Logarithm of the retention factor
$F_{tot,max}$	Maximum total flow
$F_{tot,min}$	Minimal total flow
$S_{1,M} - S_{2,M}$	S-parameters of the MM model
$S_{1,NK} - S_{2,NK}$	S-parameters of the NK model
$S_{1,Q} - S_{2,Q}$	S-parameters of the Q model (S_1 and S_2 in Chapter 4)
S_{LSS}	S-parameter of the LSS model
V_0	Column dead volume
V_{ex}	Extra-column volume
V_{inj}	Injection volume
V_{max}	Maximum volume
V_R	Retention volume
V_m	Mobile phase volume
V_s	Stationary phase volume
a_i	Analyte parameters
b_{LSS}	Effective gradient slope

⁸ This list only includes the symbols that are used throughout the manuscript. Singly used abbreviations from Chapter 2 are omitted from the table.

C_m	the analyte concentrations in the mobile phase
C_s	the analyte concentrations in the stationary phase
k_{init}	Retention factor at the start of the gradient
$k_{LSS,p}$	Calculated retention factor with dilution flow p with LSS model
k_{min}	Minimal retention factor
$k_{QUA,p}$	Calculated retention factor with dilution flow p with Q model
k_e	Retention factor at the time of elution
k_{final}	Retention factor at the end of the gradient
n_{LCW}	The number of LCW cells installed on the mHC deck
n_{parch}	The number of parallel channels
n_{ADS}	Solvation parameter of the ADS model
n_c	Peak capacity
q_m	the total mass of analyte in the mobile phase
q_s	the total mass of analyte in the stationary phase
s_i	System parameters
t_0	Column dead time
t_{deg}	Degradation time
t_{init}	Initial time (<i>i.e.</i> time before start of the gradient)
t_{max}	Maximum time
$t_{mod,max}$	Maximum modulation time
$t_{mod,min}$	Minimal modulation time
t_{mod}	Modulation time
$t_{R,p}$	Retention time at dilution flow p
$t_{R,pred}$	Predicted retention time
$t_{R,q}$	Retention time at dilution flow q
t_D	Dwell time
t_G	Gradient time
t_R	Retention time
ϵ_{pred}	Prediction error

φ_{init}	Initial organic-modifier concentration
φ_e	Organic-modifier concentration at the time of elution
φ_{final}	Final organic-modifier concentration
Γ	Gradient-slope factor
B	Slope of the gradient
F	Flow rate
K	Distribution coefficient
N	Plate number
SSE	Sum-of-squares error
T	Temperature
k	Retention factor
n	Number of observations
p	Number of parameters
p	Dimensionless dilution flow (smallest)
q	Dimensionless dilution flow (largest)
τ	Sum of t_D , t_{init} and t_0
φ	Volume fraction of strong solvent

CHAPTER 12

Appendices

Appendix A

Tables and figures in this appendix are related to Chapter 3: Measuring and using scanning-gradient data for use in method optimization for liquid chromatography

A-1. Overview of studied compounds

In this section an overview is given on the measured samples for the retention study. In the table the solvent of the sample is shown with the resulting concentration of the compounds. This is shown for Set X in Table A-1 and for Set Y in Table A-2

Table A-1. Overview of compounds investigated for Set X in this study.

Sample mixture	Compound	v/v				Concentration (ppm)
		THF	DMSO	ACN	H ₂ O	
A	Indigotin	0	1	1	0	263
B	Purpurin	0	1	19	0	500
A	Emodin	0	1	9	0	500
B	Toluene	0	0	1	0	500
C	Propylparaben	0	0	1	0	493
D	Uracil	0	0	19	20	500
C	Sudan I	0	0	1	0	200
D	Rutin	0	0	13	60	407
D	Martius Yellow	0	1	19	0	500
B	Naphthol Yellow S	0	5	19	0	416
A	Orange IV	0	1	19	0	500
B	Flavazine L	0	9	19	0	357
C	Picric Acid	0	1	19	0	500
A	Fast Red B	0	5	19	0	416
A	Tyramine	0	0	19	35	500
B	Cytosine	0	0	3	10	462
D	Trimethoprim	0	0	127	300	500
D	Propranolol	0	0	2	11	500
E	Peptide 1	0	0	0	1	500
E	Peptide 2	0	0	0	1	500
E	Peptide 3	0	0	0	1	500
E	Peptide 4	0	0	0	1	500
E	Peptide 5	0	0	0	1	500

Table A-2. Overview of compounds investigated for Set Y in this study.

Sample Mixture	Compound	v/v				Concentration (ppm)
		THF	DMSO	ACN	H ₂ O	
B	Purpurin	0	0	1	1	1000
B	Emodin	0	0	4	0	100
A	Toluene	0	0	1	0	1000
A	Propylparaben	0	0	1	0	100
A, B, C	Uracil	0	0	1	1	100
A	Sudan I	0	0	1	0	1000
B	Rutin	0	0	25	75	100
B	Martius Yellow	0	0	1	0	1000
B	Naphthol Yellow S	0	0	1	1	1000
B	Orange IV	0	0	1	1	1000
A	Flavazine L	0	0	1	0	1000
A	Tyramine	0	0	0	1	100
B	Cytosine	0	0	1	1	100
A	Trimethoprim	0	0	1	1	1000
A	Propranolol	0	0	1	1	1000
C	Peptide 1	0	0	0	1	500
C	Peptide 2	0	0	0	1	500
C	Peptide 3	0	0	0	1	500
C	Peptide 4	0	0	0	1	500
C	Peptide 5	0	0	0	1	500
A	Berberine	0	0	1	1	1000

A-2. Retention time peak tables

These tables can be found online (DOI: 10.1016/J.CHROMA.2020.461780).

A-3. AIC Values

These tables can be found online (DOI: 10.1016/J.CHROMA.2020.461780).

A-4. AIC plot for Set Y

In Fig. A-1 the average AIC values for all components are shown for the five different models. The models are constructed with a 1, 1.5, 3, 3.75, 4.5, 6, 7.5, 9, 12, and 18 min scanning gradient.

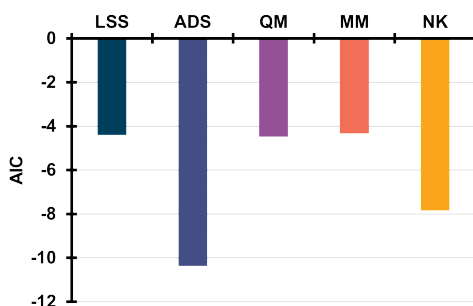


Figure A-1. Comparison of average AIC values for all studied components for the five different models using all repeats from all ten measured gradients for the repeatable data set (Set Y).

A-5. Prediction error for different models.

In Fig. A-2 the error in the prediction is shown for the extra compounds of Set X and Set Y that are not shown in Fig. 3.3. The models are based on a 3, 6, and 9 min scanning gradient.

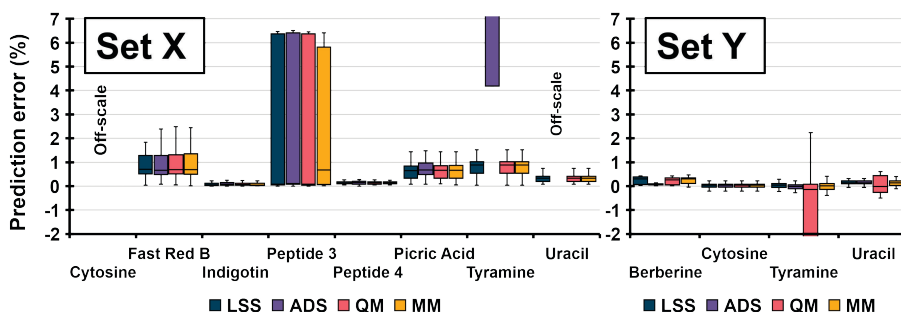


Figure A-2. Comparison of the relative prediction error for the extra compounds of Set X (left) and Set Y (right) using retention parameters obtained through a gradient time of 3, 6, and 9 min in the linear solvent strength (LSS, dark blue), adsorption (ADS, blue), quadratic (QM, purple) and the mixed mode (MM, pink) model. The box-and-whisker plots are all based on a total of 30 prediction errors, *i.e.* ten replicates for three different predicted gradients. The whiskers represent the distance from the minimum to the first quartile (0%-25%) and from the third quartile to the maximum (75%-100%) of each set of predictions. The box indicates the interquartile range between the first and third quartile (25%-75%), and the median (50%) is indicated by the horizontal line inside the box.

A-6. Retention plots for all models

The retention plots (Figs. A-3-12) can be found online (DOI: 10.1016/J.CHROMA.2020.461780).

A-7. Effect of scanning speed

In Fig. A-13 the effect of different scanning gradient speeds on the prediction of the remainder of compounds from Fig. 3.4.

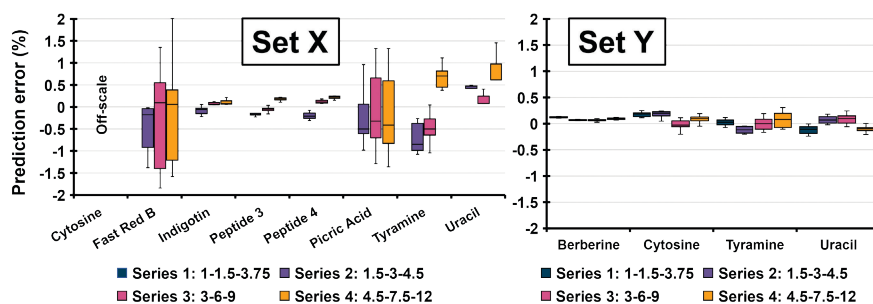


Figure A-13. Comparison of the relative prediction errors of the predicted retention times for the extra compounds of both sets using three (Set X, left) and four (Set Y, right) different sets of scanning gradients (effectively at different speeds), with different total durations. Predictions were made with the LSS model for Set X and the ADS model for Set Y. The box-and-whisker plots are all based on a total of 10 prediction errors, *i.e.* ten replicates for one predicted gradient.

A-8. Effect of number of repeats

In Fig. A-14 the pooled prediction error is shown over the number of repeats. Two gradients (4.5 and 7.5 min) are predicted with the standard set of a 3, 6, and 9 min gradient. This is done on Set X with the LSS model and for Set Y with the ADS model.

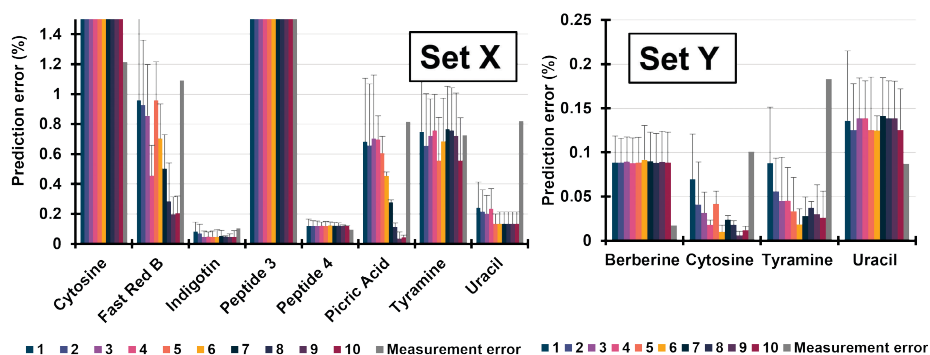


Figure A-14. Average prediction error of the retention times relative to the measured values of the remainder of compounds of Fig. 6 under a gradient time of 4.5 and 7.5 min, using 1 to 10 repeats of the recorded scanning gradients for Set X (left, using LSS model) and Set Y (right, using ADS model). The error of the predicted retention time is shown with the error bar and the measurement error is shown in grey on the right. Note that the y-axis scale is different.

A-9. Effect of scanning gradient-length distribution vs. the number of repeats

In Fig. A-15 two different sets of scanning gradients were compiled, each using a total of number of six retention times per compound for fitting the model. The first set consisted of three repeats of the 3 and the 9 min scanning gradient, henceforth referred to as set A,

whereas the second set comprised one repeat of six different scanning gradient times (1.5, 3, 3.75, 6, 9, 12 min), now referred to as set B. Both sets predicted a 4.5 and a 7.5 min gradient.

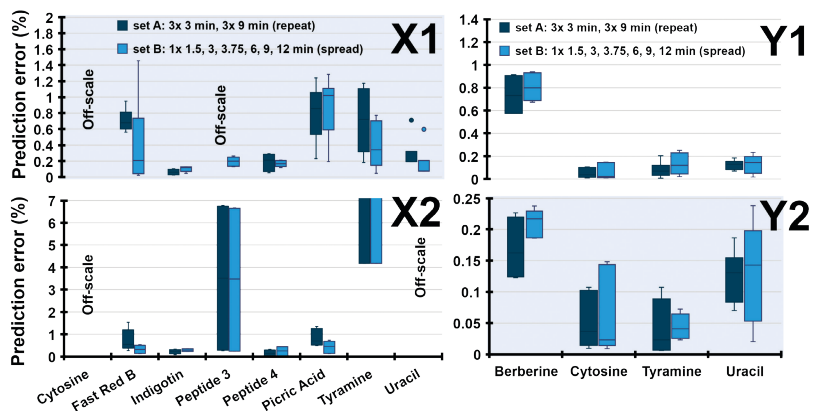


Figure A-15. Prediction error relative to the measured gradient time for two different sets of input scanning gradient data built by repeating measurement or spread measurements. Prediction performed in triplicate for both a 4.5 and a 7.5 min gradient for Set X (with a LSS model, X1; with an ADS model; X2) and for Set Y (with a LSS model, Y1; with an ADS model; Y2). The models with the best fit are indicated by the blue fill. Note the different y-axes. The box-and-whisker plots are all based on a total of 6 prediction errors, *i.e.* three replicates for two predicted gradient times.

A-10. Effect of the gradient-slope factor of the two most extreme scanning gradients

In Fig. A-16 the retention parameters calculated with the LSS model for Set X for different Γ values containing a scanning gradient of 3 min and another, yielding different factors. The top left figure shows the $\ln k_0$ parameter and the bottom left shows the S parameter. The retention parameters of Set Y are calculated with the ADS model with different gradient slopes containing a scanning gradient of 3 min and another, yielding different factors. The top right figure shows the $\ln k_0$ parameter and the bottom right shows the R parameter.

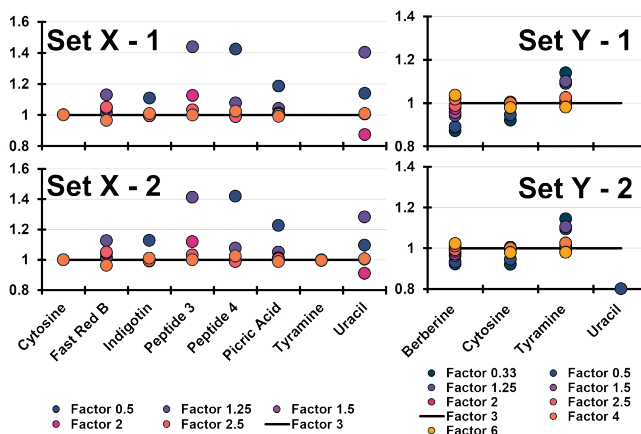


Figure A-16. Normalized $\ln k_0$ parameters of all DFs relative to the $\ln k_0$ parameter of DF = 3 for Set X (top left, Set X - 1) and the normalized s parameters of all DFs relative to the s parameter of DF = 3 for Set X (bottom left, Set X-2). Normalized $\ln k_0$ parameters of all DFs relative to the $\ln k_0$ parameter of DF = 3 for Set Y (top right, Set Y - 1) and the normalized R parameters of all DFs relative to the R parameter of DF = 3 for Set Y (bottom right, Set Y - 2). The black line represents the DF = 3 line. Data reflects average based on ten repeats.

In Fig. A-17 the prediction error in a 7.5 min gradient is shown for different Γ values between scanning gradients. This is performed with the LSS model for Set X and with the ADS model for Set Y. DFs 0.33, 0.5, 1.25, 1.5, 2, 2.5, 3, 4, and 6 are constructed with a 3 min gradient and a 1, 1.5, 3.75, 4.5, 6, 7.5, 9, 12, and 18 min gradient, respectively.

In Fig. A-18 the different approaches of calculating the effect of the DF are shown, where the purple lines indicate the coupled scanning gradients used to build the model, and the yellow boxes indicate the predicted gradient. The results of approach II, in which a 7.5 min gradient is predicted with different DFs, are shown in Fig. 9 and Fig. A-17 for Set X and Set Y, where the latter shows the remainder of compounds. The results of approach I are shown in Fig. A-19 and A-20 for Set X and Set Y. Approach III, IV, V and VI are calculated for Set Y and shown in Fig. A-21, Fig. A-22, Fig. A-23 and Fig. A-24 respectively.

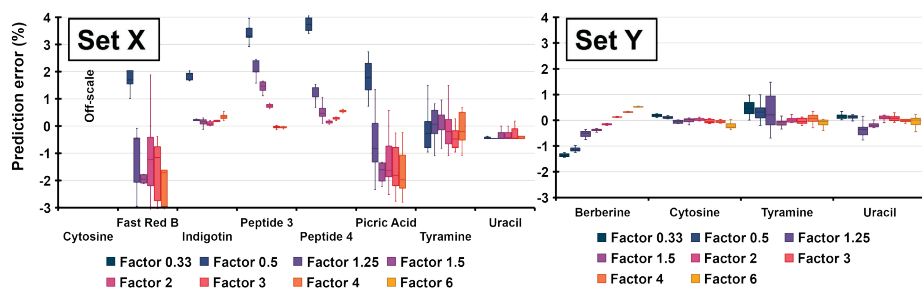


Figure A-17. Prediction error of the retention relative to the measured values in a 7.5 min gradient calculated with DFs for Set X (left) and Set Y (right). Predictions are made with the LSS model for Set X and the ADS model for Set Y. The box-and-whisker plots are all based on a total of 10 prediction errors, *i.e.* ten replicates for one predicted gradient (7.5 min). The whiskers represent the distance from the minimum to the first quartile (0%-25%) and from the third quartile to the maximum (75%-100%) of each set of predictions. The box indicates the interquartile range between the first and third quartile (25%-75%), and the median (50%) is indicated by the horizontal line inside the box.

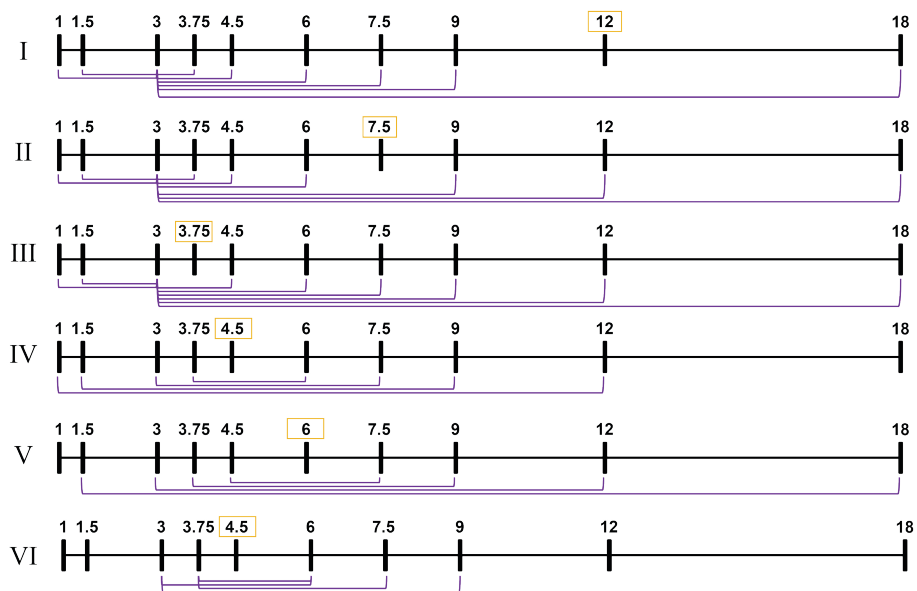


Figure A-18. Different approaches (I to IV) performed to determine the effect of the gradient-slope factor between gradient slopes. The purple lines indicate the two coupled scanning gradients, creating a specific gradient-slope factor. The yellow box indicates the predicted gradient.

In Fig. A-19 and A-20 the prediction error is shown for a predicted 12 min gradient, calculated with different Γ values. This is performed with the LSS model for Set X and with the ADS model for Set Y. DFs 0.33, 0.5, 1.25, 1.5, 2, 2.5, 3, and 6 are constructed with a 3 min gradient and a 1, 1.5, 3.75, 4.5, 6, 7.5, 9, and 18 min gradient, respectively.

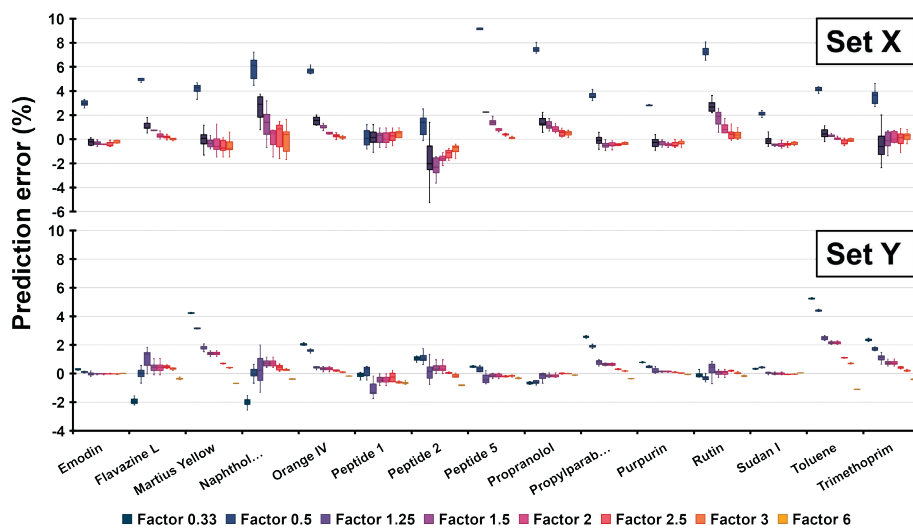


Figure A-19. Prediction error of the retention relative to the measured point in a 12 min gradient calculated with DFs for Set X (top) and Set Y (bottom) (Approach I). Predictions are made with the LSS model for Set X and the ADS model for Set Y. The box-and-whisker plots are all based on a total of 10 prediction errors, *i.e.* ten replicates for one predicted gradient (12 min).

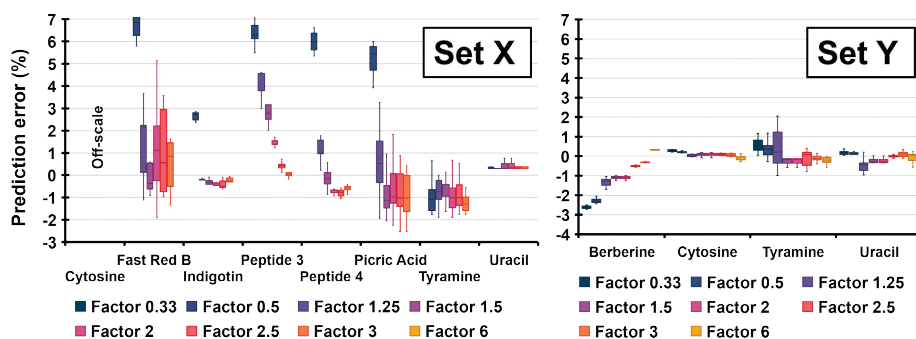


Figure A-20. Prediction error of the retention relative to the measured point in a 12 min gradient calculated with DFs for Set X (top) and Set Y (bottom) for the remainder of compounds (Approach I). Predictions are made with the LSS model for Set X and the ADS model for Set Y. The box-and-whisker plots are all based on a total of 10 prediction errors, *i.e.* ten replicates for one predicted gradient (12 min).

In Fig. A-21 the prediction error is shown for a predicted 3.75 min gradient, calculated with different Γ values. This is performed with the ADS model for Set Y. DFs 0.33, 0.5, 1.5, 2, 2.5, 3, 4, and 6 are constructed with a 3 min gradient and a 1, 1.5, 4.5, 6, 7.5, 9, 12, and 18 min gradient, respectively.

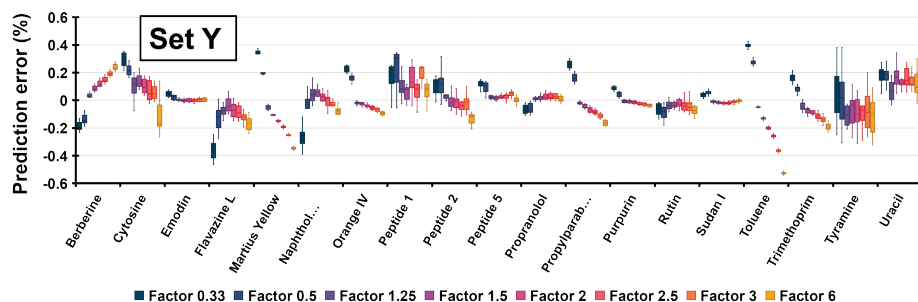


Figure A-21. Prediction error of the retention relative to the measured point in a 3.75 min gradient calculated with DFs for Set Y (Approach III). Predictions are made with the ADS model for Set Y. The box-and-whisker plots are all based on a total of 10 prediction errors, *i.e.* ten replicates for one predicted gradient (3.75 min).

Fig. A-22 shows the effect of an increasing Γ values by increasing the distance between both scanning gradients and the predicted gradient, which is 4.5 min in this case. This results in 4 combinations of scanning gradient with increasing DFs of 1.6 (3.75 and 6), 2.5 (3 and 7.5), 6 (1.5-9), and 12 (1 and 12). This has only been calculated for the data of Set Y.

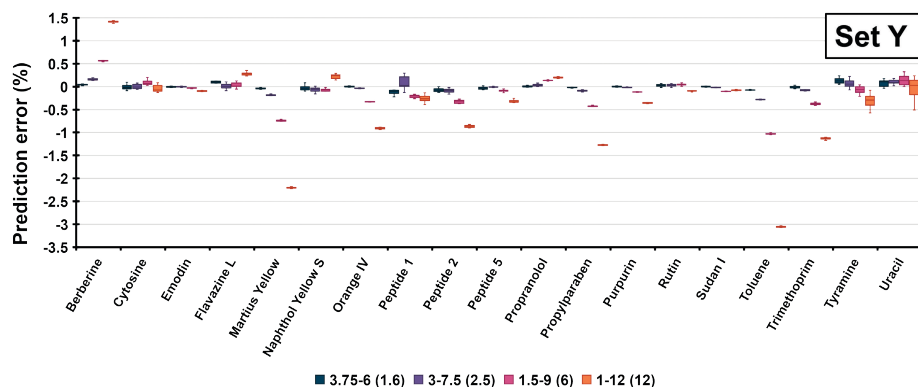


Figure A-22. Prediction error of the retention relative to the measured point in a 4.5 min gradient calculated with data of Set Y for different gradient-slope factors (Approach IV). Predictions are made with the ADS model for Set Y. The box-and-whisker plots are all based on a total of 10 prediction errors, *i.e.* ten replicates for one predicted gradient (4.5 min).

Fig. A-23 shows the effect of an increasing Γ values by increasing the distance between both scanning gradients and the predicted gradient, which is 6 min in this case. This results in 4 combinations of scanning gradient with increasing DFs of 1.67 (4.5 and 7.5), 2.4 (3.75 and 9), 4 (3-12), and 12 (1.5 and 18). This has only been calculated for the data of Set Y.

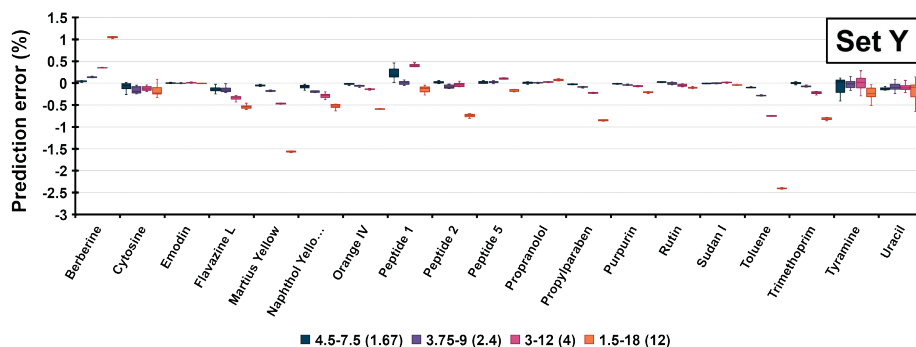


Figure A-23. Prediction error of the retention relative to the measured point in a 6 min gradient calculated with data of Set Y for different gradient-slope factors (Approach V). Predictions are made with the ADS model for Set Y. The box-and-whisker plots are all based on a total of 10 prediction errors, *i.e.* ten replicates for one predicted gradient (6 min).

Fig. A-24 shows the effect of different distances to the predicted gradient with similar factors by varying the scanning gradients. This has only been calculated for Set Y. The predicted gradient was a 4.5 min gradient, and this resulted in four different combinations of scanning gradients yielding the following Γ values: 1.6 (3.75 and 6), 2 (3.75 and 7.5), 2 (3-6), and 2.5 (3 and 7.5).

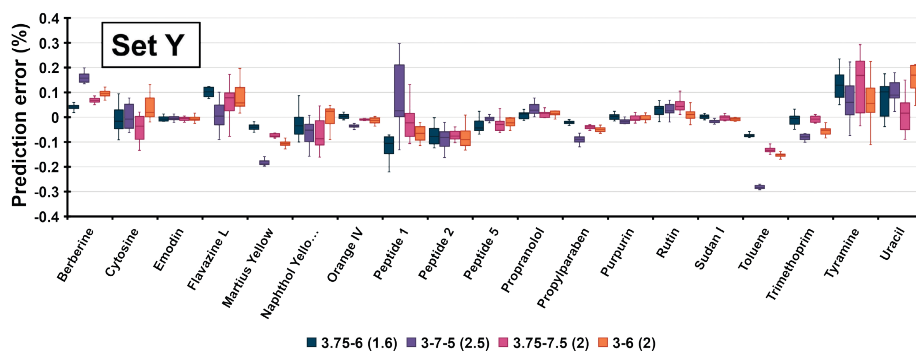


Figure A-24 Prediction error of the retention relative to the measured point in a 4.5 min gradient calculated with data of Set Y for different gradient-slope factors (Approach VI). Predictions are made with the ADS model for Set Y. The box-and-whisker plots are all based on a total of 10 prediction errors, *i.e.* ten replicates for one predicted gradient (4.5 min).

Fig. A-19 to A-24 and Fig. 3.9 together confirm the hypothesis that proximity of (at least one of) the slopes of the scanning gradients to the slope of the predicted gradient is a better indicator for a low prediction error than the gradient slope factor.

A-11. Limits of use

In Fig. A-25 the prediction error is shown for a 1.5 min gradient (*i.e.* steeper gradient) as a function of the number of sampled repeats. This is calculated with the LSS model for Set X and for the ADS model for Set Y. The remainder of compounds is shown in the figure.

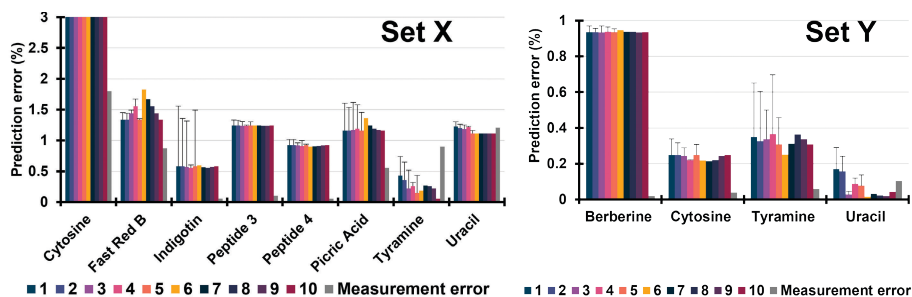


Figure A-25. Relative prediction errors per compound as a function of the number of sampled repeats for the 1.5-min gradient (*i.e.* the faster gradient) using the reference scanning gradient set (3, 6, and 9 min) for the remainder of compounds of Set X (left) and Set Y (right). Predictions are made with the LSS model for Set X and the ADS model for Set Y. The measured error is showed in grey.

In Fig. A-26 the prediction error is shown for a 12 min gradient (*i.e.* shallower gradient) as a function of the number of sampled repeats. This is calculated with the LSS model for Set X and for the ADS model for Set Y. The remainder of compounds is shown in the figure.

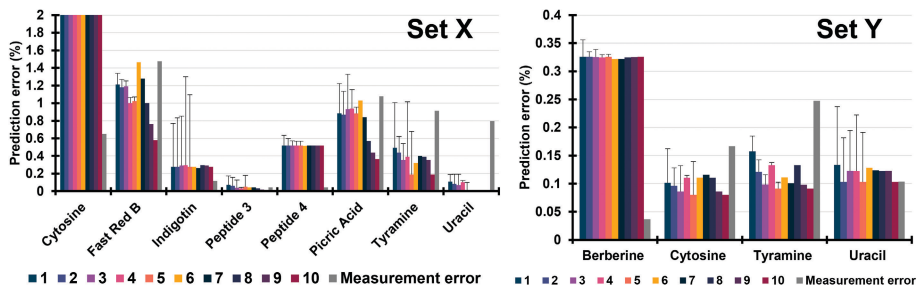


Figure A-26. Relative prediction errors per compound as a function of the number of sampled repeats for the 12-min gradient (*i.e.* the slower gradient) using the reference scanning gradient set (3, 6, and 9 min) for the remainder of compounds of Set X (left) and Set Y (right). Predictions are made with the LSS model for Set X and the ADS model for Set Y. The measured error is showed in grey.

In Fig. A-27 faster sets of gradients have been used to predict shallow gradients. The maximum gradient length of both data sets has been chosen, yielding a 12 min gradient for Set X and an 18 min gradient for Set Y. Both gradients have been predicted with two or three sets of gradients (see legend Fig. A-27).

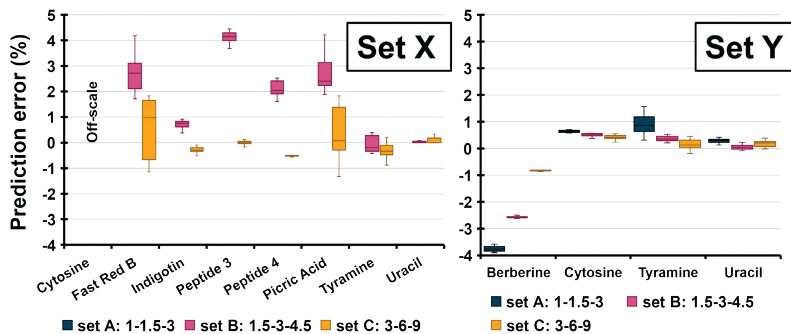


Figure A-27. Prediction error for the retention time relative to the measured point of all compounds in a 12 min (left) and in an 18 min (right) gradient calculated using two or three different sets of gradients (see legend). Predictions are made with the LSS model for Set X and the ADS model for Set Y. The box-and-whisker plots are all based on a total of 10 prediction errors, *i.e.* ten replicates for one predicted gradient (either 12 or 18 min).

Appendix B

Tables and figures in this appendix are related to Chapter 4: Assessing the Feasibility of Stationary-Phase-Assisted Modulation for Two-Dimensional Liquid-Chromatography Separations.

B-1. Overview of studied compounds

In this research, compounds were studied by introducing mixtures into the liquid chromatography separation. Table B-1 indicates the concentrations of all compounds in the mixtures.

Table B-1. Stock solutions and final concentrations of the used samples. The solvent for both stock solutions is H₂O/ACN (50:50%, v/v).

Stock solution 1		Stock solution 2	
Compound	Final concentration (ppm)	Compound	Final concentration (ppm)
Crystal violet	5	Toluene	100
Phenol	25	Acetaminophen	25
Uracil	25	Propranolol	50
4-Hydroxy benzoic acid	25	Trimethoprim	50
Orange G	50	Riboflavin	100

B-2. Dilution flow methods

In this research, four dilution flow series were performed starting at four ϕ concentrations (0.75, 0.5, 0.25 and 0.1) at a flow rate of 50 $\mu\text{L}\cdot\text{min}^{-1}$. All effluents were diluted 1:0, 1:1, 1:2, 1:3, 1:4, 1:6.5, 1:9, 14:1 and 19:1, corresponding to total flow rates of 50, 100, 150, 200, 250, 375, 500, 750 and 1000 $\mu\text{L}\cdot\text{min}^{-1}$. Details are shown in Table B-2 and Fig. B-1.

Table B-2. The four dilution flow series with corresponding flow rates and ϕ

Dilution ratio	1:0	1:1	1:2	1:3	1:4	1:6.5	1:9	1:14	1:19
Flow rate ($\mu\text{L}\cdot\text{min}^{-1}$)	50	100	150	200	250	375	500	750	1000
DF1	0.75	0.375	0.25	0.1875	0.15	0.1	0.075	0.05	0.0375
DF2	0.5	0.25	0.1667	0.125	0.1	0.0667	0.05	0.0333	0.025
DF3	0.25	0.125	0.0833	0.0625	0.05	0.0333	0.025	0.0167	0.0125
DF4	0.1	0.05	0.0333	0.025	0.02	0.0133	0.01	0.0067	0.005

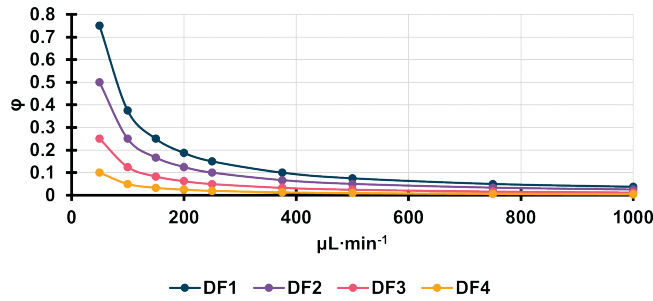


Figure B-1. Overview of the four dilution flow series starting at ϕ is 0.75 (DF1, blue), 0.5 (DF2, purple), 0.25 (DF3, pink), and 0.1 (DF4, yellow). All series consist of nine steps.

B-3. Overview of the gradient sets

In this research, five sets of gradients were used. The first four sets used three repeats of three different gradients, while set 5 consists of a single measurement of nine different gradients, yielding a total number of nine gradients of every set. Set 1 consists of 1-, 2-, and 3-min gradients, set 2 of 3-, 6-, and 9-min gradients, set 3 of 9-, 12-, and 15-min gradients, set 4 of 15-, 24-, and 48-min gradients, and set 5 consists of a 1-, 2-, 3-, 6-, 9-, 12-, 15-, 24-, and 48-min gradient.

B-4. Prediction error for the LSS and QUA model

The isocratic retention was predicted on analytical columns and trap columns with scanning-gradient data from analytical columns. The results are shown in Fig. B-2.

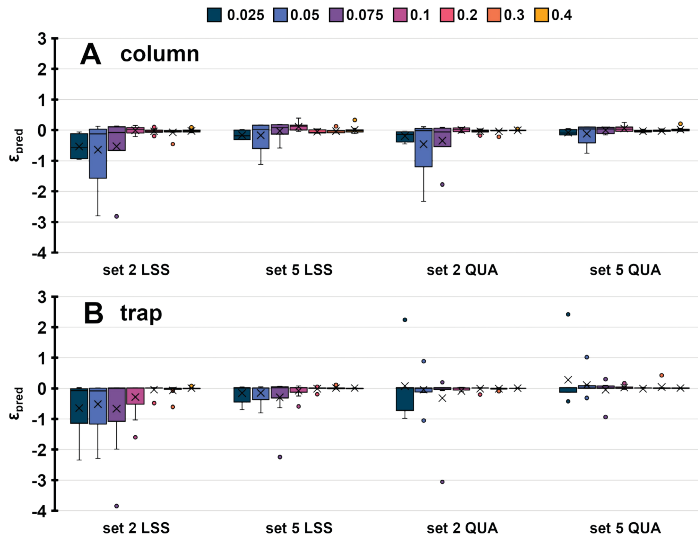


Figure B-2. Prediction error for the LSS and QUA model with gradient sets of 3, 6, and 9 min (set 2), and all gradients (1, 2, 3, 6, 9, 12, 15, 24, and 48 min, set 5) on the column (A) and trap (B). The colours indicate the different ϕ levels. The crosses indicate the average, while the points indicate outliers.

B-5. Deduction of compounds-specific dilution effect

To describe the effect of the dilution flow for a specific compound, the effect of the increasing flow on the retention time first has to be described (Eqs. B.1-B.7).

$$t_{R1} = (1 + k_1) \cdot t_0 \quad (\text{B.1})$$

$$t_{R,p} = (1 + k_p) \cdot \frac{V_0}{F_p} \quad (\text{B.2})$$

$$t_{R,q} = (1 + k_q) \cdot \frac{V_0}{F_q} \quad (\text{B.3})$$

$$\frac{t_{R,q}}{t_{R,p}} = \frac{1+k_q}{1+k_p} \cdot \frac{\frac{V_0}{F_q}}{\frac{V_0}{F_p}} \quad (\text{B.4})$$

$$\frac{t_{R,q}}{t_{R,p}} = \frac{1+k_q}{1+k_p} \cdot \frac{F_p}{F_q} \quad (\text{B.5})$$

$$\frac{t_{R,q}}{t_{R,p}} = \frac{1+k_q}{1+k_p} \cdot \frac{1F \cdot (1+p)}{1F \cdot (1+q)} \quad (\text{B.6})$$

$$\frac{t_{R,q}}{t_{R,p}} = \frac{1+k_q}{1+k_p} \cdot \frac{(1+p)}{(1+q)} \quad (\text{B.7})$$

Where q and p are two different dilution flows, V_0 and t_0 are the dead volume and dead time, respectively, F_q and F_p are the two different flow rates, $t_{R,q}$ and $t_{R,p}$ are the retention times at those dilutions flows and k_q and k_p are the retention factors at those dilution flows. When only the flow is changed, but the φ is kept constant, these two retention factors would be identical.

How the compounds retention changes at different flow rates, depends on their retention parameters of either the LSS model (Eqs. B.8 and B.9) or QUA model (Eqs. B.10 and B.11).

$$k_{p,LSS} = \exp\left(\ln k_0 - S_{LSS} \cdot \frac{\varphi}{1+p}\right) \quad (\text{B.8})$$

$$k_{q,LSS} = \exp\left(\ln k_0 - S_{LSS} \cdot \frac{\varphi}{1+q}\right) \quad (\text{B.9})$$

$$k_{p,QUA} = \exp\left(\ln k_0 - S_1 \cdot \frac{\varphi}{1+p} + S_2 \cdot \left(\frac{\varphi}{1+p}\right)^2\right) \quad (\text{B.10})$$

$$k_{q,QUA} = \exp\left(\ln k_0 - S_1 \cdot \frac{\varphi}{1+q} + S_2 \cdot \left(\frac{\varphi}{1+q}\right)^2\right) \quad (\text{B.11})$$

This can be combined into the ratio for the two models (LSS, Eq. B.12, QUA, Eq. B.13) to describe the change in retention time when a dilution flow is increased.

$$\frac{t_{R,q}}{t_{R,p}} = \frac{1 + \exp\left(\ln k_0 - S_{LSS} \cdot \frac{\phi}{1+q}\right)}{1 + \exp\left(\ln k_0 - S_{LSS} \cdot \frac{\phi}{1+p}\right)} \cdot \frac{1+p}{1+q} \quad (\text{B.12})$$

$$\frac{t_{R,q}}{t_{R,p}} = \frac{1 + \exp\left(\ln k_0 - S_1 \cdot \frac{\phi}{1+q} + S_2 \cdot \left(\frac{\phi}{1+q}\right)^2\right)}{1 + \exp\left(\ln k_0 - S_1 \cdot \frac{\phi}{1+p} + S_2 \cdot \left(\frac{\phi}{1+p}\right)^2\right)} \cdot \frac{1+p}{1+q} \quad (\text{B.13})$$

B-6. Dilution flow prediction error for different models

The retention of analytes under a dilution flow was predicted for four different dilution flow series with the LSS and the QUA model with a 3-, 6-, and 9-min gradient set (set 2) and an all-gradient set (1, 2, 3, 6, 9, 12, 15, 24, 48 min, set 5). Results are shown in Fig. B-3.

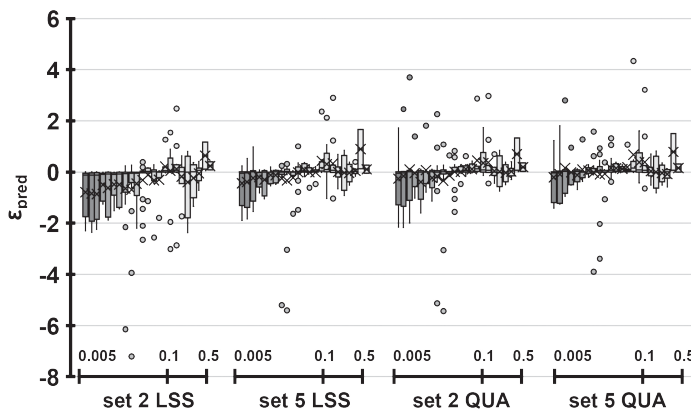


Figure B-3. Prediction errors for all compounds calculated with the LSS and QUA models with a gradient set of 3, 6, and 9 min (set 2) or with all gradients (1, 2, 3, 6, 9, 12, 15, 24, and 48 min, set 5); C18 trap column; four dilution-flow series (overlapping in the figure). The final composition is depicted on the horizontal axis for each cluster; the darkness of the bars also decreases with increasing ϕ values. The crosses indicate the average, the points indicate outliers.

B-7. Dilution flow prediction error for different gradient sets

The retention of analytes under a dilution flow was predicted for four different dilution flow series with the QUA model with a 1-, 2- and 3-min; 3-, 6- and 9-min; 9-, 12-, and 15-min; and 15-, 24-, and 48-min gradient sets or one repeat of nine different gradients (1, 2, 3, 6, 9, 12, and 15 min). The results are shown in Fig. B-4A and B-4B.

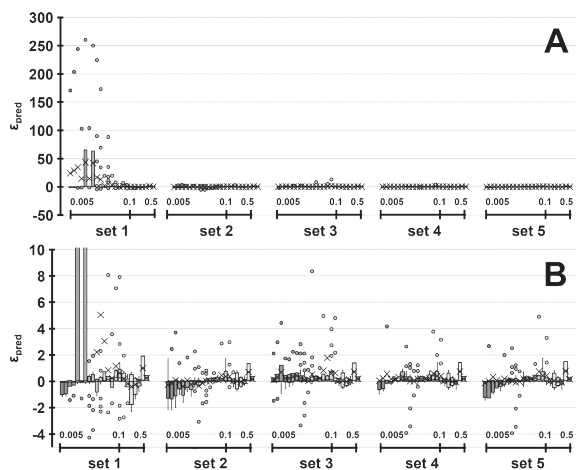


Figure B-4. A) Prediction error for all compounds calculated with five different gradient sets (three repeats of 1-, 2-, and 3- min; 3-, 6-, and 9-min; 9-, 12-, and 15-min; and 15-, 24-, and 48-min gradients or a single repeat of all nine gradients, set 1-5 respectively) for the trap columns subjected to four different dilution-flow series. The final composition is depicted on the horizontal axis for each cluster; the darkness of the bars also decreases with increasing ϕ values. The crosses indicate the average, the points indicate outliers. B) Close up of Fig. B-4A.

B-8. Effect of the mixer

To test the effect of the mixer, the same mix was injected into the setup used in this research and a setup with a mixer, resembling a two-dimensional liquid chromatography setup with a dilution flow. In Fig. B-5, the setup with mixer is indicated with yellow, while the one without mixer is shown in blue. It can be seen that the early eluting compounds have broader peaks, but that their peak top is at the same retention time. This can be accounted for in the tool by decreasing the plate number. For compounds eluting later, such as orange G, the peaks become very broad, but the retention is of the compound is also increased, not leading to sample loss.

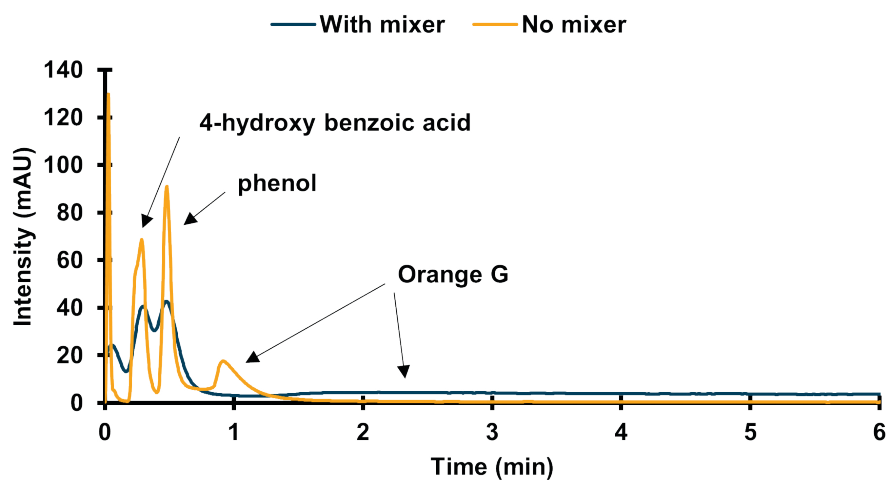


Figure B-5. Chromatogram of a mix of 4-hydroxy benzoic acid, phenol, orange G in the setup with mixer (blue) and without mixer (yellow).

Appendix C

Tables and figures in this appendix are related to Chapter 5: Comparing different light-degradation approaches for the degradation of Crystal Violet and Eosin Y.

C-1. Degradation procedure of the Xenotest

The Xenotest experiment was conducted with the following (ISO 105-B02) parameters: an irradiance of $E_{UV} = 42 \text{ W/m}^2$ and $E_v = 100.128 \text{ lux}$, a black standard temperature at 47°C , the chamber temperature at 32°C , and a relative humidity of 40%. Five samples of EY, CV and undyed silk were placed in the sample holders and sample were taken at: 0h, 2h, 4h (only EY), 6h, 15h, 35h and 80h (only CV). Afterwards, the colour change of the samples was tested with a spectrometer.

C-2. Degradation procedure of the Microfading Tester

For the fading experiments performed with the MicroFading tester, two different fading settings were used. The first setting is the standard and is as follows:

- > The distance between the lamp and the objective, called the distance illumination, is set at 24 mm
- > A spot size of 0.3 mm
- > A fading time of 10 minutes
- > With UV-IR filter

The second setting was used to induce fading on a bigger spot, which could be visible and would increase the chance of a successful extraction. The settings were as follows:

- > A distance illumination of 28 mm
- > The spot size could not be estimated with the microscope as it was outside its framework
- > A fading time of 20 minutes
- > No UV-IR filter

All measurements were conducted in threefold.

C-3. Degradation procedure of Spectrolinker

C-3.1. Degradation procedure for in-solution degradation in the Spectrolinker

For the degradation in solution, 10 mL of each dye solution was poured into a beaker. Subsequently, the beaker was placed inside the UV light box and covered with a glass plate. Samples were taken at: 0, 0.01, 0.02, 0.03, 0.04, 0.05, 0.1, 0.15, 0.2, 0.3, 0.45, 0.6, 0.8, and 1 J/mm². The solution was weighted when the samples were taken to correct for evaporation of the solvent.

C-3.2. Degradation procedure for on-textile degradation in the Spectrolinker

Each textile sample (EY, CV and undyed silk) was cut in small strips of approximately 15 by 30 mm. One strip of each sample was not degraded and used as non-degraded sample. Subsequently, the other strips are placed in the UV light box and the cover is moved along with increasing dose to create a stepwise degradation process to follow the degradation of the dyes on the silk. The uncovered samples were placed underneath a glass plate to filter the deep UV wavelengths. The total dose of energy was 1 J/mm². An undyed silk sample was degraded in the same manner to correct for the degradation products of the silk itself. Five samples of dose 0, 0.55, 0.80, 0.90 and 1 J/mm² were extracted and measured with LC-MS.

C-4. Online coupling of liquid-core waveguide to LC

For this research, the liquid-core-waveguide cell (LCW cell) of Groeneveld *et al.* was used [18]. For the coupling of the liquid-core-waveguide light cell, the cell was coupled to a six-port injection valve with a 50 μ L loop. This six-port valve was connected within a LC system as injector. The volume of the LCW cell is 60 μ L and the volume of the tubing between the LCW and the six-port valve is 12 μ L. The LCW is flushed with a volume of 60 μ L to transfer the sample to the loop. The sample is then injected in the LC system when the run is started. This setup is shown in Fig. C-1.

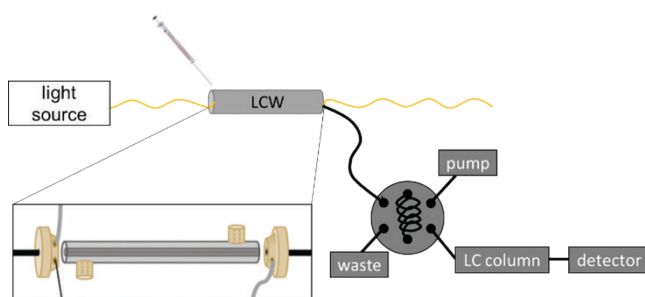


Figure C-1. Schematic setup of the coupling of the liquid-core waveguide to the liquid chromatography system.

C-5. Mass spectrometric data EY and CV

To examine the mass-spectral and absorption spectra of EY and CV and their degradation products, the absorption maxima and the m/z values are shown in Table C-2 for EY and Table C-3 for CV.

Table C-1. Overview of the identified degradation products of EY with their chemical formula, the absorbance maxima, and the m/z values used for the detection of the precursor and product ions.

Name	Formula	Abs (nm)	Precursor ion (m/z)	Product ions (m/z)
EY	$C_{20}H_7Br_4O_5^-$	530	646.7	602.7, 522.8 , 442.9
EY-1Br	$C_{20}H_8Br_3O_5^-$	522	566.8	522.8, 442.9
EY-2Br	$C_{20}H_9Br_2O_5^-$	522	488.88	444.9 , 381.0, 365.0, 363.0
EY-2Br		522	488.8	444.9 , 365.0
EY-3Br	$C_{20}H_{10}Br_1O_5^-$	516	410.9	366.9 , 355.0, 329.0, 301.0, 285.0, 273.0
EY-3Br		516	411.1	366.9 , 343.0, 322.3, 285.0, 263.1
BHBA	$C_{14}H_8Br_2O_5$	226/286/342	414.8	370.9, 266.8

Table C-2. Overview of the identified degradation products of CV with their chemical formula, the absorbance maxima, and the m/z values used for the detection of the precursor and product ions.

Name	Formula	Abs (nm)	Precursor ion (m/z)	Product ions (m/z)
CV	$C_{25}H_{30}N_3^+$	590	372.2	356.2 , 328.3, 251.2, 236.2
CV-1Me	$C_{24}H_{28}N_3^+$	582	358.2	342.2 , 251.16, 237.12
CV-2Me	$C_{23}H_{26}N_3^+$	575	344.2	329.2, 237.12 , 223.0
CV-2Me		580	344.2	328.2, 300.2, 251.08 , 223.08
CV-3Me	$C_{22}H_{24}N_3^+$	570	330.2	315.16 , 237.12, 223.08, 209.08
CV-4Me	$C_{21}H_{22}N_3^+$	560	316.2	301.16 , 223.12, 209.08
MK	$C_{17}H_{21}N_2O^+$	375	269.1	148.04
MK-1Me	$C_{16}H_{19}N_2O^+$	370	255.1	134.04, 148.04

C-6. Sample preparation

C-6.1. Stock solution

The stock solutions of the dyes were made by dissolving the dyes in ultrapure water. The concentrations were as high as possible without precipitation of the dyes: 100 μ M for Eo and 250 μ M for CV.

C-6.2. Textile dyeing procedure

The dyeing processes of EY and CV are slightly different as the former is an acid dye and the latter a basic dye. For both processes, the water to textile ratio was 75:1. See recipe for 10 g of textile below.

For the dyeing process of EY on silk, a 1000 ml beaker is filled with 750 mL ultrapure water and heated to 70°C in an oven. Then 50 g of sodium sulphate is added with 75 mg EY and 200 μ L sulphuric acid is added to the water. The silk (10g) is then soaked in the dye bath for 30 minutes at 70°C while stirred every 5 minutes. The silk is then cooled in the dye bath and subsequently rinsed with ultrapure water.

For the dyeing process of CV on silk, a 1000 mL beaker is filled with 750 mL ultrapure water and heated to 70°C. Then 50 mg of CV is added to the solution and 10 g of silk is soaked in the dye bath. The dyeing solution is kept constant at 70°C for 30 minutes and stirred every 5 minutes. The dye bath is then cooled to room temperature and subsequently rinsed with ultrapure water.

The amount of dye is dependent on the weight of the silk and the desired intensity. The amount of sodium sulphate and sulphuric acid is dependent on the volume of the water. The total weight of the silk was 13 g for EY and 11 g for CV.

C-6.3. Extraction Procedure

For the extraction procedure of EY and CV, the same method was used. A sample of 1 mg textile was taken and placed inside a 1 mL glass vial, 200 μ L DMSO was added to fully wet the textile with the solvent. Subsequently, the glass vials were vertically placed in a water bad at 80°C for 10 minutes. Then the solution was pipetted in a 250 μ L insert vial for a HPLC vial and centrifuged for 10 minutes. Finally, the sample was analysed with HPLC. The extraction was conducted in threefold per sample and each extract was analysed in duplicate. Since the Microfading tester (MFT) samples were smaller than 1 mg, the volume of DMSO added was adjusted to their weight to ensure that the ratio silk/DMSO was similar for all samples.

C-7. Reflectance measurements of MFT samples

The first experiments of the MFT were recorded with the standard setting, resulting in a spot size which was too small to observe with the naked eye (0.3 mm). Therefore, the degradation is monitored by the colour change of the textile (see Fig. C-2). After 10 minutes of fading the total energy dose was 24 J/mm² and the total light dose was 1.8 Mlx.hr.

In Figure C-2A, the ΔE_{76} values over time for EY, CV and undyed silk are depicted together with the blue wool standards 1 to 3 (BW1, BW2, BW3). The ΔE_{76} value of CV is higher than that of BW1 and EY is between BW2 and BW3 (Figure C-2A). The ΔE_{00} values over time of EY, CV, undyed silk and the blue wool standards 1 to 3 are shown in Figure C-2B. The ΔE_{00} values of CV and the BW1-3 values have decreased compared to the ΔE_{76} values while the values

for EY did not decrease (Figure C-2B). The colour change of CV- and EY-dyed silk are close together (Figure C-2B). An undyed silk sample was also faded under the same conditions with minimal colour change.

The same trend is found in the Xenotest results, with a ΔE_{76} for CV larger than for EY while the ΔE_{00} for CV is (slightly) smaller than EY. Furthermore, the degradation of the undyed silk resulted in hardly any colour change during degradation in the Xenotest as well.

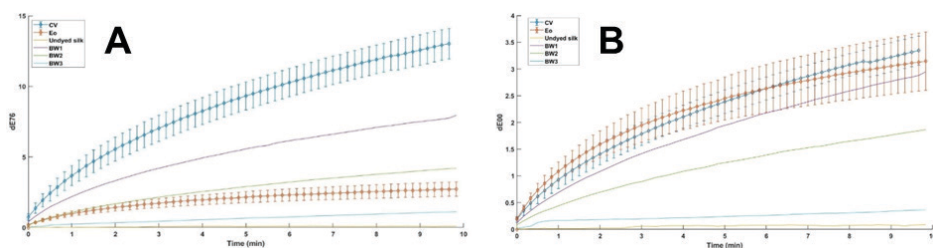


Figure C-2. Colour change over time for EY, CV, and undyed silk compared to the blue wool standards 1, 2 and 3 for ΔE_{76} (A) and for ΔE_{00} (B). In both graphs, the last data point of CV is missing.

Appendix D

Tables and figures in this appendix are related to Chapter 6: Combining photodegradation in a liquid-core-waveguide cell with multiple-heart-cut two-dimensional liquid chromatography. Appendix D-1 and D-4 are also related to Chapter 7: Incorporating a liquid-core-waveguide cell in recycling liquid chromatography for detailed studies of photodegradation reactions.

D-1. Schematic overview of the LCW-cell box

In Fig. D-1, the LCW-cell box is shown. The sample is introduced at A, where it is transferred to the LCW cell (E). After degradation, the sample is flushed from the cell through PEEK tubing (G) to the ^2D -injection loop (I). If the loop is overfilled, the sample is flushed to the waster (K). The ^2D binary pump (H) empties the loop onto the ^2D column (J). The light comes in through the light fibre cable on the left (B) and moves through the filter wheel (C), which was not operated in this research. In this research, the gas inlet was not controlled (D and F) and the absorption spectra were not collected (right, B).

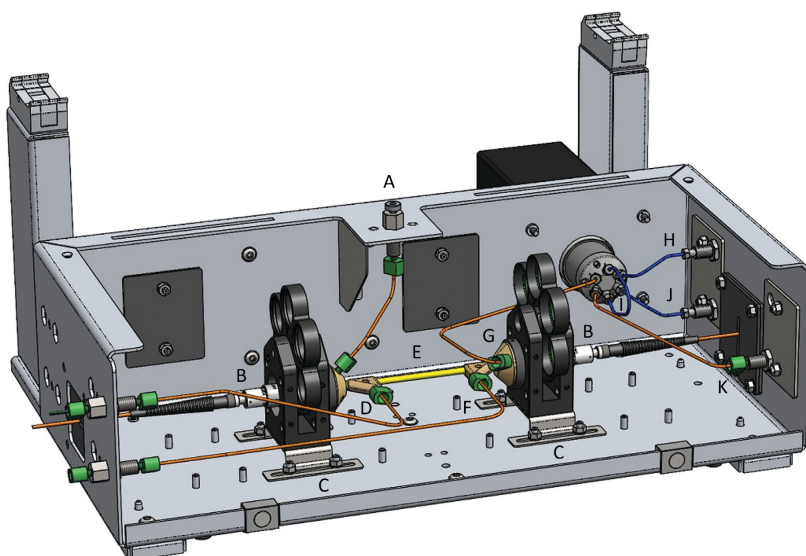


Figure D-1. Schematic overview of the box of the liquid-core-waveguide (LCW) cell. Design and drawings by courtesy of Edwin Beekwilder.

D-2. Optimization of time-based multiple-heart-cut 2DLC method

In Table D-1, the cut times of the four different multiple-heartcut methods are shown.

Table D-1. The start and end times of the cuts of the multiple-heart-cut methods. The last column indicates the method.

Compound	Start time	End time	Method
Fake cut	5.0	5.1	Test mix
Riboflavin	5.2	5.3	Test mix
Crystal Violet	7.69	7.79	Test mix
Eosin Y	8.81	8.91	Test mix
Fake cut	5.00	5.1	Fuchsin
M0	5.83	5.93	Fuchsin
M1	6.14	6.24	Fuchsin
M2	6.44	6.54	Fuchsin
M3	6.73	6.83	Fuchsin
Fake cut	5.00	5.1	Annatto
Bixin	10.61	10.71	Annatto
Fake cut	5.00	5.1	Vitamin B
Riboflavin	5.54	5.64	Vitamin B

D-3. Time schedule of the multiple-heart-cut two-dimensional liquid chromatography method for different degradation intervals

In this research, different methods were used for different samples. In Table D-2-4, these methods are described with their corresponding times and the isocratic-pump flow rate. In Table D-2, the methods are described for the test mix at different degradation periods. In Table D-3, the methods are described for the different degradation times for fuchsin. In Table D-4, the methods are described for both bixin from the annatto extract and for riboflavin from the vitamin-B extract.

Table D-2. Timings and flow of the multiple-heart-cut 2DLC method for 0-, 10-, 20- and 30-min degradation of the test mix.

Test mix 0 / 10 min	Test mix 20 min	Test mix 30 min	Flow ^{iso} P (mL/min)	Remarks
0.00	0.00	0.00	0.05	Start run
5.00	5.00	5.00	0.05	First (fake) cut
5.20	5.20	5.20	0.05	RF cut
7.69	7.69	7.69	0.05	CV cut
8.70	8.70	8.70	0.05	EY cut
8.81	8.81	8.81	0.05	EY from loop to the LCW
9.81	9.81	9.81	0.05	EY in the LCW
9.82	9.82	9.82	0.00	Stop flow and start degradation EY
19.20	29.20	39.20	0.00	End of degradation EY
19.21	29.21	39.21	0.05	Start EY flow to ² D loop
20.81	30.81	40.81	0.05	EY in the ² D loop + ² D injection valve switch
21.81	31.81	41.81	0.05	CV in the LCW
21.82	31.82	41.82	0.00	Stop flow and start degradation CV
31.20	51.20	71.20	0.00	End of degradation CV
31.21	51.21	71.21	0.05	Start CV flow to ² D loop
32.81	52.81	72.81	0.05	CV in the ² D loop + ² D injection valve switch
33.81	53.81	73.81	0.05	RF in the LCW
33.82	53.82	73.82	0.00	Stop flow and start degradation RF
43.20	73.20	103.20	0.00	End of degradation RF
43.21	73.21	103.21	0.05	Start RF flow to ² D loop
44.81	74.81	104.81	0.05	RF in the ² D loop + ² D injection valve switch
45.81	75.81	105.81	0.05	Fake cut in the LCW
45.82	75.82	105.82	0.00	Stop flow and start degradation fake cut
55.20	95.20	135.20	0.00	Stop degradation fake cut
55.21	95.21	135.21	0.05	Start fake cut flow to ² D loop
56.81	96.81	136.81	0.05	End run

Table D-3. Timings and flow of the multiple-heart-cut 2DLC method for 0- and 60-min degradation of all four fuchsin components (M0, M1, M2, and M3) and for 240 min degradation of M1. The fourth column indicates the remarks about the all-four method, while the fifth column indicates the remarks for 240-min degradation of only fuchsin (magenta I, M1).

Fuchsin all 0 / 10 min	Fuchsin all 60 min	Fuchsin only M1 240 min	Flow ^{iso} P (mL/min)	Remarks fuchsin all	Remarks fuchsin only M1
0.00	0.00	0.00	0.05	Start run	Start run
5.00	5.00	5.00	0.05	Fake cut	Fake cut
5.83	5.83	-	0.05	M0 cut	-
6.14	6.14	6.14	0.05	M1 cut	M1 cut
6.44	6.44	-	0.05	M2 cut	-

Table D-3. (continued)

Fuchsin all 0 / 10 min	Fuchsin all 60 min	Fuchsin only M1 240 min	Flow ¹⁸O-P (mL/min)	Remarks fuchsin all	Remarks fuchsin only M1
6.73	6.73	-	0.05	M3 cut	-
7.73	7.73	7.14	0.05	M3 from loop to the LCW	M1 from loop to the LCW
7.74	7.74	7.15	0.00	Start degradation M3	Start degradation M1
17.12	67.12	246.53	0.00	End of degradation M3	End of degradation M1
17.13	67.13	246.54	0.05	Start M3 flow to ² D loop	Start M1 flow to ² D loop
18.73	68.73	248.14	0.05	M3 in the ² D loop + ² D injection valve switch	M1 in the ² D loop + ² D injection valve switch
19.73	69.73	249.14	0.05	M2 from loop to the LCW	Start flow fake cut to the LCW
19.74	69.74	249.15	0.00	Start degradation M2	Stop flow and start degradation fake cut
29.12	129.12	258.53	0.00	End of degradation M2	Stop degradation fake cut
29.13	129.13	258.54	0.05	Start M2 flow to ² D loop	Start fake cut flow to ² D loop
30.73	130.73	260.14	0.05	M2 in the ² D loop + ² D injection valve switch	End run
31.73	131.73	-	0.05	M1 from loop to the LCW	
31.74	131.74	-	0.00	Start degradation M1	
41.12	191.12	-	0.00	End of degradation M1	
41.13	191.13	-	0.05	Start M1 flow to ² D loop	
42.73	192.73	-	0.05	M1 in the ² D loop + ² D injection valve switch	
43.73	193.73	-	0.05	M0 from loop to the LCW	
43.74	193.74	-	0.00	Start degradation M0	
53.12	253.12	-	0.00	End of degradation M0	
53.13	253.13	-	0.05	Start M0 flow to ² D loop	
54.73	254.73	-	0.05	M0 in the ² D loop + ² D injection valve switch	
55.73	255.73	-	0.05	Fake cut in the LCW	
55.74	255.74	-	0.00	Stop flow and start degradation fake cut	
65.12	315.12	-	0.00	Stop degradation fake cut	

Table D-3. (continued)

Fuchsin all 0 / 10 min	Fuchsin all 60 min	Fuchsin only M1 240 min	Flow ^{iso} P (mL/min)	Remarks fuchsin all	Remarks fuchsin only M1
65.13	315.13	-	0.05	Start fake cut flow to ² D loop	
66.73	316.73	-	0.05	End run	

Table D-4. Timings and flow of the multiple-heart-cut 2DLC method for 0-, 10-, 30-, 60- and 120-min degradation of bixin from an annatto extract (columns one to four) and the 0-, 10-, and 30-min degradation of riboflavin from a vitamin-B complex sample (columns five and six).

Annatto 0 / 10 min	Annatto 30 min	Annatto 6 0 min	Annatto 120 min	Vit. B 0 / 10 min	Vit. B 30 min	Flow (mL/min)	Remark
0.00	0.00	0.00	0.00	0.00	0.00	0.05	Start
5.00	5.00	5.00	5.00	5.00	5.00	0.05	Fake cut
10.61	10.61	10.61	10.61	5.54	5.54	0.05	Cut bixin / RF
11.61	11.61	11.61	11.61	6.54	6.54	0.05	Sample to the LCW
11.62	11.62	11.62	11.62	6.55	6.55	0.00	Start degradation sample
21.00	41.00	71.00	131.00	15.93	35.93	0.00	End degradation sample
21.01	41.01	71.01	131.01	15.94	35.94	0.05	Start flow sample to ² D loop
22.61	42.61	72.61	132.61	17.54	37.54	0.05	Sample in the ² D loop + ² D injection valve switch
23.61	43.61	73.61	133.61	18.54	38.54	0.05	Fake cut in the LCW
23.62	43.62	73.62	133.62	18.55	38.55	0.00	Stop flow and start degradation fake cut
33.00	53.00	83.00	143.00	27.93	47.93	0.00	Stop degradation fake cut
33.01	53.01	83.01	143.01	27.94	47.94	0.05	Start fake cut flow to ² D loop
34.61	54.61	84.61	144.61	29.54	49.54	0.05	End run

D-4. Structures of fuchsin and its derivatives

In Figs. D-2-4 the main components of the fuchsin mixture are shown. The structures have a different methylation degree, with pararosanine (M0, Fig. D-2) being the demethylated form, fuchsin the singly methylated product (M1, Fig. D-3), magenta II having two methylated sites (M2, Fig. D-4) and new fuchsin being the completely methylated form (M3, Fig. D-5).

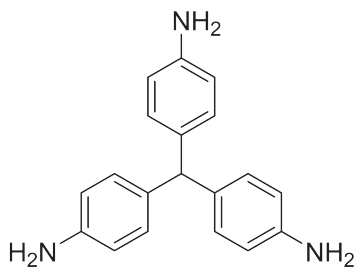


Figure D-2. Structure of pararosaniline or magenta 0 (M0).

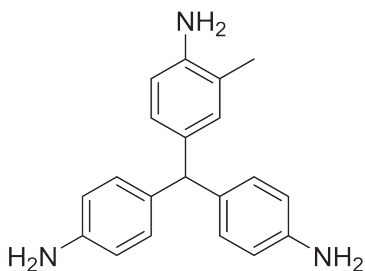


Figure D-3. Structure of fuchsin or magenta I (M1)

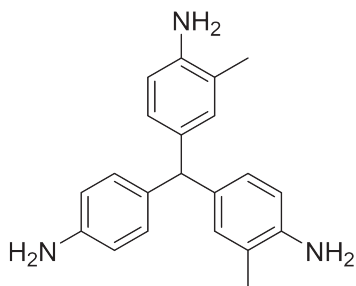


Figure D-4. Structure of magenta II (M2)

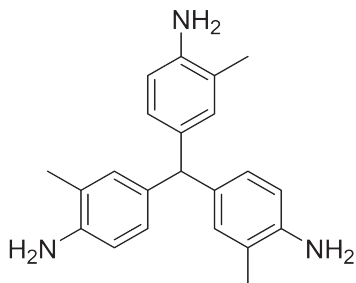


Figure D-5. Structure of new fuchsin or magenta III (M3).

Appendix E

Tables and figures in this appendix are related to Chapter 7: Incorporating a liquid-core-waveguide cell in recycling liquid chromatography for detailed studies of photodegradation reactions.

E-1. Time schedule of the LC-(LCW)LCn setup

In this research, several methods were used for the samples measured. In Table E-1-7, these methods are described with their corresponding times, the composition of the gradient pump and the isocratic-pump flow rate. In Table E-1, the methods are described for the transfer of RF one or two times. In this method the riboflavin (RF) has a residence time in the LCW of 10 min, which is repeated twice.

Table E-1. Timings, composition, and flow of the transfer of riboflavin.

Binary pump				Isocratic pump		Comment
Time [min.]	A [%]	B [%]	Flow [ml/min]	Time [min.]	Flow [ml/min]	
0.00	100.00	-	0.400	0.00	0.050	
1.00	100.00	-	0.400	6.21	0.050	
10.00	-	100.00	0.400	6.22	0.050	1st RF peak
11.00	-	100.00	0.400	7.27	0.050	
11.01	100.00	-	0.400	7.28	0.000	
20.03	100.00	-	0.400	17.27	0.000	
21.03	100.00	-	0.400	17.28	0.050	
30.03	-	100.00	0.400	20.03	0.050	valve to B
31.03	-	100.00	0.400	26.53	0.050	
31.04	100.00	-	0.400	26.54	0.050	2nd RF peak
40.36	100.00	-	0.400	27.59	0.050	
41.36	100.00	-	0.400	27.60	0.000	
50.36	-	100.00	0.400	34.00	0.000	valve to A
51.36	-	100.00	0.400	37.60	0.000	
51.37	100.00	-	0.400	37.61	0.050	
55.00	100.00	-	0.400	40.36	0.050	valve to B
end time: 55.00 min.				55.00	0.050	valve to A

Valve switch (min.)						
Selection valve	6.22	to position 1	Recycling valve	20.03	to B	
	26.54	to position 2		34.00	to A	
				40.36	to B	
				55.00	to A	

In Table E-2 the method is described of the 0-h degradation of fuchsin. In this method the selection valve switched from position 2 to position 1 at 6.47 min and the recycling valve was switched to B at 12.76 min. In Table E-3, the method is described for the 4-h degradation of fuchsin. In this method the selection valve switched from position 2 to position 1 at 6.47 min and the recycling valve was switched to B at 250.29 min.

Table E-3. Timings, composition, and flow of 0-h degradation of fuchsin.

Binary pump				Isocratic pump		
Time [min.]	A [%]	B [%]	Flow [ml/min]	Time [min.]	Flow [ml/min]	Comment
0.00	100.00	-	0.400	0.00	0.050	
1.00	100.00	-	0.400	6.46	0.050	
10.00	-	100.00	0.400	6.47	0.050	Fuchsin peak
11.00	-	100.00	0.400	7.52	0.050	
11.01	100.00	-	0.400	7.53	0.000	
12.76	100.00	-	0.400	10.00	0.000	
13.76	100.00	-	0.400	10.01	0.050	
22.76	-	100.00	0.400	12.76	0.050	valve to B
23.76	-	100.00	0.400	27.00	0.050	
23.77	100.00	-	0.400			
27.00	100.00	-	0.400			

end time: 27.00 min.

Table E-3. Timings, composition, and flow of 4-h degradation of fuchsin.

Binary pump				Isocratic pump		
Time [min.]	A [%]	B [%]	Flow [ml/min]	Time [min.]	Flow [ml/min]	Comment
0.00	100.00	-	0.400	0.00	0.050	
1.00	100.00	-	0.400	6.46	0.050	
10.00	-	100.00	0.400	6.47	0.050	Fuchsin peak
11.00	-	100.00	0.400	7.52	0.050	
11.01	100.00	-	0.400	7.53	0.000	
15.00	100.00	-	0.400	247.53	0.000	
15.01	100.00	-	0.050	247.54	0.050	
224.00	100.00	-	0.050	250.29	0.050	valve to B
225.00	100.00	-	0.400	265.00	0.050	
250.29	100.00	-	0.400			
251.29	100.00	-	0.400			
260.29	-	100.00	0.400			
261.29	-	100.00	0.400			
261.30	100.00	-	0.400			
265.00	100.00	-	0.400			

end time: 265.00 min.

In Table E-4, the method is described of the 0-h degradation of annatto. In this method the selection valve switched from position 2 to position 1 at 11.55 min and the recycling valve was switched to B at 17.76 min. In Table E-5, the method is described for the 4-h degradation of fuchsin. In this method the selection valve switched from position 2 to position 1 at 11.55 min and the recycling valve was switched to B at 135.37 min.

Table E-4. Timings, composition, and flow of 0-h degradation of bixin.

Binary pump				Isocratic pump		
Time [min.]	A [%]	B [%]	Flow [ml/min]	Time [min.]	Flow [ml/min]	Comment
0.00	100.00	-	0.400	0.00	0.050	
1.00	100.00	-	0.400	11.54	0.050	
10.00	-	100.00	0.400	11.55	0.050	Bixin peak
11.00	-	100.00	0.400	12.60	0.050	
11.01	100.00	-	0.400	12.61	0.000	
17.76	100.00	-	0.400	15.00	0.000	
18.76	100.00	-	0.400	15.01	0.050	
27.76	-	100.00	0.400	17.76	0.050	valve to B
28.76	-	100.00	0.400	32.00	0.050	
28.77	100.00	-	0.400			
32.00	100.00	-	0.400			

end time: 32.00 min.

Table E-5. Timings, composition, and flow of 2-h degradation of bixin.

Binary pump				Isocratic pump		
Time [min.]	A [%]	B [%]	Flow [ml/min]	Time [min.]	Flow [ml/min]	Comment
0.00	100.00	-	0.400	0.00	0.050	
1.00	100.00	-	0.400	11.54	0.050	
10.00	-	100.00	0.400	11.55	0.050	Bixin peak
11.00	-	100.00	0.400	12.60	0.050	
11.01	100.00	-	0.400	12.61	0.000	
15.00	100.00	-	0.400	132.61	0.000	
15.01	100.00	-	0.050	132.62	0.050	
120.00	100.00	-	0.050	135.37	0.050	valve to B
120.01	100.00	-	0.400	150.00	0.050	
135.37	100.00	-	0.400			
136.37	100.00	-	0.400			
145.37	-	100.00	0.400			
146.37	-	100.00	0.400			
146.38	100.00	-	0.400			
150.00	100.00	-	0.400			

end time: 150.00 min.

In Table E-6, the method is described of the 30-min degradation of formyl-methyl flavin, a degradation product of riboflavin. The riboflavin was degraded for 30 min.

Table E-6. Timings, composition, and flow of the 30-min degradation of formyl-methyl flavin.

Binary pump				Isocratic pump		
Time [min.]	A [%]	B [%]	Flow [ml/min]	Time [min.]	Flow [ml/min]	Comment
0.00	100.00	-	0.400	0.00	0.050	
1.00	100.00	-	0.400	6.21	0.050	
10.00	-	100.00	0.400	6.22	0.050	1st RF peak
11.00	-	100.00	0.400	7.27	0.050	
11.01	100.00	-	0.400	7.28	0.000	
40.03	100.00	-	0.400	37.27	0.000	
41.03	100.00	-	0.400	37.28	0.050	
50.03	-	100.00	0.400	40.03	0.050	valve to B
51.03	-	100.00	0.400	46.66	0.050	
51.04	100.00	-	0.400	46.67	0.050	FMF peak
80.49	100.00	-	0.400	47.72	0.050	
81.49	100.00	-	0.400	47.73	0.000	
90.49	-	100.00	0.400	55.00	0.000	valve to A
91.49	-	100.00	0.400	77.73	0.000	
91.50	100.00	-	0.400	77.74	0.050	
95.00	100.00	-	0.400	80.49	0.050	valve to B
end time: 95.00 min.				95.00	0.050	valve to A

Valve switch (min.)					
Selection valve	6.22	to position 1	Recycling	40.03	to B
	46.67	to position 2	valve	55.00	to A
				80.49	to B
				95.00	to A

In Table E-7, the method is described of the 30-min degradation of lumichrome, a degradation product of riboflavin. The riboflavin was degraded for 30 min.

Table E-7. Timings, composition, and flow of the 30-min degradation of lumichrome.

Binary pump				Isocratic pump		
Time [min.]	A [%]	B [%]	Flow [ml/min]	Time [min.]	Flow [ml/min]	Comment
0.00	100.00	-	0.400	0.00	0.050	
1.00	100.00	-	0.400	6.21	0.050	
10.00	-	100.00	0.400	6.22	0.050	1st RF peak
11.00	-	100.00	0.400	7.27	0.050	
11.01	100.00	-	0.400	7.28	0.000	
40.03	100.00	-	0.400	37.27	0.000	
41.03	100.00	-	0.400	37.28	0.050	
50.03	-	100.00	0.400	40.03	0.050	valve to B
51.03	-	100.00	0.400	48.13	0.050	
51.04	100.00	-	0.400	48.14	0.050	2nd RF peak
81.96	100.00	-	0.400	49.19	0.050	
82.96	100.00	-	0.400	49.20	0.000	
91.96	-	100.00	0.400	55.00	0.000	valve to A
92.96	-	100.00	0.400	79.20	0.000	
92.97	100.00	-	0.400	79.21	0.050	
96.00	100.00	-	0.400	81.96	0.050	valve to B
end time: 96.00 min.				96.00	0.050	valve to A

Valve switch (min.)					
Selection	6.22	to position 1	Recycling	40.03	to B
valve	48.14	to position 2	valve	55.00	to A
				81.96	to B
				96.00	to A

CHAPTER 13

Acknowledgements

Dit proefschrift zou er vandaag de dag niet zijn geweest, als ik op 6 oktober 2017 geen mail had ontvangen van ene **Maarten van Bommel**. Deze professor, die ik alleen kende van verhalen van een vriendin van mij, mailde mij met het statement dat er binnenkort 2 promotieplekken vrijkwamen en of ik wellicht belangstelling had daarop te solliciteren. Ook stond er in deze mail dat Maarten had vernomen van ene **Peter Schoenmakers** dat ik op zoek was naar een promotieplek. Hoewel ik in deze tijd weinig dingen zeker dacht te weten, wist ik wél zeker dat een promotieplek niets voor mij was. Mijn nieuwsgierigheid naar het project won het van mijn voorbedachte plan en in het begin van 2018 besloot ik te solliciteren op deze nieuwe stap in mijn loopbaan.

Dankjewel, **Maarten**, dat jij mij dit leerproces hebt gegund. Ik denk niet dat er een betere PhD positie zou zijn geweest die mij het onderzoeksveld in had kunnen trekken. Je hebt me vanaf het begin het gevoel gegeven dat ik de doelen van TooCOLD wel zou halen en gaf me daarin ontzettend veel vrijheid. Een beetje meer retention modelling? Geen probleem. Meer wetenschapscommunicatie? Leuk! Zeker in het laatste jaar waar we TooCOLD doelen met de maand behaalden had ik echt het gevoel dat we dit samen deden. Elke woensdag 'even kort' overleggen, om vervolgens 2 uur lang koffie te drinken en nieuwe plannen door te spreken. Elk verhaal leidde wel weer tot een nieuw plan of een andere associatie, waardoor we altijd eindigden met 'Goed plan! Maar eerst die andere dingen'. Jij als bèta in een alfa wereld, ik misschien wel als een alfa in een bèta wereld. We begrepen elkaar en dat had ik niet willen missen.

Dankjewel, **Peter**, voor die mooie jaren aan jouw zijde. Het begon ergens in 2016 toen ik me aanmeldde voor het MSc+ programma. Ik kan me dat interview met jou en Michelle nog goed herinneren, je vroeg me toen namelijk of scheikunde logisch was, omdat ik het vak Logica had gevolgd. Op het moment dat ik het ene pad koos (ja, het is logisch), begon jij met allerlei argumenten te komen waarom dit niet zo was. Eigenlijk is dat proces niet echt meer veranderd toen ik met mijn PhD begon. Elke keer als ik met een mooi verhaal kwam, ging jij altijd de discussie me aan. Ik heb hierdoor zoveel geleerd. In al die één-op-ééntjes hadden we elkaar altijd veel te vertellen en ik weet zeker dat ik zonder die meetings een heel andere beleving had gehad. Ik heb niet alleen veel van jouw kennis mogen proeven, ook van jouw skills heb ik veel geleerd. Ik kon bijvoorbeeld altijd bij je terecht als ik weer een nieuw presentatie idee had. Jouw presentaties zijn wereldwijd bekend en het was een eer om van jou te leren. Ik zie jou als een mentor, iemand bij wie ik kom als ik het zelf even niet meer weet. Iemand die mij helpt als het even niet goed gaat, maar ook bij wie ik graag kom als het heel goed gaat. Je schroomt niet om mij advies te geven wat ik zelf niet wil horen, maar staat ook echt voor me klaar als het nodig is. Laten we vooral onze kwart-voor-acht kopjes koffie

niet vergeten tijdens het afronden van de thesis. Waar we het wel over wetenschap hadden, maar ook over alle andere dingen die ons bezighielden. Ik wil je ontzettend bedanken voor de mooie jaren en hoop op nog een mooiere toekomst.

De helft van deze thesis zou er helemaal niet zijn geweest zonder **Iris**. Onze TooCOLD reis begon op die middag in januari toen wij bij elkaar werden gezet in de wachtruimte voor de sollicitatie. Het was heel fijn om een bekend gezicht te zien, maar we realiseerden ons ook dat we wellicht concurrenten waren. Gelukkig hadden we dat snel uit de lucht, jij ging voor spectroscopie en ik voor chromatografie. We bleken een mooi duo, die verschillende hordes kon overwinnen. Altijd maar met z'n tweeën met ál die supervisors, zowel in de tweewekelijkse meetings, als in de usermeetings. Het was leuk om met jou te groeien en ik ben trots op hoe wij in 4 jaar zijn ontwikkeld.

Bob, onze reis is niet zo vanzelfsprekend geweest. Toen ik in 2018 begon, was jij net bezig met het afronden van jouw PhD. Een fase die ik op dit moment veel beter begrijp dan toen als broekie. Het was een bijzondere periode, omdat we merkten dat we erg op 1 lijn zaten en altijd bij elkaar terecht konden. Toen wij een half jaar later besloten om jou toe te voegen als officiële copromotor, vond ik dat alleen maar leuk. Terwijl ik in mijn PhD groeide, groeide jij in jouw nieuwe functie, waardoor wij soms onder wat spanning kwamen te staan, maar vooral in nieuwe vruchtbare situaties kwamen. We hebben zoveel met elkaar gecreëerd! Het hele retention modelling stuk uit deze thesis was er denk ik niet geweest zonder jou. Maar we konden ook als vrienden bij elkaar terecht en daar ben ik je heel dankbaar voor. Ik kijk uit naar de toekomst, waar ik zeker weet dat je het fantastisch gaat doen.

Binnen TooCOLD hadden wij elke twee weken meetings, eerst vroeg op de vrijdag middag, later vlak voor de vrijmibo. Ik wil graag jullie waardevolle input bedanken **Govert, Freek, Hans-Gerd, Pim, Thomas. Govert**, dankjewel voor de discussie in de meetings, als op de borrels. **Freek**, bedankt voor je eindeloze geduld om mij spectroscopie uit te leggen. **Hans-Gerd**, dankjewel voor je moeilijke chromatografie vragen tijdens de meetings en de leuke gesprekken op de borrels! **Pim** en **Thomas**, ik vond het heel leuk dat mijn water-achtergrond uit de bachelor bij jullie nog een plekje kon vinden. **Pim**, ik heb genoten van onze gesprekken over SETAC.

Within TooCOLD there was another group that played an important role in this thesis, **Carl, Rick**, and **Ingrida**. After one year, **Carl** joined the TooCOLD team. I enjoyed the contact we had, but unfortunately it was short and limited because of COVID. **Rick**, while you were my daily supervisor in my BSc project, we reconnected when you decided to join the TooCOLD

team. I enjoyed the project we did together and am hopeful for a great ending. **Ingrida**, you have really been a TooCOLD-child. After your MSc project with Iris, you could stay a little longer at the VU, and when we opened up a new position to help us with the water project, it was you again! I enjoyed having you in the group in my last phase. But for now: doe het lekker zelf!

Behalve de researchgroup, hadden we bij het TooCOLD project ook een **usergroup**. Ik wil deze groep graag bedanken voor de aangename meetings die we op bijzondere locaties hebben gehad.

Ik was nooit aan mijn PhD begonnen als ik niet zo'n leuke ervaring met wetenschap had gehad tijdens mijn afstudeerstage. Deze periode was een vrij moeilijke periode voor mij, maar ik kijk er met heel veel geluk op terug. **Wim, Marco, Floran, Tessa, Julija, Jan, Hassan**, bedankt. Dankjewel **Wim**, dat je mij zo veel verantwoordelijkheid gaf om het maar uit te zoeken met onze **Aviv**, dat je zo trots was op de uitkomst en dat we zo'n leuke band hebben gekregen. **Marco** en **Floran**, jullie hebben de tijd bij Shell zo gezellig gemaakt en ik denk dat het heel bijzonder is dat we elkaar nog zien. Jullie hebben een speciaal plekje in mijn hart.

During my time at the analytical-chemistry group I met some amazing colleagues. Because my PhD was separated by a pandemic, there really were two phases: the pre-covid time and the post-covid time. I would like to thank the first group for their guidance into my PhD. **Gino, Marta, Alan, Liana, Dorina, Iro, Pascal, Karlijn, Suhas, Fleur, Eleni, Kristina, Robert**, thank you for embracing me in a warm group and CASA! **Marta**, we enjoyed so many fantastic days and nights with many warm memories. Sometimes I feel like those 1.5 good years were just a little short. **Alan, Liana, Dorina**, it has been a pleasure working and borrelling with you. **Iro**, we already met in MSc+ and I am really happy how our friendship evolved. You were always there when we needed to go for coffees or gossip about who-knows-what. Thank you for that. **Suhas**, thank you for all your help in TooCOLD. Even with a sea between us, you were still there for us. **Robert & Kristina**, bedankt voor de leuke sfeer bij de VU. **Gino**, hoewel het even duurde voordat jij weer aansloot bij de groep na jouw tijd bij DOW hebben we een korte maar hele leuke tijd gehad met elkaar. Zonde dat het zo kort was, maar daarom misschien ook wel leuker!

When the worst lockdown was over, I returned to the UvA as a different person. I crossed the two-year mark and was much more serious about how I was going to round off my PhD. I worked with many other PhD students that started after me and that played a much bigger role in the second phase of my PhD. **Stef, Leon, Wouter, Tijmen, Jordy, Denice, Ruben**,

Rianne, Nino, Rick, Joshka, Mirjam, Irene, Ziran, Jim, Maria, Cloé. Lieve Unmatched-boys, de boy-band, het grootste deel van mijn PhD heb ik met jullie mogen doorbrengen. **Stef**, kantoormaatje, wat hebben wij veel biertjes met elkaar gedronken. Soms leek het wel dat door de corona-periode, er nog 10x zoveel biertjes gedronken werden bij elk zonnetje dat zich liet zien. Ik heb er ontzettend van genoten. **Leon**, wat is onze band ontwikkeld in die vier jaar en wat vond ik al onze ochtend koffies fijn. Lekker met z'n tweetjes, we hoefden het eigenlijk niet aan elkaar te vragen. Dankjewel dat je al mijn gelul altijd maar wilde aanhoren. Oh! En bedankt voor die mooie reis terug uit Gent. **Wouter**, je zat een kantoor verder, dus dat was natuurlijk mega ongezellig, maar ook wij hadden het leuk met elkaar. Ik zal je missen. Wat fijn dat je geloofde dat ik uiteindelijk kwam mee-gymmen. **Tijmen**, hoewel een rivier ons scheidde, maakte dat helemaal niks uit. Twee papers hebben we samen geschreven! Ik vind het leuk hoe we allebei als mens zijn gegroeid en de passie voor de wetenschap hebben kunnen delen. **Jordy**, MSc+ maatje, dankjewel voor onze gezellige momenten. **Jim**, dankjewel voor alle lekkere setjes die je me stuurde om die laatste fase door te komen, tot het volgende feestje! **Ruben**, ik kijk ontzettend blij terug op onze lange koffie sessies waar we zowel het verleden als de toekomst in bespraken. En natuurlijk niet te vergeten onze passie voor de marathons! **Rianne**, hoewel wij precies niks gemeen hadden in ons onderzoek, vond ik het altijd heel gezellig met je. **Denice**, in mijn eerste week op de UvA, was jij degene die me moest uitleggen hoe ik mobiele fase moest maken. Ik kan me nog goed herinneren dat je daar een beetje om moest lachen, en achteraf ik eigenlijk ook... **Mirjam**, dankjewel dat je je passie voor wetenschapscommunicatie zo hebt willen delen. Je bent een talent! Lieve **Annika**, we go way back, maar écht! Mijn tijd bij Shell was ook leuker door jouw aanwezigheid. We hielden contact, ook door COAST, en nu ben je opeens mijn collega! Hoewel we maar een korte tijd (8 maanden?) van elkaar hebben genoten, vond ik het heel erg fijn om m'n maatje weer bij me te hebben, dankjewel! Lieve **Rick**, mijn andere kantoormaatje! Dankjewel voor al je slechte grappen en de vruchtbare discussies die we met elkaar konden voeren. Bedankt dat je al-tijd even mee naar het lab liep en met mij problemen wilde oplossen. **Joshka**, dankjewel voor je support voor de SiS en je hulp op Expeditie NEXT. Er komen nog mooie jaren aan! **Nino**, dankjewel voor je kopjes koffie en je gezellige gesprekken. In mijn laatste schrijfperiode wil ik sowieso de pre-8-uur gang (**Annika, Rick, Nino, Joshka, Wouter, Peter, Maarten** en **Tijmen**) bedanken voor de gezelligheid om mij door die thesis heen te trekken! **Irene, Ziran, Maria, Cloé**, while our contact was only short, I wish you all the best!

Some people at CASA stayed with me throughout the years. **Tom, Garry, Aleksandra, Pascal, Anouk, Isabelle, Arian, Raya, Henrik, Saer, Alina, Andrea, Rob**, thanks for guiding me in my PhD journey. **Tom**, dankjewel voor onze eindeloze Ajax-gesprekken. **Pascal**, thank you for your ultimate positivity to help me and my students with LC and our small obsessions with

Tour de Tietema. **Arian**, thank you for introducing me to the bird-brewery. I enjoyed working in such a big group and loved the CASA events we did together. Many Friday afternoon borrels pre-COVID and post-COVID, but also our borrels in COVID times. I think the security of our big group created an environment to achieve great things.

I also want to thank some people from HIMS that I enjoyed some fun moments with. **Tom, Marie, Pim**, dankjewel voor jullie gezelligheid op tijden dat ik even geen zin meer had. **Marcel**, dankjewel voor je support voor SiS.

This thesis would definitely not be here without the help of a big group of students. I was fortunate enough to work with a big talented group of students that I am very grateful for. First of all, **Joshka, Anika, Gerben, Julia**, you all worked on literature theses with me. Thank you for joining me in this, rather boring, project. Many students did practical work. **Tao**, thank you for doing the first annatto experiments. **Dieu**, you were my first real student. Thank you for taking the chance and exploring the water-application with me. **Tobias**, you continued the water project and worked very independently. Pursuing your passion for water research inspires me! **Marie-lou & Alissa**, thank you for joining the fun forensic project. **Alissa**, I admired the fact that you insisted on getting to know everything about a technique you had never heard of. **Marie-lou**, your creativity to solve problems was amazing. Then the TooCOLD people, **Anika, Bob, Nienke, Yorn** and **Jasper**, each one of you worked on a separate part of TooCOLD and you all had fantastic results. **Anika**, you were a spider in a cultural-heritage-research web and created great results. **Bob**, I always enjoyed being your supervisor. You were always so goal-oriented, petje af. **Nienke**, met een introductie via zoom wisten we allebei dat het erg gezellig ging worden. Hoppa, lekker 3D printen en celletjes maken. Helaas waren de resultaten niet fantastisch, het was wel de basis voor het project van **Jasper! Yorn**, speciale man! Terwijl je eigenlijk een hersenschudding had, zat jij weer op die knop te drukken. Samen hebben we het gewoon geflikt. Jammer dat je voor PSV was. **Jasper**, gewoon even zelf een lichtcel creëren en daar het ultieme TooCOLD doel mee behalen. Ik had het zonder jou echt niet gekund. Trots ben ik op je groei, je gaat nog fantastische dingen behalen. Dan het groepje studenten dat ik zover heb gekregen om retention modellering met mij te doen. **Jesper**, dankjewel dat je het aandurfde. Samen wisten we de eerste stappen te zetten voor hoofdstuk 4. **Tim**, wat een slimme man ben jij. We gaven je het project en op het einde zat je er zo in dat je eigenlijk niet wou dat het ophield. Samen met **Yorn** hebben we het zo gezellig gehad in mijn laatste jaar, daar ben ik jullie heel dankbaar voor. Doe nog een kapsalon voor mij! Dan als laatste, **Vivian**, hoewel wij al eerder met elkaar in zee wilden, kwam er wat tussendoor. Dankjewel voor het vertrouwen wat je mij hebt gegeven, ik vind dat heel bijzonder.

Naast mijn collega's boven, mocht ik ook veel met de werkplaats werken. Dankjewel **Hans, Sven, Gertjan, Tristan**, voor jullie eindeloze geduld.

Binnen mijn PhD heb ik me veel beziggehouden met nieuwe vormen van wetenschapscommunicatie. Dit is ook de reden dat er in mijn thesis een hoofdstuk 0 en hoofdstuk 9 te vinden zijn. Ik was al vroeg bezig met wetenschapscommunicatie. Ik maakte een filmpje voor HPLC2019 en deed mee aan Famelab (dankjewel voor je support **Nadine**). Ik was erg op zoek naar nieuwe vormen van wetenschapscommunicatie. Ik wilde bijvoorbeeld gaan vloggen, maar dat bracht zo'n berg werk mee dat ik daar weer vanaf zag. Ik sprak hier veel met **Noor** over. Toen begin 2020 **Lotte** begon bij ons in de groep, hadden we het er samen over. We besloten begin 2021 **Sisters in Science** met elkaar te beginnen; een avontuur dat ik niet had willen missen. Lieve **Noor**, kantoormaatje, duootje, dankjewel voor al die momenten die we samen hebben beleefd. Mijn PhD was écht niet hetzelfde geweest zonder jou erbij. Lekker met elkaar klagen, koffietjes drinken, en samen lachen. We hebben zelfs (heel) even met elkaar gewerkt in het 3D-print lab! Toen we SiS startten werd het allemaal meer en nóg leuker. Lieve **Lot**, wat ben ik dankbaar dat onze wegen weer kruisten toen jij bij ons kwam werken. We hadden aan een blik genoeg, waardoor deze plek nog fijner was. Hoewel dit allemaal gebeurde tijdens COVID, heb ik dit gevoel terugkijkend helemaal niet. Lieve meiden, samen in de krant, samen op tv, samen prijzen winnen, samen filmpjes maken, samen reel-challenges doen, samen zelfs op live tv, we hebben het allemaal gedaan. Ik kijk uit naar onze nieuwe fase, want wie weet wat ons nog te wachten staat. Dankjulliewel voor alle liefde die ik heb gevoeld.

In onze SiS periode hebben we met heel veel leuke mensen mogen werken. Allereerst de groep van de KNCV: **Jan-Willem, Hanneke, Frank**, dankjewel voor jullie vertrouwen in ons. C3, **Marijn, Susanne, Winnie**, bedankt voor de support voor de filmpjes met Vraagbaak. VNCI, **Roderik, Vicky, Manon**, zonder jullie waren we misschien helemaal niet geweest waar we nu zijn. Dan de groep van Warner & VPRO die bij ons aanklopten om mee te doen bij **Anna's Brains**. Dankjewel voor de leuke tijd **Anna, Jorn, Boy, Thierry** en de rest! Als laatste de UvA communicatiegroep, **Kim, Bregje**, bedankt voor de mogelijkheden.

Dan nog iets dichterbij huis. Ik wil graag al mijn **lieve vrienden**, jong en oud, en **mijn familie** bedanken voor jullie support. Hoewel je misschien denkt dat je ver van dit proefschrift af staat, kan je ik je verzekeren dat daar niks van waar is. Door mijn bewogen leven buiten de universiteit hield ik de energie over om me volledig op de wetenschap te werpen. Veel dank aan degenen die mij wat reuring gaven toen het universiteitsleven wat saaier was.

In het speciaal wil ik mijn lieve paranimfen bedanken, **Lot, Saar & Char**. Hoe bijzonder is het dat wij 9 jaar geleden in de collegebanken zaten en dat we nu samen dit met elkaar kunnen beleven. Ik wil jullie ontzettend bedanken dat jullie de wereld waarin ik werkte altijd hebben begrepen en de steun die ik daaruit heb kunnen halen. Dankjewel ook dat jullie met mij dit avontuur aan wilden gaan. Ik ben trots op jullie.

Nu komen we toch echt bijna aan het einde van dit dankwoord. Heel dichtbij zijn er nog een paar speciale mensen die ik wil bedanken. Lieve **Annemarieke, Raouf, Yara, Jasper**, dankjewel dat jullie me zo hebben opgenomen in huize Basta en wat fijn dat ik twee sparringpartners had als het om PhD gaat. Lieve **Luuk & Kaj**, kleine rakkers. Wat ben ik trots om jullie tante te zijn.

Dan mijn lieve **oma**. Met bewondering kijk ik op naar de positieve vrouw die jij bent. We hebben geen makkelijke jaren gehad, maar je staat altijd op met een glimlach. Met zon, een lekker terrasje en een koud biertje kan je ons allebei uren stilhouden, want samen genieten is dubbel genieten.. Ik proost met jou op nog vele jaren en ben zo gelukkig dat jij bij mijn grote dag kan zijn.

Toen ik in 2018 begon aan mijn PhD, was mijn gezinssituatie aan verandering onderhevig. Nu 4 jaar later, ben ik veranderd, maar die situatie ook. Samen zijn we gegroeid naar een nieuwe vorm. Lieve **Mama**, dankjewel voor je steun in die moeilijke jaren. Ik ben blij dat het leven ons toelicht en trots op jou als persoon. Je hebt altijd begrip voor me gehad en mij de ruimte gegeven. Ik vind het fantastisch dat je het geluk hebt gevonden bij **Tom**. Tom, dankjewel dat je zo gek bent op mijn moeder. Ik vind het heel bijzonder dat we elkaar zo goed hebben leren kennen in die korte tijd. **Shifra**, dankjewel voor jouw open blik en enthousiasme. Ik ben heel gelukkig dat ik zo'n stiefzus erbij heb gekregen. Lieve **Papa**, wat ben ik trots op ons. Ik had niet durven dromen van de band die wij nu met elkaar hebben. Ik ben ook trots op jou, dat je beter naar jezelf luistert en de rust op zoekt. Stiekem vind ik Groenekan ook mooi, hoor. Ik ben ook blij dat je **Marlies** hebt gevonden. Marlies, bedankt voor je rust en je aandacht. Ik prijs mezelf gelukkig met zo iemand in mijn kring. Ik kijk ook uit om jullie beter te leren kennen, **Koen en Sterre**.

Loek, zonder jou was die periode helemaal niks geweest. Ben jij nou mijn zusje of mijn zus? In tijd van onzekerheid was jij mijn baken, en dat ben je eigenlijk nog steeds. Een stabiele factor, die al-tijd begrip zal hebben voor mij (tenzij het niet eerlijk is, natuurlijk). Lieve Loek, ik ben zo blij dat jij mijn zus bent, net zoals de dag dat je geboren werd. Dat ik je dan een beetje moet delen met **Laura** vind ik natuurlijk niet erg. **Laura**, dankjewel dat je in het leven van Loek bent gewandeld. Ik kan niet wachten om met herinneringen met je te maken.

En dan, als aller, allerlaatste, **Didi**. Best bijzonder dat jij de hele rit aan mijn zijde stond. Hoewel je er natuurlijk niks van snapte, gaf je me wel altijd het gevoel dat je luisterde. Toen we even in corona op 50 m² moesten gaan samenwerken vond ik het eerder gezellig dan ongezellig (maar je praat wel echt heel erg hard). Dankjewel dat je me op hoge stress momenten altijd weer even naar de grond haalde, of me toch overhaalde om dat ene feestje of borreltje mee te pakken. Jij was mijn grootste toevluchtsoord van de PhD en daar ben ik je ontzettend dankbaar voor. Daarnaast heb ik ook altijd het gevoel gehad dat je mijn grootste fan was. Altijd meekijken, altijd feedback geven, altijd vieren. Ik kijk uit naar de toekomst met jou.

Heb je nou nóg niet genoeg?!

Dan heb ik nog een toetje: <https://linktr.ee/mimidenuyl>

